Theoretical Study on Pd-catalyzed Cross-Coupling Reactions.

Maximiliano García Melchor

Ph.D. Thesis
Ph.D. in Chemistry

Supervisors:
Gregori Ujaque Pérez
Agustí Lledós Falcó

Departament de Química,
Facultat de Ciències
2012

Universitat Autònoma de Barcelona
Departament de Química
Unitat de Química Física

Memòria presentada per aspirar al Grau de Doctor per Max García Melchor.

Max García Melchor

Vist i plau,

Gregori Ujaque Pérez

Agustí Lledós Falcó

Bellaterra, 9 de Març de 2012.

List of abbreviations

Abbreviation	Meaning
Ar	Any aromatic group
B3LYP	Becke's three-parameter, Lee-Yang-Parr exchange-correlation functional
^{t}Bu	*tert*-butyl
dba	dibenzylideneacetone
DCM	Dichloromethane
DMF	N,N-Dimethylformamide
DFT	Density Functional Theory
DMSO	Dimethyl sulfoxide
ee	Enantiomeric excess
GGA	Generalized Gradient Approximation
HF	Hartree-Fock
IUPAC	International Union of Pure and Applied Chemistry
KS	Kohn-Sham
LDA	Local Density Approximation
LSDA	Local Spin Density Approximation
MA	Maleic Anhydride
Me	Methyl
MeCN	Acetonitrile
MM	Molecular Mechanics
MP2	Møller-Plesset perturbation theory to second order
NHC	N-Heterocyclic Carbene
NMR	Nuclear Magnetic Resonance
ONIOM	Our own N-layered integrated molecular orbital + molecular mechanics
PCM	Polarizable Continuum Model

Abbreviation	**Meaning**
PES	Potential Energy Surface
Ph	Phenyl
^{i}Pr	Isopropyl
QM	Quantum Mechanics
SDD	Stuttgart-Dresden effective core potential
S_N2	Bimolecular nucleophilic substitution
THF	Tetrahydrofuran
ZPE	Zero Point Energy

Contents

"In all science, error precedes the truth, and it is better it should go first than last."

Hugh Walpole

1 General introduction

As the title above suggests, this first chapter is devoted to make a general introduction to the main topic of this present thesis: the *Pd-catalyzed cross-coupling reactions*. With this aim, in the first part of this chapter the concept of catalysis, its origin, as well as other related topics will be briefly introduced.

Next, in the second part of this chapter, the definition of cross-coupling reactions and a summary of their generally accepted reaction pathway will be presented.

Finally, the elementary steps that take part in this type of reactions will be described separately. Furthermore, for each of these steps, the most relevant mechanistic studies on Pd-catalyzed cross-coupling reactions reported in the last years, with particular attention to the theoretical ones, will be reviewed.

In principle, all the concepts provided in this first chapter may be more than enough to contextualize all the results obtained in the course of this thesis, and that are presented in Chapters 4, 5 and 6.

1.1 Catalysis

1.1.1 Origin and basic concepts

The term "catalysis"[†] was introduced by Berzelius when in 1836 in an effort of accounting for a series of chemical transformations and decompositions, wrote:[1,2]

"This new force, which was unknown until now, is common to organic and inorganic nature. I do not believe that this is a force entirely independent of the electrochemical affinities of matter; I believe, on the contrary, that it is only a new manifestation, but since we cannot see their connection and mutual dependence, it will be easier to designate it by a separate name. I will call this force catalytic force. Similarly, I will call the decomposition of bodies by this force catalysis, as one designates the decomposition of bodies by chemical affinity analysis".

Hence, Berzelius used the concept of catalysis to bring together a series of phenomena that could not be explained with the common conception of that time of reactions being caused by chemical affinity. The term, however, was originally purely descriptive because Berzelius intentionally refrained from attempting to explain the nature of catalysis. Specifically, he called "catalytic force" to a new force, but emphasized that he expected to be able to explain its operation within the framework of electrochemical theory.

At present, the International Union of Pure and Applied Chemistry (*IUPAC*) defines catalysis as *"the action of a substance (i.e. catalyst) that increases the rate of a reaction without modifying the overall standard Gibbs energy change in the reaction"*. In fact, this definition is quite similar to the one provided in 1895 by Ostwald:[‡] *"a catalyst accelerates a chemical reaction without affecting the position of the equilibrium"*. Thus, a catalyst does not influence the thermodynamic equilibrium of reactants and products but affects the rates of the chemical reactions. In other words, the reaction Gibbs energy (ΔG) in a catalyzed reaction does not change whereas the activation energy (E_a) certainly does it (Figure 1.1).

Nevertheless, catalysts can influence the reaction equilibria for more subtle reasons and, for example, result in higher concentrations of the product. It is well known that equilibria can be shifted by changing conditions, such as temperature, and that *Le Châtelier's principle* predicts that an exothermic reaction will lead to

[†]The word "catalysis" originates from the Greek words "$\kappa\alpha\tau\acute{\alpha}$" and "$\lambda\acute{\upsilon}\sigma\iota\varsigma$" and has the sense of "dissolution".

[‡]Wilhelm Ostwald was awarded with the Nobel Prize in Chemistry in 1909 *"in recognition of his work on catalysis and for his investigations into the fundamental principles governing chemical equilibria and rates of reaction"*.

higher equilibrium concentrations of product at lower temperatures than at higher temperatures. Thus, a catalyst that allows to conduct an exothermic reaction at a lower temperature than in its absence will lead to a higher concentration of product.

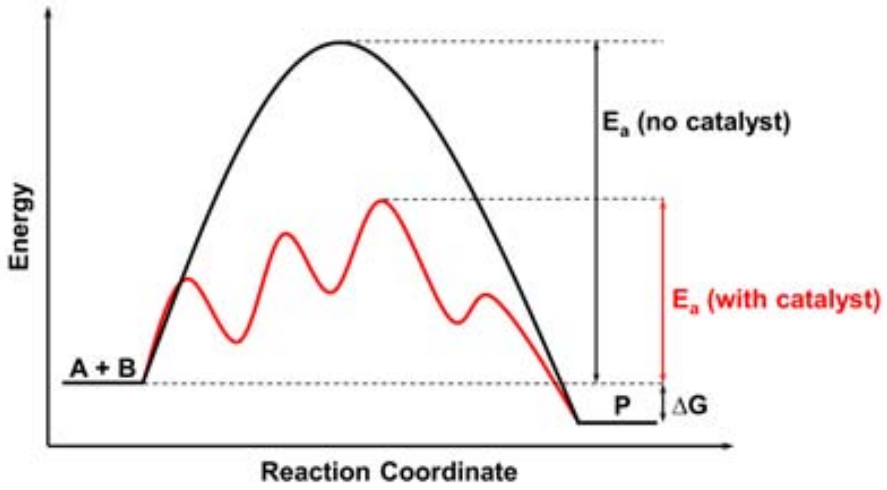

Figure 1.1: General representation of an arbitrary reaction profile for a catalyzed (red curve) and uncatalyzed (black curve) reactions.

1.1.2 Transition state stabilization

During a catalytic reaction, the catalyst decreases the activation energy, relative to that of the uncatalyzed reaction, by stabilizing the transition state(s). However, as the transition state is an unstable and fleeting species, the catalyst can not affect it alone. Instead, it coordinates to one or more of the reactants and remains coordinated throughout the transition state(s) of the catalytic process. Along this process, the dissociation of the product either regenerates the starting catalyst directly or generates a species that will be converted to the starting catalyst. Consequently, catalysts can be used in sub-stoichiometric amounts relative to the reagents.

On the other hand, catalysts can lower the energy of the highest energy transition state by interacting with and stabilizing a structure that is similar to that of the uncatalyzed reaction, or can present a completely different reaction pathway (Figure 1.1). The former is typical in enzyme-catalyzed processes while the latter occurs more often in organometallic chemistry. In this last case, the reaction normally takes place in more steps, but the activation energy of each of the individual steps is always lower than the activation energy of the uncatalyzed process.

1.1.3 The catalytic cycle

The combination of steps of a catalytic reaction is commonly known as *catalytic cycle*. As shown in Figure 1.2, this series of reactions is generally depicted in the form of a cycle because the starting point of the catalytic process is also the ending point of the reaction (i.e. the catalyst is regenerated).

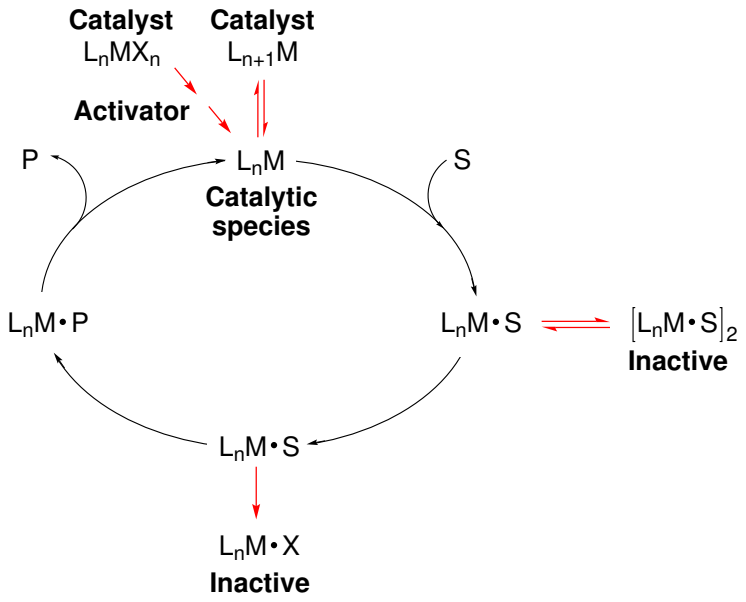

Figure 1.2: Example of a catalytic cycle with both the reversible and irreversible formation of inactive species.

Often, the added catalyst is not in the active form. This is, the catalyst is a precursor and do not correspond to the species that enters into the catalytic cycle (Figure 1.2). The species that runs in the catalytic cycle is generally named *catalytic species*, and can be generated either by the dissociation of a ligand or by the assistance of an *activator*. Once this active species is formed, it undergoes a series of transformations eventually giving rise to the formation of the final product and its concomitant regeneration. In some cases, however, during the catalytic cycle there can appear competitive reactions that give birth to inactive species, which produce the deactivation of the catalyst or the retard of the catalytic process. Examples of catalyst deactivation and retardation of the catalytic activity in the catalytic cycle shown in Figure 1.2, are the irreversible reaction of $[L_nM{\cdot}S]$ to form $[L_nM{\cdot}X]$, and the formation of the dimeric species $[L_nM{\cdot}S]_2$, respectively.

1.1.4 Quantification of the activity and efficiency of catalytic processes

Even though in a catalytic reaction, in principle, the catalyst should be fully regenerated at the end of the process, it really rarely happens. As above mentioned, catalytic species can undergo competitive reactions and decrease their activity (i.e. catalyst deactivation). Thus, obtaining magnitudes that allow measuring their activity and efficiency is crucial for their comparison and the further design of more active and efficient catalysts.

A widely used manner of measuring the catalytic activity is to calculate the reaction rate constant, k. There exists different ways of obtaining this parameter. Probably, the simplest one is to use the empirical relation between the reaction rate constant and the temperature, derived by Arrhenius[3] in 1899 and that receives his own name:†

$$k = Ae^{\frac{-E_a}{RT}} \tag{1.1}$$

where A is the *pre-exponential factor* (sometimes called *frequency factor*), E_a is the *activation energy*, R is the *universal gas constant*, and T is the *absolute temperature*.[4]

In the Arrhenius equation (Eq. 1.1), the term A also changes with temperature. However, since its dependence compared to that of the exponential term is usually low, it can be neglected. On the other hand, the activation energy of a reaction is a very important term in catalysis because it dictates the barrier that must be overcome for a reaction to happen. The expression for this term can be easily obtained from equation (1.1) after simple mathematical treatment,

$$E_a = RT^2 \frac{d(ln\ k)}{dT} \tag{1.2}$$

and provides an empirical estimation of the energy barrier for a given reaction. A useful rule of thumb states that the reaction rate roughly doubles for every 10 ℃ increase in temperature. Moreover, in cases in which E_a is lower than ∼5 kcal·mol^{-1}, we say that the reaction is diffusion-controlled, which means that the reaction rate is controlled by how fast the molecules move toward one another. Alternatively, when E_a is higher than ∼5 kcal·mol^{-1}, we say that the reaction is chemically-controlled.[4]

†Although this expression applies only to gas phase reactions, it is often applied in general.

Another way of calculating the reaction rate constant is by means of the transition state theory (TST). This theory was developed simultaneously in 1935 by Eyring[5] and by Evans and Polanyi.[6] There exists different formulations of the TST, but only the thermodynamical formulation will be described herein.

Let us consider a reaction between two reactants, A and B, that results in an activated species $[AB]^{\ddagger}$ (or transition state) such that it spontaneously evolves to the final product P, and further, is in equilibrium with the starting reactants

$$A + B \underset{k_{-1}^{\ddagger}}{\overset{k_1^{\ddagger}}{\rightleftharpoons}} AB^{\ddagger} \xrightarrow{k^{\ddagger}} P \tag{1.3}$$

The equilibrium constant for the reaction between reagents A and B, and the activated species, is given by:

$$K_c^{\ddagger} = \frac{k_1^{\ddagger}}{k_{-1}^{\ddagger}} = \frac{[AB^{\ddagger}]}{[A][B]} \tag{1.4}$$

The concentration of the activated species $[AB^{\ddagger}]$ is considered to be negligible towards the concentration of reagents A and B. Thus, the concentration of the reagents can be assumed constant. On the other hand, the reaction rate can be expressed as a function of the formation of product P,

$$\frac{d[P]}{dt} = k^{\ddagger}[AB^{\ddagger}] \tag{1.5}$$

where $k^{\ddagger}$ is the rate constant for the reaction going from $[AB^{\ddagger}]$ to P. The value of this rate constant can be obtained by statistical mechanics and equals to $k_B T/h$, being k_B the *Boltzmann constant* ($1.38{\cdot}10^{-23}$ J·K^{-1}), and h the *Planck constant* ($6.626{\cdot}10^{-34}$ J·s).

Now, if we combine the equations (1.5) and (1.4) we arrive at:

$$\frac{d[P]}{dt} = \underbrace{\frac{k_B T}{h} K_c^{\ddagger}}_{k}[A][B] \tag{1.6}$$

Finally, the *van't Hoff equation* states the relation between the equilibrium constant and the variation in the *activation Gibbs energy* ($\Delta G_0^{\ddagger}$) by means of the following expression,

$$\Delta G_0^{\ddagger} = -RT\ ln\ K_c^{\ddagger} \tag{1.7}$$

where $\Delta G_0^{\ddagger}$ is defined as the difference between the standard Gibbs energy of the transition state and the reagents A and B. Introducing the value of $K_c^{\ddagger}$ in equation (1.7) into the equation (1.6), we obtain that the reaction rate constant of the overall reaction is:

$$k = \frac{k_B T}{h}\ e^{-\frac{\Delta G_0^{\ddagger}}{RT}} \tag{1.8}$$

In this last equation $\Delta G_0^{\ddagger}$ can be alternatively expressed in terms of enthalpy and entropy of activation ($\Delta H_0^{\ddagger}$ and $\Delta S_0^{\ddagger}$, respectively), which leads to the widely known *Eyring equation*:

$$k = \frac{k_B T}{h}\ e^{\frac{\Delta S_0^{\ddagger}}{R}}\ e^{-\frac{\Delta H_0^{\ddagger}}{RT}} \tag{1.9}$$

So far, we have seen that the reaction rate constant is used to quantify the catalytic activity and how it can be calculated. But, how is the efficiency of a catalytic process measured? In general, two quantities are used for this purpose. The first one is the is the *turnover number*, *TON*. As its name suggests, it can be seen as the number of turns that a catalyst does within the catalytic cycle before it is deactivated. It can be calculated as the number of moles of product per mole of catalyst (Eq. 1.10). Hence, for an ideal catalyst, the *TON* should be infinite. So that you can get an idea of the range of *TON* values, commodity-scale reactions, such as rhodium-catalyzed hydroformylation occur with hundreds of thousands of turnover numbers, whereas other reactions that are less developed might occur with 10 to 20 turnovers.[7]

$$TON = \frac{moles\ of\ product}{moles\ of\ catalyst} \tag{1.10}$$

The other quantity used to measure the efficiency of a catalytic process is the *turnover frequency*, *TOF*, which is defined as the number of moles of product per mole of catalyst per unit time. Therefore, the *TOF* is simply the *TON* per unit time:

$$TOF = \frac{TON}{time} \tag{1.11}$$

The above presented definitions for the *TON* and *TOF*, however, vary slightly depending on the type of catalyst. In heterogeneous catalysis, for example, the *TON* and *TOF* are often defined per active site or per gram catalyst. In contrast, in biocatalysis, they are defined by the rate measured when all the enzyme molecules are complexed with a reactant, divided by the total enzyme concentration. Thus, when dealing with *TON* and *TOF* data it is important to provide the units in order to avoid misunderstandings.

Up to a few years ago, there was no simple way to calculate the efficiency of a catalytic cycle (i.e. *TOF*), from a theoretically obtained energy profile. It was Kozuch and Shaik who recently introduced the so-called *energetic span model*, which enables evaluating *TOFs* in a straightforward manner.[8–11] The formulation of this model is based on *Eyring's TST* and corresponds to a steady-state regime. One of the most interesting conclusions derived by the authors from this model is that in catalytic cycles there are no rate determining steps, but *rate determining states*.

With the concept of catalysis and some of their related aspects already introduced, the following section will be devoted to describe the type of catalytic reactions that have been studied in this present thesis: the *cross-coupling reactions*.

1.2 C–C cross-coupling reactions

1.2.1 What are C–C cross-coupling reactions?

The C–C cross-coupling reactions are undoubtedly one of the most important and useful reactions in organic synthesis and organometallic chemistry, since a huge variety of complex compounds can be synthesized from readily accessible reactants.[12–16] These reactions consist in the carbon-carbon bond formation between an organic electrophile (R^1–X) and an organometallic nucleophile (R^2–m) in the presence of a metal catalyst [M] (Scheme 1.1). Generally, the most widely used metal catalysts are transition metal complexes from groups 8-10, especially Ni and Pd.[17–19] The reason for

which these metals are the most common ones originates from their Ni(II)/Ni(0) and Pd(II)/Pd(0) ease of redox exchange, which is an indispensable condition for the catalytic cycle to be completed. Between these two catalysts, however, Pd catalysts have been demonstrated to have more advantages for cross-coupling reactions than those of Ni.[7] For example, they tend to be less sensitive to oxygen, and are believed to be less toxic. Moreover, unlike the Ni catalysts, Pd complexes tend to react without the intervention of radical intermediates, which can eventually lead to side products such as those from homocoupling.† Consequently, Pd-catalyzed cross-coupling reactions have been the most developed ones.

As regards to the organometallic nucleophile (R^2–m), depending on the metal or semi-metal involved, cross-coupling reactions receive different names, which usually correspond to their discoverers' name (Scheme 1.1). For instance, Stille[20–22] reaction is tin-mediated; Suzuki-Miyaura,[23,24] boron-mediated; Negishi,[25] zinc-mediated, etc. The relevance of these reactions in the last decades has been such that three of their developers were awarded with the Nobel Prize in Chemistry in 2010.‡ Additionally, their mild reaction conditions along with their wide tolerance of functional groups have substantially contributed to their application in many areas, such as the synthesis of natural products,[26–28] fine chemicals,[29–31] and polymers.[32–34]

Scheme 1.1: General scheme for C–C cross-coupling reactions.

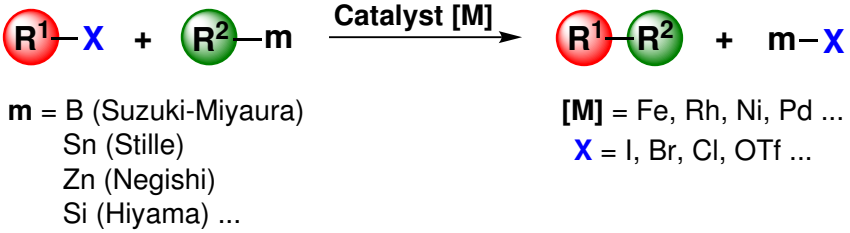

Among the numerous advantages of these reactions, probably the most remarkably is the manifold variety of organometallic reagents and organic electrophiles that can be employed to assemble C–C bonds. However, not all the reactions involving different organic groups (e.g. R = alkyl, allyl, aryl, alkenyl, alkynyl) and different heteroatoms (e.g. X = Cl, Br, I) have been studied to the same extent. For example, cross-coupling reactions involving aryl or vinyl electrophiles have been by far the most extensively

†The *homocoupling* is the coupling of two identical molecules.

‡Richard F. Heck, Ei-ichi Negishi and Akira Suzuki shared the Nobel Prize in Chemistry in 2010 *"for palladium-catalyzed cross couplings in organic synthesis"*. These scientists are the developers of the widely known Heck, Negishi, and Suzuki reactions, respectively.

studied mainly because they are readily accessible reagents and, further, their reactions have wide applicability and high selectivities. Conversely, alkyl electrophiles, and specially those that possess β-hydrogens (i.e. unactivated alkyl electrophiles), have been much less studied. In this case, it is mainly due to their lack of reactivity towards oxidative addition and their ease of participating in competitive reactions, such as β-elimination and hydrohalogenation. In fact, it was not until the appearance of some pioneering works, such as the ones from Kochi and Tamura,[35–37] Suzuki et al.,[38] and other recent works, such as the ones from Knochel[39–42] or Beller,[43] that it was demonstrated that cross-coupling reactions employing alkyl electrophiles are feasible. Thereafter, the interest in these reactions has become increasingly important to the point that the development of efficient Csp^3–Csp^3 coupling is at present one of the active research topics within cross-coupling reactions.

On the other hand, cross-coupling reactions involving organic halides initially had the important limitation that only aryl bromides and iodides could be employed. However, as aryl chlorides are more profusely available and, in general, less expensive than their bromide and iodide analogs, many efforts to overcome that issue have been made since then.[44] In particular, important advances in the past few years have been achieved mainly owing to the development of new transition metal complexes containing electron rich and bulky ligands (mostly phosphines,[45–47] but also carbenes[48,49]).

1.2.2 The catalytic cycle

C–C cross-coupling reactions follow a general accepted reaction pathway named *catalytic cycle* that consists of three steps (Figure 1.3): *i) oxidative addition* or insertion of the low valent transition metal into the electrophilic carbon-heteroatom bond; *ii) transmetalation* or displacement of the heteroatom leaving group by the nucleophile; and finally, *iii) reductive elimination* to form the new C–C bond with the concomitant regeneration of the catalyst. The former and the latter steps are common to all cross-coupling reactions and have been studied in depth both by experimental[50–53] and computational methods.[54–57] Hence, the mechanisms for these two steps are quite well understood. In contrast, the various cross-coupling reactions differ in the nucleophile used for transmetalation and, consequently, in the transmetalation step. Furthermore, experimental evidence for this process is particularly difficult to obtain due to the complexity that involves the isolation and characterization of key intermediates. Thus, it is not surprising that the transmetalation step is the less studied and considered as the most complex one within the catalytic cycle (Figure 1.3). Even so, in the last years several mechanistic studies on this step have appeared.[58–64] In particular, in our group we have carried out several theoretical studies concerning this step in several cross-coupling reactions, some of them in collaboration with experi-

mental groups.[65–72] In fact, some of these theoretical studies are part of the results of this thesis and will be presented in Chapters 4, 5 and 6.

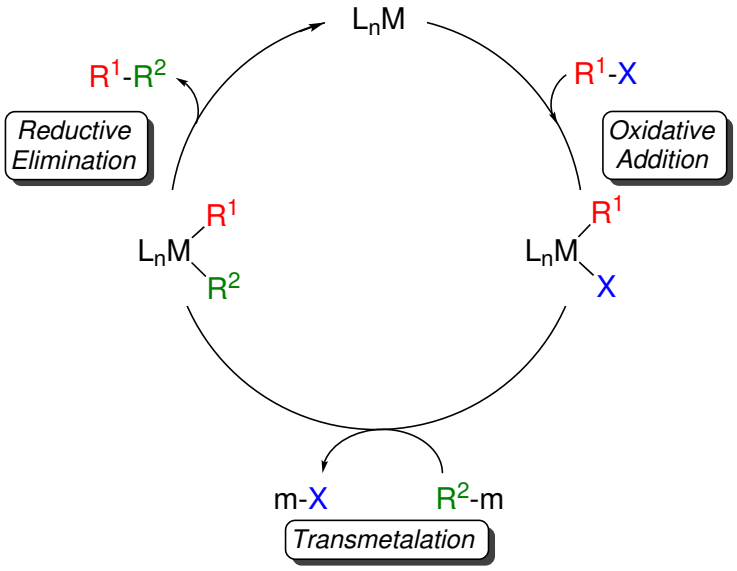

Figure 1.3: General catalytic cycle for C–C cross-coupling reactions.

In the following sections, a brief description of the three elementary steps of the catalytic cycle (Figure 1.3) will be presented separately. More specifically, I will briefly describe each of these steps, and what has been reported about them in the last years.

1.2.3 Oxidative addition

Oxidative addition reactions are processes in which the bond in an organic or main group reagent A–B breaks, and two new bonds with the metal are formed (Scheme 1.2). In this overall process, since A and B are anionic ligands, the metal is formally oxidized. More specifically, oxidative additions to mononuclear metal complexes (Eq. 1, Scheme 1.2) results in an increase in the oxidation state of the metal from n to n+2, whereas oxidative additions to dinuclear metal complexes (Eq. 2, Scheme 1.2) increase the oxidation state of each metal from n to n+1.

The opposite reaction to the oxidative addition is the reductive elimination, where the A–B molecule is expelled from the [M(A)(B)] complex. In principle, these reactions can be reversible but, in practice, they tend to evolve in either one or other

Scheme 1.2: General scheme for the oxidative addition reaction of an A–B molecule to a mononuclear (Eq. 1) and dinuclear (Eq. 2) metal complexes.

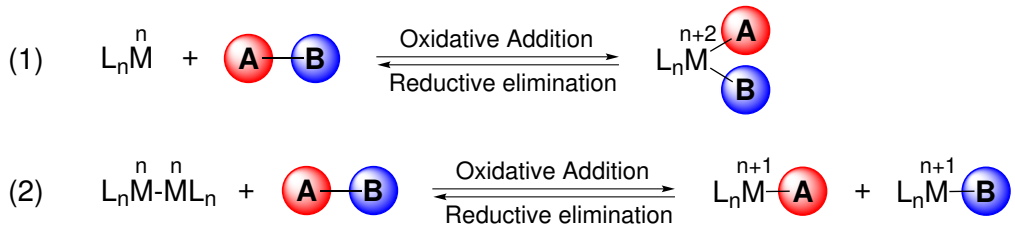

direction. In fact, the position of equilibrium in any particular case depends on the overall thermodynamics, which in turn depends on the relative stability of the metal in each oxidation state and the strength of the A–B bond with respect to the M–A and M–B bonds. On the basis of these dependences and other chemical concepts (e.g. coordination number of the metal), we can consider the following series of trends as a guide for predicting the reactivity of metal complexes towards oxidative addition:[†]

- *Oxidative additions to more electron-rich metal centers tend to be more favorable than oxidative additions to more electron-poor metal centers.*
- *Oxidative additions to less-hindered metal centers tend to be more favorable than oxidative additions to more-hindered metal centers.*
- *Rates and equilibrium constants for ligand dissociation or association previous to oxidative additions affect the rates of the overall addition processes.*

Probably, one of the best features of oxidative addition reactions is the unusual wide range of reagents A–B that can be involved. These can be divided into three groups: *i)* species that are non-polar or have low polarity (e.g. H_2, silanes); *ii)* reagents that are highly polar (e.g. alkyl halides, strong acids); and *iii)* reagents that are intermediate in polarity (e.g. amines, alcohols). A direct consequence derived from this wide range of A–B molecules that can undergo oxidative addition is the existence of multiple reactions mechanisms for this process. In particular, in the literature there are described four reaction mechanisms for oxidative addition (Figure 1.4): *concerted mechanism*, *S_N2 mechanism*, *radical mechanism*, and *ionic mechanism*.

In oxidative additions via a *concerted mechanism* (Figure 1.4), the A–B molecule binds firstly to the metal center and then, the cleavage of the A–B bond and the

[†]These trends are only given by way of guidance; there may be exceptions.

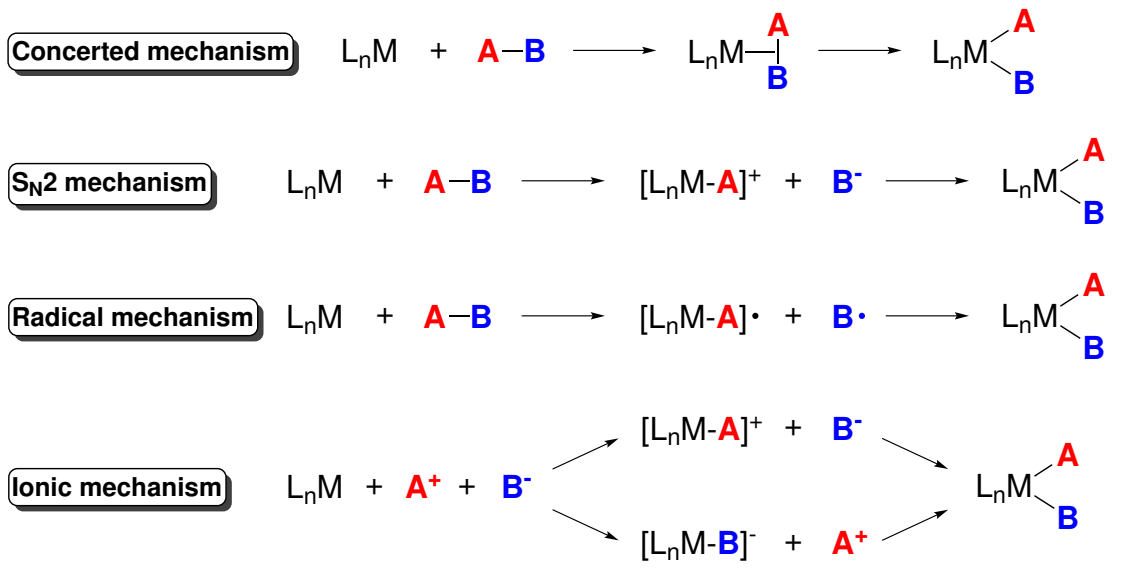

Figure 1.4: Reaction mechanisms for the oxidative addition of an A–B molecule to a metal complex.

formation of the new M–A and M–B bonds take place simultaneously through a three-centered transition state. This mechanism is normally found in oxidative additions of non-polar reagents[73–76] and aryl halides.[77–80] Experimental evidences for this mechanism are the retention of configuration at a stereogenic center in the case of chiral A–B reagents, and the relative *cis* disposition of the ligands A and B in after the oxidative addition.[81] The latter, however, may be not observed in the cases in which the cis-to-trans isomerization reaction of the oxidative product is very fast.[82]

On the other hand, the *S_N2 mechanism* is an associative bimolecular process that consists in two steps (Figure 1.4): first, the ligand A is attacked by a metal electron pair and the anionic ligand B^- is expelled giving rise to the cationic species $[L_nM–A]^+$; subsequently, the two charged species collapse to yield the oxidative addition product. Unlike the concerted mechanism, the relative position of the ligands A and B in the final product via this mechanism can be either *cis* or *trans*, depending on where the anionic ligand B ends up coordinated after the second step.† This S_N2 mechanism is often found in oxidative additions of polar reagents and in polar solvents, and results in the inversion of configuration of a stereogenic center.[81,83–85]

The third mechanism in Figure 1.4 is a type of *radical mechanism* known as *non-*

†This may be governed by the *trans-effect*.
Trans-effect: is the effect that produces a ligand that facilitates the exchange or substitution of a second ligand that is in *trans* position respect to the former. We refer to ligands with high trans-effect when these facilitate that substitution.

chain radical mechanism.† This non-chain variant is generally believed to operate in oxidative additions of certain alkyl halides[87] and consists in the one-electron oxidation of the metal by the A–B molecule giving rise to the radical species $[L_nM–A]^{\bullet}$ and $B^{\bullet}$, which rapidly recombine to yield the oxidative addition product $[L_nM(A)(B)]$. Similarly to the S_N2 mechanism, the rate of this radical mechanism increases as more basic is the metal, and the more easily the ligand A is transferred to the metal. Experimental evidences for this type of mechanism can be the significant changes in the reaction rate produced by the introduction of slight modifications of the substrate, the metal complex, or the solvent. Another alternative to confirm this mechanism is to use radical scavengers, such as $RNO^{\bullet}$. This alternative, however, has been somewhat criticized on the basis that the presence of such species may initiate a radical pathway for a reaction that otherwise would have followed a non-radical mechanism.

Finally, the last mechanism proposed for oxidative addition is the *ionic mechanism* (Figure 1.4). This mechanism is adopted for A–B molecules that are completely dissociated in solution, and consists in the consecutive coordination of the two charged ligands to the metal complex. Thus, this mechanism can evolve through two possible variants. The first one involves the initial coordination of the cation A^+ to the metal complex and the subsequent coordination of the anionic ligand B^-. On the contrary, in the second alternative the coordination of the anionic ligand B^- to the metal complex occurs first, followed by the coordination of the cation A^+. In general, the first variant is the most common one, and is favored by basic ligands and a low oxidation state of the metal.[86]

Overall, we have seen that the reaction mechanism for the oxidative addition is highly sensitive to the nature of the reagent A–B. Thus, depending on the reagent one or another mechanism might be favored. However, this is not the unique factor that influences the oxidative addition. Other factors that can affect this process are, for instance, the nature of the solvent, the metal-bound ligands, or the added additives. An illustrative example of this is the oxidative addition of allylic chloride to Pd(0) and Pt(0) complexes.[88,89] In these reactions, the use of polar solvents, such as MeCN or DMSO, was found to favor the S_N2 mechanism leading to complete or nearly complete inversion of configuration. Conversely, complete or predominant retention of configuration was observed in less coordinating solvents, such as benzene or dichloromethane.

Among the manifold variety of A–B molecules that can undergo oxidative addition, the ones possessing C–X bonds are typically involved in the oxidative addition step of cross-coupling reactions. Hence, since this thesis is focused on the theoretical study of these reactions catalyzed by Pd complexes, I found appropriate to include

†There is also another variant of radical mechanism called *chain mechanism*. This, however, will not be discussed here. More details on this type of mechanism can be found in books on general organometallic chemistry.[7,86]

at the end of this section a brief overview of this type of oxidative additions. The aim of this overview is just to provide a general picture of which have been the main research interests related to this process, paying especial attention on the reported theoretical works.

Oxidative addition of C–X bonds to Pd(0) complexes

Oxidative additions of substrates possessing C–X bonds, and specially those possessing Ar–X bonds, have been extensively studied because they are the first step in cross-coupling reactions. In particular, the focus of computational attention on this step is probably related to the fact that it has been postulated to be rate-limiting in a few cross-coupling reactions, specially when X = Cl.[44]

One of the earliest theoretical studies on C–X oxidative addition to a Pd complex was reported by Bickelhaupt et al.[76] These authors investigated the addition of chloromethane to a ligand-free palladium atom by means of density functional theory (*DFT*) calculations showing a preference for the concerted pathway toward the S_N2 substitution. Few years later, the oxidative addition of PhX (X = Cl, Br, I) to palladium(0) complexes containing bidentate phosphanes was investigated by Senn and Ziegler.[54] Interestingly, the authors could not locate in solution the concerted transition state reported for the gas phase. Instead, they found that the dissociation of the halide and its subsequent recombination with the cationic phenyl complex (i.e. the S_N2 mechanism) was energetically a facile process in solution even without accounting for favorable entropic contributions that such a dissociative mechanism may have.

As previously stated, the oxidative addition reaction is highly sensitive to the nature of the reagent, the added additives, the metal-bound ligands, and the solvent. Hence, all these factors have been also of particular interest in this type of oxidative additions and have been studied in some depth. Regarding the influence of added additives, the role of anionic additives in improving the oxidative addition step has been analyzed by several authors. Jutand et al.[50,90,91] provided a significant amount of experimental evidences suggesting an anionic form for the catalyst, $[Pd(Cl)(L)_n]^-$. Calculations by Bickelhaupt and co-workers on the activation of H–H, C–H, C–C and C–Cl bonds showed that the anionic species $[PdCl]^-$ favors the S_N2 pathway even in gas phase, and revealed that the lowering of activation barriers through anion assistance is caused by the more stabilizing interaction between the reactants in the transition state.[92] On the other hand, Thiel et al.[55] explored the reaction of $[Pd(OAc)(PMe_3)_2]^-$ with Ph–I. In this case, however, the mechanism is quite subtle; the acetate ligand moves away from palladium when iodobenzene coordinates, and returns afterwards to the metal to displace another ligand. Two different paths of similar energies were characterized for this process (Figure 1.5): the most favored

one (pathway A, Figure 1.5) ends up with departure of iodide, and resembles the S_N2 pathway; the least favored one (pathway B, Figure 1.5), involves the displacement of a phosphine ligand and the transition state associated to C–I cleavage is of a concerted type.

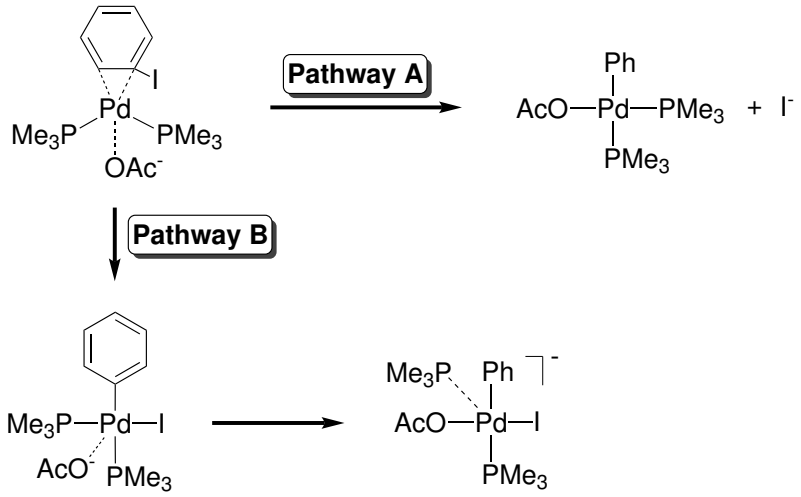

Figure 1.5: Reaction pathways proposed by Thiel et al. for the oxidative addition of Ph–I to $[Pd(OAc)(PMe_3)_2]^-$.[55]

As regards to the influence of the nature of the substrate, so far we have seen that the prototypical substrates for oxidative addition reactions are aryl halides, but fragments different from aryl are also relevant. Aimed at providing a better understanding of what is responsible for the higher reactivity of aryl halides compared to alkyl halides, Ariafard and Lin recently reported a *DFT* study on the oxidative addition of different reagents R–Br (R = methyl, benzyl, phenyl, vinyl) to $[Pd(PH_3)_2]$.[93] In this study, however, the authors only considered the oxidative addition reaction via a concerted pathway. As expected, the calculated barriers with the systems involving sp^2 carbons were lower than those involving sp^3 carbons. In particular, the Gibbs energy values in gas phase increased in the order: vinyl > phenyl > benzyl > methyl. The authors attributed this order in the reactivity to kinetic factors rather than thermodynamic factors. More specifically, they demonstrated that the lowering of the reaction barriers is consequence of the existence of low-lying C–Br π^* orbitals in the transition states structures of the unsaturated systems.

Last but not least, the effect of the donating character of the ligands and the number of them bound to the metal center in the active form of the catalyst, has been one of the factors that have drawn more attention. Usually, in palladium systems, the catalyst is introduced as a precursor, often as $[Pd_2(dba)_3]$ or $[Pd(PPh_3)_4]$;

however, this is clearly not the active form. The bis-ligated form has been postulated in most experimental proposals, and accordingly used in calculations, because of the well established stability of d^{10} $[ML_2]$ complexes, but the mono-ligated form [ML] can be also envisaged (Figure 1.6). In fact, the enhanced reactivity of transition metal complexes containing electron-rich and bulky phosphine ligands has been attributed to the formation of mono-ligated [ML] species, which can undergo oxidative addition more rapidly than the corresponding bis-ligated ones $[ML_2]$.[44,94,95] On this issue, several authors have recently gone even further and have revealed that the rate constants for the oxidative addition depend more on the identity of the halide in the Ar–X reagent rather than on the steric bulk of the phosphine ligands.[96–98] In particular, these authors independently came to the same conclusion that the use of bulky ligands for the oxidative addition of ArCl and ArBr promotes the reaction because such ligands favor the mono-ligated pathway, while ArI species are more susceptible to oxidative addition and therefore, they favor the bis-phosphine pathway.

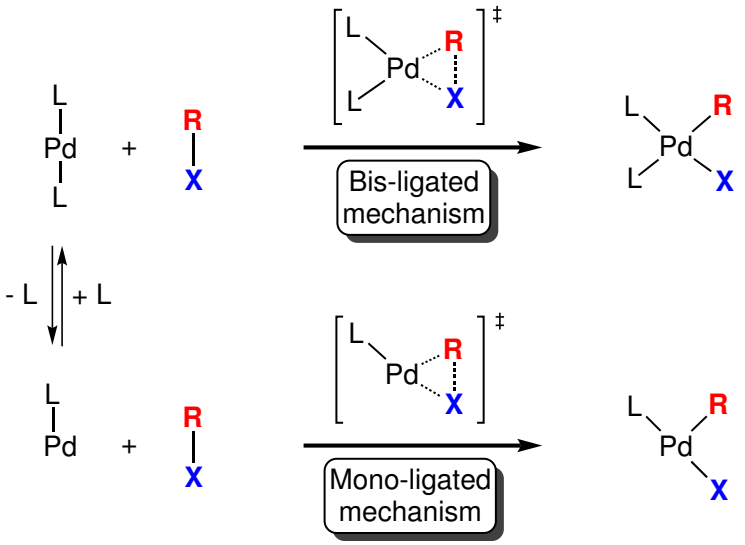

Figure 1.6: Bis-ligated and mono-ligated reaction pathways proposed for the oxidative addition of R–X to $[PdL_2]$ complexes.

Besides the all above mentioned works, there are many other theoretical studies related to the effect of phosphine ligands on cross-coupling reactions, but for the lack of space and time only some of them have been cited herein. Nevertheless, if you have further interest, you can look up our book chapter[99] in which most of the relevant theoretical studies on phosphine effects in the different steps of some Pd-catalyzed cross-coupling reactions are reviewed. This book chapter is included as part of the Appendix B.

1.2.4 Transmetalation

Transmetalation reactions consist in the transfer of an organic group R (e.g. alkyl, aryl, vinyl) from one metal (M^1) to another one (M^2).[100–102] Thus, these reactions entail the cleavage of a M^1–C bond and the concomitant formation of a new M^2–C bond. Regarding the metal centers, these can be both transition metals and main group elements. As a result, depending on the type of the metal atoms involved in transmetalation we can distinguish between three different processes: *i)* organic ligand transfer between two main group elements; *ii)* that between one main group element and one transition metal; and *iii)* transmetalation involving two transition metals.

Compared to other fundamental organometallic reactions involving transition metal complexes (e.g. oxidative addition), transmetalation reactions have been much less studied to the point that have even been considered simply as ligand substitutions. Recently, however, as a consequence of its participation in relevant catalytic processes (e.g. C–C cross-coupling reactions), they have started being more studied and, at present, are recognized as a differentiated process. A prove of its increasingly importance is the number of citations per year in scientific journals for *"transmetalation"* as topic (Figure 1.7).

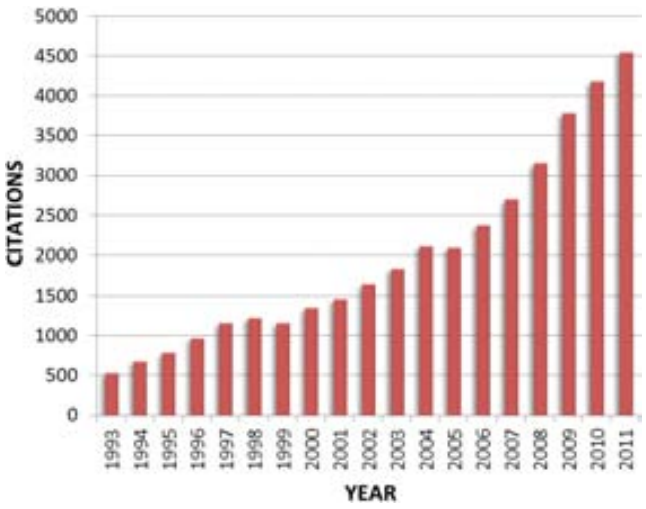

Figure 1.7: Plot of the number of citations per year between 1993 and 2011 for the topic "transmetalation". Data from the *Web of Knowledge* database.

A common classification for transmetalation reactions is the one based on the reaction mechanisms, depicted in Figure 1.8. In the first category of this classification we can find those transmetalations that follow a *redox-type mechanism*, which consists

in the intermolecular transfer of the organic ligand accompanied by the oxidation and reduction of the metal centers involved. The thermodynamics of this type of transmetalation reactions will be governed by the relative stability of the metal-carbon bonds of the started and produced organometallic compounds.

In the second category of that classification we have those transmetalation reactions that evolve through a *metal exchange mechanism* (Figure 1.8). As its name suggests, this mechanism entails the metal-ligand exchange between an organometallic compound M^1–R and a metal complex with a halogen or pseudo-halogen ligand M^2–X (e.g. X = Cl, Br, CN). This type of transmetalation is the most common among the three types of reactions and is characteristic of cross-coupling reactions. On the other hand, the exchange reaction of alkyl or aryl ligands between two organometallic compounds (i.e. X = R') is also included within this category.

Lastly, within the third type of transmetalation reactions we find those that follow a mechanism dubbed as *"ate" complex mechanism* (Figure 1.8). In this mechanism, the transfer of the organic ligand from M^1 to M^2 gives birth to an ion-pair formed between the metal cation and the anionic organometallic complex. This mechanism differs from the metal exchange mechanism in that this one only involves the transfer of the organic group from M^1 to M^2, and not the simultaneous intermolecular transfer of both the organic and the halogen (or pseudo-halogen) ligands between M^1 and M^2.

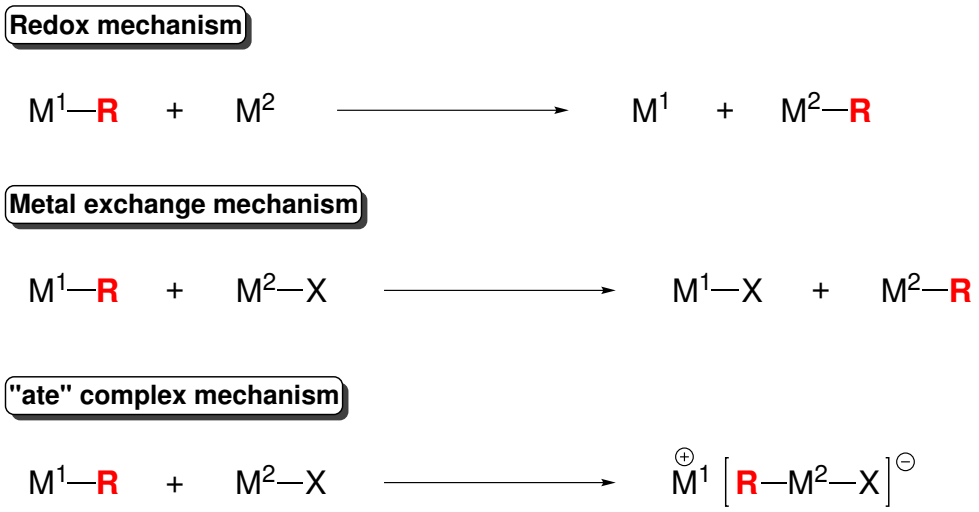

Figure 1.8: Mechanisms proposed for transmetalation reaction.

Given that the carbon-bonded ligand does not easily dissociate, all the above mentioned reaction mechanisms involve transition states (or intermediates) where the organic group acts as a bridging ligand connecting the two metal centers (Figure

1.9). Additionally, in some exchange mechanisms the halide or pseudo-halide can also act as stabilizing bridging ligand in the transition state. In such cases, the transition states are usually called *"cyclic"*, whereas the rest are referred to as *"open"*. On the other hand, the formation of these bimetallic species and its dissociation into two metal complexes via a concerted pathway suggest that transmetalation reactions may be reversible.[†] However, the reversibility or not of these reactions might be dictated by the influence of several factors, such as the reaction rate of the reaction following transmetalation, the nature of the ligands bound to the metal complex, or the nature of the organic group. Thus, the reversibility of these reactions needs to be evaluated for each particular case.

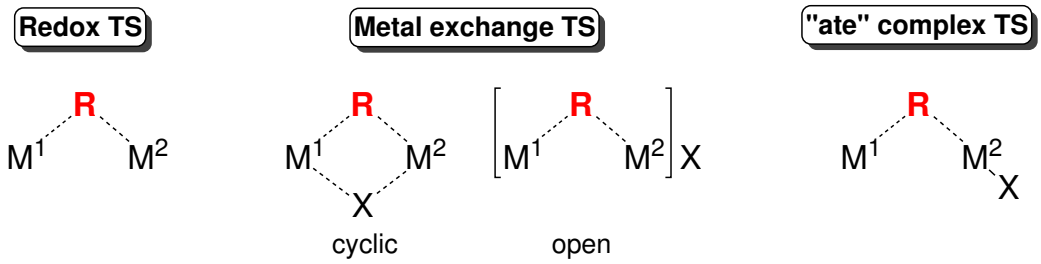

Figure 1.9: Schematic representation of the transition states proposed for the different types of transmetalation reactions.

As far as the applications of transmetalation reactions is concerned, these reactions are very important, on the one hand, because they are employed for the synthesis of new organometallic complexes, and on the other hand, because they are part of catalytic cycles for preparing organic compounds. In particular, within the transmetalation reactions used for the synthesis of organometallic compounds there are included all the reactions in which halides (or pseudo-halides) of transition metals (or main group elements) react with organometallic complexes of main groups elements to yield new organometallic complexes. The most common reagents that act as a alkylating agents of other metals are the Grignard reagents and the organolithiates.[86] Some examples for these reactions are shown in Figure (1.10). Interestingly, unlike most of the Grignard reagents that react through metal-exchange reactions (Eqs. 1 and 2, Figure 1.10), organolithiates are stronger alkylating agents and thus, they often undergo transmetalation via an "ate" complex mechanism (Eq. 3, Figure 1.10).

Among the different roles of transmetalation within catalytic cycles, its role within

[†]The reverse of the transmetalation reaction is commonly known as "retrotransmetalation".[69]

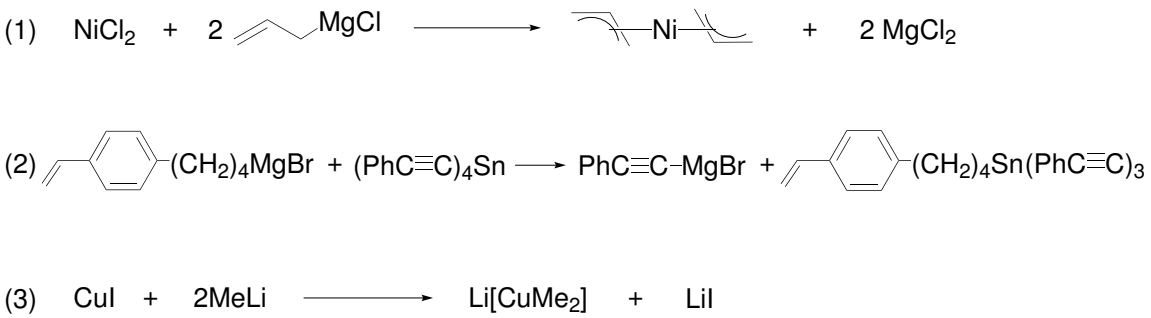

Figure 1.10: Examples of transmetalation reactions used for the synthesis of organometallic compounds that involve Grignard and organolithiate reagents.

cross-coupling reactions is, perhaps, the most relevant one. In fact, the different cross-coupling reactions differ in the organometallic nucleophile used and, accordingly, in the transmetalation step (Scheme 1.3). This step takes place from the oxidative addition product *cis* or *trans*-[M(R^1)(X)$(L)_n$] and results in the formation of the complex [M(R^1)(R^2)$(L)_n$], where the two organic groups can also be in a *cis* or *trans* disposition. Importantly, the subsequent reductive elimination step must occur from the *cis* isomer. Thus, in the cases in which transmetalation leads to the *trans* product, the trans-to-cis isomerization has to take place in order to successfully complete the catalytic cycle. On the other hand, the product of the oxidative addition is commonly assumed to be *trans* because this isomer is more stable than the *cis* one and, further, the cis-to-trans isomerization is usually fast. However, when this is not the case and that isomerization is not fast, both *cis* and *trans* isomers can compete for transmetalation and affect the final outcome of the reaction. Therefore, in such cases, the transmetalation reactions starting from both the *trans* and *cis* isomers have to be considered. An example of this situation was exposed meticulously and with an expert hand in a recent experimental work on the Stille coupling of alkynyl stannane and aryl iodide reported by Espinet et al.[103]

Scheme 1.3: General scheme for the transmetalation reaction in cross-coupling reactions.

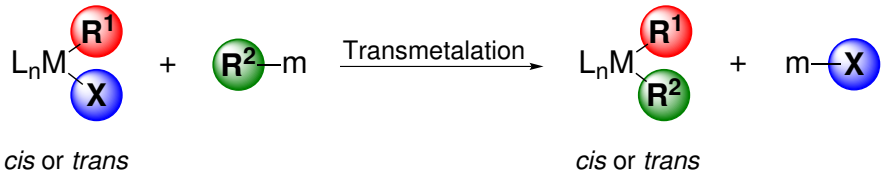

Similarly to oxidative addition, the transmetalation step can be also influenced by

slightly modifications on the reaction conditions (e.g. nature of the R group, metal-bound ligands, solvent). In this case, however, this influence is not so straightforward as in the oxidative addition. This is because, since cross-coupling reactions differ in the transmetalation step, the reaction mechanisms proposed for these processes are more varied and complex. Thus, only the reaction mechanisms proposed for the transmetalation step of the cross-coupling reactions that have been studied in this thesis will be presented. Specifically, they will be presented in the introduction of the chapter of the corresponding cross-coupling reaction.

1.2.5 Reductive elimination

Reductive elimination is the reverse of oxidative addition. Thus, in the overall process, two metal-ligand bonds are broken and one new ligand-ligand bond is formed (Scheme 1.4). This coupling of two covalent ligands can further take place both at a single metal center (Eq. 1, Scheme 1.4) and between two ligands from two different metal centers (Eq. 2, Scheme 1.4). In any case, as expected for the reverse process of the oxidative addition, the oxidation state of the metal is reduced. More specifically, it is reduced by two units in the case of mononuclear metal complexes, and by one in each of the two metal centers in the case of dinuclear metal complexes.

Scheme 1.4: General scheme for the reductive elimination of an A–B molecule from a mononuclear (Eq. 1) and dinuclear (Eq. 2) metal complexes.

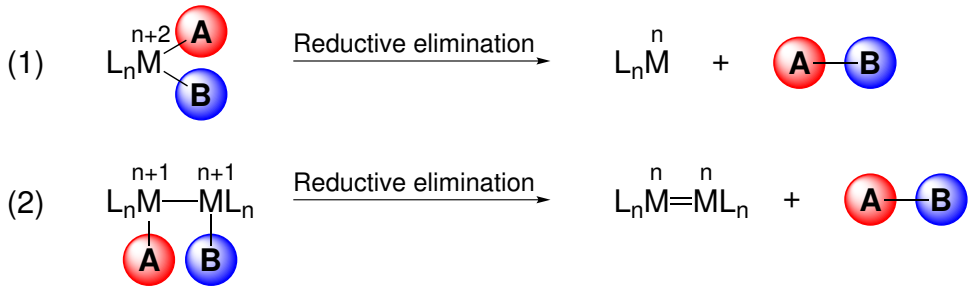

Similarly to oxidative addition, there are many factors that control the rates of reductive elimination reactions. In many cases, some of these factors have the opposite effect on the rate of reductive elimination than in the oxidative addition because these effects originate from thermodynamic factors. Thus, those factors that thermodynamically favor oxidative addition must thermodynamically disfavor the opposite reductive elimination reaction. On this basis, we can consider the following series of trends as a guide for predicting the reactivity of metal complexes towards

reductive elimination:[†]

- *Reductive eliminations in first row metal complexes tend to be more favorable than in second row metal complexes, which tend to be more favorable than in third row metal complexes.*
- *Reductive eliminations in more electron-poor complexes tend to be more favorable than in more electron-rich complexes.*
- *Reductive eliminations in more-hindered complexes tend to be more favorable than in less-hindered complexes.*
- *Reductive eliminations of H ligands are faster than those of R ligands.*

As regards to the reaction mechanisms involved in this type of reactions, the principle of microscopic reversibility[‡] suggests that reductive elimination reactions should show the same variety of mechanisms than oxidative additions (Figure 1.4). Furthermore, it implies that the intermediates and transition states involved in these two reactions should be the same. Hence, reductive eliminations can occur through a concerted mechanism, a S_N2 mechanism, a radical mechanism or an ionic mechanism. All these mechanisms have been previously described in the section devoted to oxidative addition (Figure 1.4); thus, they will be not described again herein.

Concerning the applications of reductive elimination, this reaction is the product-forming step of many catalytic processes.[7] In this thesis, however, since it is focused on the study of Pd-catalyzed cross-coupling reactions, only the role of reductive elimination in these reactions will be discussed. In particular, I will lay stress on some of the most relevant theoretical studies on this step that have been recently reported.

Reductive elimination in Pd-catalyzed cross-coupling reactions

The reductive elimination in cross-coupling reactions is the last step of the catalytic cycle and results in the final C–C coupling and the concomitant regeneration of the catalytic species. The generally accepted mechanism for this process is concerted and features a cyclic three-coordinated transition state (Figure 1.11). Moreover, as reductive elimination is usually irreversible, this step is often taken for granted to be

[†]As in oxidative addition, these trends are only given by way of guidance, because always there may be exceptions.

[‡]This principle holds that a reversible reaction proceeds by the same mechanism in both forward and reverse directions.

critical for the success of the whole reaction because it must pull the catalytic cycle forward.

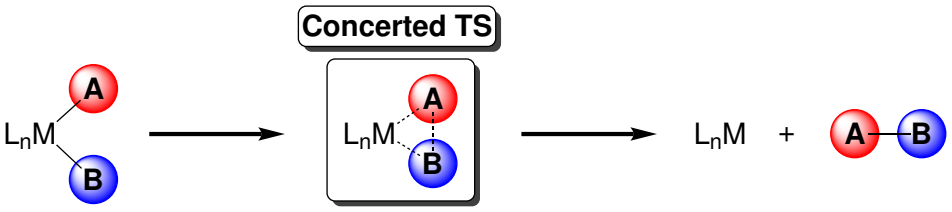

Figure 1.11: Generally accepted mechanism for the reductive elimination step in cross-coupling reactions.

Since the early theoretical works of Tatsumi, Hoffmann, Yamamoto and Stille[104] and Low and Goddard,[105, 106] the reductive elimination step had received scant attention, but in the last decade, extensive studies on C–C reductive elimination have appeared. In particular, most of these theoretical studies are concerning the effect of different factors on this step.

In 2002, Ananikov, Musaev, and Morokuma reported a theoretical study on the effect of different X ligands on the reductive elimination reaction from bis-σ-vinyl complexes [Pd(CH=CH$_2$)$_2$(X)$_2$] (X = Cl, Br, I, NH$_3$, PH$_3$) revealing that the computed activation barriers decrease in the following order: Cl > Br, NH$_3$ > I > PH$_3$.[107] A few years later, the same authors investigated most of the common types of coupling partners in the square-planar *cis*-[Pd(R)(R')(PH$_3$)$_2$] complexes (R or R' = Me, vinyl, Ph, ethynyl) and found that the Gibbs energy barrier for the carbon-carbon coupling from the symmetrical complex [Pd(R)$_2$(PH$_3$)$_2$] increases in the order: vinyl < Ph < ethynyl < Me.[108] Interestingly, the energy barriers and the exothermicities for the asymmetrical coupling from *cis*-[Pd(R)(R')(PH$_3$)$_2$] resulted to be very close to the averages of the corresponding values with the symmetrical R–R and R'–R' coupling reactions from [Pd(R)$_2$(PH$_3$)$_2$] and [Pd(R')$_2$(PH$_3$)$_2$], respectively.

As the other steps in cross-coupling reactions, the rate of the reductive elimination step is also influenced by the steric and electronic effects induced by the ancillary ligands bound to the metal center. Consequently, the influence of the steric and electronic properties of these ligands on this step has been theoretically investigated by several groups. Ananikov, Musaev and Morokuma analyzed by means of the *ONIOM* approach the C–C coupling from the complexes *cis*-[Pd(R)$_2$(L)$_n$] (R = Me, Ph, vinyl, ethynyl; L = PPh$_3$, PCy$_3$, PMe$_3$, and PH$_3$; n = 1, 2).[109] According to the authors, the steric effects mainly influence the energy of the initial complex, whereas the electronic effects have the largest impact on the energy of the transition state. Furthermore, the results revealed that different L ligands may involve differ-

ent mechanisms of the reductive elimination (Figure 1.12). Specifically, the PCy_3 ligand was proposed to promote the mono-ligated reaction pathway resulting in an increase in the reactivity, while the PMe_3 ligand was proposed to stabilize the four-coordinated complexes, thus decreasing the reactivity toward reductive elimination. In the particular case of the PPh_3 ligand, this ligand exhibited good reactivity for both mechanisms; hence, the authors referred to this ligand as a "more universal choice".

The influence of the bite angle in chelating bis-phosphine ligands was investigated by Bo et al. revealing that wide bite angle ligands destabilize the four-coordinated intermediate and stabilize the transition state, which reflects in the acceleration of reductive elimination.[110]

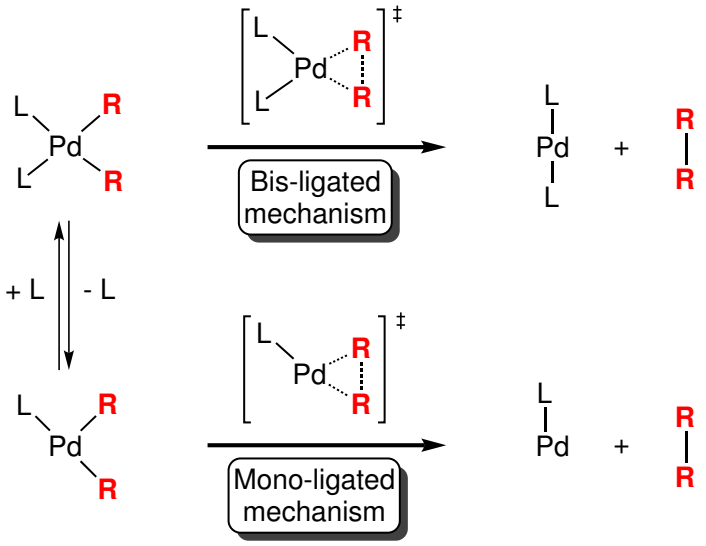

Figure 1.12: Proposed mechanisms for the reductive elimination reaction from a general *cis*-$[Pd(R)_2(L)_2]$ complex.

More recently, the steric and electronic effects of several phosphine ligands (L = PMe_3, PH_3, PCl_3, PPh_3, PPh_2Me, $PPhMe_2$) on the Me–Me coupling through the mono-ligated and bis-ligated reaction pathways was investigated by Ariafard and Yates.[111] On the basis of the reported energy barriers, the electronic properties of the ligand (i.e. L = PMe_3, PH_3, PCl_3) were found to have a significant influence on the energy of the four-coordinated transition state, whereas its effect on the energy of the three-coordinated transition state was much lower. More specifically, for the bis-ligated mechanism, the authors concluded that the greater the electron-donation of L the higher the energy barrier for this process. In contrast, for the mono-ligated

mechanism, the authors proposed the dissociation of the phosphine ligand, which is controlled by the basicity of L, as responsible for the different overall energy barrier; this is, the stronger electron donation leads to a stronger Pd–L bond and, accordingly, to a higher dissociation energy that results in a higher overall barrier.

On the other hand, the energy-decomposition analyses[112,113] of the reaction barriers with the larger ligands (L = PPh_3, PPh_2Me, and $PPhMe_2$) revealed that the electronic effects are similar in all the series and that the lowering of the energy barrier originates from the steric effects that destabilize the complex *cis*-[$Pd(R)_2(L)_2$] but not the transition state. Thus, the sterically larger phosphines tend to reduce the energy required to dissociate one L ligand, which results in the lowering of the coupling barrier via the mono-ligated mechanism. However, these steric effects do not play a role in the reductive elimination from the three-coordinated complex [$Pd(R)_2(L)$]. In fact, the coupling from this complex was found to be almost independent of the bulk of the L. This fact was supported by very small steric repulsions between the L ligand and the Me group calculated in the mono-phosphine species. The reported energy barriers with the larger ligands resulted to increase in the order: $PPh_3 < PPh_2Me < PPhMe_2$ regardless of the mechanism, which agrees with the experimental observations.[114]

At the same time that the publication of the work of Ariafard and Yates,[111] we reported in collaboration with Espinet, Álvarez et al. a combined experimental and theoretical study on the C–C coupling from complexes *cis*-[$Pd(R)_2(PMe_3)(L)$].[56] Specifically, in this study, the mono-phosphine and bis-phosphine pathways (L = "empty" and PMe_3, respectively) with different organic groups (R = Me, Ph, vinyl), as well as the influence on the reaction rate of the addition of several coupling promoters (L = acetonitrile, ethylene, maleic anhydride (MA)), was investigated. As shown in Table 1.1, the trend of computed Gibbs energy barriers at the DFT-B3LYP level with different R groups was Csp^3–Csp^3 > C_{Ar}–C_{Ar} > Csp^2–Csp^2 for any series with an identical ligand, which agrees with the reported sequence for *cis*-[$Pd(R)_2(PH_3)_2$] complexes.[108]

Table 1.1: Gibbs energy barriers (in kcal·mol^{-1}) for the reductive elimination from *cis*-[Pd(R)$_2$(PMe$_3$)(L)] complexes.[56]

R	Ligand L	$\Delta G^{\ddagger}$
Me	MA	8.6
	empty	13.2
	CH_2CH_2	21.7
	MeCN	27.0[a]
	PMe_3	28.6
Ph	MA	2.9
	empty	4.9
	CH_2CH_2	11.3
	MeCN	13.2
	PMe_3	12.8
vinyl	MA	0.6
	empty	4.9
	CH_2CH_2	8.9
	MeCN	11.9
	PMe_3	11.5

[a] For this weak ligand a stepwise mechanism consisting in the MeCN dissociation followed by the coupling from the resulting three-coordinated complex was predicted. This value corresponds to the overall energy barrier for the reductive elimination reaction through this stepwise mechanism.

On the other hand, the addition of a coupling promoter led to the following order in the computed energy barriers: L = MA < "empty" < ethylene < $PMe_3 \approx$ MeCN, pointing out that the energy barrier decreases with the π-acceptor ability of L. Thus, the addition of MA consistently produces a lower coupling barrier because it is a better π-acceptor than ethylene, which in turn is better than PMe_3. Furthermore, the energy barrier with L = MA was found to be lower to the point that the coupling with this ligand from the four-coordinated complex resulted to be easier than from the three-coordinated species (L = empty). On this basis, we concluded that in cases where a low coupling barrier is operating via a three-coordinated intermediate (e.g. with bulky phosphines), the addition of small electron-deficient olefins with

coordinating ability can still help considerably to further accelerate the coupling rate by forming a *cis*-[Pd(R)$_2$(bulky phosphine)(acceptor olefin)] intermediate, from which the coupling takes place with a lower activation energy.

The mono-phosphine and bis-phosphine pathways, as well as the effect of some selected ligands (L = empty, PMe_3, ethylene, maleic anhydride (MA)), was also computationally analyzed very recently by Álvarez, Espinet et al. for the reductive elimination reaction from the palladium complexes *cis*-[Pd(η^1-allyl)$_2$(PMe_3)(L)] and [Pd(η^1-allyl)(η^3-allyl)(L)].[115] Unexpectedly, among all the possible carbon-carbon couplings (Figure 1.13), the C3–C3' bond formation and not the classical C1–C1' was found to be the most favored one in *cis*-[Pd(η^1-allyl)$_2$(PMe_3)(L)] complexes, in coincidence with the results previously reported by Echavarren et al. for *cis*-[Pd(η^1-allyl)$_2$(PH_3)$_2$] complexes.[116] For this favored coupling, the activation energies with the different ligands resulted to increase in the order: empty < MA < CH_2CH_2 < PMe_3.

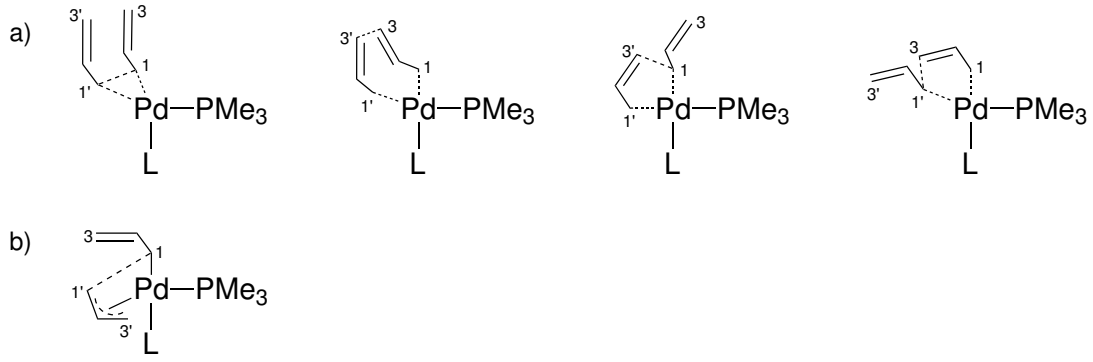

Figure 1.13: Possible C–C couplings in: a) *cis*-[Pd(η^1-allyl)$_2$(PMe_3)(L)] complex; and b) [Pd(η^1-allyl)(η^3-allyl)(L)] complex.[115]

Interestingly, the order in the activation energies of the two most favored C3–C3' allyl couplings (i.e. empty < MA) is reversed with respect to the trend found earlier for the (necessary C1–C1') coupling of alkyl, aryl and alkenyl organic groups.[56] This trend, however, reverts to the usual one (i.e. empty > MA) in the case of the less favored C1–C1' allyl coupling mechanism. Structural analysis on this particular behavior in the allyl-allyl coupling revealed that the C3–C3' coupling from *cis*-[Pd(η^1-allyl)$_2$(PMe_3)] is particularly favored by stereoelectronic effects associated with the small distortion required by the original T-shaped geometry to adopt the transition state geometry while maintaining the stabilizing side-by-side hyper-conjugative dσ-(C1–Pd)$\rightarrow \pi^*$(C2=C3) type interaction.

"We are perhaps not far removed from the time when we shall be able to submit the bulk of chemical phenomena to calculation."

Joseph Louie Gay-Lussac (1888)

2

Computational methods

The aim of this chapter is not just to make a general description of the computational methods used in this thesis (as it is usually the case), but also to try to provide an overview of what quantum mechanics is, and how do we use it to study chemical reactions. In particular, the first part of this chapter will be devoted to make a brief introduction on the origin and some basic concepts of quantum mechanics. In general, this is a part that is usually skipped by the Ph.D. candidates probably because they are not experts on it, or just because collecting the main ideas of quantum mechanics in a reasonable space is too much work. Honestly, I would probably be in the first group. However, when I started "doing bibliography" for this chapter, I found something that changed my mind. Specifically, it was a sentence from one of most brilliant physicists, Richard Feynman, who said: *"I think I can safely say that nobody understands quantum mechanics"*. Obviously, this sentence comforted me and was what prompted me to write and include this first part of the chapter. In any case, I am aware that there may be people that may know much more about quantum mechanics than I do, and that might not agree with some aspects of this first part of the chapter. To those, I sincerely apologize.

In the second part of this chapter, I will explain how we, the computational

chemists, apply quantum mechanics to the study of chemical reactions, which are the approximations that we do, and how do we obtain valuable information by means of applying these approximations.

Finally, in the last part of this chapter, I will briefly describe the methods that I have used during this thesis. This last part is probably the part that involves more mathematical equations, but don't worry about it because I will only include the most important ones. Furthermore, my intention in this last part of the chapter is not to do an exhaustive description of the methods, but to provide a comprehensive view of the original concepts, approximations and ideas that are behind them.

2.1 Quantum mechanics basis

2.1.1 Origin and basic concepts

As we go deeper into the microscopic world, classical mechanics laws start failing and do not provide the good results that they are used to. This impossibility of reproducing some observations by means of classical mechanics is a consequence of the so-called *quantum realm*, which is a term applied in Physics that refers to the scales where quantum mechanical effects become important.[†] This fact, in particular, was what led to the development of quantum mechanics in the first half of 20^{th} century. However, it is important not to forget that, despite the differences between classical and quantum mechanics, they are not independent. In fact, according to the *correspondence principle* between classical and quantum mechanics, all objects obey the laws of quantum mechanics, and classical mechanics is just an approximation for large systems (or a statistical quantum mechanics of a large collection of particles). Thus, classical and quantum mechanics provide the same answer when the systems under study become large. These conditions under which quantum and classical mechanics agree are commonly known as the *correspondence limit* or *classical limit*.

One of the basic concepts derived from quantum mechanics is the *discretization of magnitudes* (e.g. energy), which states that magnitudes can only have discrete values or *quantized* values. Other derived basic concepts are the *wave-particle duality*, which postulates that all particles exhibit both wave and particle properties, and the *uncertainty principle*. This last principle, formulated by Werner Heisenberg in 1927,[117] states a fundamental limit on the accuracy with which certain pairs of physical properties of a particle, such as position and momentum, can be simultaneously known. In other words, the more precisely one property is measured, the less precisely the other can be determined. Thus, quantum mechanics only provides a range of probabilities of where a particle might be given its momentum and momentum probability. This range of probabilities are described by the *wavefunction* (Ψ) and depends on the quantum state at the "instant" of the measurement. Hence, uncertainty is indeed involved in the value. Nevertheless, there are certain states that are associated with a definite value of a particular measured property (i.e. *observable*); these states are the *eigenstates* of the observable. Unfortunately, usually a system is not in an eigenstate of the observable that we are interested in. However, if we measure the observable, the wavefunction will instantaneously be an eigenstate of that observable. This process, known as *wavefunction collapse*, has been a much debated process but due to the lack of space, time, and deeper knowledge, it will not be further discussed in this thesis.

[†]Interestingly, these scales are typically distances of 100 nm or less, which is (and not coincidentally) the same scale as Nanotechnology.

2.1.2 The Schrödinger equation

With a role similar to *Newton's second law* in classical mechanics, the *Schrödinger equation* (Eq. 2.1) in quantum mechanics describes how the wavefunction evolves in time.

$$i\hbar\frac{\partial}{\partial t}\Psi(x,t) = H\Psi(x,t) \tag{2.1}$$

In this last equation, H is the *Hamiltonian*, an operator that generates the time evolution of quantum states and provides the value for the total energy of the system. By analogy with classical mechanics, this operator is generally expressed as the sum of the operators for the kinetic (T) and potential (V) energies:[†]

$$H = T + V \tag{2.2}$$

As with all the operators, there are a series of states that are eigenstates of the Hamiltonian, whose eigenvalues correspond to the energies of those states. In fact, if we assume that the Hamiltonian does not contain time,[‡] the spatial and time dependences of the wavefunction for these states can be treated separately

$$\Psi(x,t) = f(t)\Psi(x) \tag{2.3}$$

Then, if the wavefunction $\Psi(x)$ is an eigenstate of the Hamiltonian, the equation (2.1) can be written as:

$$i\hbar\frac{1}{f(t)}\frac{\partial f(t)}{\partial t} = \frac{1}{\Psi(x)}H\Psi(x) = E \tag{2.4}$$

[†]In this general definition of the Hamiltonian, relativistic effects are neglected. These effects are normally negligible for the first three rows in the periodic table (i.e. $Z < 36$), but become important for the fourth and fifth rows, and for transition metals. Other operators such as the ones describing spin-orbit, orbit-orbit, or spin-spin couplings are also neglected because their contributions are, in most cases, rather small.

[‡]This implies that the total energy of the system remains constant; thus, the system is conservative.

where the constant E that appears in this equation is the total energy of the system in the quantum state described by the wavefunction.

Now, if we isolate the two function parts of equation (2.4) we obtain the following two equations:

$$f(t) = e^{-iEt/\hbar} \tag{2.5}$$

and

$$H\Psi(x) = E\Psi(x) \tag{2.6}$$

This last equation (2.6) is usually called *time-independent Schrödinger* equation to distinguish it from equation (2.1), commonly named *time-dependent Schrödinger* equation. It is interesting to note that equation (2.6) can also be seen as the spatial part of the time-dependent Schrödinger equation (Eq. 2.1), because the time dependency is always an exponential function of the type represented in the equation (2.5).

Hence, the eigenstates of the Hamiltonian are of the type:

$$\Psi(x,t) = e^{-iEt/\hbar}\ \Psi(x) \tag{2.7}$$

Importantly, these eigenstates have the peculiarity that they produce probability distributions that are independent of time and, accordingly, their properties do not depend on it either. For this reason, they are called *stationary states*. Among these stationary states, the one with the lowest energy value is commonly known as the *ground state* and the other ones as *excited states*.

In general, most of the methods used for the study of chemical reactions focus on the resolution of the time-independent Schrödinger equation (Eq. 2.6). Thus, from now on, we will refer to this last equation simply as "*Schrödinger equation*", unless specified otherwise.

2.2 Theory applied to reactivity

After having summarized the origin and some of the basic concepts of quantum mechanics in the previous sections, the next step is to understand how quantum mechanics is applied to the study of chemical reactions.

The application of quantum mechanics to the study of reactivity results in very complex equations, which have led to the appearance of multiple approximations. These approximations allow obtaining approximate values for many properties of molecules. However, their acceptance without having checked their validity can occasionally lead to cases where they are not valid and, consequently, to incorrect results. On the other hand, the no acceptance of approximations, even when they are valid, restricts the study to only very small systems though, in such cases, we have the certainty of obtaining the correct results. Hence, when facing chemical problems, the choice (or not) of these approximations is crucial.

This section, in particular, will be devoted to summarize which are the common approximations that we use when applying quantum mechanics for studying chemical reactions, and how do we obtain valuable information of these reactions by means of these approximations. It should be said, however, that this section does not intend to be exhaustive on the theoretical methods to study reactivity, but just to introduce how do we approach to such analysis.

2.2.1 The Born-Oppenheimer approximation and the concept of electronic structure

The *Born-Oppenheimer* approximation is probably the approximation that has been most successfully applied in Theoretical Chemistry. In general terms, we could say that it allows the decomposition of the Schrödinger equation in two parts: one part that describes the electronic wavefunction for a fixed nuclear geometry, and the other part that describes the nuclear wavefunction, where the energy from the electronic wavefunction plays the role of a potential energy. This is, however, a very generalized description of this approximation, so let us go into a more detailed description of it.

The Born-Oppenheimer approximation is based on the following two assumptions:

- *The wavefunction can be separated by the product of an electronic wavefunction and a nuclear wavefunction:*

$$\Psi_{tot}(R,r) = \Psi_{el}(R,r)\ \Psi_{nuc}(R) \tag{2.8}$$

(R and r denote the nuclear and the electronic coordinates, respectively).

- *The electronic wavefunction depends parametrically*[†] *on the coordinates of the nuclei, but not on their momenta.*

The basis for these two assumptions is the high mass ratio between nuclei and electrons, which reflects in a much faster movement of the electrons compared to the nuclei. In general, we can safely say that this is a very good approximation because for the lightest nuclei, the *proton* or ^1H, that ratio is: $\frac{m_{^1H}}{m_{e^-}} \approx 1836$.

The Born-Oppenheimer approximation consists of two steps that we will discuss below. First, let us start by writing the Schrödinger equation for a given molecule:

$$H_{tot}\Psi_{tot}(R,r) = E_{tot}\Psi_{tot}(R,r) \tag{2.9}$$

The total Hamiltonian, H_{tot}, in equation (2.9) is

$$H_{tot} = T_{tot} + V_{tot} = (T_{el} + T_{nuc}) + (V_{ne} + V_{ee} + V_{nn}) \tag{2.10}$$

where T_{el} and T_{nuc} stand for the kinetic energy of electrons and nuclei, respectively, V_{ne} stands for the coulombic attraction between electrons and nuclei, and V_{ee} and V_{nn} stand for the coulombic repulsion between electrons and between nuclei, respectively.

Now, assuming that nuclei move much more slowly than electrons, and that the latter are moving in the potential of fixed nuclei, it results that the term corresponding to the nuclear kinetic energy can be dropped from equation (2.10) and that the repulsion between the nuclei can be considered to be constant. At this point, we can define the *electronic Hamiltonian* as:

$$H_{el} = T_{el} + (V_{ne} + V_{ee} + \underbrace{V_{nn}}_{ct}) = T_{el} + V \tag{2.11}$$

Then, if we apply this electronic Hamiltonian to the electronic wavefunction, we obtain the electronic state of the molecule by solving the equation

[†]By *parametrically* we mean that for different arrangements of the nuclei, the electronic wavefunction is a different function of the electronic coordinates.

$$(T_{el} + V)\Psi_{el}(R, r) = U_n(R)\Psi_{el}(R, r) \tag{2.12}$$

where U_n is the sum of the electronic energy and the potential energy of the nuclei, for a fixed nuclear coordinates. This dependence of U_n on the nuclear coordinates means that for each nuclear positions, we will have a different electronic wavefunction and a different electronic energetic spectrum. The resolution of this equation (2.12) is the first of the two steps in the Born-Oppenheimer approximation.

Once the electronic Schrödinger equation (2.12) has been solved, the second step is to solve the complete Schrödinger equation. For this step, we just have to apply the complete Hamiltonian (2.10) to the nuclear wavefunction:

$$(T_{nuc} + T_{el} + V)\Psi_{nuc}(R) = E_{tot}\Psi_{nuc}(R) \tag{2.13}$$

Then, as the electrons move much faster than the nuclei, it is a reasonable approximation to replace the electronic Hamiltonian by its average value. This generates a nuclear Hamiltonian for the motion of the nuclei in the average potential of the electrons, which transforms equation (2.13) into

$$(T_{nuc} + U_n(R))\Psi_{nuc}(R) = E_{tot}\Psi_{nuc}(R) \tag{2.14}$$

This potential U_n, also known as *adiabatic potential*, comes from the resolution of the electronic Schrödinger equation (2.12) and, as above mentioned, corresponds to the sum of the electronic energy and the coulombic repulsion between the nuclei, for a fixed nuclear arrangement. This adiabatic potential calculated for a large number of nuclear geometries is known as *potential energy surface* (*PES*).

Overall, in the Born-Oppenheimer approximation, the nuclei move on a potential energy surface obtained by solving the electronic Schrödinger equation. This assumption of the nuclei moving on a potential energy surface was, in particular, what led to the development of methods aimed at solving the electronic Schrödinger equation. These methods are broadly referred to as *electronic structure calculations*, and allow obtaining molecular properties that result very useful in the study of chemical reactions.

2.2.2 The potential energy surface (*PES*)

As previously stated, the potential energy surface (*PES*) is nothing else than the terms U_n that one obtain in the Born-Oppenheimer approximation by solving the electronic Schrödinger equation for a set of fixed nuclear coordinates (Eq. 2.12). Hence, once the electronic Schrödinger equation has been solved for all the possible nuclear configurations, the complete *PES* is known. Unfortunately, the construction of the complete *PES* for molecules containing more than 3-4 atoms is virtually impossible given that it is a $3N$-6 dimension space, where N is the number of atoms.

Hence, a general strategy in computational chemistry consists in restricting the calculations to the chemically interesting part of the *PES*, which usually allows extracting useful information. The most interesting points from the chemical perspective are, in general, the points on the *PES* where the energy is stationary with respect to the nuclear coordinates. Particularly, those that are minima and first-order saddle points (Figure 2.1).

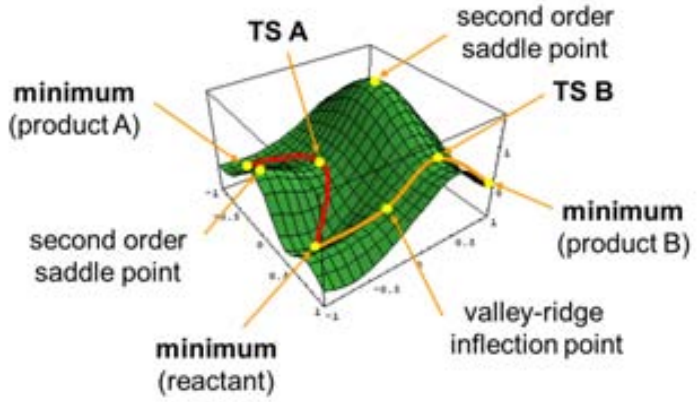

Figure 2.1: Example of a *3D*-representation of an arbitrary *PES*.

The energy minima give us an idea of the expected nuclear configuration of an isomer of a molecule, and are potentially observables as stable products or reaction intermediates. On the other hand, the first-order saddle points (or *transition states, TSs*) are points on the *PES* that are minima in all directions but one, which are maxima. Furthermore, the energy of these transition states provide an estimation of the reaction rate when going from one minimum to another one. Thus, the reaction minima and the transition states that relate these minima, are usually the stationary points on the *PES* that we look for when we are interested in the reaction mechanism and/or the kinetics of a particular reaction. Finding these stationary points, however,

is frequently not trivial[†] and requires the choice of an appropriate methodology, which entails a right balance between accuracy and computational cost. This choice of the methodology includes the selection of the level of theory (e.g. Molecular Mechanics, Quantum Mechanics, *QM/MM*), the method (e.g. Force Field, Hartree-Fock, *DFT*, *MP2*), the basis sets (e.g. double-ζ, pseudo-potentials, polarization functions), the chemical model (i.e. the simplification or not, of parts of the system), and the solvent (e.g. continuum model, explicit solvent molecules).

Once the energy minima and the corresponding transition states have been located, then we obtain a potential energy profile from which we can extract the reaction energy (ΔE) and the energy barrier(s) ($\Delta E^{\ddagger}$). It is important to remark that these potential energies are only valid for one molecule and not for an ensemble of molecules, as it is the case in a real reaction. Thus, if we want to calculate a thermodynamic property and compare its value with the experimental one, we have to use statistical thermodynamics in order to estimate this thermodynamic property for the whole ensemble of molecules. This is a lengthy process and thus, it will not be discussed here. However, if you have further interest in it, there are excellent books on statistical mechanics where you can find a detailed description of it.[118–120]

As we will see in the next chapters, one of the most common thermodynamic properties that we compute for its further comparison with the experimental value is the *Gibbs energy* in solution (G_s).[‡] Generally, this thermodynamic magnitude is estimated by computing the entropic contributions for the solute in gas phase (i.e. in vacuum). This, of course, is a rough approximation, but normally provides good results except for associative and dissociative processes. In these last cases, the results through this approximation are not so good mainly because, in gas phase, the translational and rotational contributions to the entropy are overestimated. This overestimation stems from the fact that, in solution, the molecules are surrounded by the solvent and consequently, they can not freely move and rotate as they do in gas phase. Hence, the computation of dissociative processes in condensed phases, such as the dissociation of one molecule into two fragments, results to be more favorable than what they really are. On the contrary, the computation of associative processes turn out to be less favorable than what they are. On this issue, several approaches have been developed and proposed in the last decades.[121, 122] For example, some authors[123–125] have proposed to only consider the vibrational contribution to the entropy, but if the previous approximation overestimates the entropy, this one under-

[†]Some of us even think that the location of transition states can be considered as an "art".

[‡]When we talk about "experimental Gibbs energies", we should be aware that these are not truly experimental values, since there is no *"Gibbs-meter"* that enables measuring this thermodynamic property. In fact, these experimental Gibbs energies are always based on theoretical models. Thus, even though we use the term "experimental Gibbs energies", they are as theoretical as the ones that we compute.

estimates it. Another approximation is the one proposed by Ziegler et al.[126–128] and based on the *Wertz model*.[129] This approximation, however, requires the knowledge of reference quantities, which sometimes might be not available.† On the other hand, Martin et al.[130] proposed simulating the condensed phase by computing the Gibbs energies in gas phase at high pressure. More specifically, the authors suggested that the computation of the Gibbs energies at the pressure: $p = \rho_W RT$, is a good estimation.‡ This is also a rough approximation because it involves the modification of the standard state (T = 298.15 K, and p = 1 atm) but, somehow, it allows simulating the constraints imposed by the solvent over the free movement of the molecules.

Obviously, apart from all these approximations, there are other methods that, in principle, deliver better Gibbs energy values (e.g. molecular dynamics simulations, Monte-Carlo-based methods). These methods, however, are too computationally demanding and thus, they are normally restricted to small systems.

2.2.3 Approximate resolution of the Schrödinger equation

In the case of one-electron systems, like in the H_2^+ molecule, the electronic Schrödinger equation (2.12) can be solved exactly; however, this is not the case when we are in front of many-electron systems. Typically, we say that this impossibility of solving exactly this equation is because the Schrödinger equation is a *many-body interacting* problem. But, what does it exactly mean? Well, this means that, as a consequence of the electron-electron repulsive interactions, we can not solve the problem of N-interacting electrons as a sum of N one-electron problems. In order to overcome this issue, several methods have been developed, which, by means of different approximations, deal with this electronic problem. These methods aimed at solving the electronic Schrödinger equation can be classified in two well differentiated classes: the methods that are based on the wavefunction, and the methods that are based on the electron density. Among the first class of methods, probably the most important one is the *Hartree-Fock* (*HF*) method, since most of the precise methods are based on corrections to this method. As far as the methods based on the electron density is concerned, these methods have received special attention and are being increasingly used due to the good results that they provide at a reasonable computational cost.

In this thesis, all the calculations have been performed using methods based on the electron density. Thus, the following section will be exclusively devoted to describe these methods, and the approximations that there are behind them.

†This approximation in the case of solvation entropies in water states that they can be approximated in qualitative discussions as 50% of the gas phase entropy, with the opposite sign.

‡In this formula, ρ_W is the experimental density of the solvent, R is the ideal gas constant, and T is the temperature.

2.3 The density functional theory (*DFT*)

In the methods based on the wavefunction, the resolution of the electronic Schrödinger equation implies the computation of the wavefunction for a given nuclear coordinates, which is a function of $3N$ spatial coordinates plus N spin variables, where N is the number of electrons. This, in the systems that we are usually interested in, where there are many atoms and many more electrons, becomes a very complicated problem. But, is there any other formulation that allows simplifying this problem? The answer is *yes*. This alternative formulation is the so-called *Density Functional Theory* (*DFT*) and is based on the calculation of electronic properties from the electron density, instead of from the wavefunction. This formulation has the main advantage that the electron density depends only on the three spatial coordinates (*x, y, z*), which simplifies considerably the problem.

The electron density $\rho(\vec{r})$ is defined as the multiple integral over the spin variables of all the electrons and over all but one of the spatial coordinates,

$$\rho(\vec{r}_1) = N \int \cdots \int |\Psi(\vec{x}_1, \vec{x}_2, ..., \vec{x}_N)|^2 ds_1 d\vec{x}_2 ... d\vec{x}_N \tag{2.15}$$

where

$$d\vec{x}_i = ds_i d\vec{r}_i$$

The electron density represents the probability of finding any of the N electrons within the volume element $d\vec{r}_1$ but with arbitrary spin, while the other N-1 electrons have arbitrary positions and spin in the state represented by Ψ. Thus, strictly speaking $\rho(\vec{r})$ is a probability density although, in practice, it is commonly known simply as electron density. Furthermore, since the electrons are indistinguishable, the probability of finding any electron at that position is just N times the probability for one particular electron. Therefore, we can say that $\rho(\vec{r})$ is a non-negative function of only three spatial coordinates that vanishes at infinity and integrates to the total number of electrons:

$$\rho(\vec{r} \to \infty) = 0, \tag{2.16}$$

$$\int \rho(\vec{r}_1) d\vec{r}_1 = N \tag{2.17}$$

2.3.1 The Hohenberg-Kohn theorems

The density functional theory as we know it today was born in 1964 with the appearance of the seminal paper of Hohenberg and Kohn.[131] In this paper, the authors stated two theorems that now represent the major theoretical bedrock of *DFT*. Quoting directly from the Hohenberg and Kohn's paper, the first theorem states:

"The external potential $V_{ext}(\vec{r})$ is (to within a constant) a unique functional of $\rho(\vec{r})$; since, in turn, $V_{ext}(\vec{r})$ fixes H we see that the full many-particle ground state is a unique functional of $\rho(\vec{r})$".

The authors demonstrated this first theorem by proving by *reductio ad absurdum* that there can not be two different $V_{ext}(\vec{r})$[†] that result in the same ground state electron density; or what is the same, the ground state density uniquely specifies the external potential $V_{ext}(\vec{r})$. A direct consequence derived from this first principle is that all the ground state properties of a system are defined by its electron density. On the other hand, given that the complete ground state energy is a functional[‡] of the ground state electron density so must be its individual components. Thus, the expectation value for the energy of the system can be written as:[§]

$$E[\rho] = T[\rho] + V_{ee}[\rho] + V_{ne}[\rho] \tag{2.18}$$

Now, if we separate the terms that are dependent on the external potential and those which are *universal* or independent on it, we arrive at

$$E[\rho] = \underbrace{T[\rho] + V_{ee}[\rho]}_{independent} + \underbrace{V_{ne}[\rho]}_{dependent} = F_{HK}[\rho] + \int \rho_r V_{ne} d\vec{r} \tag{2.19}$$

where the independent terms have been collected into a new quantity, the *Hohenberg-Kohn functional*, $F_{HK}[\rho]$:

[†]This external potential is the potential that the nuclei exert over the electrons.

[‡]A functional is a prescription for producing a number from a function, which in turn depends on variables. Thus, the wavefunction and the electron density are functions, whereas the energy that depends on the wavefunction or the electron density, is a functional.

[§]In this expression, the Born-Oppenheimer approximation has been adopted.

$$F_{HK}[\rho] = T[\rho] + V_{ee}[\rho] \tag{2.20}$$

According to the equation (2.19), if we know $F_{HK}[\rho]$ then, we can solve the Schrödinger equation exactly. Moreover, it is noteworthy to note that since this is a functional that is completely independent of the system, it applies equally well to the hydrogen atom as to huge molecules such as the *DNA*! Unfortunately, things usually are not as easy as they seem, and this case will not be an exception. Here, the main problem is that the exact form of the functional $F_{HK}[\rho]$ is not known. Hence, the pursuit of the explicit expression for this unknown functional is the major challenge in the *DFT* and, at the same time, represents the weakest point of this theory.

Up to this point, we have seen that the ground state density is, in principle, sufficient to obtain all the properties of interest. However, how can we know that a certain density is indeed the ground state density that we are looking for? Well, here is where the second Hohenberg-Kohn theorem takes part. This second theorem states:

The functional $F_{HK}[\rho]$, which provides the ground state energy of the system, provides the lowest energy if and only if the input density is truly the ground state density.

This statement is nothing else than applying the variational principle established for wavefunctions, to the present case:

$$E_0 \leq E[\tilde{\rho}] = T[\tilde{\rho}] + V_{ee}[\tilde{\rho}] + V_{ne}[\tilde{\rho}] \tag{2.21}$$

In this last equation, the density $\tilde{\rho}(\vec{r})$ represents a trial density that defines a trial external potential, a trial Hamiltonian, and a trial wavefunction, and leads to an energy that is higher than or equal to the exact energy of the system. Thus, in order to obtain the exact energy of the system we will have to find the electron density that minimizes the energy,

$$\left[\frac{\partial E[\rho]}{\partial \rho}\right] = 0 \tag{2.22}$$

Overall, the second Hohenberg-Kohn theorem establishes the variational principle

in the *DFT*. However, we have to be aware of what it implies and do not overinterpret this result. Many conventional methods based on the wavefunction, such as the *HF* method, are strictly variational and, consequently, the expectation value of the energy is an indicator of the quality of the trial wavefunction. This means that the lower the energy the better approximated the trial wavefunction to the ground state wavefunction. However, this is not the case in the "real" *DFT*.[†] The variational principle stated by the second Hohenberg-Kohn theorem applies only for the exact functional, which is not known. Thus, the energy provided by a trial functional has absolutely no meaning in that respect.

2.3.2 The Kohn-Sham method

As above mentioned, the ignorance of the exact expression of the functional $F_{HK}[\rho]$ is undoubtedly the major drawback when trying to solve a system of N electrons by means of the *DFT*. An alternative to overcome this issue is to use an approximate expression for this functional and solve the N-electron problem approximately. In fact, if the approximate functional $F_{HK}[\rho]$ is good enough, we should obtain an energy value close to the exact energy of the system. This aim at obtaining an approximate expression for $F_{HK}[\rho]$ was what led to the formulation of the *Thomas-Fermi* (*TF*) and *Thomas-Fermi-Dirac* (*TFD*) methods.[132–134] These two methods are normally viewed as precursors of modern *DFT*, and further represent the basis of the formulation of the widely known *Kohn-Sham* (*KS*) method.[135] In particular, this last method is considered as the second major paper of the modern *DFT*, and is based on corrections to the *TF* and *TFD* methods. Thus, let us first start by making a brief summary of these two methods before going into the description of the Kohn-Sham method.

In the *TF* and *TFD* methods, the general expression for the energy functional (Eq. 2.18)

$$E[\rho] = T[\rho] + V_{ee}[\rho] + V_{ne}[\rho]$$

is approximated as follows: the first term $T[\rho]$, which corresponds to the kinetic energy of the N-electron system, is substituted by the functional corresponding to a non-interacting and uniform electron gas, $T_{TF}[\rho]$. On the other hand, the term that stands for the electron-electron repulsion, $V_{ee}[\rho]$, is replaced by the classic coulombic

[†]When I say "real" *DFT* I am assuming that the exact expression of the functional $F_{HK}[\rho]$ is not known.

repulsion between two electrons, $J[\rho]$, and the exchange energy, $K[\rho]$.[†] Taking into account all these approximations, the equation for the energy functional $E[\rho]$ in the *TFD* method can be written as:

$$E_{TFD}[\rho] = T_{TF}[\rho] + J[\rho] + K[\rho] + V_{ne}[\rho] \tag{2.23}$$

With the expression for the energy functional already defined, let us see now how do the terms in (2.23) look like. In the *TF* and *TFD* methods, the terms $V_{ne}[\rho]$ and $J[\rho]$ are treated in a completely classical way, so they can be easily obtained from their classical expressions,

$$V_{ne}[\rho] = -\sum_{a}^{M} \int \frac{Z_a \rho(\vec{r})}{|R_a - \vec{r}|} d\vec{r} \tag{2.24}$$

$$J[\rho] = \frac{1}{2} \iint \frac{\rho(\vec{r_1})\rho(\vec{r_2})}{|\vec{r_1} - \vec{r_2}|} d\vec{r_1} d\vec{r_2} \tag{2.25}$$

where the factor of $1/2$ in $J[\rho]$ allows the integration to run over all space for both variables.

As regards to the terms $T_{TF}[\rho]$ and $K[\rho]$, it can be demonstrated that their expressions for a non-interacting uniform gas of electrons are:

$$T_{TF}[\rho] = C_F \int \rho^{5/3}(\vec{r}) d\vec{r} \tag{2.26}$$

$$K[\rho] = -C_x \int \rho^{4/3}(\vec{r}) d\vec{r} \tag{2.27}$$

with

$$C_F = \frac{3}{10}(3\pi^2)^{2/3} = 2.8712 \tag{2.28}$$

$$C_x = \frac{3}{4}\left(\frac{3}{\pi}\right)^{1/3} = 0.7386 \tag{2.29}$$

[†]This exchange energy term is only added in the *TFD* method.

Hence, introducing the expressions for $T_{TF}[\rho]$, $J[\rho]$, $K[\rho]$, and $V_{ne}[\rho]$ into the equation for the energy functional $E[\rho]$ (Eq. 2.23), we obtain that the expression for the energy functional in the *TFD* method is given by:

$$E_{TFD}[\rho] = \underbrace{C_F \int \rho^{5/3}(\vec{r})d\vec{r}}_{T_{TF}[\rho]} + \underbrace{\frac{1}{2}\iint \frac{\rho(\vec{r_1})\rho(\vec{r_2})}{|\vec{r_1}-\vec{r_2}|}d\vec{r_1}d\vec{r_2}}_{J[\rho]} - \underbrace{C_x \int \rho^{4/3}(\vec{r})d\vec{r}}_{K[\rho]} - \underbrace{\sum_a^M \int \frac{Z_a\rho(\vec{r})}{|R_a-\vec{r}|}d\vec{r}}_{V_{ne}[\rho]} \tag{2.30}$$

This expression (2.30) but without the term $K[\rho]$ corresponds to the energy functional in the *TF* method.

To summarize, with the *TF* and *TFD* methods all the terms included in the energy functional (Eq. 2.30) are explicit functionals of the electron density, which simplifies considerably the problem of the N-electron system. However, these two methods fail miserably in many cases, mainly because the approximation that these models do for the kinetic energy term is rather simple. Here was when, in 1965,[135] Kohn and Sham realized that if we are not able to accurately determine the kinetic energy through an explicit functional of the density, we should concentrate on calculating as much as we can the true kinetic energy exactly. Thus, their basic idea was to obtain from a Slater determinant† the exact kinetic energy of a non-interacting reference system with the same density as the real one (i.e. the interacting system),

$$T_S = -\frac{1}{2}\sum_i^N \langle\varphi_i|\nabla^2|\varphi_i\rangle \tag{2.31}$$

Of course, the kinetic energy of this non-interacting system is not equal to the kinetic energy in the real system, even if both systems share the same density. In order to account for this and the other approximations present in the universal functional

†A Slater determinant is an antisymmetrized product of N one-electron wavefunctions (*spin orbitals*). In this determinant, the columns are the one-electron wave functions while the electron coordinates are along the rows.

$F_{HK}[\rho]$ (Eq. 2.20), Kohn and Sham collected all the necessary corrections into a new term E_{XC}, so that the expression for $F_{HK}[\rho]$ becomes

$$F[\rho] = T_S[\rho] + J[\rho] + E_{XC}[\rho] \tag{2.32}$$

This term $E_{XC}[\rho]$ is known as *exchange-correlation energy*, and is defined as:

$$E_{XC}[\rho] \equiv (T[\rho] - T_S[\rho]) + (V_{ee}[\rho] - J[\rho]) \tag{2.33}$$

The two first terms in $E_{XC}[\rho]$ correct the difference between the true and the approximate kinetic energies, while the last two terms correct the difference between the classical electron-electron interaction $J[\rho]$ defined in (2.25) and the real one. Thus, we can say that the exchange-correlation energy $E_{XC}[\rho]$ is the functional that contains everything that is unknown.

Introducing the expression (2.33) into (2.32), we can write down the expression for the energy functional of the real system as:

$$\begin{aligned} E[\rho(\vec{r})] &= T_S[\rho] + J[\rho] + E_{XC}[\rho] + V_{ne}[\rho] \\ &= -\frac{1}{2}\sum_{i}^{N}\langle\varphi_i|\nabla^2|\varphi_i\rangle \quad + \quad \frac{1}{2}\iint\frac{\rho(\vec{r_1})\rho(\vec{r_2})}{|\vec{r_1}-\vec{r_2}|}d\vec{r_1}d\vec{r_2} \quad + \\ &+E_{XC}[\rho] \quad - \quad \sum_{a}^{M}\int\frac{Z_a\rho(\vec{r})}{|R_a-\vec{r}|}d\vec{r} \end{aligned} \tag{2.34}$$

Now, introducing into this last equation the restriction that the electron density resulting from the summation of the moduli of the squared orbitals φ_i exactly equals the ground state density of our real system of interacting electrons,

$$\rho(\vec{r}) = \sum_{i}^{N}\sum_{s}|\varphi_i(\vec{r},s)|^2 = \rho_0(\vec{r}) \tag{2.35}$$

and imposing the constraint that the orbitals φ_i have to be orthonormal,

$$\int \varphi_i(\vec{r})^* \varphi_j(\vec{r}) = \delta_{ij} \tag{2.36}$$

$$\begin{aligned} \delta_{ij} &= 1 \quad i = j \\ \delta_{ij} &= 0 \quad i \neq j \end{aligned}$$

we finally arrive to the Kohn-Sham equations:

$$\underbrace{\left(-\frac{1}{2}\nabla^2 + v_{eff}\right)}_{h_{KS}} \varphi_i = \varepsilon_i \varphi_i \tag{2.37}$$

where h_{KS} is the Kohn-Sham monoelectronic hamiltonian and the term v_{eff} is the *effective potential*, which is defined as:

$$v_{eff}(\vec{r}) = \int \frac{\rho(\vec{r}_2)}{r_{12}} d\vec{r}_2 + V_{XC}(\vec{r}_1) - \sum_a^M \frac{Z_a}{r_{1a}} \tag{2.38}$$

In this last equation, the only term that is unknown is the potential V_{XC} due to the exchange-correlation energy E_{XC}. This potential is simply defined as the functional derivative of E_{XC} with respect to the electron density:

$$V_{XC} \equiv \frac{\partial E_{XC}}{\partial \rho} \tag{2.39}$$

It is very important to realize that if the exact forms of E_{XC} and V_{XC} were known, the Kohn-Sham method would provide the exact energy. Unfortunately, this is not the case. Furthermore, since the effective potential depends on the electron density, the Kohn-Sham equations (2.37) have to be solved in an iterative way. For this process, we define a trial electron density from which we can calculate the effective potential through equation (2.38). Then, with this effective potential we solve the Kohn-Sham equations (2.37) and obtain the orbitals φ_i, which are introduced into

the equation (2.35) resulting in a new electron density. This process is iteratively repeated until the difference between this new electron density and the trial density satisfies the desired convergence criterion. Once this is done, the energy can be easily computed from equation (2.34) using the converged electron density.

Another important point that should be remarked is that unlike the *HF* method, where the approximation is introduced right from the start,[†] the Kohn-Sham method is in principle exact! The approximation in this last method only comes into play when we choose an explicit form of the unknown exchange-correlation functional E_{XC} and the corresponding potential V_{XC}. Therefore, the difference between *DFT* methods stem from the form of these unknown functionals.

2.3.3 Exchange-correlation functionals

The form of exchange-correlation functionals is often designed to have a certain limiting behavior (e.g. including the uniform electron gas limit), and fitting parameters to known accurate data. A common approach in the design of these functionals consists in splitting them into two parts: the exchange part E_X, and the correlation part E_C

$$E_{XC}[\rho] = E_X[\rho] + E_C[\rho] \tag{2.40}$$

These exchange and correlation parts are normally calculated separately by means of different approximations and then, combined into the exchange-correlation functional. Based on these approximations, John P. Perdew presented by analogy with the biblical referent of *Jacob's ladder*,[136] his particular vision of which are the rungs to be climbed in the *DFT* for going from the Earth (i.e. the *HF* world) to Heaven (i.e. the chemical accuracy) (Figure 2.2).

[†]In the *HF* method the wavefunction is assumed to be a single Slater determinant, which therefore, can never provide the true solution.

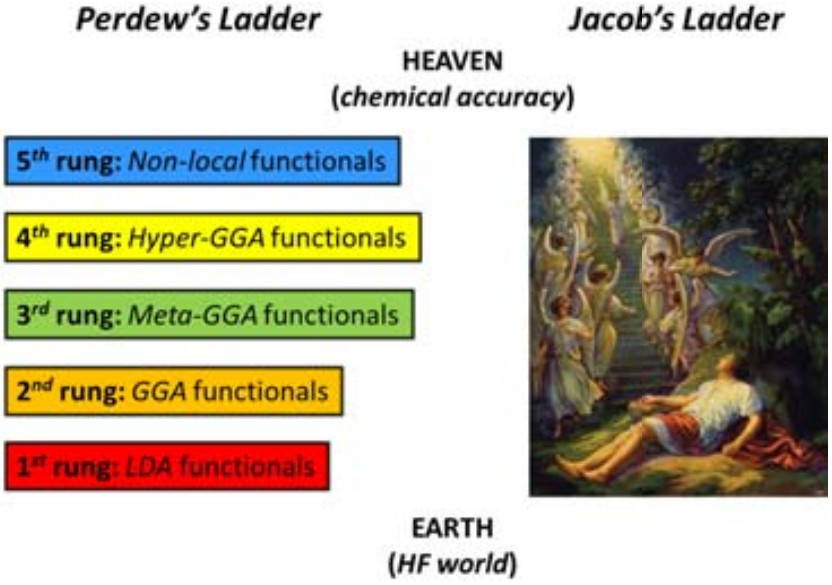

Figure 2.2: Graphical representation of the 'Perdew's functionals ladder' (left) and the Jacob's Ladder (right).

According to Perdew, the main advantage of the *DFT* is that we can go up or down this ladder of functionals depending on our necessities. In principle, going up this ladder involves an improvement of the results but also, an increase in the computational cost. Thus, when choosing an exchange-correlation functional, we should arrive to a good compromise between accuracy and computational cost. It is important, however, to keep in mind that despite of this general classification of functionals, the typical one million dollar question *'which is the best functional?'* does not have a unique answer, and needs to be settled for each particular case by comparing the performance of functionals with experiments or high-level wave mechanics calculations.

In the next pages, I will briefly describe the different types of exchange-correlation functionals that appear in the Perdew's ladder (Figure 2.2), and which are the approximations that are behind them.

Local density and local spin density approximations (LDA/LSDA)

The *local density approximation* (*LDA*) constitutes the simplest way of representing the exchange-correlation functional. In particular, this approximation assumes that the density can be locally treated as a uniform electron gas. The general expression for the functional E_{XC} in the *LDA* is:

$$E_{XC}^{LDA}[\rho] = \int f(\rho) d\vec{r} = E_X^{LDA}[\rho] + E_C^{LDA}[\rho] \tag{2.41}$$

The exchange part in a uniform electron gas is nothing else that the exchange functional that we met in the Thomas-Fermi-Dirac method (Eq. 2.27). Thus, the exchange energy E_X in this *LDA* approximation is also given by:

$$E_X^{LDA}[\rho] = -\frac{3}{4}\left(\frac{3}{\pi}\right)^{1/3} \int \rho^{4/3}(\vec{r}) d\vec{r} \tag{2.42}$$

As far as the correlation part E_C^{LDA} is concerned, no such explicit expression for this term is known. However, there are highly accurate numerical quantum Monte-Carlo simulations of the uniform electron gas[137] from which several authors have derived analytical expressions by means of sophisticated interpolation schemes. One of the most widely used representations for this term is the one developed by Vosko, Wilk, and Nusair (*VWN*).[138]

In the *LDA*, the total density is considered to be the sum of α and β spin densities. This assumption is satisfied in closed-shell systems, but not in open-shell systems. If we extend the *LDA* to the latter case, we arrive to the so-called *local spin density approximation* (*LSDA*). The exchange energy in this *LSDA* is:

$$E_X^{LSDA}[\rho] = -(2)^{1/3} \quad \frac{3}{4}\left(\frac{3}{\pi}\right)^{1/3} \int [\rho_\alpha^{4/3} + \rho_\beta^{4/3}] d\vec{r} \tag{2.43}$$

Despite the simplicity of these *LDA* or *LSDA* approximations, it has been proven that they can deliver results with a similar accuracy than those obtained with the *HF* method. However, we should not get overexcited about these results because a look at energetical properties, such as bond energies, immediately shows that the performance of these approximations is rather poor. Hence, there is still a long way to go in the development of exchange-correlation functionals before the chemical accuracy can be reached. The next step on this way is the introduction of the gradient of the density, which takes us to the next rung of the Perdew's ladder (Figure 2.2): the *generalized gradient approximation* (*GGA*) functionals.

The generalized gradient approximation (GGA)

Probably the most logical and intuitive way of improving the *LDA*-based functionals is to try to account for the non-homogeneity of the true electron density. A first approximation to this aim is to consider that exchange and correlation energies not only depend on the electron density, but also on its derivatives. This, in particular, represents the basis of the *generalized gradient approximation* (*GGA*) functionals.[†] The general expression for the exchange-correlation functional in the *GGA* is:

$$E_{XC}^{GGA}[\rho] = \int f(\rho, \nabla\rho) d\vec{r} = E_X^{GGA}[\rho] + E_C^{GGA}[\rho] \tag{2.44}$$

The exchange part in this approximation can be expressed as

$$E_X^{GGA}[\rho] = E_X^{LDA}[\rho] - \sum_\sigma \int F(s_\sigma) \rho_\sigma^{4/3}(\vec{r}) d\vec{r} \tag{2.45}$$

where F is a function whose argument is the *reduced density gradient* for spin σ,[‡]

$$s_\sigma(\vec{r}) = \frac{|\nabla\rho_\sigma(\vec{r})|}{\rho_\sigma^{4/3}(\vec{r})} \tag{2.46}$$

In general, most of the *GGA* exchange functionals are developed following two main philosophies. The first one, initiated with the formulation of the *GGA* exchange functional *B* (or *B88*) by Becke,[139] is based on fitting empirical parameters usually considering experimental data for a set of atoms or model molecules. Some examples of *GGA* exchange functionals that follow this philosophy are the *PW91*,[140–143] the *OPTX* (*O*),[144,145] and the modified Perdew-Wang (*mPW*) functional.[146] On the other hand, the second philosophy considers that the development of exchange functionals should be based on principles derived from quantum mechanics. Examples of *GGA* exchange functionals following this second philosophy are the *B86* functional from Becke,[147] the *P* functional from Perdew,[148] and the *PBE* functional from Perdew, Burke, and Ernzerhof.[149]

[†]These functionals are sometimes referred to as non-local functionals in order to distinguish them from the *LDA* ones. However, it is more appropriate to consider them as local functionals because they depend only on the density (and derivatives) at a given point, and not on a space volume as the *HF* exchange energy.

[‡]The term s_σ can be understood as a local inhomogeneity parameter.

Regarding the *GGA* correlation functionals, these have an even more complicated analytical form than the exchange functionals. Thus, I will merely enumerate some of the most commonly used correlation functionals. For example, it is worth highlighting the correlation counterpart of the exchange functional *P* from Perdew (*P* or *P86*),[148] the *LYP* functional from Lee, Yang and Parr,[150] and the parameter-free correlation functional *PW91* from Perdew and Wang.[140–143] In principle, all the correlation functionals could be combined with any of the exchange functionals, but in practice, only some combinations are currently in use.

Meta-GGA functionals

According to Perdew's ladder (Figure 2.2), the next rung corresponds to the *meta-GGA* functionals.[151] The difference between this third rung and the previous one (i.e. the *GGA* rung) is that this type of exchange-correlation functionals expands GGA to include further the kinetic energy density τ (i.e. the Laplacian of the occupied orbitals) and/or the Laplacian of the density $\nabla^2\rho(r)$.

$$\tau(\vec{r}) = \frac{1}{2}\sum_{i}^{occupied} |\nabla\varphi_i(\vec{r})|^2 \tag{2.47}$$

Thus, the *meta-GGA* functionals are functionals of the density, the gradient of the density, and the kinetic energy density.

$$E_{XC}^{meta-GGA}[\rho] = \int f(\rho, \nabla\rho, \tau)d\vec{r} \tag{2.48}$$

Some examples of this type of functionals are the exchange-correlation functionals *B98*,[152] *TPSS*,[153] *VSXC*[154] and the correlation functional *KCIS*.[155–158]

The adiabatic connection: hybrid functionals

Keeping up with the quest for a most accurate exchange-correlation functional, another appropriate strategy is to use the exact exchange energy calculated with the *HF* method and the Kohn-Sham orbitals, and rely on approximate functionals only for the part that *HF* misses, i.e. the electron correlation (Eq. 2.49). The exchange-correlation functionals based on this strategy are commonly known as *hybrid functionals*.

$$E_{XC} = E_X^{exact} + E_C^{KS} \tag{2.49}$$

The connection between these two components of the exchange-correlation energy is achieved by means of the so-called *adiabatic connection formula* (*ACF*),

$$E_{XC}[\rho] = \int_0^1 E_{ncl}^{\lambda}[\rho] d\lambda \tag{2.50}$$

where λ is the *coupling strength parameter* (with values between 0 and 1), and E_{ncl} is nothing else than the non-classical contribution to the electron-electron interaction for different values of λ. In particular, at the integration limit $\lambda = 0$, we are dealing with a non-interacting system and accordingly, $E_{ncl}^{\lambda=0}$ is composed of exchange only. Hence, this limiting case (i.e. $\lambda = 0$) simply corresponds to the exact exchange. On the other hand, at $\lambda = 1$, the non-classical contributions are those of the fully interacting system, which contains both exchange and correlation terms. This interacting exchange-correlation is not known and therefore, has to be approximated by any E_{XC} functional.

The simplest approximation to solve the equation (2.50) is to assume that E_{ncl}^{λ} is a linear function in λ, and use the *LDA* exchange-correlation functional for $E_{ncl}^{\lambda=1}$. This approximation leads to the so-called *half-and-half* (*HH*) combination proposed by Becke,[159] in which a 50% of exact exchange and a 50% of *LDA* exchange, is included.

$$E_{XC}^{HH} = \frac{1}{2} E_X^{\lambda=0} + \frac{1}{2} E_X^{\lambda=1} \tag{2.51}$$

One of the most widely used variants of this combination is the *BHandHLYP*,[139,150,159] which has been shown to deliver particularly good results for radical systems.[160–163]

$$E_{XC}^{BHandHLYP} = \frac{1}{2} E_X^{exact} + \frac{1}{2} E_X^{LSDA} + \frac{1}{2} \Delta E_X^{B88} + E_C^{LYP} \tag{2.52}$$

During the same year than the proposal of the *HH* combination and following the same scheme, Becke developed one of the most famous hybrid functionals, i.e. the

Becke 3 parameter functional (*B3*).[164] For this functional, the expression for the exchange-correlation is given by:

$$E_{XC}^{B3} = aE_X^{exact} + (1-a)E_X^{LSDA} + b\Delta E_X^{B88} + E_C^{LSDA} + c\Delta E_C^{PW91} \tag{2.53}$$

where a, b, and c are parameters that weigh the various terms in this *B3* functional. In particular, these three parameters were chosen to optimally reproduce a set of properties such as total energies, atomization and ionization energies, and proton affinities. The resulting values for these parameters are: $a = 0.20$, $b = 0.72$, and $c = 0.81$. Note that in this functional, the parameter a determines the amount of exact exchange (i.e. 20%).

The substitution of the correlation terms in this *B3* functional (Eq. 2.53) by the correlation functional *LYP* was proposed by Stevens et al.,[165] and gave birth to the appearance of the widely known *B3LYP* functional.†

$$E_{XC}^{B3LYP} = aE_X^{exact} + (1-a)E_X^{LSDA} + b\Delta E_X^{B88} + cE_C^{LYP} + (1-c)E_C^{VWN} \tag{2.54}$$

Since its appearance in 1994, the *B3LYP* functional has experienced an unprecedented success to the point that, in the last years, it has been by far the most popular and most widely used functional. This hegemony, however, is presently getting lost mainly because *B3LYP* (as most of the functionals) fails in certain aspects, such as the bad description of non-covalent interactions (e.g. van der Waals interactions) and the underestimation of energy barriers,.[166,167] Thus, new functionals and/or correction terms have been developed to overcome these lacks. Among these new functionals one could highlight the appearance of the *"MXX"* series of functionals of Truhlar et al., which have shown to provide satisfactory results. The first of these series of functionals are the *M05* functionals,[168–170] which consist of two functionals: the *M05*[168] and the *M05-2X*.[169] In particular, the *M05* functional (with 28% of exact exchange) is recommended by the authors for reactivity studies involving metals, while the *M05-2X* functional (with 56% of exact exchange) is recommended for reactivity studies without metals. The second of these series are the *M06* functionals,[170–173] which includes four functionals: the *M06* functional[171] (with 27% of

†In this functional, since the *LYP* functional contains a local part besides of the correction to the gradient, the term E_C^{VWN} is also added in order to subtract this local part. This last term corresponds to the *LSDA*-based correlation functional derived from Vosko, Wilk, and Nusair.[138]

exact exchange), the *M06-2X* functional[171] (with 54% of exact exchange), the *M06-L* functional[172] (without exact exchange), and the *M06-HF* functional[173] (with 100% of exact exchange). At present, the last of theses series of functionals are the *M08* functionals, which includes the *M08-HX* functional (with 52.23% of exact exchange) and the *M08-SO* functional (with 56.79% of exact exchange),[174] and the *M11* functional.[175]

Unlike the *B3LYP* functional, where the non-covalent interactions are not well described, most of Truhlar's *"MXX"* functionals are designed in order to provide a good description of these interactions. This, in particular, is carried out by means of implicit parametrization of these functionals. However, there are other ways of improving the description of non-covalent interactions in *DFT*.[176–179] Among them, probably the most popular and in fashion strategy up-to date is the method of dispersion correction (*DFT-D*), commonly known as *Grimme's dispersion correction*.[176] This correction consists in the addition to the Kohn-Sham energy of a dispersion energy term defined as

$$E_{disp} = -s_6 \sum_{i=1}^{N_{at}-1} \sum_{j=i+1}^{N_{at}} \frac{C_6^{ij}}{R_{ij}^6} f_{dmp}(R_{ij}) \tag{2.55}$$

where N_{at} is the number of atoms in the system, C_6^{ij} denotes the dispersion coefficient for atom pair ij, s_6 is a global scaling factor that only depends on the density functional used, f_{dmp} is a damping function, and R_{ij} is an interatomic distance. Recently, some additional corrections to this dispersion term have been added resulting in a considerably improvement of the performance of these dispersion corrected density functionals.[180–182]

Hyper-GGA functionals

Going another rung up in the Jacob's ladder of functionals (Figure 2.2) we arrive to the level of the *hyper-GGA* functionals. Some books and articles define the *hyper-GGA* functionals as functionals that include exact exchange. This definition, however, is rather incomplete because it does not specify whether a functional that includes part of exact exchange (e.g. hybrid functionals) can be considered as a *hyper-GGA* functional or not. On the other hand, there are many articles and books that consider that the term *hyper-GGA* applies to functionals that include part of exact exchange. Thus, according to this last definition, hybrid functionals can be considered as *hyper-GGA* functionals. Honestly, I have to recognize that even after having surfed the literature looking for the exact meaning of this *hyper-GGA* term, its exact definition

remains still not clear for me. In fact, in my humble opinion, its general definition entails certain ambiguity. In any case, this is just a mere question of nomenclature and has no further relevance, but it is interesting to see how this term can lead to two different concepts.

Importantly, even though the *hyper-GGA* functionals appear as the last rung in the Perdew's ladder (Figure 2.2), there is still another rung before reaching the chemical accuracy. This last level corresponds to fully *non-local functionals*, which includes the exact exchange and refines the correlation part by evaluating part of it exactly. Examples of this last type of functionals are the *generalized random phase approximation* (*RPA*)[183–188] and the *interaction strength interpolation* (*ISI*).[189]

2.3.4 Self-interaction error

Apart from the problem of the ignorance of the exact form of the exchange-correlation functional, there is one more typical problem in the *DFT* methods: the so-called *self-interaction error*. Probably the easiest way of understanding this error is to consider the particular case of a one-electron system and compare the energies obtained with the Kohn-Sham method and the *HF* method, which is free of self-interaction errors. Let us first start by the *HF* method.†

In the *HF* method, the electronic energy of the system is given by:

$$E_{HF} = \sum_{i=1}^{N} \varepsilon_i - \frac{1}{2} \sum_{i=1}^{N} \sum_{j=1}^{N} (J_{ij} - K_{ij}) \tag{2.56}$$

where ε_i is the energy of the electron i, and J and K are the coulombic and exchange integrals, respectively. In a monoelectronic system, since there is no electron-electron repulsion, the terms J and K in (2.56) are equal with opposite sign, which leads to the complete cancellation of the self-interaction of the electron i.

On the other hand, in the Kohn-Sham scheme,

$$E[\rho(\vec{r})] = T_S[\rho] + J[\rho] + E_{XC}[\rho] + V_{ne}[\rho]$$

†For the lack of time and space, the expression for the electronic energy in the *HF* method has not been derived in this thesis. Even so, I will use this expression in order to explain the concept of self-interaction error. Details on the derivation of this equation can be found in many books on general quantum chemistry.[190–192]

the term $J[\rho]$

$$J[\rho] = \frac{1}{2}\iint \frac{\rho(\vec{r_1})\rho(\vec{r_2})}{|\vec{r_1} - \vec{r_2}|} d\vec{r_1} d\vec{r_2}$$

is also different from zero because it contains the spurious interaction of the density with itself, but in this case, does not cancel completely with E_{XC}. This no complete cancellation stems from the approximate expressions we have to do for the unknown term E_{XC}. A solution to this problem is the *self-interaction corrected* (*SIC*) form of approximate functionals suggested by Perdew and Zunger.[193]

2.4 Computation of solvent effects

In general, most of the chemical reactions are carried out in the presence of a solvent, which can, in some cases, be crucial for the final outcome of the reaction (e.g. stabilizing species, acting as a reactant). Thus, when studying chemical reactions, an appropriate description of solvent effects is highly recommended. But, how do we introduce solvent effects into calculations? One alternative for evaluating solvent effects is to consider individual solvent molecules explicitly. This alternative, however, involves dealing with a higher number of molecules, which increases the number of degrees of freedom and therefore, the computational cost. Furthermore, other problems that can arise related to this alternative are, for example, which is the number of molecules that should be included, and where should they be placed.† Hence, this alternative is normally used only in specific cases where the solvent actively participates in the reaction, and provided they were not too computationally demanding.

A more affordable alternative is to treat the solvent as a continuous medium with the commonly named *continuum methods*. Among this type of methods, probably the most widely used is the *Self-Consistent Reaction Field* (*SCRF*),[194] which considers the solvent as a uniform polarizable medium with a dielectric constant ε, and with the solute placed in a suitable shaped hole in the medium. In this method, the electric charge distribution of the solute polarizes the medium, which in turn acts back on the solute, thereby producing an electrostatic stabilization. This process is iteratively repeated until the mutual polarization between the solute and solvent achieves the self-consistency.‡

†To overcome this issue one should use methods such as molecular dynamics or Monte-Carlo-based methods.

‡This is the reason for the name of this method.

The solvation *"free"* energy[†] in the *SCRF* method can be calculated as a sum of different energy contributions:

$$\Delta G_{solvation} = \Delta G_{cav} + \Delta G_{disp} + \Delta G_{rep} + \Delta G_{elec} \tag{2.57}$$

In this expression, the ΔG_{cav} term corresponds to the energetic cost that is needed to create the cavity for the solute and thus, this term is always positive. On the other hand, the ΔG_{disp} term is associated with the dispersive interactions between solute and solvent, and contributes positively to the solvation. In contrast, the ΔG_{rep} term is associated with the repulsive interactions between solute and solvent, and is always positive. Finally, the term ΔG_{elec} is an stabilizing term that accounts for the electrostatic interactions between the solute and solvent.

Within the *SCRF* method, we can distinguish between different models depending on several features:

- How the size and shape of the cavity is defined.
- How the dispersion contributions are calculated.
- How the charge distribution of the solute is represented.
- How the solute is described (i.e. classically or quantally).
- How the dielectric constant is described.

In this thesis, the models that have been used for all the calculations are the widely known *polarizable continuum model* (*PCM*),[195] and the recently developed *SMD* model.[196] These two models define the cavity for the solute as the union of a series of interlocking spheres centered on the atoms and differ only in that the latter includes the radii and non-electrostatic terms as suggested by Truhlar and coworkers. Other variants of the *PCM* model are, for example, the *Isoelectronic-PCM* (*IPCM*), which uses a static isodensity surface for the cavity, and its improved version *self-consistent isodensity-PCM* (*SCI-PCM*).[197]

In all *PCM* methods, the radii of the spheres used to create the cavity can be further defined in different ways, but in the course of this thesis only the two most common radii have been employed: the *UA0* and *UFF*. These two radii use the united atom topological model applied on atomic radii of the *UFF* force field for

[†]Even though it is generally considered as a Gibbs energy, it is really not, because entropic terms are not included.

heavy atoms and only differ in how the spheres for hydrogen atoms are described. More specifically, in the *UA0* radii the hydrogen atoms are enclosed in the sphere of the heavy atom to which they are bonded, while in the *UFF* radii they have individual spheres.

In a compromise between good description of solvent effects and computational cost, combinations of discrete (i.e. with explicit solvent molecules) and continuum methods are a good alternative. An example of combination of these methods is to consider explicitly the first solvation sphere, and treat the rest with a continuous method. This combination is commonly referred to as *discrete-continuum* methods and has been used in some parts of the present thesis.

"All successful people men and women are big dreamers. They imagine what their future could be, ideal in every respect, and then they work every day toward their distant vision, that goal or purpose."

Brian Tracy

3 Objectives

The main objective of this thesis is to apply computational methods to the study of Pd-catalyzed cross-coupling reactions with the aim of determining and/or better understanding their reaction mechanisms. In particular, three different Pd-catalyzed cross-coupling reactions have been investigated in this thesis. A brief summary of the reasons that prompted us to study these reactions and the particular objectives established for each these studies are summarized next.

The Negishi reaction

Despite the numerous applications of Pd-catalyzed Negishi reactions in many useful synthetic processes, such as the synthesis of fine chemicals, pharmaceuticals or natural products, the understanding of the details of its reaction mechanism is rather scarce. Thus, we decided to investigate computationally the reaction mechanism for the transmetalation process between the complex *trans*-$[Pd(Me)(Cl)(PMePh_2)_2]$ and the organozinc reagents ZnMeCl and $ZnMe_2$. This study was carried out in close collaboration with the experimental group of Prof. Pablo Espinet and Prof. Juan Casares. The main objectives of this study are:

- Determining and evaluating the mechanisms that give rise to *trans*- and *cis*-$[Pd(Me)_2(PMePh_2)_2]$ the transmetalation products.
- Comparing the reaction mechanisms for the transmetalation processes with the $ZnMe_2$ and ZnMeCl reagents.
- Investigating the effect of the additional ligands (e.g. phosphine) in the transmetalation reaction mechanism with $ZnMe_2$.
- Providing a plausible explanation for the experimental observation of the cationic complex $[Pd(Me)(PMePh_2)_3]^+$ in the transmetalation reaction with $ZnMe_2$.
- Compare our theoretical results with the experimental results provided by the experimental group.

The Cu-free Sonogashira reaction

Over the last years, two reaction mechanisms proposed for the copper-free Sonogashira reaction have been somewhat discussed in the literature. Recently, the experimental group of Mårtensson demonstrated that one of them can be discarded,

and further proposed two alternatives for the other mechanism on the basis of the electronic nature of the alkyne's substituents. Hence, in order to shed light on the reaction mechanism for this process, we decided to carry out a theoretical study in close contact with the experimental group of Prof. Carmen Nájera with the following main objectives:

- Evaluating all the mechanistic pathways proposed in the literature for the copper-free Sonogashira reaction.
- Exploring new alternatives for the reaction mechanisms.
- Analyzing the effect on the reaction rate of the electronic nature of different 4-substituted phenylacetylenes (R = H, CF_3, OMe, NMe_2).
- Comparing our theoretical results with the experiments and putting them into context with the ones reported by the group of Mårtensson.

An asymmetric Suzuki-Miyaura reaction

Recently, the experimental research group of Prof. Rosario Fernández and Prof. José M. Lassaletta reported an asymmetric version of the Suzuki-Miyaura coupling. In particular, the use of (*S,S*)-2,5-diphenyl-pyrrolidine-derived glyoxal bis-hydrazone ligand in conjunction with Cs_2CO_3 as base and toluene as solvent, allowed the asymmetric Suzuki-Miyaura coupling of a broad variety of substrates in high yields and enantioselectivities. In order to get a deeper understanding of this reaction, we decided to carry out a theoretical study in collaboration with the group of professors Fernández and Lassaletta with the following main objectives:

- Characterizing the intermediates and transition states involved in the full catalytic cycle for this asymmetric Suzuki-Miyaura coupling.
- Rationalizing where the stereochemistry of the final product is defined.
- Determining which are the factors responsible for the high enantioselectivities observed.

"Every science begins as philosophy and ends as art"

Will Durant, The Story of Philosophy, 1926

4

The Negishi reaction mechanism

The results presented in this chapter have been published in the following two articles:

Article I: Fuentes, B.; **García-Melchor, M.**; Lledós, A.; Maseras, F.; Casares, J. A.; Ujaque, G.; Espinet, P. *Chem. Eur. J.* **2010**, *16*, 8596-8599.

Article II: **García-Melchor, M.**; Fuentes, B.; Lledós, A.; Casares, J. A.; Ujaque, G.; Espinet, P. *J. Am. Chem. Soc.* **2011**, *133*, 13519-13526.

4.1 Introduction

The Negishi reaction is a C–C cross-coupling reaction that involves the coupling between an organic halide (or triflate) R^1–X and an organozinc compound (Scheme 4.1).[7,13] This reaction was first reported by Prof. Negishi in 1977 showing that the reaction of aryl- and benzylzinc derivatives with aryl halides in the presence of a catalytic amount of a Ni or Pd catalyst provided a general and highly chemo- and regioselective route to unsymmetrical biaryls and diarylmethanes.[25] Thus, as most of the C–C cross-coupling reactions, the Negishi reaction is catalyzed by Ni or Pd catalysts, though the latter have been much more developed.[17]

Scheme 4.1: General scheme for Negishi cross-coupling reaction.

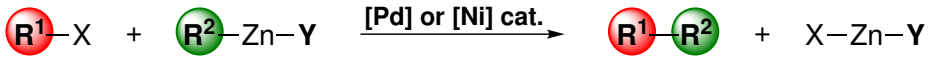

R^1 = aryl, alkynyl, alkyl, vinyl
R^2 = aryl, benzyl, vinyl
Y = X or R^2
X = I, Br, Cl, OTf

Most of the advantages and disadvantages of the Negishi reaction compared to other C–C cross-coupling reactions lie on the intrinsic properties of organozinc compounds. These nucleophiles, unlike other organometallic reagents such as organolithium and organomagnesium compounds, have a carbon-metal bond with a high covalent character, which makes them less reactive and, consequently, more tolerant of functional groups. Moreover, organozinc reagents have the ability of providing fast transmetalation reactions with transition metal salts, specially with those of Pd.[198,199] Therefore, despite of their moderate reactivity toward most of the organic electrophiles, organozinc compounds are one of the most reactive nucleophilic agents employed in Pd-catalyzed cross-coupling reactions.

Other of the main advantages of the Negishi reaction, and related to the above mentioned wide tolerance of functional groups at the organozinc reagents, is that it can be applied to every possible combination of carbon types (i.e. sp, sp^2, or sp^3). These two specific features, in particular, are responsible for the numerous applications of this reaction in many useful synthetic processes, such as the synthesis of fine chemicals, pharmaceuticals or natural products.[28,200–203] Furthermore, the Negishi reaction has the peculiarity that it can be carried out using two types of organometallic reagents, ZnR_2 or ZnRX. The choice of one or the other usually depends on the

more readily accessibility of the two nucleophiles, though, as we will see in the next sections, the different nucleophilic character of these nucleophiles can be also considered in order to influence the reaction outcome.

As in all cross-coupling reactions, the Negishi reaction mechanism consists in three steps (Figure 4.1): oxidative addition, transmetalation, and reductive elimination. The former and the latter are common to all the other cross-coupling reactions, whereas the transmetalation step is particular of this reaction. Unfortunately, very little is known about this transmetalation compared to the ones in the Stille[22,58,63,68,204,205] or Suzuki reactions,[60,66,67,206] in spite of the fact that the transmetalation between organozinc and palladium complexes is also involved in other relevant processes, such as the hydroalkylation of styrenes,[207] the asymmetric allylation of aryl aldehydes,[208] the coupling propargylic benzoates and aldehydes,[102] or the double-transmetalation oxidative cross-coupling reaction.[209,210]

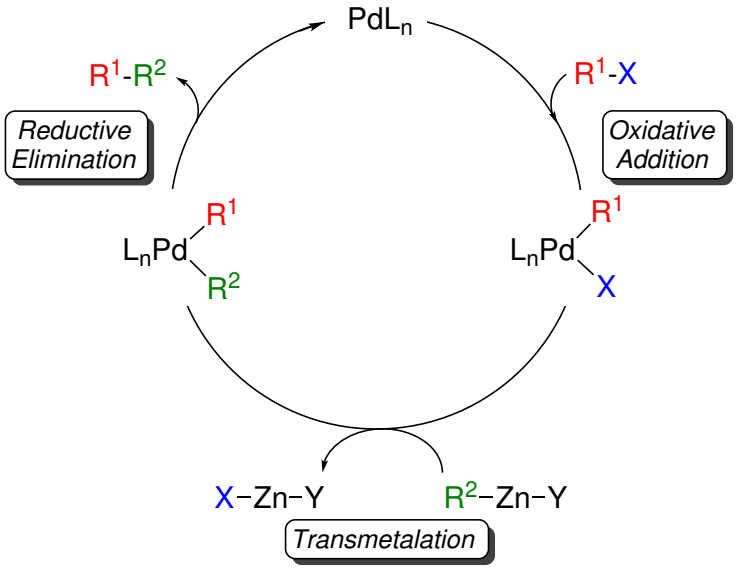

Figure 4.1: General reaction mechanism for the Pd-catalyzed Negishi reaction.

The first experimental observations on the transmetalation step in the Negishi coupling were recently reported by Espinet et al.[62] for the transmetalation reaction between *trans*-[Pd(Rf)(Cl)(PPh_3)$_2$] (Rf = 3,5-dichloro-2,4,6-trifluorophenyl) and the organozinc reagents $ZnMe_2$ and ZnMeCl, in *THF*. Interestingly, this study revealed that each organozinc reagent affords a different isomer (*trans* or *cis*, respectively) of the coupling intermediate [Pd(Rf)(Me)(PPh_3)$_2$], and warned on the existence of

secondary undesired transmetalations[†] (i.e. methyl by aryl exchanges, Figure 4.2) that could eventually lead to homocoupling products. This last phenomenon had been previously observed by Elsevier et al.[211] and, after the work of Espinet et al.,[62] was also noted by Lei et al. on related reactions with aryl derivatives.[61] In particular, in this last study, the competition between a second transmetalation reaction between [Pd(Ar^1)(Ar^2)(dppf)] (dppf = 1,1'-bis(diphenylphosphino)ferrocene) and Ar^2ZnCl yielding [Pd(Ar^2)(Ar^2)(dppf)] and Ar^1ZnCl, and the reductive elimination reaction providing the coupling product Ar^1–Ar^2, was identified as responsible for the experimental observation of a mixture of heterocoupling product (Ar^1–Ar^2), homocoupling product (Ar^2–Ar^2) and dehalogenated product (Ar^1–H) (the last two in equal amounts). The theoretical calculations on a model system reported therein shed light on this issue revealing that an ortho substituent in Ar^1I favors the second transmetalation reaction, while an ortho substituent in Ar^2ZnCl significantly disfavors this second transmetalation.

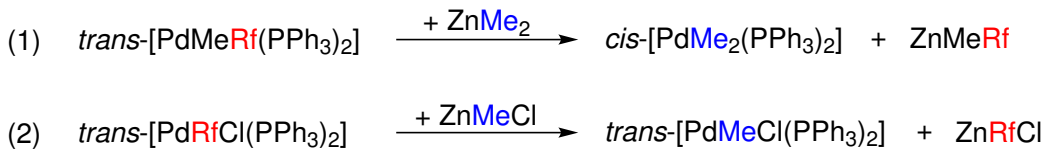

Figure 4.2: Undesired transmetalation reactions in the Pd-catalyzed Negishi reaction between *trans*-[Pd(Rf)(Cl)(PPh_3)$_2$] and $ZnMe_2$ or ZnMeCl.[62]

It is worth mentioning that, besides the studies of Espinet et al.[62] and Lei et al.[61] above mentioned, the number of mechanistic studies reported to date concerning the Negishi reaction are more than scarce.[‡] In fact, to our knowledge, there are only the ones from Organ et al.[212] and Mézailles et al.[213] The former, published the same year than Lei et al.'s paper,[61] involved the theoretical investigation of the full catalytic cycle for the Negishi Csp^3–Csp^3 coupling between EtBr and EtZnBr catalyzed by mono-ligated *NHC*–Pd complexes. Therein, the authors concluded that the use of *NHC* ligands introduce important differences into the traditionally accepted mechanism. For example, the transmetalation and not the oxidative addition, which is considered to be slow in comparison with that for aryl halides, is the rate-limiting step within the whole catalytic cycle. Moreover, the resulting inorganic salt $ZnBr_2$ from the transmetalation reaction not only does not dissociate prior to reductive elimination, but also helps to release the coupling product.

[†]By "undesired transmetalations" we mean transmetalations other than the one desired to produce the heterocoupling product.

[‡]Actually, when we started our studies on the Negishi reaction mechanism, no related studies were reported yet.

On the other hand, in the work of Mézailles et al.[213] the Negishi reaction between bromoarenes and arylzinc derivatives catalyzed by an air-stable Pd(II) complex bearing a bulky electron-withdrawing phosphine ligand was investigated both experimentally and theoretically. The *DFT* calculations on this catalytic system showed that the three elementary steps (i.e. oxidative addition, transmetalation and reductive elimination) possessed low to very low energy barriers, which agreed with the high reaction rates observed experimentally. Thus, the authors brought up the idea of replacing the bulky electron-rich phosphines, extensively used at present in cross-coupling processes, by electron-poor phosphines.

4.2 The transmetalation step in the Negishi coupling of *trans*-[PdMeCl(PMePh$_2$)$_2$] with ZnMeCl

As a result of the scant information available concerning the Negishi reaction mechanism and prompted by the undesired (and unexpected) transmetalations reported by Espinet et al.[62] (Figure 4.2), we decided to investigate computationally the reaction mechanism for the transmetalation process between the complex *trans*-[Pd(Me)(Cl)(PMePh$_2$)$_2$] (**1**) and ZnMeCl (Scheme 4.2). We chose **1** in particular because it is analogous to the complex that was supposed to be generated by a Rf-for-Me substitution in the reaction reported by Espinet et al.[62] between the starting complex *trans*-[Pd(Rf)(Cl)(PPh$_3$)$_2$] and ZnMeCl (Eq. 2, Figure 4.2).[62] Hence, the purpose of our study was to cast light on how complex **1** undergoes transmetalation with ZnMeCl, and which is the stereoselectivity of the final dimethylated product obtained in this process (Scheme 4.2).

Scheme 4.2: Transmetalation reaction between *trans*-[Pd(Me)(Cl)(PMePh$_2$)$_2$] (**1**) and ZnMeCl.

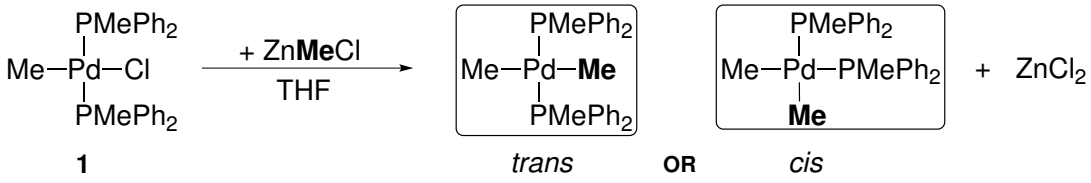

This mechanistic study was carried out in collaboration with the experimental group of Prof. Espinet and Prof. Casares at the University of Valladolid. Importantly, this study represented the first experimental determination of thermodynamic parameters of a Negishi transmetalation reaction. Furthermore, these results were

complemented with *DFT* calculations that provided a detailed picture of the reaction pathway and whose calculated energy barriers resulted to be in good agreement with the experimental parameters. In the next subsections, a summary of these experimental results followed by the theoretical results obtained in this work will be presented.

4.2.1 Experimental data

As mentioned, all the experiments in this study were performed in the research group of Prof. Espinet and Prof. Casares at the University of Valladolid. The reactions between **1** and ZnMeCl (Scheme 4.2) were carried out (with one exception) in 1:20 ratio, simulating catalytic conditions with 5% of Pd in *THF*, and at different temperatures.

Interestingly, experiments revealed significant differences between the transmetalation reactions carried out at different temperatures. Thus, when the transmetalation reaction was carried out at room temperature, the only product that could be observed (in equilibrium with the starting complex **1**) was the complex *cis*-[$Pd(Me)_2(PMePh_2)_2$] (**2**), which slowly underwent reductive elimination to give ethane. In contrast, when the same reaction was monitored by ^{31}P NMR spectroscopy at 223 K (Figure 4.3 a), the coupling rate to yield ethane became negligible and the formation of *trans*-$Pd(Me)_2(PMePh_2)_2$] (**3**) as well as *cis*-[$Pd(Me)_2(PMePh_2)_2$] (**2**) was observed. Furthermore, at this temperature, the *trans* product **3** seemed to be formed first and then fade out in favor of **2**. Hence, in order to get deeper insight into this exciting finding, the same reaction but now at 203 K and in 1:1 ratio to get a slower rate of transformation, was also carried out (Figure 4.3 b). In effect, the transmetalation reaction monitored by ^{31}P NMR in these conditions confirmed that **3** is formed noticeably faster than **2**, which allowed us to conclude that the only observation of the *cis* product **2** at room temperature is deceptive for the stereoselectivity of the transmetalation.

The behavior of **3** found in these experiments resembles to the one of a kinetic product of considerably lower stability than the thermodynamic product (**2**). That is, it disappears from observation as the reaction evolves and gets closer to the equilibrium concentrations, where the concentration of **3** is very small. Indeed, this can be observed from the concentration versus time data obtained by monitoring the reaction at 223 K (Figure 4.3 a): the concentration of **2** increases continuously, whereas a small accumulation of **3** is initially produced followed by a decrease in its concentration, so that after 300 minutes it has practically disappeared.[†]

[†]After about 10 h at this temperature, the system has reached equilibrium between the starting material **1** and the final thermodynamic product **2** ([**1**] = 5.8 x 10^{-3} M, [**2**] = 4.4 x 10^{-3} M, and K_{eq} = 2.0 x 10^{-2}). The concentration of **3** is not given because it is below the limit of NMR observation.

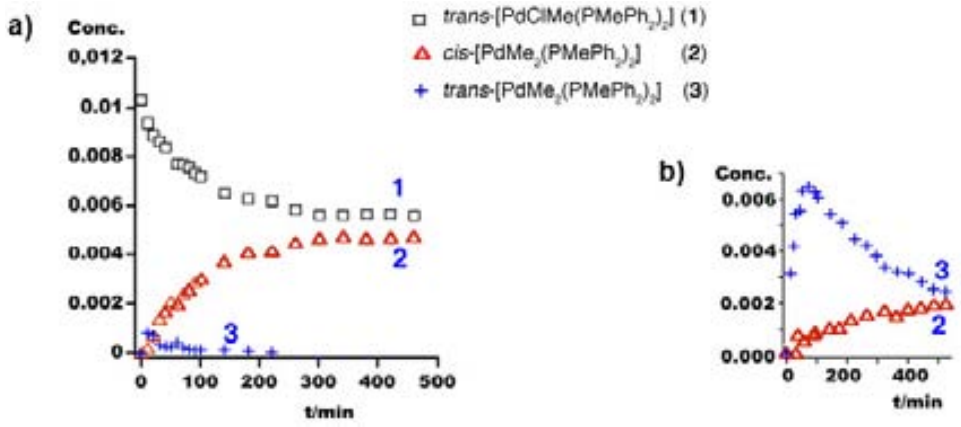

Figure 4.3: Concentration versus time data obtained by ^{31}P NMR spectroscopy for the reaction of **1** with ZnMeCl in different conditions: a) ratio 1:20, in *THF* at T = 223 K. Starting conditions: $[\mathbf{1}]_0 = 0.01$ M; $[\text{ZnMeCl}]_0 = 0.20$ M; b) ratio 1:1, in *THF* at T = 203 K (in this case **1** is not plotted because its abundance is above the values represented in the ordinate axis). Starting conditions: $[\mathbf{1}]_0 = 0.056$ M; $[\text{ZnMeCl}]_0 = 0.056$ M.

Another surprising finding was the fact that despite the transient existence of **3** in the transmetalation reactions, this species prepared by an alternative method was found to be fairly stable. In particular, it took 10 h in *THF* at 273 K for about half of it to isomerize to **2**, whereas at 223 K the **3** to **2** isomerization rate was negligible. On the other hand, the addition of $ZnCl_2$ to a solution of **3** in *THF* at 223 K, produced the instantaneous and complete transformation of **3** to **1**. In the same conditions (i.e. addition of $ZnCl_2$), compound **2** was also transformed into **1** until equilibrium was reached. In other words, the transmetalations between **1** and ZnMeCl to give **2** or **3** are quickly reversible. Hence, these experiments demonstrated that the fast **3** to **2** isomerization observed in Figure 4.3 is not a direct isomerization, which is slow, but a retrotransmetalation of **3** to **1** followed by transmetalation to **2**.

Finally, the concentration versus time data for the reaction monitored at 223 K (Figure 4.3 a) were fitted to the kinetic model shown in Figure 4.4, thereby allowing the calculation of the transmetalation and retrotransmetalation rates at this temperature.[†] Then, from these rates, the relative Gibbs energies at that temperature (ΔG_{223K}) for **1**, **2**, **3** and for the transition states that connect these species ($\mathbf{TS_{1-2}}$ and $\mathbf{TS_{1-3}}$) were obtained (Figure 4.4). The calculated Gibbs energies indicate that the transmetalation from **1** to **3** requires 1 kcal·mol^{-1} less than the transmetalation from **1** to **2**. This, in terms of reaction rates, means that the transmetalation from **1** to **3** (at 223 K) is about 10 times faster than that to **2**. Furthermore, the values

[†]This fitting was also performed by the group of Prof. Espinet and Prof. Casares using the multivariable adjust program *Gepasi*.[214]

indicate that the retrotransmetalations from **3** or **2** to **1** are still faster than their respective transmetalations.

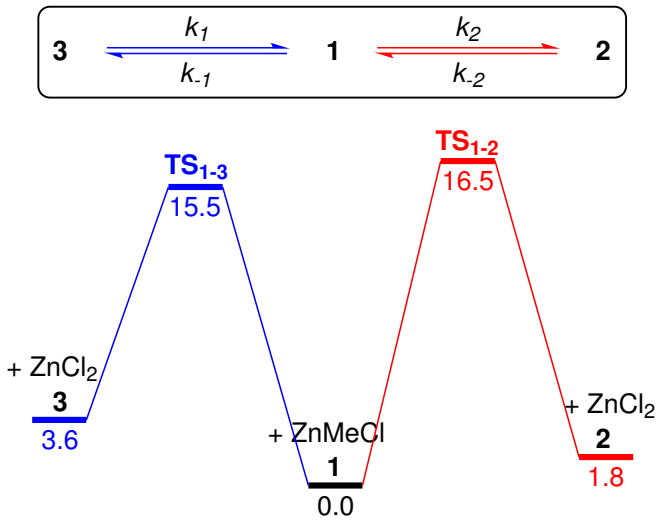

Figure 4.4: Kinetic model (top) and experimental ΔG_{223K} profiles (bottom) (kcal·mol^{-1}) for the reaction of **1** with ZnMeCl. k_1 and k_2 are the transmetalation rate constants, whereas k_{-1} and k_{-2} are the retrotransmetalation rate constants.

It is noteworthy to mention that the fact that the experimental results have been summarized first does not necessarily mean that all the events in this study followed this particular chronological order. In fact, experiments and theoretical calculations were carried out hand in hand. Thereby, the proposal of additional experiments and/or calculations during the course of this study was, in many cases, instigated by theoretical and experimental evidences, respectively. Consequently, many of the results that have been described in this section (or that will be described in further sections) are fruit of the rationalization of a series of experimental and theoretical findings.

In the following sections, the computational details of the theoretical calculations performed in this study, followed by the results derived from these calculations, will be described.

4.2.2 Computational details

All the theoretical calculations in this study were carried out at the *DFT* level by means of the dispersion-corrected *M06* functional[171] and using the *Gaussian09* program.[215] We selected this functional in purpose because it has been shown to deliver good results for both organometallic systems and non-covalent interactions.[171] The mechanistic study was performed on the very Pd catalyst used for experiments, thus including the real phosphine ligands bound to the metal center. Moreover, for the ZnMeCl reactant two additional explicit solvent molecules (i.e. *THF*) were included to fulfill the coordination sphere of Zn. The choice of this methodology allowed us to consider tetrahedral Zn species coordinated with *THF* along all the studied reaction pathways, rather than the unrealistic linear dicoordinated Zn species often used and that lead to calculated species of unlikely existence in *THF* solution.[216]

For geometry optimizations, the standard 6-31G(d) basis set was used to describe the C, Cl, O, P, and H atoms, and the *LANL2DZ* effective core potential[217,218] for the Pd and Zn atoms. We denoted the combination of these two basis sets as *BSI*. Geometries of all the reactants, intermediates, and transition states were fully optimized without symmetry constraints. The nature these stationary points was characterized by a vibrational analysis performed within the harmonic approximation. In particular, transition states were identified by the presence of one imaginary frequency and minima by a full set of real frequencies. Each of the computed reaction pathways was further checked by connecting transition states to the corresponding reactants and products following the displacement associated to the imaginary frequencies.

Potential energies (both in gas phase and solution) were also obtained by performing single point calculations at the above optimized geometries using the all electron basis set *DGDZVP* (double-ζ valence plus polarization)[219] for Pd, and the *TZVP* basis set (triple-ζ valence plus polarization)[220] for Zn and the main group elements. We denoted the combination of these two basis sets as *BSII*. Relative Gibbs energies were obtained by adding to the potential energies calculated with *BSII* the zero point energy (*ZPE*) and the vibrational, rotational, and translational entropic contributions of all the species calculated with *BSI* and at the temperature of 223 K.

Solvent effects (i.e. *THF*, $\varepsilon = 7.4257$) were introduced by a discrete-continuum model: two *THF* molecules were explicitly included in the calculations as potential ligands (see above), and the effect of the bulk solvent was considered with a continuum method, the *PCM* approach,[195] by means of single point calculations at all optimized gas phase geometries. In this method, the radii of the spheres employed to create the cavity for the solute were defined with the *UFF* model,† which is the default in *Gaussian09*.

†For further details on this model, see the last section of Chapter 2.

Unless specified otherwise, all the energies shown in this study correspond to Gibbs energies in *THF* (ΔG_{THF}) at 223 K, obtained by employing the following scheme:

$$\Delta G_{THF} = \Delta E_{THF} + (\Delta G_{gas} - \Delta E_{gas})$$

4.2.3 The concerted mechanism to the *trans* product

As commented, experiments revealed with the reaction of **1** with ZnMeCl at 203 K that the *trans* product (**3**) is formed at a higher rate than the *cis* one (**2**), thus demonstrating that the unique observation of **2** when the reaction is carried out at room temperature is deceptive. Hence, with the aim of providing a better understanding of this complex transmetalation process, we first focused our attention on computing a reaction pathway for the transmetalation of **1** leading to *trans* product **3**. In particular, we computed a reaction mechanism similar to the typical exchange-type mechanism described in Chapter 1 and that entails the concerted ligand exchange between two metal centers. The Gibbs energy profile obtained for this reaction pathway is depicted in Figure 4.5.

This concerted mechanism starts with the dissociation of a *THF* molecule from the organozinc reagent $ZnMeCl(THF)_2$ and the concomitant chlorine coordination to Zn. The resulting intermediate from this first step is **CT-1**, with an energy of 3.1 kcal·mol^{-1} relative to reactants. In this first intermediate, the Pd complex adopts a square planar geometry, whereas the Zn reagent adopts a Y-type geometry placed at 3.397 Å from Pd and 2.562 Å from the Cl atom (Figure 4.6). Then, from this species, the concerted transmetalation reaction occurs with a relative energy barrier of only 7.4 kcal·mol^{-1}. This step takes place through the four-membered ring transition state **CT-TS1** and involves the simultaneous methyl and chloride exchange between the Zn and Pd centers. Thus, in **CT-TS1** the two Pd–Cl (2.883 Å) and Zn–Me (2.071 Å) bonds are being broken at the same time that the two new Pd–Me (2.794 Å) and Zn–Cl (2.391 Å) bonds are being formed.

Interestingly, the intermediate that results from the concerted transmetalation (**CT-2**) features a relatively short Pd–Zn distance (2.710 Å), which suggests the existence of a metal-metal interaction between the electron rich Pd center and the fairly positive Zn center.[†] Once **CT-2** is formed, this last intermediate affords the final product **3** by coordination of a *THF* molecule to the Zn reagent and subsequent Pd–Zn dissociation.

[†]Such Pd–Zn interactions were also noticed by Álvarez et al.[221] in the formation of nucleophilic allenylzincs from allenylpalladium complexes, and by Organ et al.[212] in the alkyl-alkyl Negishi coupling catalyzed by (*NHC*)-Pd complexes.

The optimized geometries for the transition state and the intermediates involved in this concerted mechanism are shown in Figure 4.6.

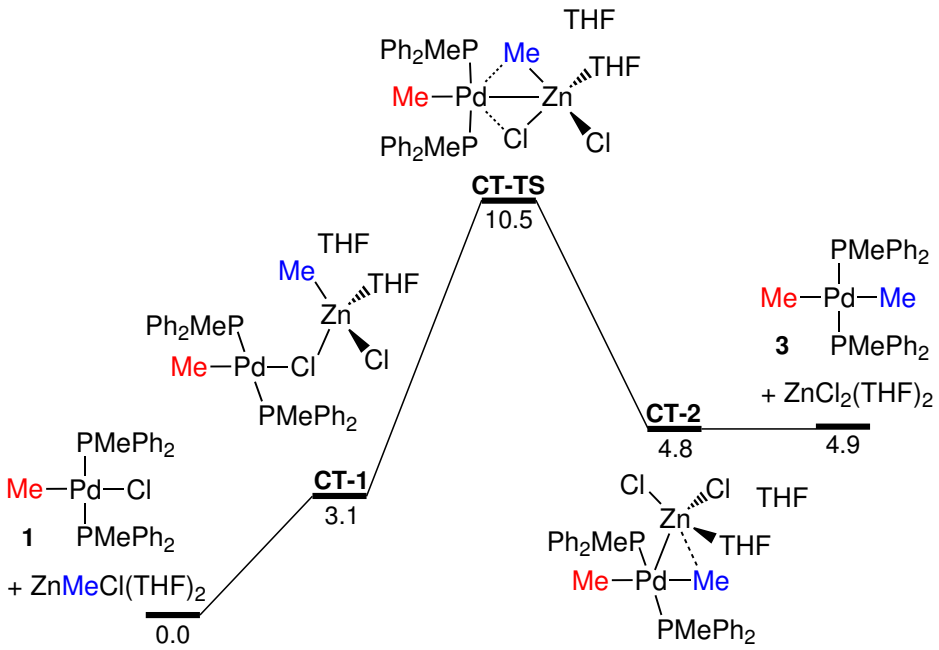

Figure 4.5: Gibbs energy profile in *THF* (ΔG_{THF}, kcal·mol^{-1}) at 223 K for the transmetalation with ZnMeCl leading to the *trans* product (**3**) via a concerted mechanism.

Overall, the computed concerted mechanism for the transmetalation reaction of **1** to the *trans* product **3** (Figure 4.5) shows that this process is endergonic by 4.9 kcal·mol^{-1}. Therefore, the reaction equilibrium is displaced toward the starting materials (**1** + ZnMeCl(THF)$_2$). On the other hand, the energy difference between the products (**3** + $ZnCl_2(THF)_2$) and the starting materials is responsible for the lower energy barrier for the reverse reaction (i.e. retrotransmetalation from **3** to **1**) compared to the forward reaction (i.e. transmetalation from **1** to **3**). This difference in the energy barriers reflects in a faster retrotransmetalation compared to transmetalation.

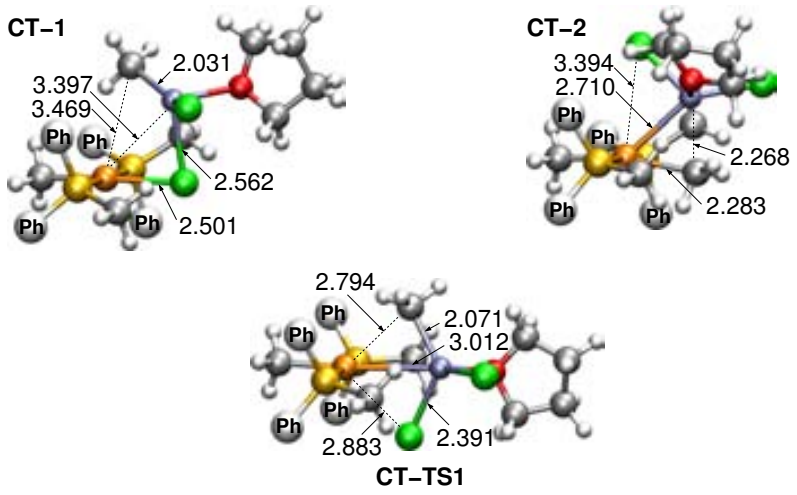

Figure 4.6: Optimized structures for the transition state and all the intermediates involved in the transmetalation with ZnMeCl leading to the *trans* product (**3**) via a concerted mechanism. Phenyl rings of the phosphine ligands have been simplified, and the second *THF* molecule of the organozinc reactant is not shown for clarity. Distances are shown in Å.

4.2.4 The concerted mechanism to the *cis* product

With the reaction mechanism for the transmetalation of **1** to the *trans* product **3** established, we next focused on investigating the transmetalation of **1** to the *cis* product **2**. The reaction mechanism that we computed for this process is also concerted but, unlike the one that yields **3**, it involves a Me by phosphine substitution followed by a phosphine by chloride substitution. The calculated Gibbs energy profile for the transmetalation reaction through this concerted mechanism is shown in Figure 4.7.

As in the transmetalation leading to the *trans* product **3** (Figure 4.5), the first step in this mechanism corresponds to the dissociation of a *THF* molecule from the organozinc reagent $ZnMeCl(THF)_2$ and the concomitant chlorine coordination to Zn (Figure 4.7). The intermediate that results from this first step is **CC-1** (analogous to **CT-1**),[†] which undergoes Me by phosphine substitution followed by phosphine by chloride substitution. Interestingly, this double substitution was found to take place in a unique transition state (**CC-TS1**) with an energy barrier of 16.9 kcal·mol^{-1}, though, as we will see later, it can also occur in two subsequent steps.[‡]

Similarly to **CT-TS1** in Figure 4.6, **CC-TS1** features a four-membered ring

[†]The difference in energy between **CT-1** and **CC-1** stems from the different conformation of the Zn reactant in these complexes.

[‡]This is the case of the transmetalation reaction of **1** with $ZnMe_2$ via this mechanism.

formed between the Pd, Cl, Me and Zn atoms (Figure 4.8). Moreover, the Pd–Zn distance in this transition state is rather short (2.592 Å), which seems to indicate that indeed there exists an interaction between these two metal centers. This transition state results in the last intermediate **CC-2**, in which the Pd–Zn interaction is maintained with a distance of 2.586 Å. Finally, **CC-2** affords the *cis* product **2** by coordination of a *THF* molecule to the Zn reagent and subsequent Pd–Zn dissociation. The optimized geometries for all the species that take part in this concerted mechanism are shown in Figure 4.8.

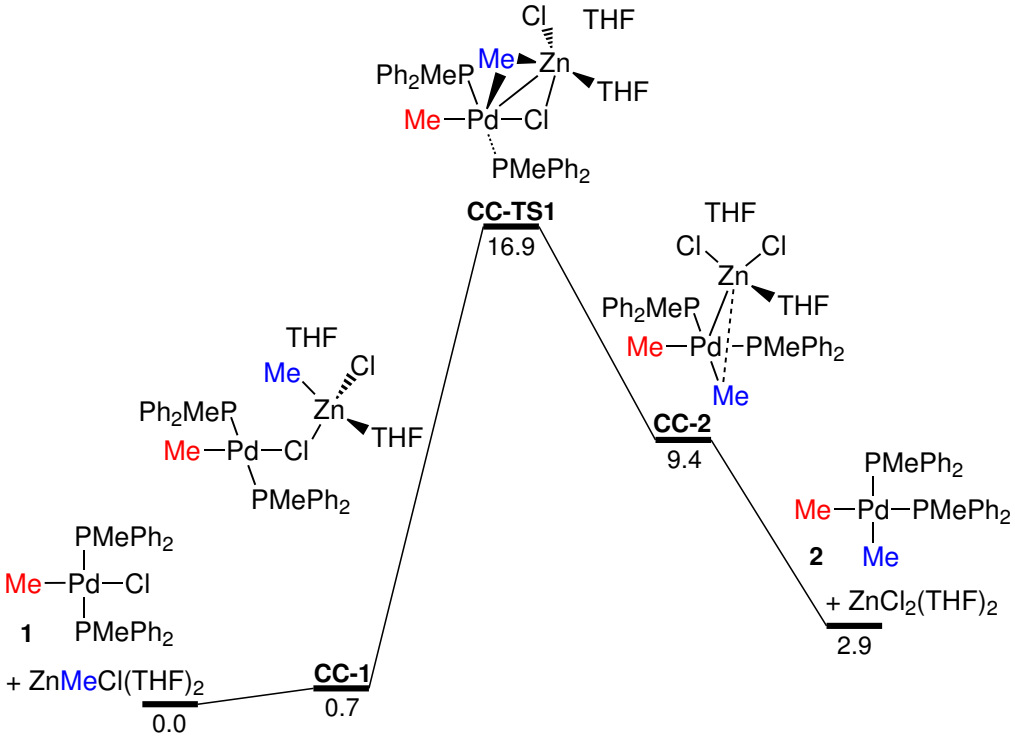

Figure 4.7: Gibbs energy profile in *THF* (ΔG_{THF}, kcal·mol^{-1}) at 223 K for the transmetalation with ZnMeCl leading to the *cis* product (**2**) via a concerted mechanism.

According to the overall Gibbs energy profile presented in Figure 4.7, the transmetalation of **1** to the *cis* product **2** is endergonic by 2.9 kcal·mol^{-1}. Therefore, just like in the transmetalation of **1** to **3**, the reaction to **2** is displaced toward the starting reagents (**1** + ZnMeCl(THF)$_2$). Furthermore, this is energy difference between reactants and products also causes that the rate of the retrotransmetalation is higher than that for transmetalation.

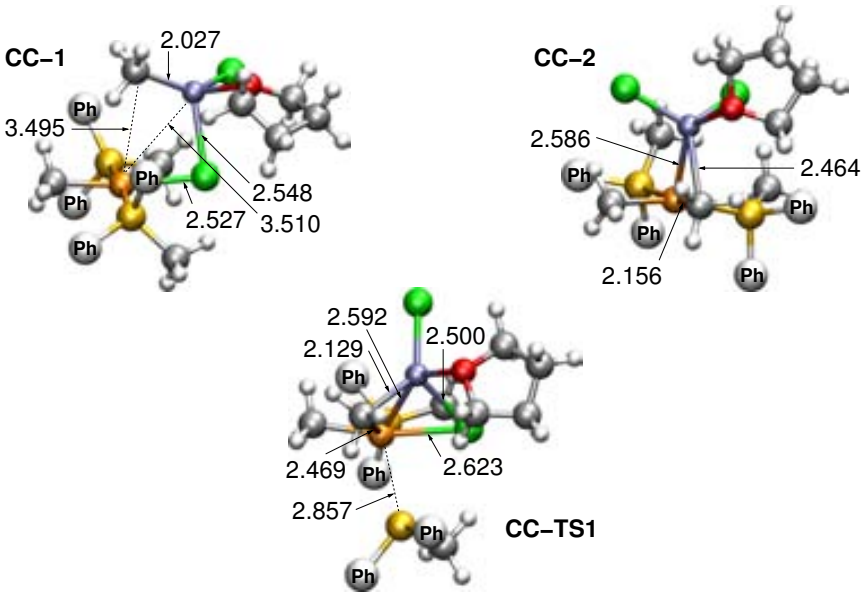

Figure 4.8: Optimized structures for the transition state and all the intermediates involved in the transmetalation with ZnMeCl leading to the *cis* product (**2**) via a concerted mechanism. Phenyl rings of the phosphine ligands have been simplified, and the second *THF* molecule of the organozinc reactant is not shown for clarity. Distances are shown in Å.

4.2.5 Comparing theoretical and experimental results

So far, the experimental and theoretical results obtained for the transmetalation reactions of **1** to **2** or **3** have been presented, but no comparison between them has been made yet. Hence, with this aim, the Gibbs energies obtained in the theoretical and experimental studies one these two transmetalations at 223 K have been summarized in the simplified reaction profiles depicted in Figure 4.9. According to these results, the theoretical calculations reproduce qualitatively all the experimental observations. In particular, from the thermodynamic point of view, both computed transmetalation reactions are endergonic, in agreement with experiments. Furthermore, the order of stability of the reagents and products in equilibrium predicted by calculations is exactly the same that the one observed in the experiments: **1** > **2** (*cis*) > **3** (*trans*). Therefore, calculations also conclude that **2** is the thermodynamic product.

As far as the kinetics is concerned, the theoretical results show that the reverse reactions (i.e. retrotransmetalations from **2** or **3** to **1**) are faster, which means that both transmetalation reactions are quickly reversible. This is consistent with the experimental observation that the addition of $ZnCl_2$ to a solution of **2** or **3** leads to the transformation of these species to **1**, and accordingly, with the fact that the

isomerization of **3** to **2** occurs via retrotransmetalation from **3** to **1** and subsequent transmetalation to **2**. On the other hand, the computed energy barriers for both reaction pathways are very low, which accounts for the fast transmetalation reactions observed in the experiments. More specifically, the global energy barrier for the transmetalation reaction to the *trans* product **3** (10.5 kcal·mol^{-1}) is lower than the one to the *cis* product **2** (16.9 kcal·mol^{-1}), which indicates that **3** is the kinetic product in agreement with experiments.

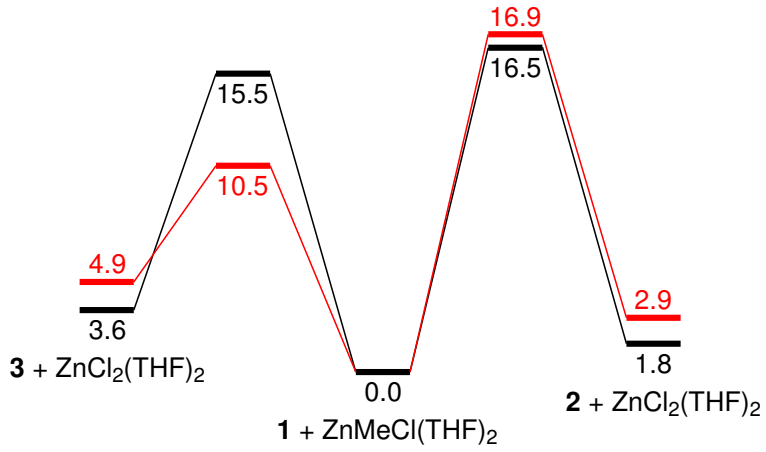

Figure 4.9: Comparison of the Gibbs energy values at 223 K (ΔG_{223K}, kcal·mol^{-1}) for the transmetalation reaction of **1** with ZnMeCl. Experimental values are shown in black, whereas calculated values are shown in red.

From the quantitative perspective, the results collected in Figure 4.9 show a good match between the computed and experimental values for the stabilities of the reagents and products in equilibrium (with energy differences about 1 kcal·mol^{-1}). On the other hand, the computed Gibbs energy barriers show an excellent fit with the experimental value for the transmetalation of **1** to **2** (with a difference of less than 0.5 kcal·mol^{-1}), but not so good for the transmetalation to **3** (calculations underestimates the Gibbs energy barrier by 5 kcal·mol^{-1}).

4.2.6 Conclusions

The transmetalation reaction between the complex *trans*-[Pd(Me)(Cl)(PMePh$_2$)$_2$] (**1**) and ZnMeCl (Scheme 4.2) was investigated combining experiments and *DFT* calculations. The theoretical and experimental results derived from this study revealed that, at variance with the unique observation of the *cis* product (**2**) when the reaction is carried out at room temperature, the *trans* product (**3**) is formed at a higher rate.

Thus, the reaction of **1** with ZnMeCl follows two competitive pathways: one, kinetically preferred that yields **3** but is unproductive for the coupling; and other, about one order of magnitude slower, that produces **2** from which the coupling will eventually take place though at a much slower rate. The computation of these two pathways showed that both involve cyclic transition states with structures very reminiscent of the one proposed for the cyclic mechanism in the Stille reaction.[22,68] However, in the case of the Negishi reaction a distinctive feature of these transition states and some intermediates was found: the existence of metal-metal interactions between the Pd and Zn centers.

Finally, this study also demonstrated that the transmetalations of **1** to **2** or **3** are quickly reversible, whereas the isomerization of **3** to **2** is very slow. Hence, since the transmetalation reactions and their respective reverse processes are much faster than the reductive elimination from **2**, it follows that the **2**-**1**-**3** round trip will take place many times before coupling occurs. Accordingly, in general catalyzed couplings of $[Pd(R^1)(X)(L)_2]$ and R^2ZnCl (or ZnR^2_2) there are statistically many chances for new intermediates $[Pd(R^2)(X)(L)_2]$ and R^1ZnCl (or ZnR^1R^2) to be formed through undesired retrotransmetalations from the initial intermediate $[Pd(R^1)(R^2)(L)_2]$, eventually affording the R^1–R^1 and R^2–R^2 homocoupling side products. All these results are summarized in the catalytic cycle shown in Figure 4.10.

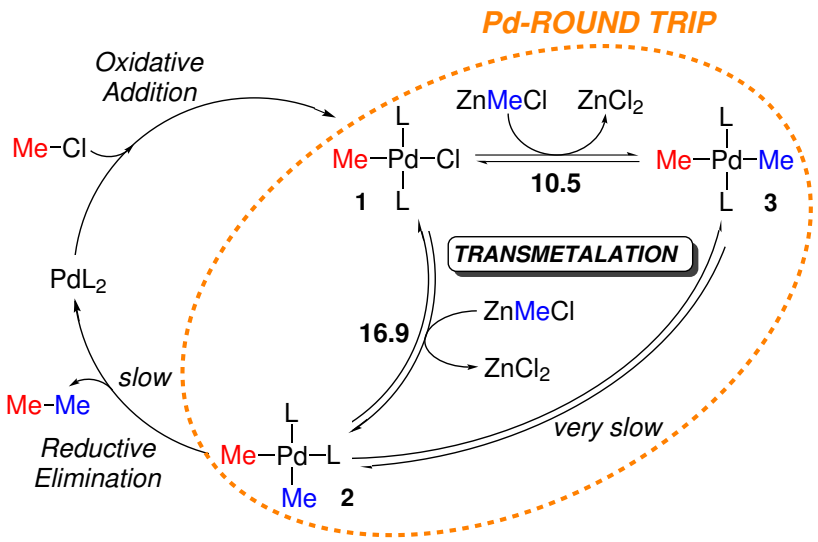

Figure 4.10: Simplified reaction mechanism for the Pd-catalyzed Negishi cross-coupling reaction with ZnMeCl (L = $PMePh_2$).

Overall, this study highlighted the complexity of the transmetalation step in the Negishi reaction. It is noteworthy to mention that this study represented the first ex-

perimental determination of thermodynamic parameters of a Negishi transmetalation reaction, and one of the earliest theoretical studies on this particular step. Furthermore, the deeper understanding provided by this study of the transmetalation of **1** with ZnMeCl is of particular importance since this type of complex can be envisaged in general catalyzed couplings of $[Pd(R^1)(X)(L)_2]$ and R^2ZnCl (or ZnR^2_2) as a result of undesired transmetalations.

4.3 The transmetalation step in the Negishi coupling of *trans*-[PdMeCl(PMePh$_2$)$_2$] with ZnMe$_2$

Due to the fact that the Negishi reaction is peculiar in that it can be carried out with two different types of organozinc nucleophiles (i.e. ZnR_2 and ZnRX), we decided, for the sake of completeness, to study the same transmetalation reaction that we investigated with ZnMeCl,[70] but with $ZnMe_2$ (Scheme 4.3).

Scheme 4.3: Transmetalation reaction between *trans*-[Pd(Me)(Cl)(PMePh$_2$)$_2$] (**1**) and ZnMe$_2$.

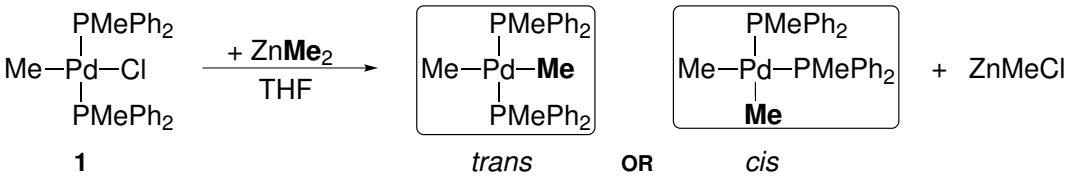

This study was also carried out in collaboration with the research group of Prof. Espinet and Prof. Casares. Hence, the reaction mechanism for the transmetalation of (**1**) with $ZnMe_2$ was investigated both theoretically and experimentally. As for the transmetalation with ZnMeCl, in the following sections the experimental and theoretical results derived from this study will be presented in this order.

4.3.1 Experimental data

A priori, with the merely change of ZnMeCl by $ZnMe_2$ as transmetalating nucleophile, only minor differences with respect to the results obtained with ZnMeCl were expected. However, as we will see next, experiments and theoretical calculations (see later) on this reaction revealed several unknown and unexpected aspects of the Negishi reaction.

As for the transmetalation with ZnMeCl, the reactions between **1** and $ZnMe_2$ (Scheme 4.3) were carried out in 1:20 ratio, simulating catalytic conditions with 5% of Pd in *THF*, and at different temperatures. In coincidence with ZnMeCl, the reaction with $ZnMe_2$ at room temperature afforded complex **2** as the only observable product, which slowly decomposed to give the Negishi coupling product ethane. In contrast, when the reaction was monitored by ^{31}P NMR at 203 K,[†] significant differences between the two organozinc reagents were observed (Figure 4.11). For example, the rate of consumption of **1** with $ZnMe_2$ (Figure 4.11 A) resulting in a mixture of **3** and **2** (being **3** very major) seemed to be too high compared to with ZnMeCl, even considering that some acceleration was expected owing to the higher nucleophilic character of $ZnMe_2$. Besides, unlike the reaction with ZnMeCl, where the reaction equilibrium is displaced toward the reagents (**1** + ZnMeCl, see Figure 4.3), in the system **1** + $ZnMe_2$ the reaction is displaced toward the products (**2** + ZnMeCl, and **3** + ZnMeCl). On the other hand, the addition to the reaction of just a small amount of $PMePh_2$ markedly decreased the rate of consumption of **1** (Figure 4.11 B), thus bringing the reaction rate into the convenient range for kinetic studies with ^{31}P NMR. Moreover, interestingly enough, further increases in the concentration of $PMePh_2$ affected only slightly the rate of consumption of **1** (Figure 4.11 C-E).

Hence, the behavior observed in the reactions with $ZnMe_2$ pointed out to the existence, in the initial reaction conditions (Figure 4.11 A), of a minute proportion of a non-observed catalytic intermediate that would open a much faster reaction pathway; this intermediate with the addition of a small amount of phosphine would be blocked, thereby causing the reaction rate to decrease. As the most plausible candidate for such catalytic intermediate we proposed the cationic species *trans*-$[Pd(Me)(PMePh_2)_2(THF)]^+$ ($\mathbf{4}^+$), which would be generated in the presence of a large amount of $ZnMe_2$ acting as Cl^- scavenger.[‡] This proposal was reinforced by the observation of the related cationic complex $[Pd(Me)(PMePh_2)_3]^+$ ($\mathbf{5}^+$) in the reactions with added $PMePh_2$ (Figure 4.11 B-E), and further supported by *DFT* calculations (see later).

Interestingly, the observation of $\mathbf{5}^+$ in variable concentration depending on the amount of added phosphine confirmed unequivocally that, in the presence of added phosphine, a second cationic species, this time observable, is made available from the very beginning of the reaction. Therefore, depending on the reaction conditions, the transmetalation with $ZnMe_2$ could take place on **1**, $\mathbf{4}^+$, or on $\mathbf{5}^+$. In order to shed light on this issue, the kinetic data collected in Figure 4.11 was fitted to two kinetic

[†]Temperature at which the coupling rate to give ethane was negligible.

[‡]Precedents for this proposal are the role of $ZnBr_2$ facilitating halide abstraction from Ni complexes, reported by Buchwald,[222,223] and the formation of [Ni(η^3-Bz)(diphosphine)][$ZnBr_3$(THF)] complexes from [Ni(σ-Bz)Br(diphosphine)] and $ZnBr_2$ in *THF*, reported by Anderson and Vicic.[224]

models:† (a) considering that the transmetalation takes place only from **1** (Eqs. 1 and 2, Figure 4.12); and (b) taking also into account the competitive transmetalation occurring from the cationic complex $\mathbf{5}^+$ (Eqs. 3 and 4, Figure 4.12).

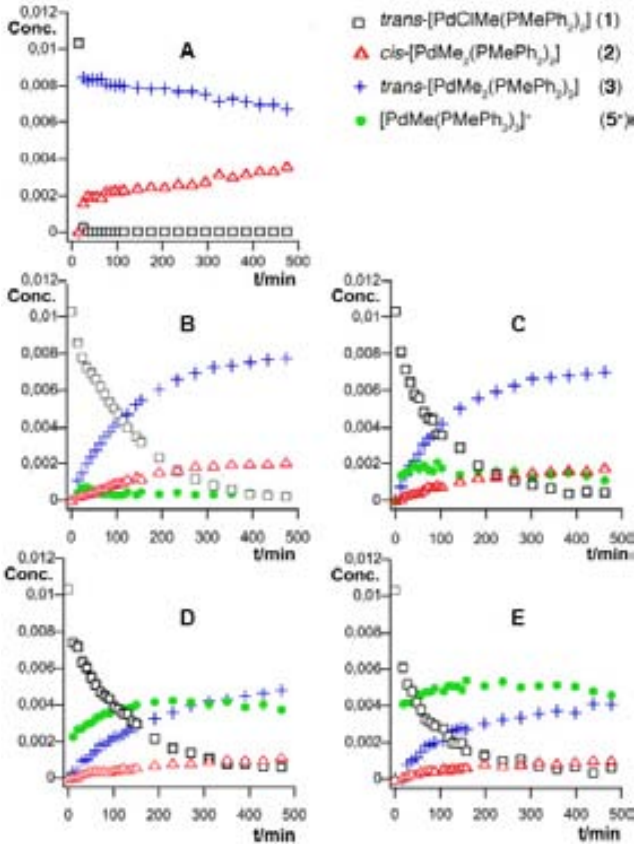

Figure 4.11: Concentration versus time data obtained by ^{31}P NMR spectroscopy for the reaction of **1** with $ZnMe_2$ in *THF* at T = 203 K. Starting conditions: $[\mathbf{1}]_0$ = 0.01 M; $[ZnMe_2]_0$ = 0.21 M. Added phosphine: (**A**) $[PMePh_2]$ = 0 M, (**B**) $[PMePh_2]$ = 6.0 x 10^{-4} M, (**C**) $[PMePh_2]$ = 2.0 x 10^{-3} M, (**D**) $[PMePh_2]$ = 5.0 x 10^{-3} M, (**E**) $[PMePh_2]$ = 1.0 x 10^{-2} M.

Importantly, the results derived from the kinetic model *b* provided negligible values for k_3^+, thus indicating that the competitive transmetalation pathway via $\mathbf{5}^+$ can be ruled out. Besides, both kinetic models consistently provided almost identical values for k_3 and for k_4.‡

Hence, according to the experiments, in the absence of added phosphine the ob-

†For further details see Tables 1 and 2 in Article II, in Appendix A.

‡The two rate constants with average values $k_3 \approx 2.8$ x 10^{-2} min^{-1}, and $k_4 \approx 6.2$ x 10^{-3}, differ in less than 1 order of magnitude.

served rate is too fast for the transmetalation to occur on **1**; consequently, the reaction must be going via the non-observed cationic intermediate $\mathbf{4}^+$. Similarly to the reaction with ZnMeCl, the transmetalation reaction affords the *trans* product **3** at a higher rate than the *cis* product **2**. Furthermore, the isomerization of **3** to **2** is also slow. On the other hand, in the presence of added phosphine, the cationic intermediate $\mathbf{4}^+$ is not available and, accordingly, the transmetalation takes place on **1**, but at a lower rate.

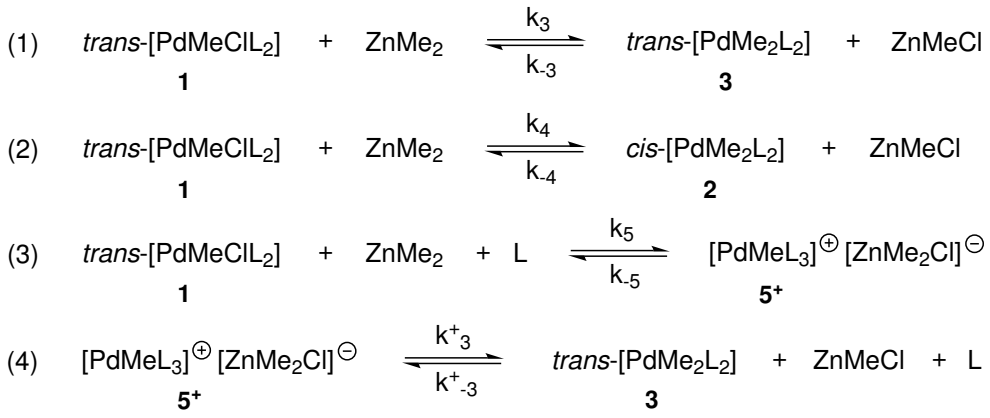

Figure 4.12: Reactions considered for the two applied kinetic models.

As commented for the reaction with ZnMeCl, the experiments and theoretical calculations in this study were performed alongside each other. Thus, in spite of the fact that the experimental results have been presented first, it should be said that many of the mechanistic suggestions or proposals presented in this section are fruit of the profitable feedback between experiments and theory.

In the following sections, the computational details of the theoretical calculations performed in this study, followed by the results derived from these calculations, will be presented.

4.3.2 Computational details

On the basis of the good results obtained in the study on the transmetalation reaction of **1** with ZnMeCl, and in order to further compare the results obtained with both organozinc compounds, we adopted essentially the same methodology than for that study. Hence, all the calculations were performed with the *Gaussian09* program,[215] and at the *DFT* level by means of the *M06* functional.[171] The mechanistic study was also carried out considering the same molecules (i.e. reactants and catalyst)

employed for the experiments, thus without modeling the phosphine ligands bound to the Pd catalyst (i.e. methyldiphenylphosphine). Moreover, as for the study with ZnMeCl, two additional explicit solvent molecules (i.e. *THF*) were included to fulfill the coordination sphere of $ZnMe_2$.[216]

For geometry optimizations the 6-31G(d) basis set for C, Cl, O, P, and H, along with the *LANL2DZ* effective core potential[217,218] for Pd and Zn atoms were used. We denoted the combination of these two basis set (*LANL2DZ* for Pd and Zn, 6-31G(d) for the main group elements) as *BSI*. Geometries were fully optimized without symmetry constraints. Harmonic force constants were computed at the optimized geometries to characterize the stationary points as minima or saddle points. The latter were confirmed by having a unique imaginary frequency and correlating the corresponding reactants and products.

Potential energies (both in gas phase and in solution) were refined by performing single point calculations at the optimized geometries with *BSI* using the all electron basis set *DGDZVP* (double-ζ valence plus polarization)[219] for Pd, in conjunction with the *TZVP* (triple-ζ valence plus polarization)[220] basis set for Zn and the main group elements. We named the combination of these two basis sets as *BSII*. Relative Gibbs energies in *THF* of the species were obtained by adding the gas phase Gibbs energy corrections of the solute calculated with *BSI* at 203 K to the energies in solution calculated with *BSII*.

Solvent effects (i.e. *THF*, $\varepsilon = 7.4257$) were introduced by a discrete-continuum model: two *THF* molecules were explicitly included in the calculations to fulfill the coordination sphere of the Zn reagent, and the effect of the bulk solvent was taken into account with a continuum method, the *SMD*[196] solvation model† implemented in *Gaussian09*, by means of single point calculations at all optimized gas phase geometries.

All the energies shown in this study correspond to Gibbs energies in *THF* (ΔG_{THF}) at 203 K calculated by employing the following scheme:

$$\Delta G_{THF} = \Delta E_{THF} + (\Delta G_{gas} - \Delta E_{gas})$$

4.3.3 The concerted mechanism to the *trans* product

The mechanistic study on the transmetalation of **1** with ZnMeCl revealed that the *trans* product **3** is formed through a reaction pathway that involves the concerted Cl for Me exchange in a cyclic transition state (Figure 4.5). Thus, for the sake of completeness, the analogous mechanism for the reaction of **1** with $ZnMe_2$ was

†For further details on this model, see the last section of Chapter 2.

computed. The calculated Gibbs energy profile for the reaction occurring via this mechanism is depicted in Figure 4.13.

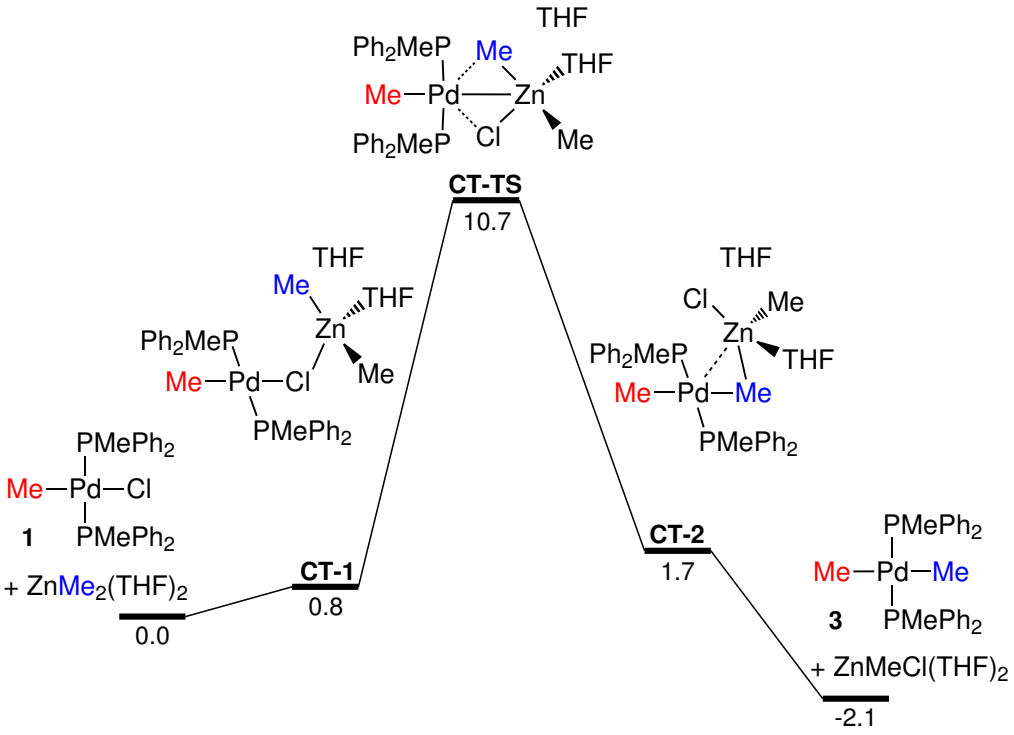

Figure 4.13: Gibbs energy profile in *THF* (ΔG_{THF}, kcal·mol^{-1}) at 203 K for the transmetalation with $ZnMe_2$ leading to the *trans* product (**3**) via a concerted mechanism.

Similarly to the concerted pathway with ZnMeCl, the first step in this mechanism corresponds to the dissociation of a *THF* molecule form the starting Zn reagent and the chlorine coordination to Zn. This initial step is almost thermoneutral (0.8 kcal·mol^{-1}) and results in the formation of the intermediate **CT-1**. Subsequently, this species evolves to the transition state **CT-TS1**, where the transmetalation properly speaking occurs with a global energy barrier of 10.7 kcal·mol^{-1}. The optimized geometry for **CT-TS1** is practically the same than the calculated for the transition state with ZnMeCl (**CT-TS1**, Figure 4.6), with distances differing in less than about 0.1 Å (Figure 4.14). This transition state affords the last intermediate **CT-2**, which features a rather short Pd–Zn distance (2.794 Å), again in coincidence with the calculated for ZnMeCl (2.710 Å). Finally, **CT-2** yields the *trans* product **3** by coordination of a *THF* molecule to the Zn reagent and subsequent Pd–Zn dissociation. The optimized geometries for the transition state and intermediates involved in this mechanism are shown in Figure 4.14.

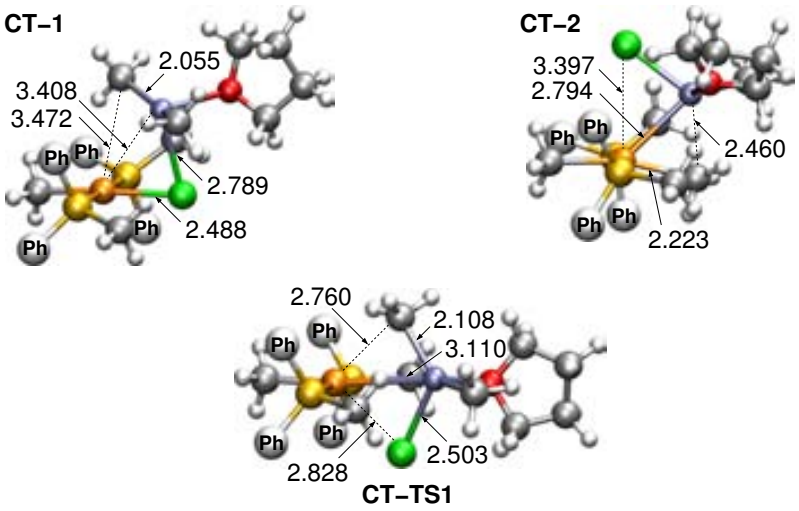

Figure 4.14: Optimized structures for the transition state and all the intermediates involved in the transmetalation with $ZnMe_2$ leading to the *trans* product (**3**) via a concerted mechanism. Phenyl rings of the phosphine ligands have been simplified, and the second *THF* molecule of the organozinc reactant is not shown for clarity. Distances are shown in Å.

Unlike the reaction of with ZnMeCl, which was found to be endergonic, the overall Gibbs energy profile for the reaction with $ZnMe_2$ indicates that this reaction is exergonic by 2.1 kcal·mol^{-1}. Thus, the reaction equilibrium, in this case, is displaced toward the products (**3** + $ZnMeCl(THF)_2$). As a consequence, the reverse reaction (i.e. retrotransmetalation from **3** to **1**) is slower than the forward reaction (i.e. transmetalation from **1** to **3**).

4.3.4 The concerted mechanism to the *cis* product

Following the same concerted mechanism than the one proposed in the study with ZnMeCl (Figure 4.7), the transmetalation of **1** with $ZnMe_2$ leading to the *cis* product **2** was computed. The Gibbs energy profile obtained for the reaction through that mechanism is shown in Figure 4.15.

As the other concerted pathways, this mechanism starts with the dissociation of one *THF* molecule from the reactant $ZnMe_2(THF)_2$ and the concomitant interaction between the Cl and Zn atoms. The resulting intermediate from this first step is **CC-1**, which lies only 0.4 kcal·mol^{-1} above the separated reactants (**1** + $ZnMe_2(THF)_2$). Then, **CC-1** undergoes phosphine by Me substitution followed by phosphine by chloride substitution. Unlike the reaction with ZnMeCl, where this double substitution was found to take place in the same transition state (**CC-TS1**, Figure 4.7), with $ZnMe_2$ this process occurs in two separated steps. More specifically,

the first phosphine by Me substitution occurs through the transition state **CC-TS1** (11.5 kcal·mol^{-1}), while the following phosphine by chloride substitution takes place via **CC-TS2** (11.8 kcal·mol^{-1}). Interestingly, both transition states and the intermediate that connects these transition states (**CC-2**) have similar Gibbs energies, which indicates that once the first substitution occurs, the second one is very easy (it requires only 2.5 kcal·mol^{-1}). Furthermore, all these species feature a four-membered ring formed between the Pd, Cl, Zn, and Me atoms (Figure 4.16), and fairly short Pd–Zn distances (the largest distance is 2.707 Å, in **CC-TS1**).

The second substitution through **CC-TS2** gives rise to the last intermediate **CC-3**, where the two Me groups are in *cis* disposition and the short Pd–Zn distance is maintained (2.700 Å). Finally, this intermediate yields the final product **2** by the coordination of the *THF* molecule to the Zn reagent and the subsequent Pd–Zn dissociation.

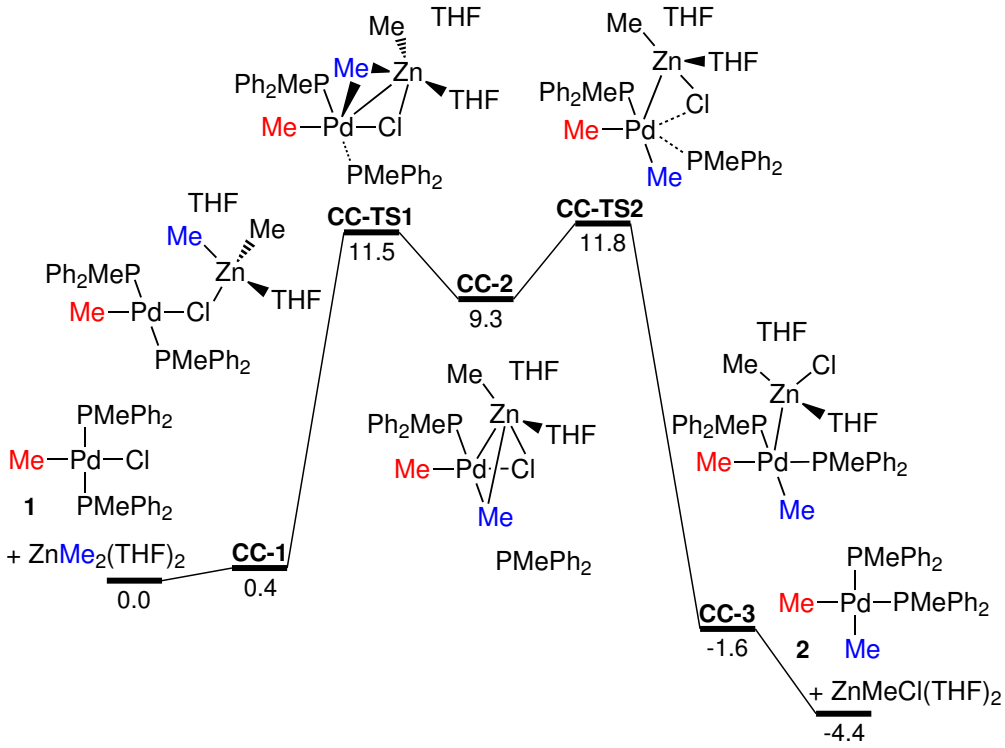

Figure 4.15: Gibbs energy profile in *THF* (ΔG_{THF}, kcal·mol^{-1}) at 203 K for the transmetalation with $ZnMe_2$ leading to the *cis* product (**2**) via a concerted mechanism.

The optimized geometries for all the transition states and intermediates that take part in this mechanism are displayed in Figure 4.16.

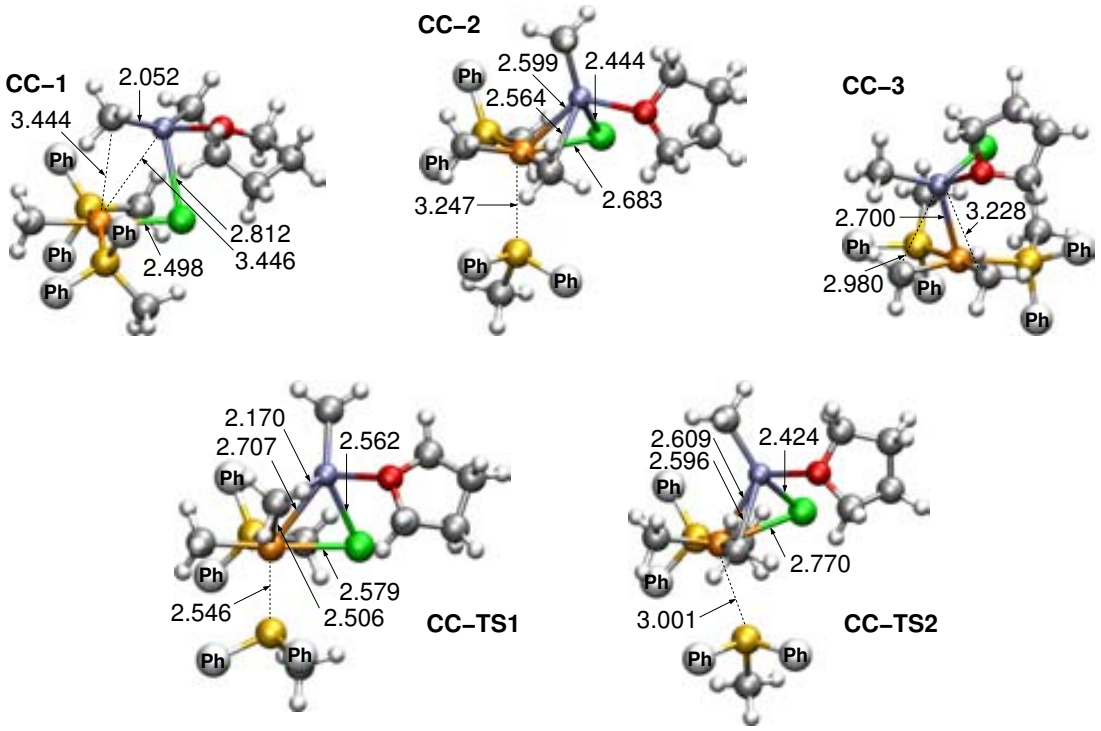

Figure 4.16: Optimized structures for all the intermediates and transition states involved in the transmetalation with $ZnMe_2$ leading to the *cis* product (**2**) via a concerted mechanism. Phenyl rings of the phosphine ligands have been simplified, and the second *THF* molecule of the organozinc reactant is not shown for clarity. Distances are shown in Å.

Overall, the Gibbs energy profile depicted in Figure 4.15 shows that transmetalation of **1** to the *cis* product **2** is endergonic by 4.4 kcal·mol^{-1}. Thus, the reaction equilibrium is displaced towards the products (**2** + $ZnMeCl(THF)_2$), which reflects in a faster transmetalation compared to the retrotransmetalation reaction. The highest energy barrier within this overall reaction profile corresponds to the chloride by phosphine substitution via **CC-TS2**, with an energy of 11.8 kcal·mol^{-1}.

4.3.5 The ionic mechanism to the *trans* product (L = THF)

According to the experimental results, a consistent explanation for the unusually fast transmetalation observed with $ZnMe_2$ would be the formation of the non-observable intermediate *trans*-$[Pd(Me)(PMePh_2)_2(THF)]^+$ ($\mathbf{4}^+$), from which the reaction would take place at a higher rate. Thus, in order to evaluate this proposal, a plausible transmetalation mechanisms involving this cationic intermediate $\mathbf{4}^+$ was theoretically investigated. In particular, the analyzed mechanism is reminiscent of the concerted mechanism leading to the *cis* product **2**, where the transmetalation reaction between Pd an Zn centers takes place in two steps (Figure 4.15). In this case, however, the Me and Cl ligands are transferred in reversed order; that is, first the Cl atom is transferred from Pd to Zn, and afterwards, the Me group from Zn to Pd. On the other hand, this mechanism involves the formation of charged species and for this reason we named it as *ionic mechanism*. The calculated Gibbs energy profile for the transmetalation reaction through this mechanism is depicted in Figure 4.17.

The first step in this ionic mechanism is the same than for the concerted mechanisms investigated so far. Thus, it entails the dissociation of a *THF* molecule from $ZnMe_2(THF)_2$ and the concomitant Cl coordination to Zn. The intermediate that results from this step is **IT-1**,[†] which undergoes chloride abstraction assisted by an external coordinating ligand (L) and the Zn reagent. In this case, since *THF* is the solvent and furthermore has a moderate coordinating ability, it can act as external ligand and assist the chloride abstraction through the transition state **IT-TS1**[‡] affording the unstable intermediate **IT-2** (corresponding to $\mathbf{4}^+$ in the experimental nomenclature). Importantly, the relative position of this last intermediate in the Gibbs energy profile is 5.3 kcal·mol^{-1} above the starting reactants, which makes its observation by ^{31}P NMR very unlikely.[§]

Once **IT-2** is formed, the *THF* molecule coordinated to the cationic Pd complex *trans*-$[Pd(Me)(PMePh_2)_2(THF)]^+$ is replaced by a Me group of the counter-ion $[ZnMe_2Cl(THF)]^-$ with a relative energy barrier of only 5.0 kcal·mol^{-1}. The transition state involved in this substitution is **IT-TS2** and results in the last intermediate **IT-3**. Finally, this last intermediate evolves to the *trans* product **3** by the coordination of a *THF* molecule to the Zn reactant and the dissociation of the Pd–Zn complex.

[†]Note that this intermediate differs from their analogous **CT-1** and **CC-1** in that the dissociated *THF* molecule is explicitly included.

[‡]This transition state appears 0.6 kcal·mol^{-1} below the following intermediate **IT-2**, which suggests that **IT-TS1** might not be a transition state in the Gibbs energy surface. In any case, the proximity in energy of **IT-TS1** and **IT-2** indicates that the backward process to generate the starting reactants is very easy.

[§]A Gibbs energy difference larger than 3 kcal·mol^{-1} with respect to the starting reactants should be sufficient to make its equilibrium concentration low enough to be non-observable by ^{31}P NMR.

The optimized geometries for the transition states and intermediates involved in this ionic mechanism are shown in Figure 4.18.

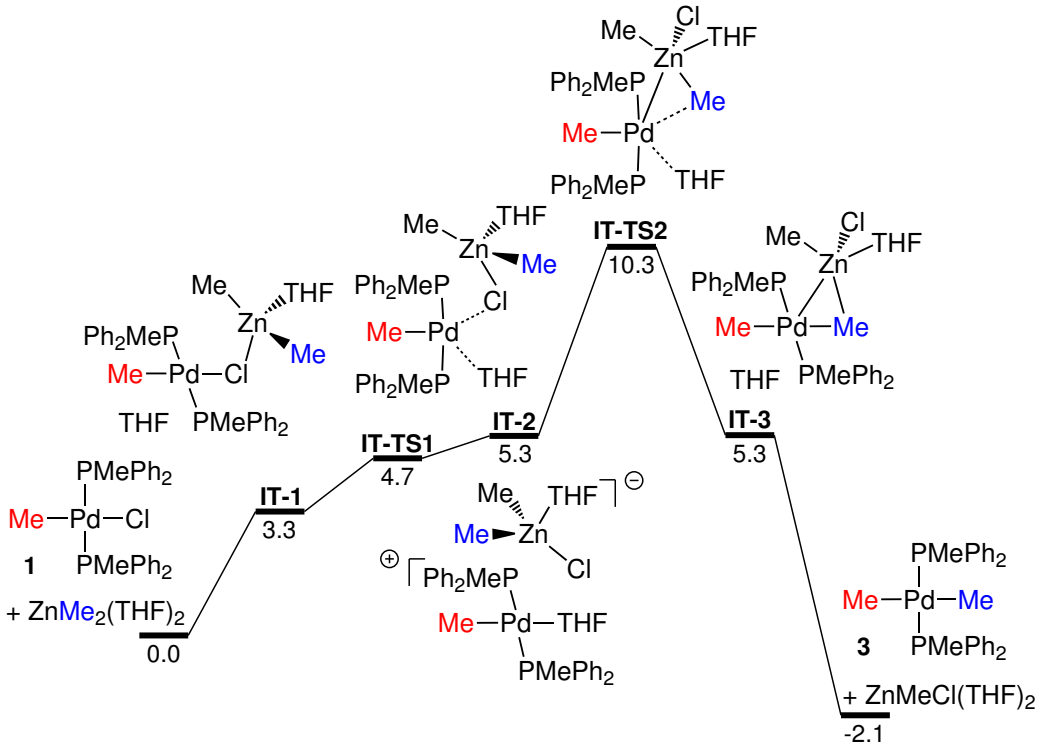

Figure 4.17: Gibbs energy profile in *THF* (ΔG_{THF}, kcal·mol^{-1}) at 203 K for the transmetalation with $ZnMe_2$ leading to the *trans* product (**3**) via the ionic mechanism with L = *THF*.

Overall, the calculated Gibbs energy profile depicted in Figure 4.17 shows that the highest energy barrier within this ionic mechanism corresponds to the transfer of the Me group from Zn to Pd through **IT-TS2** (10.3 kcal·mol^{-1}). This energy barrier is even lower than that found for the concerted mechanism leading to **3** (Figure 4.14), which consistently supports the proposal of an alternative transmetalation mechanism involving the cationic intermediate $\mathbf{4}^+$ as a plausible explanation for the unusual fast transmetalation observed.

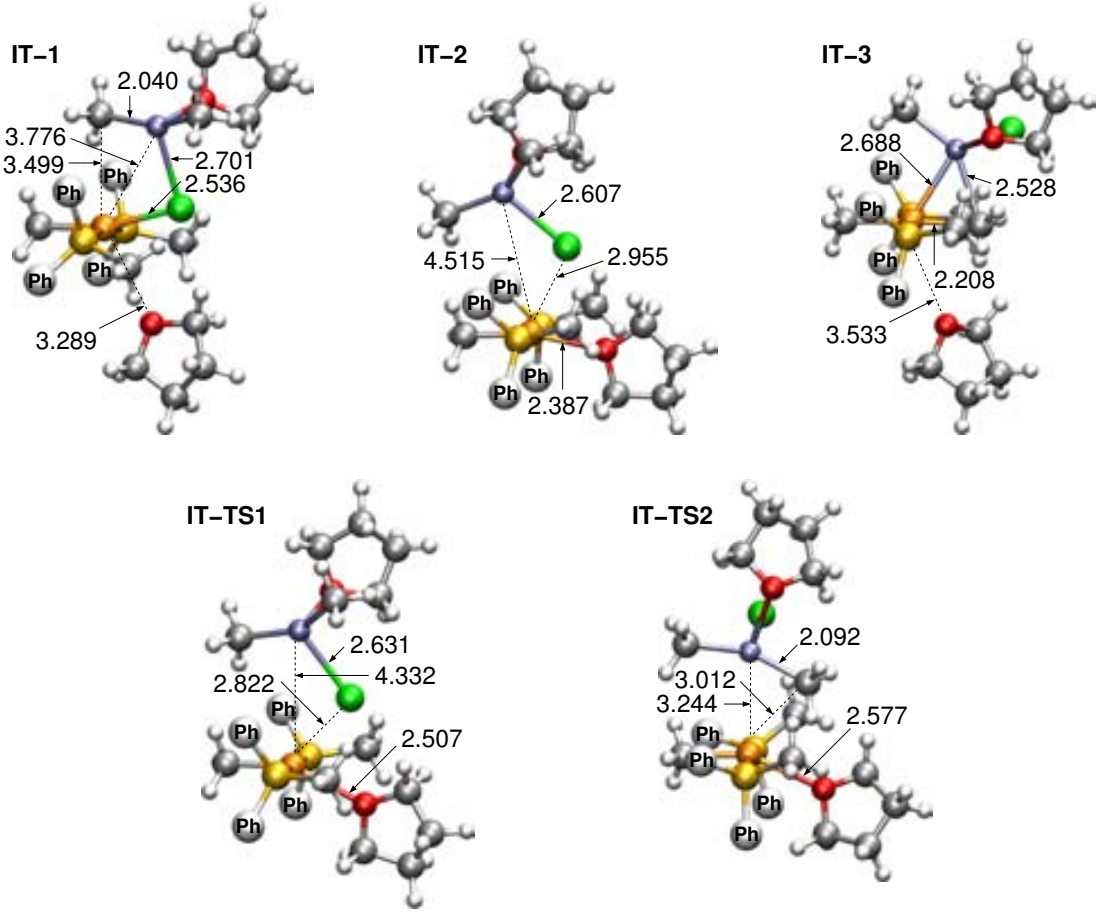

Figure 4.18: Optimized structures for all the intermediates and transition states involved in the transmetalation with $ZnMe_2$ leading to the *trans* product (**3**) via the ionic mechanism with $L = THF$. Phenyl rings of the phosphine ligands have been simplified, and the second *THF* molecule of the organozinc reactant is not shown for clarity. Distances are shown in Å.

4.3.6 The ionic mechanism to the *trans* product (L = $PMePh_2$)

Finally, in order to unravel the observed decrease of the reaction rates for the transmetalation process with added phosphine, and further support the observation of the cationic species $[Pd(Me)(PMePh_2)_3]^+$ ($\mathbf{5}^+$), a transmetalation pathway through this species was computed. This pathway involves the same steps than the ionic mechanism with $L = THF$ (Figure 4.17), but entails very different energies (Figure 4.19). Probably the most noteworthy difference between these two mechanisms is the different stability of intermediates **IT-2** corresponding to the cationic species $\mathbf{4}^+$ (i.e.

L = *THF*) and $\mathbf{5}^{+}$ (i.e. $L = \mathrm{PMePh_2}$). According to calculations, unlike the former that has a higher energy than the separated reactants (5.3 kcal·mol^{-1}), the latter lies 6.0 kcal·mol^{-1} below separate reactants, which accounts for its observation by ^{31}P NMR. This lowering in the energy of **IT-2**, however, makes the energy barrier for the following step (**IT-TS2**) to increase to 15.5 kcal·mol^{-1}. The optimized geometries for all the transition states and intermediates implicated in this ionic mechanism are shown in Figure 4.19.

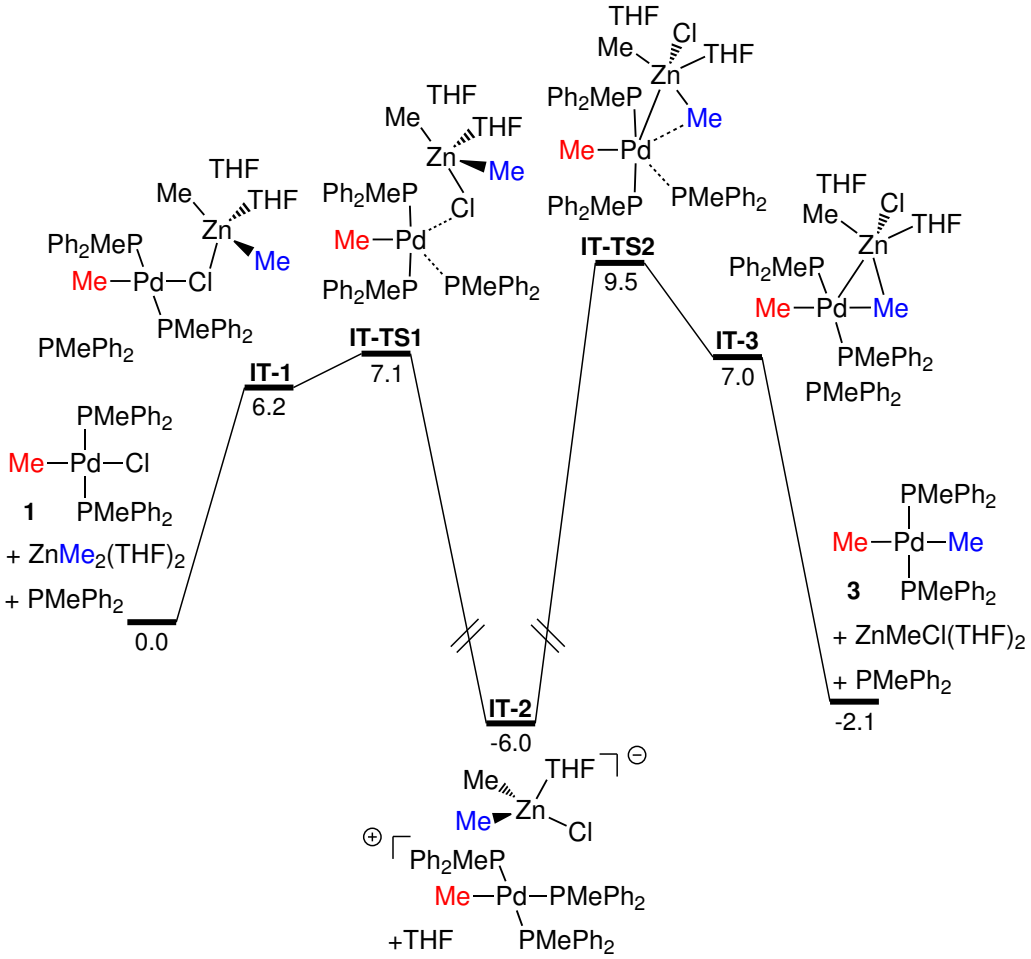

Figure 4.19: Gibbs energy profile in *THF* (ΔG_{THF}, kcal·mol^{-1}) at 203 K for the transmetalation with $ZnMe_2$ leading to the *trans* product (**3**) via the ionic mechanism with $L = \mathrm{PMePh_2}$.

In summary, the computed Gibbs energy profile for the transmetalation through this ionic mechanism with $L = \mathrm{PMePh_2}$ (Figure 4.19) reveals that the very low energy of **IT-2** makes the observation of this species by ^{31}P NMR to be very likely. Similarly

to the mechanism with $L = THF$, the highest energy barrier corresponds to the Me by phosphine substitution via **IT-TS2** (15.5 kcal·mol^{-1}). This energy is more than 3 kcal·mol^{-1} higher than those calculated for the concerted mechanisms and the ionic mechanism with $L = THF$, which in terms of reaction rates means more than 3 orders of magnitude slower. Therefore, this pathway is clearly the most disfavored one for the transmetalation of **1** with $ZnMe_2$.

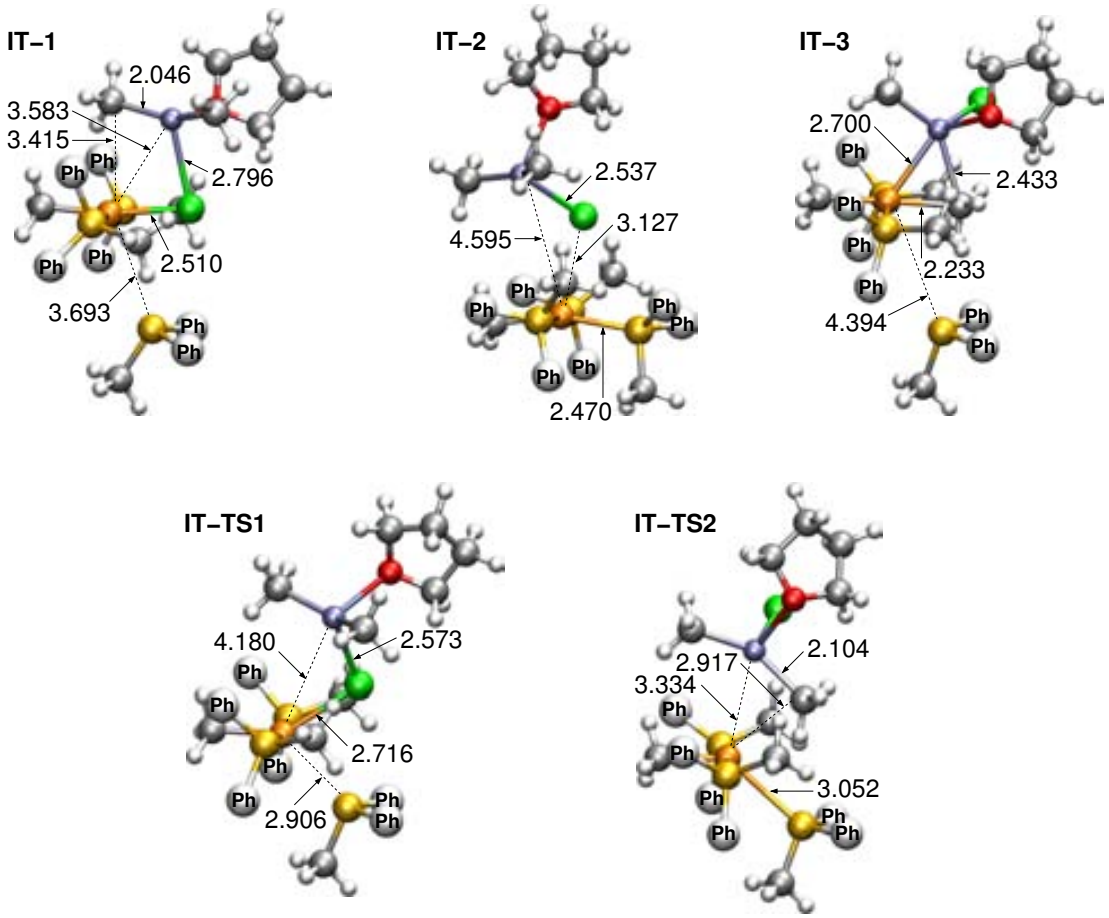

Figure 4.20: Optimized structures for all the intermediates and transition states involved in the transmetalation with $ZnMe_2$ leading to the *trans* product (**3**) via the ionic mechanism with $L = PMePh_2$. Phenyl rings of the phosphine ligands have been simplified, and the second *THF* molecule of the organozinc reactant is not shown for clarity. Distances are shown in Å.

4.3.7 Comparing theoretical and experimental results

After having summarized the experimental and theoretical results obtained for the transmetalation of **1** with $ZnMe_2$, the only thing that is left is to compare them and draw the final conclusions of this mechanistic study. With this purpose, the Gibbs energies at 203 K obtained in the experimental[†] and theoretical studies on this reaction have been summarized in the simplified reaction profiles depicted in Figure 4.21.

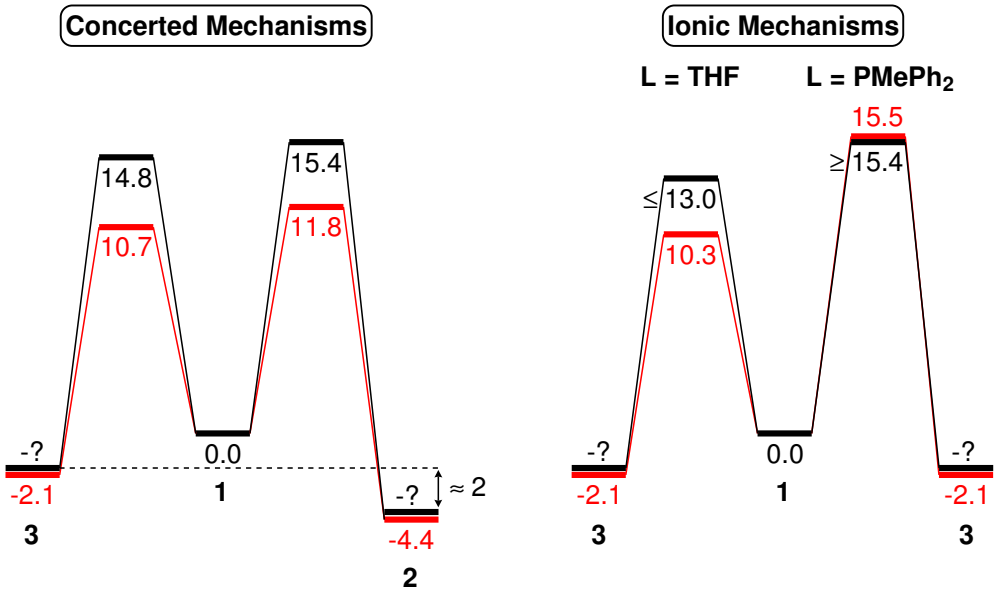

Figure 4.21: Comparison of the Gibbs energy values at 203 K (ΔG_{223K}, kcal·mol^{-1}) for the transmetalation reaction of **1** with $ZnMe_2$. Zn species are not shown for clarity. Experimental values are shown in black, whereas calculated values are shown in red.

At first glance, from Figure 4.21 it can be observed that calculations reproduce qualitatively all the experimental observations. In particular, from the thermodynamic perspective, the computed Gibbs energies confirm that transmetalation reactions leading to the *trans* and *cis* products (**3** and **2**, respectively) are exergonic, in coincidence with experiments. Furthermore, the computed order of stability of the

[†]These values were calculated using the reaction rates derived from the kinetic model *a* adopted in the experiments. Note that the experimental values for the concerted mechanisms are the quantitative kinetic results, whereas for the ionic mechanisms the values plotted correspond to the estimated maximum (i.e. $L = THF$) or minimum (i.e. $L = PMePh_2$) values compatible with the experimental observations.

reagents and products in equilibrium is the same than that observed in the experiments: **2** > **3** > **1**. On the other hand, from the kinetic point of view, the calculated Gibbs energy barriers for the transmetalation reaction through the different analyzed mechanisms decrease in the order: ionic to *trans* (L = $PMePh_2$) > concerted to *cis* > concerted to *trans* > ionic to *trans* (L = *THF*), which consistently accounts for the observation of the unusually fast transmetalation of **1** to the kinetic product **3** and the decelerating effect of the added phosphine (Figure 4.11).

Last but not least, the quantitative comparison of experimental and theoretical Gibbs energy barriers can be only strictly made for the concerted mechanisms, since only the lower (for $\mathbf{5}^+$) and higher (for $\mathbf{4}^+$) limits for the ionic mechanisms could be estimated experimentally. Thus, according to the computed barriers for the concerted mechanisms it seems that they are underestimated by about 4 kcal·mol^{-1}. Nevertheless, calculations nicely reproduce the energy difference between the concerted mechanisms (it is 0.6 kcal·mol^{-1} in the experiments, and 1.1 kcal·mol^{-1} in the theoretical values). Similarly, the relative stability of products **2** and **3** could not be quantified experimentally either, but in the study with ZnMeCl we demonstrated that **2** is about 2.0 kcal·mol^{-1} more stable than **3**. Hence, a calculated difference of 2.3 kcal·mol^{-1}, in this case, can be considered a very satisfactory fit with the experiment.

4.3.8 Conclusions

Following our research interest in the Negishi reaction, the transmetalation reaction between the complex *trans*-[$PdMeCl(PMePh_2)_2$] (**1**) and $ZnMe_2$ was investigated both experimentally and theoretically. The results derived from this study showed that all the reactions with $ZnMe_2$ are faster than with ZnMeCl. Similarly to ZnMeCl, the transmetalation with $ZnMe_2$ was found to afford the *trans* product (**3**) at a higher rate than the *cis* product (**2**). However, the **3** to **2** isomerization, necessary for the success of the coupling, resulted to be slower than with ZnMeCl. This is due to the slower retrotransmetalation reactions with $ZnMe_2$.

Probably the most interesting observation of this work was that, besides the expected concerted pathways previously proposed for ZnMeCl, alternative ionic mechanisms could be operative. These ionic pathways involve cationic intermediates of the type $[Pd(Me)(PMePh_2)_2(L)]^+$ $[ZnMe_2Cl(THF)]^-$ (L = *THF*, $PMePh_2$). In particular, the ionic mechanism with L = *THF* is faster than the concerted mechanisms, while this mechanism with L = $PMePh_2$ is much more slower. In fact, the observation of the complex $[Pd(Me)(PMePh_2)_3]^+$ ($\mathbf{5}^+$) suggests that the formation of this complex becomes a trap of the Pd catalyst. This observation consistently accounts for the decelerating effect of the addition of $PMePh_2$ to the reaction of **1** with $ZnMe_2$. Interestingly, the fact that no accelerating effect was detected in the

study with ZnMeCl can be attributed to the unlikely formation of the cationic species $[Pd(Me)(PMePh_2)_2(THF)]^+$ ($\mathbf{4}^+$), since the presence of a large number of terminal chloro donor atoms will prevent *THF* from coordinating Pd.

All the results obtained in this combined experimental and theoretical study are summarized in the catalytic cycle depicted in Figure 4.22.

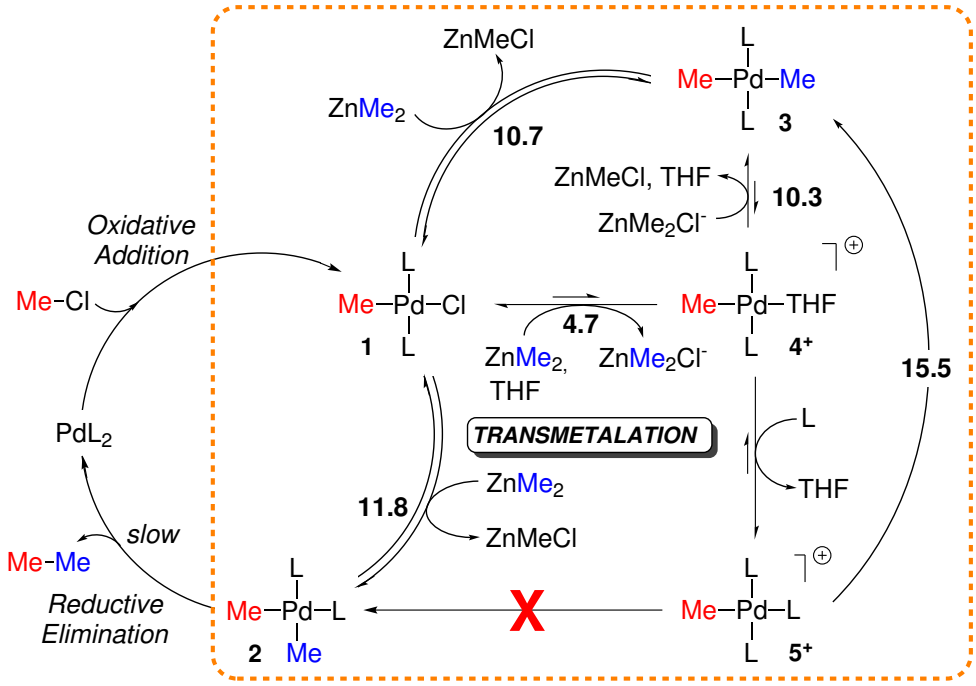

Figure 4.22: Simplified reaction mechanism for the Pd-catalyzed Negishi cross-coupling reaction with $ZnMe_2$ (L = $PMePh_2$).

Overall, this study provided a proof of existence, operation and effects of competitive transmetalation pathways, some of which had not been invoked before, but that should be considered from now on when planning or discussing Negishi syntheses. For instance, the oxidative addition products $[Pd(R)(L)_2(solvent)]^+ X^-$ generated by reaction of R–X to $[PdL_2]$, in the case of weakly coordinating anions X, are very likely to promote ionic mechanisms. Conversely, a less donating R group on Pd, instead of Me, is expected to be somewhat less prone to produce ionic species, whereas heavier halogens will promote ionic Pd species better than Cl. As far as the solvent is concerned, the use of solvents more coordinating than *THF* will also favor ionic mechanisms.

On the other hand, this study also showed that despite the fact that matching

experimental relative Gibbs energies in solution with theoretical calculations is a harsh work, the computation of energy differences between reaction mechanisms are very useful to elucidate which pathway is preferred.

"Important scientific discoveries go through three phases: first they are completely ignored, then they are violently attacked, and finally they are brushed aside as well known"

Max Tegmark, Nature, **2007**, *448*, 23-24

5

The Cu-free Sonogashira reaction mechanism

The results presented in this chapter have been published in the following article:

Article III: **García-Melchor, M.**; Pacheco, M. C.; Nájera, C.; Lledós, A.; Ujaque, G. *ACS Catal.* **2012**, *2*, 135-144.

5.1 Introduction

The palladium-catalyzed Sonogashira reaction is one of the most important and widely used methods for preparing arylacetylenes and conjugated enynes,[225–230] which are precursors for natural products, pharmaceuticals, and materials with specialized optical and electronic properties.[18,31,231–234] The two studies first reported on this field were independently published in 1975 by Heck's group[235] and Cassar.[236] The Heck and co-workers' procedure was based on the Mizoroki-Heck reaction,[237,238] namely the palladium-catalyzed arylation or alkenylation of alkenes, employing a phosphane-palladium complex as catalyst and triethylamine or piperidine both as base and solvent. On the other hand, Cassar's procedure also involved a phosphane-palladium complex as catalyst but, in this case, in combination with sodium methoxide as base and *DMF* as solvent. Both methods, however, had the disadvantage that generally required high temperatures (up to 100 °C). Afterwards but in the same year, Sonogashira and Hagihara reported that addition of a catalytic amount of CuI greatly accelerates the alkynylation reaction, thus enabling the performance of this reaction even at room temperature.[239] As a result, this Sonogashira-Hagihara reaction, commonly known simply as Sonogashira reaction, became the most popular procedure for the alkynylation of aryl or alkenyl halides replacing all the other related protocols. Thereafter, the general Sonogashira protocol for the coupling of terminal alkynes with aryl or alkenyl halides (or triflates) usually involves an organic solvent, a Pd(0)/Cu(I) catalytic system, and at least a stoichiometric amount of a base (Scheme 5.1).

Scheme 5.1: General scheme for Pd-catalyzed Sonogashira reaction.

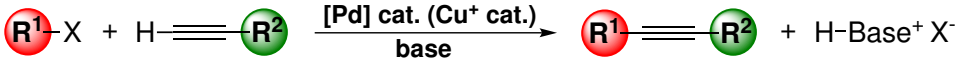

R^1 = aryl, hetaryl, alkenyl, alkyl, SiR_3
R^2 = aryl, hetaryl, vinyl
X = I, Br, Cl, OTf

Although the exact mechanism for the Sonogashira reaction is still at this moment not fully understood, it is generally supposed to occur via two coupled catalytic cycles (Figure 5.1): a *"Pd cycle"* and a *"Cu cycle"*. The former is the classical from C–C cross-coupling reactions (described in Chapter 1) and starts up with the oxidative addition of the organic electrophile R^1–X to the catalytically active species [Pd(0)] to yield a [Pd(II)] complex with two new metal-ligand bonds. At this point, the

next step in this cycle connects with the cycle of the copper co-catalyst (i.e. the Cu cycle). Unlike the Pd cycle, which is quite well understood, the Cu cycle, is poorly known. In particular, in this cycle, the base is believed to assist the copper acetylide formation through a π-alkyne copper complex, which would make the alkyne terminal proton more acidic. Once the copper acetylide is formed, then it would undergo transmetalation reaction with the [Pd(II)] complex generated in the Pd cycle resulting in the complex *cis*-[Pd(R^1)(acetylide)], which affords the final product and the regeneration of the catalytic species through a common reductive elimination.

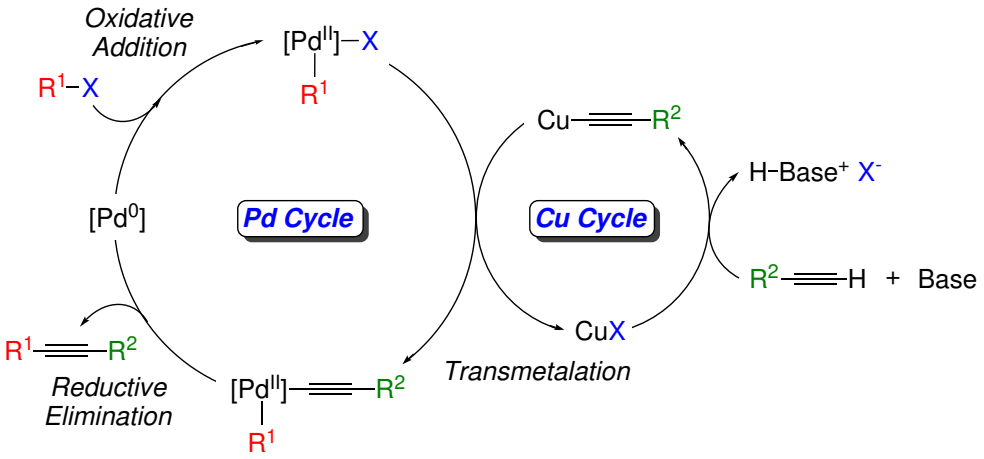

Figure 5.1: General reaction mechanism for the Pd-catalyzed Sonogashira reaction.

Hence, in principle, the presence of a copper(I) salt as co-catalyst in the typical Sonogashira reaction facilitates the reaction by the in situ generation of copper acetylide. However, the addition of this copper(I) salt under the reaction conditions entails some drawbacks,[240,241] mainly the induction of the so-called *Glaser-type* homocoupling of terminal alkynes that yields the corresponding diyne.[237,242] Aimed at suppressing the formation of this by-product, many efforts have been devoted to develop reaction procedures working in the absence of copper salts.[243–251] All these copper-free strategies are commonly known as *copper-free Sonogashira reaction*. Unfortunately, this copper-free variant usually requires the use of an excess of amine (often even acting as solvent), which proves detrimental to the environmental and economical advantages of this methodology. In order to avoid that, several modifications of the original Sonogashira reaction have been also recently reported including amine-free, ligand-free and solvent-free conditions.[252–262] These modifications, however, are based on assumptions about a hypothetical reaction mechanism since, as mentioned, very little is known about the mechanism of the Sonogashira reaction, specially for the copper-free variant.

As far as the reaction mechanism for the copper-free Sonogashira reaction is concerned, two different mechanisms have been proposed (Figure 5.2): the *deprotonation*[244] and *carbopalladation*[235] mechanisms. Both mechanisms share the initial oxidative addition of the organohalide R^1–X to the $[PdL_2(0)]$ complex giving the intermediate **1** and the subsequent ligand by alkyne substitution from this species, which results in the formation of complex **2**. At this point, the two reaction mechanisms differ in the next steps leading to the final coupled product. More specifically, in the case of the deprotonation mechanism (Figure 5.2, left), the deprotonation of the alkyne and the coordination of the ligand L take place from **2** yielding a square planar Pd complex with the two organic groups in *cis* disposition, from which the coupled product is expelled by reductive elimination. Alternatively, in the carbopalladation mechanism (Figure 5.2, right), complex **2** undergoes addition of the organic group R^1 to the terminal alkyne, followed by the coordination of the ligand L and subsequent base-mediated reductive elimination.

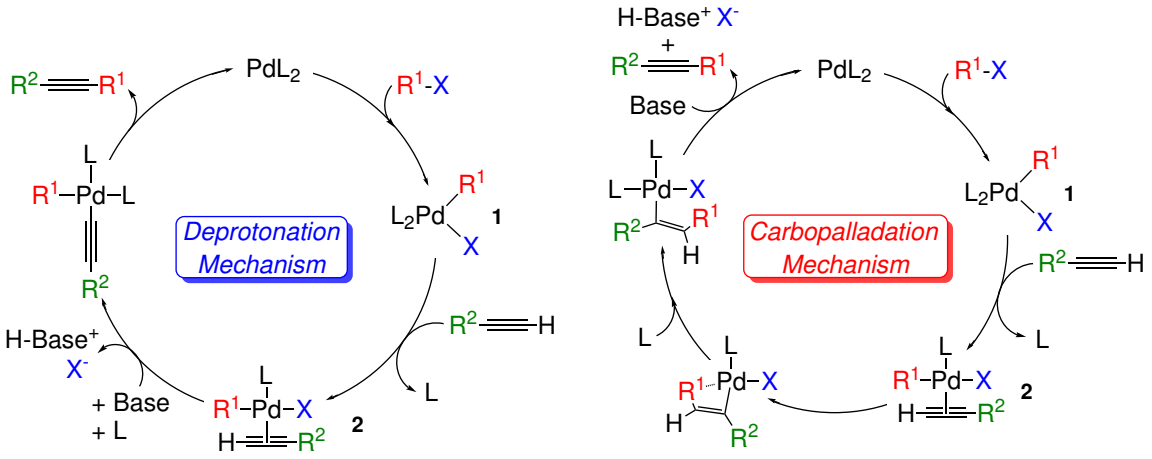

Figure 5.2: Proposed reaction mechanisms for the copper-free Sonogashira reaction: deprotonation[244] (left) and carbopalladation[235] (right) mechanisms.

Over the last years, these two mechanisms have been somewhat discussed in the literature, but the mechanism that operates in the copper-free Sonogashira reaction remains still unclear. In fact, up to date, the reported experimental and theoretical mechanistic studies on this process have been rather scarce. Among the experimental ones, one must mention the ones reported by Jutand et al.[263,264] and Mårtensson et al.[265] On the one hand, Jutand et al. by means of a thoughtful work shed light on the decelerating effect of alkynes in the oxidative addition step and suggested that amines might have multiple roles in the reaction mechanism. On the other hand, Mårtensson et al.[265] demonstrated with a simple though clever experiment, that the carbopal-

ladation mechanism can be discarded, and proposed two alternatives routes for the deprotonation pathway. These two variants of the deprotonation mechanism, labeled by the authors as *cationic* and *anionic mechanisms*, only differ in the order in which the steps in this mechanism occur (Figure 5.3). Thus, in the cationic mechanism (Figure 5.3, left), the L-for-X ligand substitution in **2** takes place first giving rise to the cationic Pd complex *cis*-$[Pd(R^1)(alkyne)(L)_2]^+$, which undergoes deprotonation of the alkyne by an external base and subsequent reductive elimination. In contrast, in the anionic mechanism (Figure 5.3, right), the deprotonation of the alkyne occurs first resulting in the anionic complex *cis*-$[Pd(R^1)(acetylide)(X)(L)]^-$, from which the L-for-X ligand substitution takes place followed by the reductive elimination step. According to Mårtensson et al.,[265] these cationic and anionic alternatives can be favored depending on the electronic nature of the substituents directly attached to the terminal alkynes. More specifically, the authors suggested that alkynes bearing electron withdrawing groups (*EWG*) may favor the anionic mechanism, whereas alkynes bearing electron donating groups (*EDG*) may favor the cationic pathway.

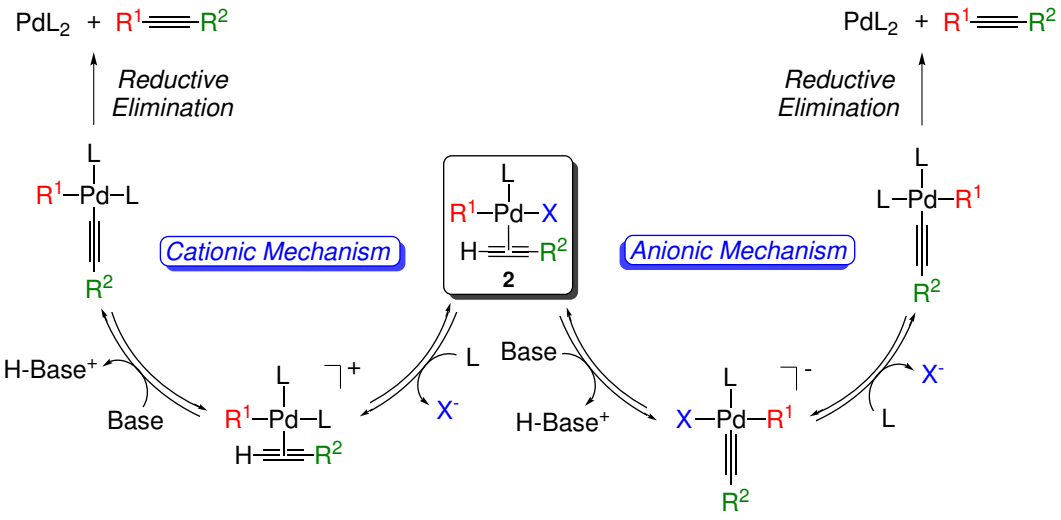

Figure 5.3: Cationic (left) and anionic (right) alternatives for the deprotonation mechanism.

As regards to the theoretical mechanistic studies on this copper-free variant, to the best of our knowledge, before we started our mechanistic study there was only the one reported by Chen et al.,[266] whereas the work of Sikk et al.[267] appeared during the revision process of our submitted article.[72] The former is on a model copper/base-free Sonogashira reaction in which the authors considered the halide (i.e. Br^-) as the species accepting the proton from the alkyne, while the latter is on a typical copper-free Sonogashira reaction but in which only a deprotonation-type

mechanism was analyzed. Thus, in spite of these works, the dichotomy between the carbopalladation and deprotonation mechanisms, as well as additional alternatives, remained still unsolved.

In view of this picture, we decided to carry out a theoretical study in order to gain a deeper understanding of the reaction mechanism for this process. In particular, the purpose of our work was to weigh up the reaction mechanisms proposed in the literature and possible alternative pathways using a general model of the typical Pd-catalyzed copper-free Sonogashira reaction. To this aim, we computed the Gibbs energy profiles of the different mechanistic proposals by means of *DFT* calculations. Additionally, we also analyzed the effect of the electronic nature of the alkyne's substituents over all the studied reaction pathways. This feature, in particular, was investigated for a set of substituents combining theory and experiments. This work was carried out in collaboration with the experimental group of Prof. Nájera at the Universidad de Alicante.

5.2 Computational details

All calculations in this study were performed at the *DFT* level, by means of the hybrid *B3LYP*[150,164] functional and using the *Gaussian03* program.[268] Pd and I atoms were described using the Stuttgart-Dresden (*SDD*) effective core potential[269] for the inner electrons and its associated double-ζ basis set for the outer ones. Additionally, for these atoms f-polarization (exponent 1.472)[270] and d-polarization (exponent = 0.289)[271] shells were added, respectively. In the case of I atoms diffuse functions were also added (exponent = 0.0308).[272] For the C, P, H atoms and the N atoms the 6-31G(d,p) and the 6-31+g(d) basis sets were used, respectively. We chose such computational level because it has been widely employed in theoretical studies on related cross-coupling reactions providing good results.[56,66,68,115,204,273,274]

All the structures of the reactants, intermediates and transition states were fully optimized without any symmetry constraint. Harmonic force constants were computed at the optimized geometries to characterize the stationary points as minima or saddle points. The latter were confirmed by having one imaginary frequency in the Hessian matrix and correlating the corresponding reactants and products. The entropic contributions were evaluated at a pressure of 382 atm following the argument in Martin's et al.[130] paper in order to model the changes in entropy for a condensed phase.

Solvent effects (i.e. dichloromethane, $\varepsilon = 8.930$) were introduced through single point calculations at optimized gas-phase geometries for all the minima and transition states by means of a continuum method, the *PCM* approach[195] implemented in

Gaussian03. Moreover, the default cavity model (i.e. *UA0*) was modified by adding individual spheres to the hydrogen atoms directly linked to the alkyne and to the nitrogen atom of the pyrrolidine molecule, using the keyword *"SPHEREONH"*.

Unless otherwise stated, all the energies shown throughout this chapter correspond to Gibbs energies in dichloromethane (ΔG_{DCM}) at 298 K, obtained by employing the following scheme:

$$\Delta G_{DCM} = \Delta E_{DCM} + (\Delta G_{gas} - \Delta E_{gas})$$

5.3 Selection of the model

In order to obtain a general overview on the process, we selected a set of model molecules for the analysis of the general reaction mechanism. Hence, phenylacetylene and iodobenzene species were selected as models for the coupling organic reactants, pyrrolidine as base, and dichloromethane (*DCM*) as solvent. On the other hand, for the additional analysis of the effect of the alkyne's substituents, several 4-substituted phenylacetylenes (R = H, CF_3, OMe, NMe_2) were considered (Scheme 5.2). As far as the catalyst is concerned, all the calculations were performed using $[Pd(PH_3)_2]$ as a model for the catalyst. Due to the increase of computational power, this model use to be considered too small, and catalysts with bigger phosphine ligands use to be calculated. Nevertheless, we chose this model in purpose for this study for the following reasons: *i)* as our group have recently shown, conformational diversity induced by bulky phosphine ligands may introduce significant errors in the calculations of the energy profiles (with modifications in energy barriers higher than 10 kcal·mol^{-1} depending on the phosphines);[275] *ii)* regarding the electronic properties of the phosphine, PH_3 can be considered as a neutral one; and *iii)* in terms of computational requirements it is by far the less demanding one.

Scheme 5.2: Copper-free Sonogashira reaction between several 4-substituted phenylacetylenes and iodobenzene.

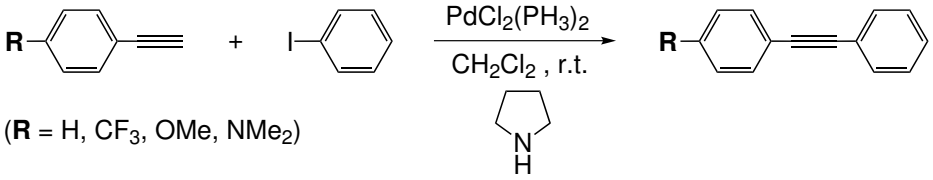

The main objective of our work was to map the potential energy surface by analyzing all the reasonable reaction profiles. Thus, in our opinion, this model covers most of the general features of the reaction system, apart from the steric effects that should be evaluated for each particular system studied.

5.4 The oxidative addition step

The first step in all the proposed mechanisms for the copper-free Sonogashira reaction corresponds to the oxidative addition of the organic halide R–X to the starting [Pd(0)] complex. This step, in particular, has been extensively studied (see Chapter 1) and is well known that in the case of organic iodides does not use to be rate-limiting. Even so, we decided to compute it for completeness. Hence, the oxidative addition of PhI to the complex $[Pd(PH_3)_2]$ was computed. The optimized structures for this process are shown in Figure 5.4.

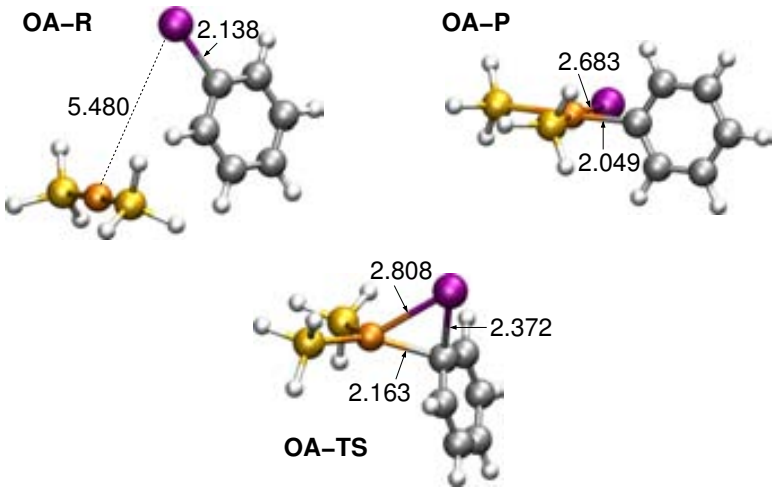

Figure 5.4: Optimized structures for the reactant (**OA-R**), product (**OA-R**), and transition state (**OA-R**) in the oxidative addition of PhI to $[Pd(PH_3)_2]$. Distances are shown in Å.

As expected for aryl iodides, the calculated energy barrier for the oxidative addition reaction was rather low (17.0 kcal·mol^{-1}) and involves the concerted formation of the Pd–I and P–C bonds, and the cleavage of the C–I bond through a three-center transition state (**OA-TS**). This transition state results in the oxidative addition product **OA-P**, which evolves to the more stable *trans* isomer through a cis-to-trans isomerization. This isomerization is known that may take place following different pathways,[66] but in any case it is an easy process.[276] Thus, we focused our further

analysis on the proposed mechanisms starting from the *trans*-[Pd(Ph)(I)(PH_3)$_2$] (**1**) complex.

5.5 The carbopalladation mechanism

Despite that Mårtensson et al.[265] experimentally showed that the carbopalladation mechanism can not be operative, in order to have a comprehensive mechanistic understanding of the reaction we decided to investigate this mechanism together with the deprotonation mechanism including their cationic and anionic alternatives (see below).

The theoretical investigation of the copper-free Sonogashira reaction with phenylacetylene as a model substrate (R = H) through a carbopalladation mechanism afforded the reaction profile shown in Figure 5.5.

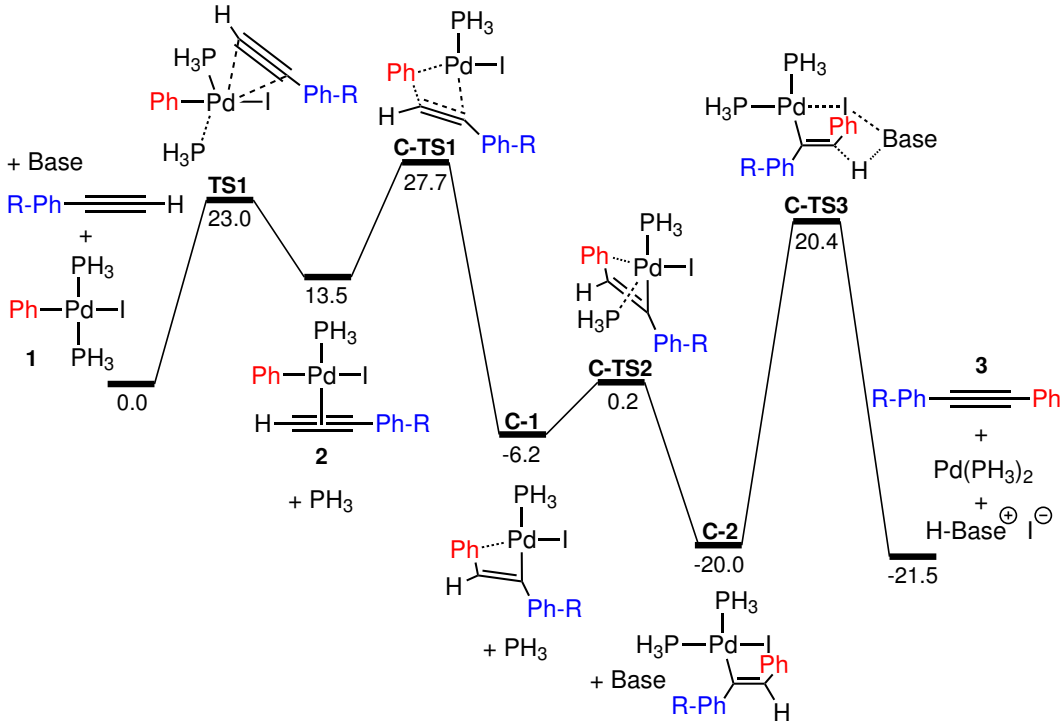

Figure 5.5: Gibbs energy profile in *DCM* (ΔG_{DCM}, kcal·mol^{-1}) at 298 K for the carbopalladation mechanism with R = H, and Base = pyrrolidine.

As previously mentioned, the carbopalladation and the deprotonation mechanisms share the initial substitution of a phosphine ligand by the alkyne, which leads

to the formation of a common intermediate (**2**). The calculation of this substitution via an associative substitution indicated that this is an endergonic process by 13.5 kcal·mol^{-1} with an energy barrier of 23.0 kcal·mol^{-1}. Once complex **2** is formed, the carbopalladation reaction occurs through the transition state **C-TS1** resulting in the intermediate **C-1** with a relative energy barrier of 14.2 kcal·mol^{-1}. Subsequently, this intermediate evolves with a low energy barrier (6.4 kcal·mol^{-1}) to the very stable intermediate **C-2** by coordination of a phosphine ligand via **C-TS2**. Finally, the alkenyl moiety in **C-2** is deprotonated by the external base through the transition state **C-TS3** yielding the final coupled product (**3**) and the regeneration of the catalytic species. This last step has the highest energy barrier in the overall energy profile (40.4 kcal·mol^{-1}), which can be attributed to the high stability of **C-2** and the difficult that entails the deprotonation of a double bond (high energy of **C-TS3**). The optimized structures for all the transition states involved in this mechanism are shown in Figure 5.6.

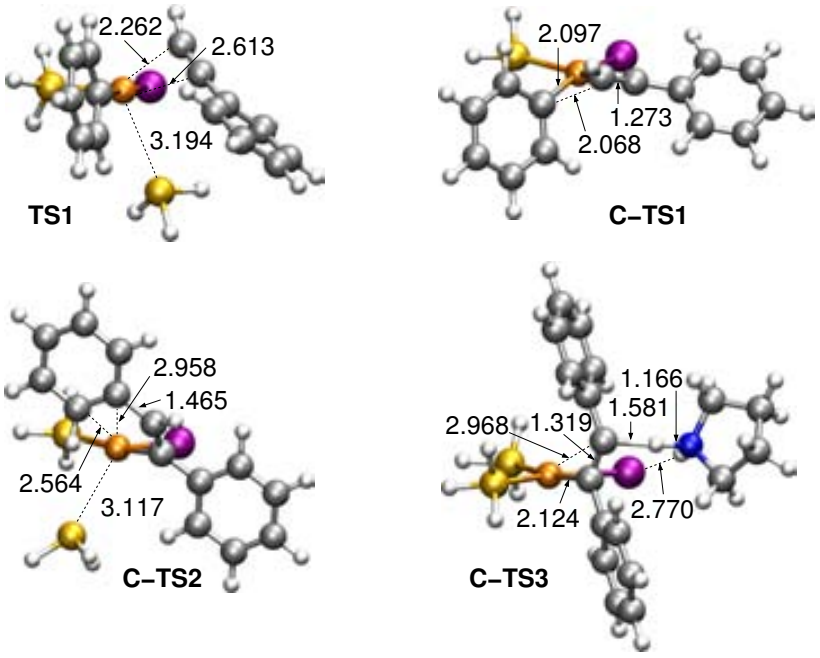

Figure 5.6: Optimized structures for the transition states involved in the carbopalladation mechanism with phenylacetylene (R = H). Distances are shown in Å.

Overall, the reaction is exergonic by 21.5 kcal·mol^{-1} but the carbopalladation mechanism has a very high energy barrier (40.4 kcal·mol^{-1}), which makes this mechanism very unlikely to be operating in the copper-free Sonogashira reaction. The occurrence of a very stable intermediate placed 20 kcal·mol^{-1} below reactants (i.e.

C-2) and the necessity of overcoming a barrier of about 40 kcal·mol^{-1} (energy from **C-2** to **C-TS3**) are responsible for the unsuitability of the carbopalladation mechanism. This theoretical finding for phenylacetylene (R = H) agrees with the experimental observation of Mårtensson et al.[265] that a complex analogous to **C-2** synthesized through an alternative route does not afford the coupled product under the Sonogashira reaction conditions.

With the carbopalladation reaction pathway established for phenylacetylene (R = H) and for the sake of completeness, the effect of the alkyne R substituent on the overall carbopalladation mechanism was next examined. With this purpose, the Gibbs energy profiles for the Sonogashira reaction with several 4-substituted phenylacetylenes (R = CF_3, OMe, NMe_2) through a carbopalladation mechanism were computed (Table 5.1).

Table 5.1: Relative Gibbs energies in *DCM* (ΔG_{DCM}, kcal·mol^{-1}) at 298 K for the carbopalladation mechanism with the different 4-substituted phenylacetylenes (R = H, CF_3, OMe, NMe_2).

	Substituent R			
Species	**H**	**CF_3**	**OMe**	**NMe_2**
1 + Base + alkyne	0.0	0.0	0.0	0.0
TS1	23.0	24.8	22.9	20.6
2 + PH_3	13.5	15.9	12.7	9.9
C-TS1	27.7	28.3	27.5	26.7
C-1	-6.2	-7.1	-5.7	-5.4
C-TS2	0.2	-1.8	0.2	-0.1
C-2	-20.0	-21.5	-19.5	-19.8
C-TS3	20.4	19.4	21.3	21.2
3 + $[Pd(PH_3)_2]$ + H-Base$^+$I$^-$	-21.5	-21.6	-21.3	-21.4

The results collected in Table 5.1 show that the influence of the substituent on the reaction energy is rather low: the reaction is highly exergonic with all the substituents by around 21 kcal·mol^{-1}. Moreover, the results also show that the most important effect of the different R groups is in the step common to all the different mechanisms, which is the coordination of the alkyne to the palladium complex **1** to yield complex **2**. The calculated energy barrier for this process (Table 5.1, **TS1**) decreases in the order: R = CF_3 > H > OMe > NMe_2, which correlates with the higher electron donor ability of the R groups, and consequently, with the higher donor ability of the alkyne. Furthermore, this higher donor ability of the alkyne with *EDGs* is responsible

for the higher stability of the corresponding complexes **2**, which feature shorter Pd–C_1 distances and higher Pd–C_1–C_2 angles with these substituents (Figure 5.7).

Similarly to the case with R = H, the deprotonation of the alkene moiety in **C-2** with the other R groups has the highest energy barrier in the overall reaction pathway, with values ranging from 40.4 to 41.0 kcal·mol^{-1} (Table 5.1). Thus, for these substituted phenylacetylenes we could also conclude that the carbopalladation mechanism is also too energy-demanding to be operative under the reaction conditions, which agrees again with the experimental findings of Mårtensson et al.[265]

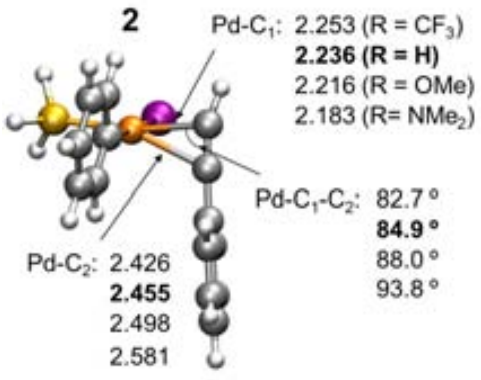

Figure 5.7: Optimized structure for intermediate **2** with phenylacetylene (R = H). Distances (shown in Å) and angles in complex **2** with the other R groups are also shown.

5.6 The deprotonation mechanism

With the carbopalladation mechanism ruled out as operative mechanism, the copper-free Sonogashira reaction through a deprotonation mechanism was next investigated. As commented in the introduction, for this mechanism two different alternatives have been proposed, namely the cationic and the anionic mechanisms (Figure 5.3).[265] This two mechanistic alternatives only differ in the order in which the steps in the deprotonation mechanism occur.

5.6.1 The cationic mechanism

The computed Gibbs energy profile for the copper-free Sonogashira reaction with phenylacetylene (R = H) through a cationic mechanism is shown in Figure 5.8.

Unlike the carbopalladation mechanism, once complex **2** is formed, the substitution of the iodide by the phosphine ligand takes place with a relative energy barrier of 14.0 kcal·mol^{-1} (**DC-TS1**) giving rise to the ion-pair formed between the cationic Pd complex and the iodide (**DC-1**). Then, from this species the deprotonation of the alkyne by the external base occurs (**DC-TS2**, 25.9 kcal·mol^{-1}) yielding the intermediate **RE-1**, where the two organic groups are in a *cis* configuration. Finally, **RE-1** undergoes reductive elimination via **RE-TS1** (17.9 kcal·mol^{-1}) resulting in the final product (**3**) and the regeneration of the catalytically active species. In the overall energy profile, the highest global energy barrier corresponds to the iodide-by-phosphine ligand substitution in **2** via **DC-TS1** (27.5 kcal·mol^{-1}). The optimized structures for the transition states involved in this mechanism are shown in Figure 5.9.

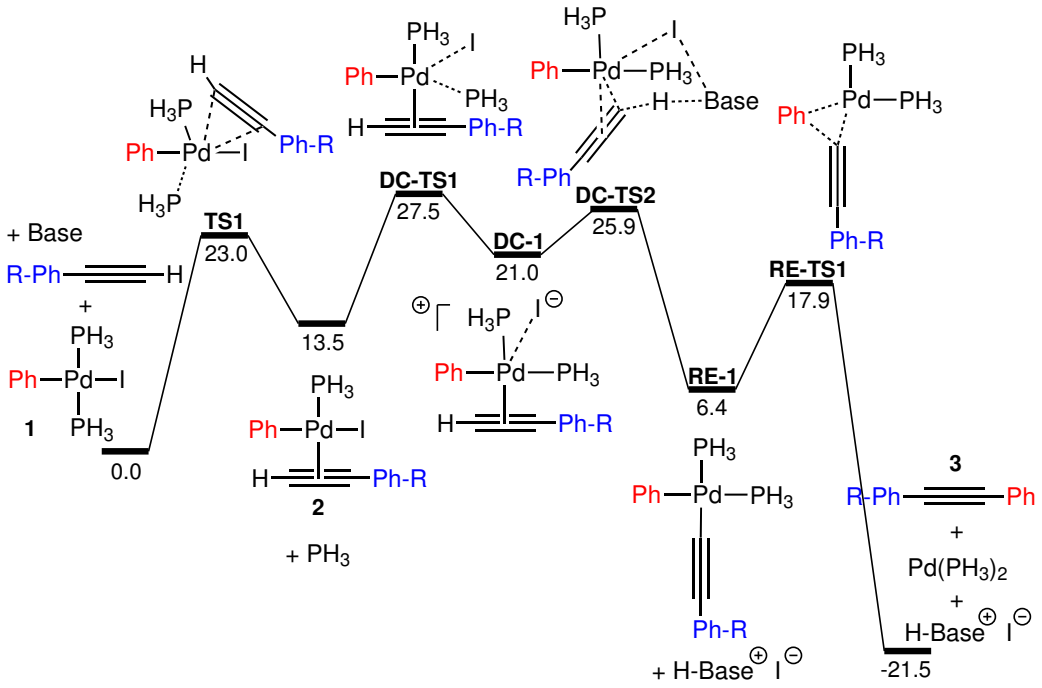

Figure 5.8: Gibbs energy profile in *DCM* (ΔG_{DCM}, kcal·mol^{-1}) at 298 K for the cationic mechanism with R = H, and Base = pyrrolidine.

Having established the cationic reaction pathway for the copper-free Sonogashira reaction with phenylacetylene (R = H), the effect of the alkyne R substituent on the overall cationic mechanism was next analyzed by computing the corresponding Gibbs energy profile for the other 4-substituted phenylacetylenes (R = CF_3, OMe, NMe_2). The relative Gibbs energies obtained with these 4-substituted phenylacetylenes are presented in Table 5.2. Interestingly, the energy of the transition state for the substi-

tution of the iodide by the phosphine ligand (**DC-TS1**) with the different R groups increases in the order: R = NMe_2 < OMe < H < CF_3. However, the relative energy barrier for this step (the energy difference between **DC-TS1** and **2**) is practically the same for all the R groups (the highest energy difference between the R groups is 0.8 kcal·mol^{-1}), which indicates that the different stability of intermediates **2** is responsible for the differences in the global energy barriers. On the other hand, Table 5.2 shows that the deprotonation of the alkyne in **DC-1** through **DC-TS2** follows a similar trend that the previous iodide-for-phosphine substitution step (i.e. R = NMe_2 < OMe < CF_3 < H). In this case, however, the differences in the relative energy barriers (the energy difference between **DC-TS2** and **DC-1**) between the different R groups is slightly higher (the lowest energy difference between the R groups is 1.5 kcal·mol^{-1}). More specifically, the relative energy barriers for the deprotonation step increase in the following order: CF_3 < OMe ≈ H < NMe_2. This trend can be rationalized as follows: the presence of a *EWG* (i.e. R = CF_3) in the alkyne makes its proton more acidic and thus, the relative energy barrier for this step decreases. Conversely, the presence of an *EDG* (i.e. R = NMe_2) makes the proton of the alkyne less acidic, which increases the relative energy barrier. The cases with the model substituent (i.e. R = H) and the moderate *EDG* (i.e. R = OMe) have similar energy barriers and lie in between the other R groups.

Table 5.2: Relative Gibbs energies in *DCM* (ΔG_{DCM}, kcal·mol^{-1}) at 298 K for the cationic mechanism with the different 4-substituted phenylacetylenes (R = H, CF_3, OMe, NMe_2).

	Substituent R			
Species	**H**	**CF_3**	**OMe**	**NMe_2**
1 + Base + alkyne	0.0	0.0	0.0	0.0
TS1	23.0	24.8	22.9	20.6
2 + PH_3	13.5	15.9	12.7	9.9
DC-TS1	27.5	29.1	26.4	23.7
DC-1	21.0	22.2	20.6	16.1
DC-TS2	25.9	25.5	25.3	21.5
RE-1	6.4	4.3	7.1	6.8
RE-TS1	17.9	15.5	18.8	18.8
3 + $[Pd(PH_3)_2]$ + H-Base$^+I^-$	-21.5	-21.6	-21.3	-21.4

Similarly to the reaction with phenylacetylene (R = H), the highest energy point in the overall energy profile corresponds to the substitution of the iodide by the

phosphine ligand (**DC-TS1**) regardless of the R groups; therefore, this step has also the highest energy barrier for all the R groups. Furthermore, these energy barriers are lower for *EDGs* than for *EWGs*, indicating that the more *EDG* the faster the process via this cationic mechanism should be.

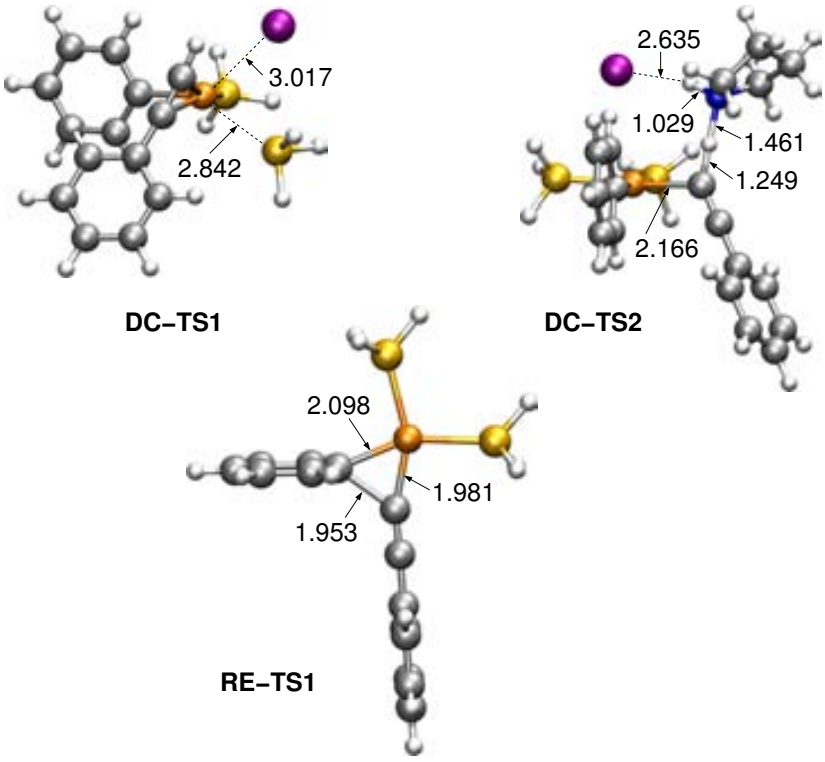

Figure 5.9: Optimized structures for the transition states involved in the cationic mechanism with phenylacetylene (R = H). Distances are shown in Å.

5.6.2 The anionic mechanism

As above stated, in the anionic mechanism the steps of the deprotonation mechanism take place in reverse order than in the cationic mechanism (Figure 5.8). Thus, in the anionic mechanism the deprotonation of the alkyne by the external base in complex **2** occurs first, followed by the iodide-for-phosphine substitution. The Gibbs energy profile obtained for the copper-free Sonogashira reaction with phenylacetylene (R = H) through the anionic mechanism is shown in Figure 5.10.

The deprotonation of the alkyne by the external base in complex **2** occurs through the transition state **DA-TS1** (23.0 kcal·mol^{-1}) and leads to the formation of the

ion-pair (**DA-1**) formed between the anionic Pd complex and the protonated base. Subsequently, this species evolves to the next intermediate, **RE-1**, by a iodide-by-phosphine substitution via the transition state **DA-TS2** with a relative energy barrier of 13.1 kcal·mol^{-1}. Finally, **RE-1** undergoes reductive elimination giving rise to the coupled product and regenerating the catalytic species. The optimized structures for the transition states involved in this mechanism are shown in Figure 5.11.

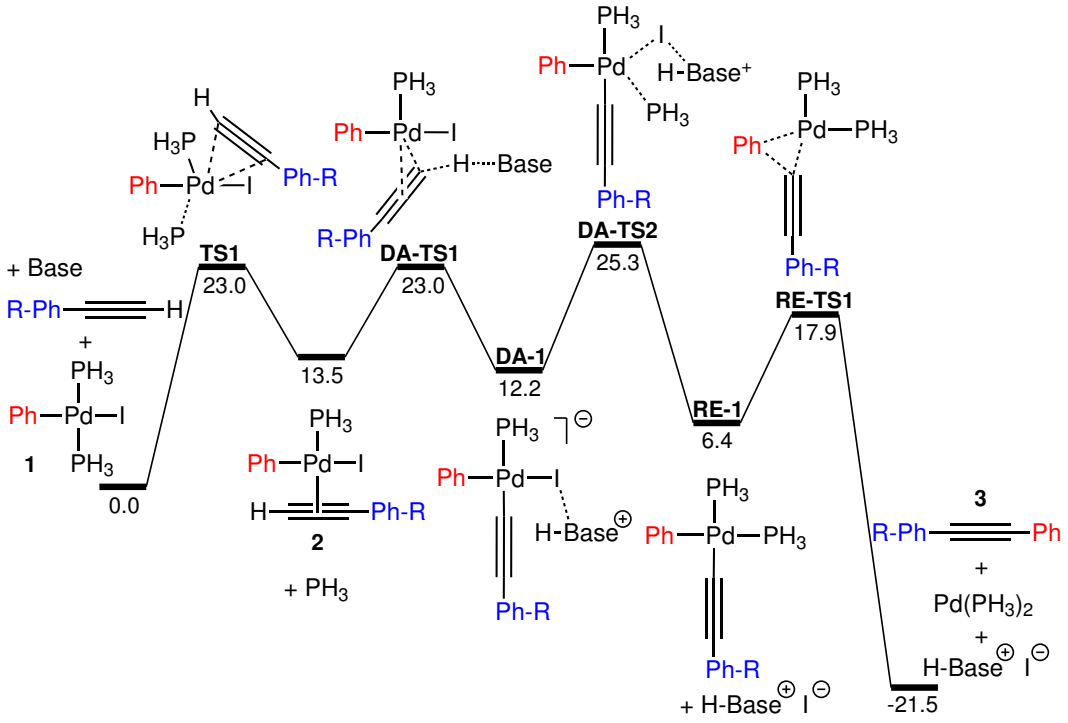

Figure 5.10: Gibbs energy profile in *DCM* (ΔG_{DCM}, kcal·mol^{-1}) at 298 K for the anionic mechanism with R = H, and Base = pyrrolidine.

Overall, the substitution of the iodide by the phosphine ligand in **DA-1** through the transition state **DA-TS2** has a global energy barrier 2.3 kcal·mol^{-1} higher than the previous transition states (**TS1** and **DA-TS1**) and 7.4 kcal·mol^{-1} higher than the next transition state (**RE-TS1**). Therefore, the highest energy point in the anionic mechanism is **DA-TS2**. Interestingly, the energy of this transition state, is a bit lower than the highest energy barrier in the cationic mechanism (**DC-TS1**, Figure 5.8), which means that, for phenylacetylene (R = H), the anionic mechanism is favored.

With the anionic reaction pathway established for phenylacetylene (R = H), we next examined the effect of the alkyne R substituent on the overall anionic mechanism

by computing the corresponding Gibbs energy profile for the other 4-substituted phenylacetylenes (R = CF_3, OMe, NMe_2). The relative Gibbs energies obtained with these 4-substituted phenylacetylenes are collected in Table 5.3.

Table 5.3: Relative Gibbs energies in *DCM* (ΔG_{DCM}, kcal·mol^{-1}) at 298 K for the anionic mechanism with the different 4-substituted phenylacetylenes (R = H, CF_3, OMe, NMe_2).

	Substituent R			
Species	**H**	**CF_3**	**OMe**	**NMe_2**
1 + Base + alkyne	0.0	0.0	0.0	0.0
TS1	23.0	24.8	22.9	20.6
2 + PH_3	13.5	15.9	12.7	9.9
DA-TS1	23.0	23.1	22.3	19.3
DA-1	12.2	10.8	12.3	12.5
DA-TS2	25.3	24.6	25.8	25.6
RE-1	6.4	4.3	7.1	6.8
RE-TS1	17.9	15.5	18.8	18.8
3 + $[Pd(PH_3)_2]$ + H-Base$^+I^-$	-21.5	-21.6	-21.3	-21.4

Similarly to phenylacetylene (R = H), the highest energy barrier with the other 4-substituted phenylacetylenes corresponds to the substitution of the iodide by the phosphine ligand via **DA-TS2**. Moreover, the small energy differences between the different transition states **DA-TS2** (all of them within 1 kcal·mol^{-1}) suggest that the electronic nature of the alkyne R substituent does not have a significant effect on the reaction rates through this mechanism.

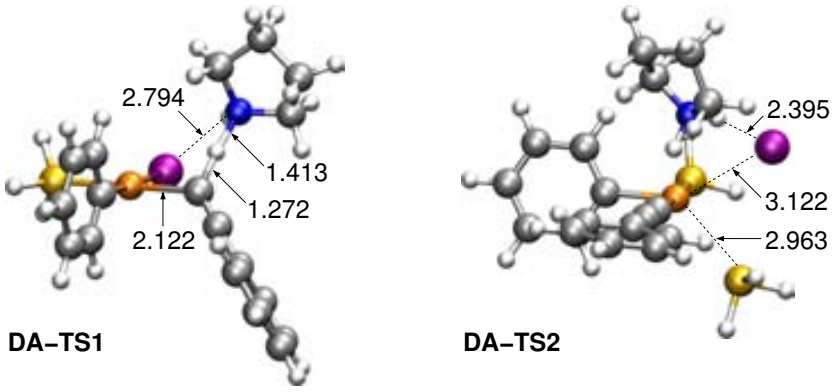

Figure 5.11: Optimized structures for the transition states involved in the anionic mechanism with phenylacetylene (R = H). Distances are shown in Å.

5.6.3 Cationic mechanism vs. anionic mechanism

According to calculations, the highest energy barrier in both cationic and anionic mechanisms corresponds to the substitution of the iodide by the phosphine ligand. However, depending on the mechanism this substitution takes place before (i.e. in the cationic mechanism) or after (i.e. in the anionic mechanism) the deprotonation of the alkyne. In particular, in the case of the cationic mechanism this substitution occurs in complex **2** via **DC-TS1** (Figure 5.8), whereas in the anionic mechanism it takes place in **DA-1** via **DA-TS2** (Figure 5.10). The computed global Gibbs energy barriers for these processes with all the 4-substituted phenylacetylenes (Table 5.4) indicate that both mechanisms are feasible. Importantly, these values also suggest that depending on the electronic nature of the R substituent there might be a change in the reaction mechanism. More specifically, the highly electron withdrawing group R = CF_3 and the model substituent R = H, favor the anionic mechanism compared to the cationic mechanism by 4.5 and 2.2 kcal·mol^{-1}, respectively. On the other hand, with the moderate electron donating group R = OMe this energy difference becomes smaller (0.6 kcal·mol^{-1}) but still in favor of the anionic mechanism. Finally, with the highly electron donating group R = NMe_2 this energy difference is reversed favoring the cationic mechanism by 1.9 kcal·mol^{-1}.

This predicted change in the reaction mechanism can be rationalized as follows: the first step in the cationic mechanism yields intermediate **2** (Figure 5.8). As previously stated, in the case of *EWGs* (i.e. R = CF_3, H) or moderate *EDGs* (i.e. R = OMe) this species is less stable than with highly *EDGs* (i.e. R = NMe_2) (the energy difference range from 2.8 kcal·mol^{-1} to 6.0 kcal·mol^{-1}). Thus, *EWGs* groups cause higher energy barriers because the following iodide-by-phosphine substitution step

Table 5.4: Global Gibbs energy barriers in *DCM* (ΔG_{DCM}, kcal·mol^{-1}) at 298 K for the cationic and anionic mechanisms with the different 4-substituted phenylacetylenes (R = H, CF_3, OMe, NMe_2).

	Global Gibbs energy barriers[a]	
Substituent R	**Cationic mechanism**	**Anionic mechanism**
CF_3	29.1	**24.6**
H	27.5	**25.3**
OMe	26.4	**25.8**
NMe_2	**23.7**	25.6

[a] The Gibbs energy barriers for the lowest-energy deprotonation pathways with the different R groups are shown in bold.

has a very similar relative energy barrier for all the R groups. In contrast, the first step in the anionic mechanism gives the intermediate **DA-1** (Figure 5.10). In this case, the anionic charge on the Pd complex is better stabilized with *EWGs*, which offsets the energy gain in complex **2** with the highly *EDGs* and leads to lower energy barriers compared to the cationic mechanism. This results in a preference for the anionic mechanism with *EWGs* (i. e. R = CF_3, H) or moderate *EDGs* (i.e. R = OMe) and a preference for the cationic mechanism with highly *EDGs* (i.e. R = NMe_2).

5.7 An alternative mechanism: the ionic mechanism

While carrying out this mechanistic study on the copper-free Sonogashira reaction, we reported the combined experimental and theoretical study on the transmetalation step in the Negishi cross-coupling reaction[71] that has been described in Chapter 4. Therein, we demonstrated that an external coordinating ligand (i.e. $PMePh_2$, THF) can easily replace the chlorine from the complex *trans*-[PdMeCl($PMePh_2$)$_2$] (complex analogous to **1**) through a mechanism that we dubbed as ionic mechanism (**Figures 4.17 and 4.19**). Based on these results and based on the fact that the coordination of the alkyne in the copper-free Sonogashira reaction requires a considerably high energy barrier (higher than 20 kcal·mol^{-1}), we decided to compute a mechanism analogous to that ionic mechanism for the copper-free Sonogashira reaction. We labeled this mechanism as *ionic mechanism* owing to its similarities with the one reported for the Negishi coupling.[71] The computed Gibbs energy reaction profile via this mechanism with phenylacetylene (R = H) is shown in Figure 5.12.

Unlike the cationic and anionic mechanisms, where the iodide is always expelled after the coordination of the alkyne, in the ionic mechanism it is replaced by the base in the first step. This process occurs through the transition state **I-TS1** and results in the formation of the cationic Pd complex **I-1**. Importantly, the energy barrier required for this process is 15.3 kcal·mol^{-1}, which is much lower (it is at least 5 kcal·mol^{-1} lower) than the energy required for the coordination of the alkyne to **1** via **TS1** (Figure 5.10). At this point, and based on the fact that the reaction is usually carried out with a large excess of base, we considered that the corresponding phenylacetylide may be present in solution as a result of the acid-base reaction. According to calculations, the phenylacetylide can replace one of the phosphine ligands in **I-1** through a barrier-less process.[†] This substitution without barrier yields the nearly isoenergetic species **RE-2**, which directly evolves to the desired alkyne (**3**) by common reductive elimination via **RE-TS2** (22.1 kcal·mol^{-1}). The optimized structures of the transition states involved in this ionic mechanism are shown in Figure 5.13.

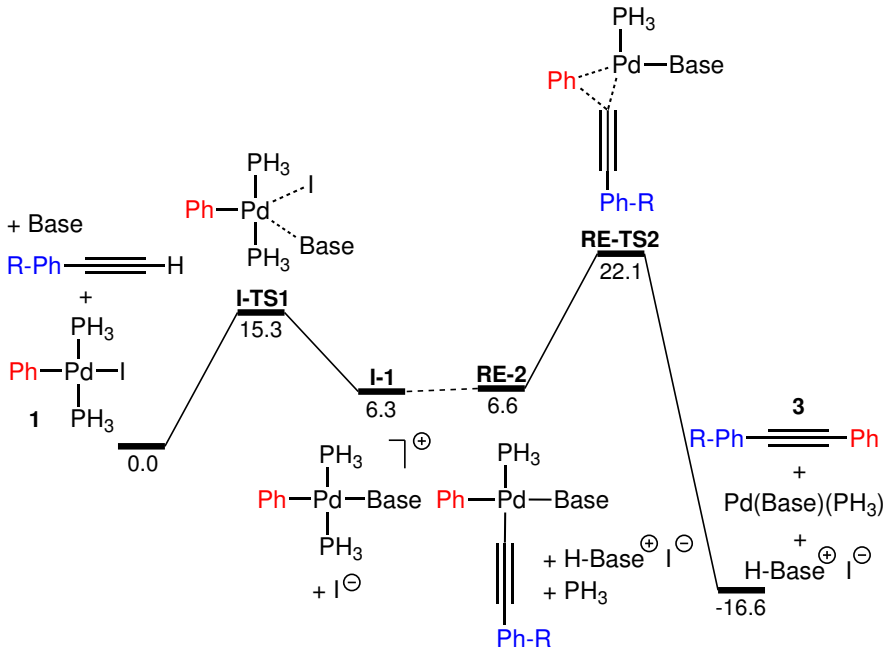

Figure 5.12: Gibbs energy profile in *DCM* (ΔG_{DCM}, kcal·mol^{-1}) at 298 K for the ionic mechanism with R = H, and Base = pyrrolidine.

Overall, the reaction through this ionic mechanism is exergonic by 16.6 kcal·mol^{-1}.

[†]This was confirmed by optimizing the full system in dichloromethane starting with the phenylacetylene at 4 Å far from the cationic complex **I-1**.

The step with the highest energy barrier corresponds to the reductive elimination step from complex **RE-2** via **RE-TS2** with an energy of 22.1 kcal·mol^{-1}. This energy barrier is lower than the ones found for the cationic and anionic mechanism, which suggests that this mechanism, in principle, should be favored. However, we have to take into account that this ionic mechanism depends on the concentration of the phenylacetylide present in solution, which is also directly linked to the concentration of the base. On this issue, the theoretical calculation of the *TOF* using the scheme developed by Kozuch et al. and by means of the *AUTOF* program[8–10] showed that the ratio between the anionic and the ionic mechanisms with phenylacetylene (R = H) is 2:1, thus indicating that both mechanisms are competitive.

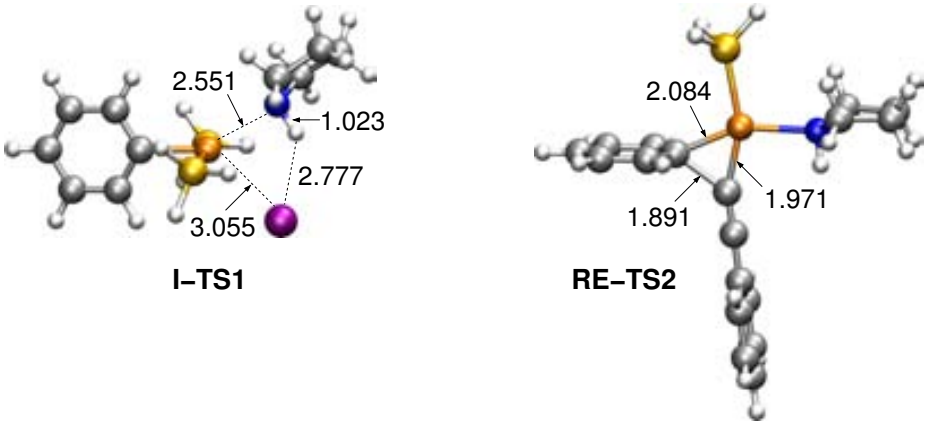

Figure 5.13: Optimized structures for the transition states involved in the ionic mechanism with phenylacetylene (R = H). Distances are shown in Å.

As for the other analyzed mechanisms, after having established this ionic reaction pathway for phenylacetylene (R = H), we next examined the effect of the alkyne R substituent on the overall ionic mechanism. The relative Gibbs energies obtained in the computed Gibbs energy profiles with the other 4-substituted phenylacetylenes (R = CF_3, OMe, NMe_2) are presented in Table 5.5.

As shown in Table 5.5, for all the R substituents the highest energy barrier corresponds to the reductive elimination step through the transition state **RE-TS2**. The calculated energy barriers for this process with the different R groups rank from 18.5 (R = CF_3) to 22.6 kcal·mol^{-1} (R = OMe), which indicates that this ionic mechanism might be competitive with the cationic and anionic mechanisms. As above mentioned, the reaction rate through this ionic mechanism depends on the concentration of acetylide present in solution, which in turn depends on the concentration of the base. In other words, this mechanism depends on the base[†] and the acidity of the

[†]The 2:1 ratio between base and alkyne molecules in this ionic mechanism is compatible with

Table 5.5: Relative Gibbs energies in *DCM* (ΔG_{DCM}, kcal·mol^{-1}) at 298 K for the ionic mechanism with the different 4-substituted phenylacetylenes (R = H, CF_3, OMe, NMe_2).

	Substituent R			
Species	**H**	**CF_3**	**OMe**	**NMe_2**
1 + Base + alkyne	0.0	0.0	0.0	0.0
I-TS1	15.3	15.3	15.3	15.3
I-1	6.3	6.3	6.3	6.3
RE-2	6.6	3.5	6.0	6.4
RE-TS2	22.1	18.5	22.6	21.8
3 + [Pd(Base)(PH_3)] + H-Base$^+$I$^-$	-16.6	-16.7	-16.4	-16.5

terminal alkyne proton, which at the same time depends on the electron withdrawing ability of the alkyne R substituent. Thus, the reaction through this mechanism is expected to be faster when alkynes bearing *EWGs* are used.

5.8 The effect of the alkyne R substituent from experiments

The theoretical calculations presented so far, demonstrated that the carbopalladation mechanism is not operating under the reaction conditions. Furthermore, calculations also showed that the other three investigated mechanisms (i.e. cationic, anionic and ionic mechanisms) may have competitive rates. Thus, a change on the reaction conditions (i.e. solvent, ligands, substrates, base, etc.) might favor one or another mechanism.

Regarding the effect of the alkyne R substituent on the analyzed mechanisms, theoretical results showed relatively small energy differences in the highest Gibbs energy barriers with the different 4-substituted phenylacetylenes (Tables 5.4 and 5.5). Thus, we decided, in collaboration with the group of Prof. Nájera, to carry out experimental copper-free Sonogashira reactions of 1-fluoro-4-iodobenzene with the 4-substituted phenylacetylenes used for the computational study for comparison. These couplings were performed in dichloromethane with $PdCl_2(PPh_3)_2$ (2 mol%) as catalyst, pyrro-

the common reaction conditions, where an excess of base is frequently added.

lidine (6 eq.) as base, and at room temperature and under Ar atmosphere.[†] Then, for these reactions, the values of conversion (%) of the desired alkyne **3** versus time were obtained by monitoring the reactions by ^{19}F NMR spectroscopy (Figure 5.14).

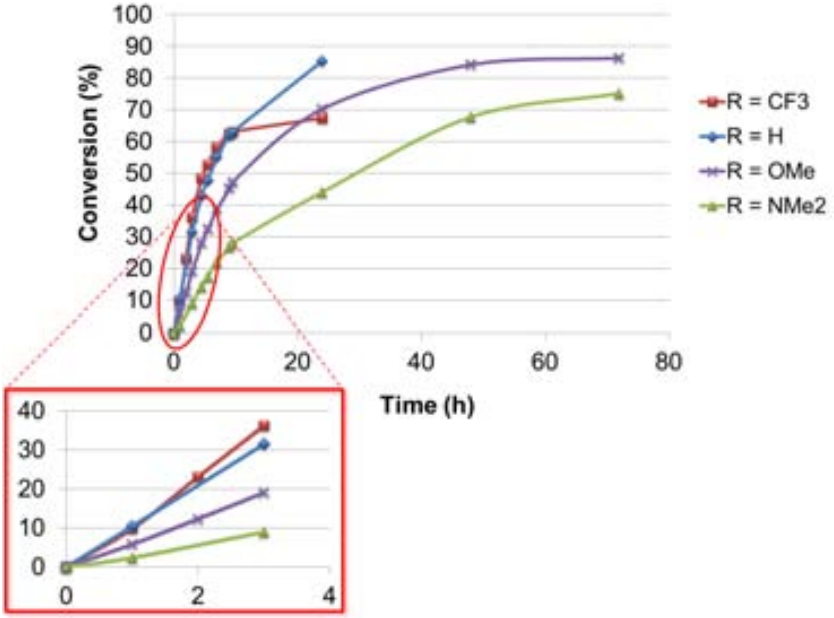

Figure 5.14: Conversion/time data, obtained by ^{19}F NMR, for the Sonogashira reaction with the analyzed 4-substituted phenylacetylenes (R = H, CF_3, OMe, NMe_2).

According to the conversion/time data plotted in Figure 5.14 the reaction rate increases with the electron withdrawing ability of the R group ($R = NMe_2 < OMe < H \approx CF_3$). Therefore, the more acidic the terminal alkyne proton is, the higher the reaction rate is; this experimental trend is supported by the ionic mechanism. Notice, however, that if we compare the ratio of conversion of **3** after 1h for the fastest (R = CF_3 or H) and the slowest ($R = NMe_2$) reaction, it is about 4:1. This ratio in terms of activation energies corresponds to an energy difference lower than 1 kcal·mol^{-1}, which means that the activation energies for the copper-free Sonogashira reactions with the different 4-substituted phenylacetylenes are very similar, in agreement with theoretical calculations. In view of these results, there is not a clear preference for either the deprotonation or the ionic mechanism. Hence, the precise mechanism for a coupling reaction needs to be evaluated in detail for each particular case, and competitive mechanisms make take place together. The analysis on a model system for the Suzuki cross-coupling reaction gave rise to similar conclusions regarding the

[†]For further details on the experimental reaction conditions, see Article III in Appendix A.

operative reaction mechanism.[66]

5.9 Conclusions

In the study presented in this chapter, the reaction mechanism for the model copper-free Sonogashira reaction between iodobenzene and several 4-substituted phenylacetylenes (R = H, CF_3, OMe, NMe_2) was investigated by means of *DFT* calculations. Importantly, to the best of our knowledge, this study was the first theoretical study that investigated all the reported mechanistic proposals for the copper-free Sonogashira reaction.

The theoretical results on the carbopalladation mechanism showed that this pathway has a very high energy barrier, which indicated that this mechanism could not be operating under the reaction conditions. On the other hand, the calculated Gibbs energy barriers for the cationic and anionic alternatives proposed for the deprotonation mechanism,[265] revealed that both alternatives are feasible. Moreover, calculations predicted that one or the other reaction mechanism may be favored depending on the electronic nature of the alkyne R substituent. Thus, *EWGs* (R = CF_3, H) or moderate *EDGs* (R = OMe) may favor the anionic mechanism, whereas highly *EDGs* (R = NMe_2) may favor the cationic mechanism. These predicted differences can be attributed to the different stability of the intermediates that precede the highest energy barrier, which depends on the R substituent. These results are in agreement with the reported experimental work of Mårtensson et al.[265]

This study also demonstrated that the presence of an excess of a coordinating ligand like pyrrolidine, the base, and the presence of phenylacetylide opens a new reaction pathway for the copper-free Sonogashira reaction: the ionic mechanism. This mechanism involves that the base substitutes the halide and helps forming the acetylide species. The theoretical results for this mechanism showed that it is competitive with the analyzed cationic and anionic mechanisms and that it may lead to higher reaction rates with terminal alkynes bearing *EWGs*, which agreed with our experiments.

In summary, this study revealed that in the copper-free Sonogashira reaction, like in other cross-coupling reactions (i.e. Stille, Negishi), there are several reaction pathways that may have competitive rates and a change on the reaction conditions (e.g. solvent, ligands, substrates, base) might favor one over the other ones. Thus, the general conclusion that we can draw from this study is that a detailed study of a particular copper-free Sonogashira reaction is required to assess which of the herein analyzed mechanisms is favored. This study of a general model of Pd-catalyzed copper-free Sonogashira reaction mapped out the reaction scenario, and showed the

complexity of this process.

"In order to succeed you must fail, so that you know what not to do the next time."

Anthony J. D'Angelo

6

An asymmetric Suzuki-Miyaura reaction mechanism

6.1 Introduction

The Suzuki-Miyaura reaction, commonly known simply as Suzuki coupling, is one of the most practiced types of C–C cross-coupling reactions. This reaction is generally catalyzed by Pd complexes and consists in the carbon-carbon bond formation between an organic halide (or triflate), R^1–X, and an organoboron compound, R^2–BY_2, in the presence of a base (Scheme 6.1).[13,14,23,24,277] The advantages of this reaction are numerous, such as the ready availability of reactants, the tolerance of a broad range of functional groups, the mild reaction conditions and high product yields, the low toxicity, etc. Consequently, the Suzuki-Miyaura coupling has been actively used not only in academic laboratories but also in industrial processes such as the large-scale synthesis of pharmaceuticals, natural products and fine chemicals.[31,278–282]

Scheme 6.1: General scheme for Pd-catalyzed Suzuki cross-coupling reaction.

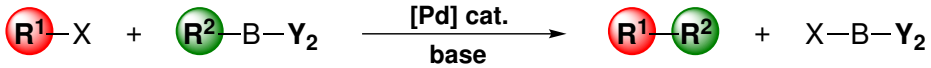

R^1, R^2 = aryl, vinyl, alkyl
X = I, Br, Cl, OTf

As the rest of cross-coupling reactions, the Suzuki-Miyaura reaction mechanism consists in three general steps: oxidative addition, transmetalation, and reductive elimination. Unlike the former and the latter that are common to all cross-coupling reactions, the transmetalation is particular of this reaction as this is the step in which the organoboron compound actively participates. Thus, it is not surprising that since the discovery of the Suzuki-Miyaura coupling in 1979,[23] many efforts have been devoted to fully understand the mechanism of this singular step. For this process, two reaction pathways involving the required base have been proposed (Figure 6.1): one consisting in the coordination of the base to the organoboron compound to form the organoboronate species, which undergoes nucleophilic attack on a palladium halide complex (pathway A, Figure 6.1), and other consisting in the base-for-halide substitution in the coordination sphere of the catalyst and the subsequent reaction with a neutral organoboron compound (Figure 6.1, pathway B). Aimed at elucidating which of these two pathways is favored, both mechanisms were theoretically investigated by our group for a model Suzuki-Miyaura reaction using *trans*-[$Pd(CH_2{=}CH)(Br)(PH_3)_2$], $CH_2{=}CH\text{-}B(OH)_2$ and OH^- species as reactants.[65] The results derived from this study indicated that the pathway involving the organoboronate species (i.e. pathway A) is the most plausible one.

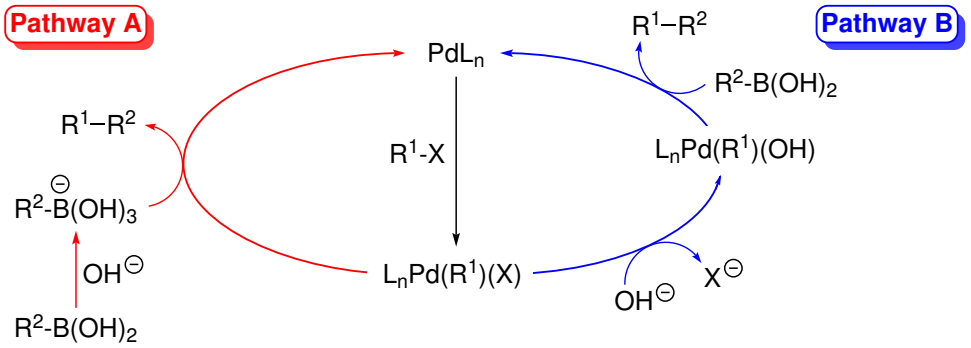

Figure 6.1: Example for the proposed reaction pathways for the transmetalation step in the Suzuki-Miyaura cross-coupling reaction.

Thereafter, the transmetalation reaction has been generally taken for granted to go through the pathway A and, consequently, considered in further mechanistic studies on related Suzuki-Miyaura reactions.[60,66,275,283,284] The transmetalation via this pathway takes place in three steps (Figure 6.2): first, the organoboronate species (generated by the reaction of the boronic acid with the base) replaces the halide in the coordination sphere of the Pd complex **S-1** (formed after the oxidative addition step) through the transition state **S-TS1**; subsequently, the resulting intermediate **S-3** undergoes intramolecular substitution of the OH ligand by the vinyl moiety via **S-TS2**, giving rise to the last intermediate **S-4**; and finally, this species evolves to the final products *trans*-[Pd(CH_2=CH)$_2$(PH_3)$_2$] (**S-5**) and B(OH)$_3$ by the concerted cleavage of the B–C bond and the coordination of the vinyl group to Pd through a single carbon atom (**S-TS3**).[†]

Very recently, however, the proposal of the pathway A as the most plausible mechanism for transmetalation has been questioned with the appearance of a kinetic study of Hartwig et al.[206] In particular, the results reported therein demonstrated that under typical Suzuki-Miyaura reaction conditions of weak base and aqueous solvent mixtures, the transmetalation process involves a palladium hydroxo complex and a neutral organoboron compound (pathway B, Figure 6.1), rather than a palladium halide complex and the organoboronate species (pathway A, Figure 6.1). The authors came to this conclusion based on the following experimental observations: *i)* the populations of palladium halide and palladium hydroxo complex were found to be similar to each other; *ii)* the populations of organoboron reagent and the corresponding organoboronate species resulted to be similar to each other in the presence

[†]The theoretical results obtained with this model system remained qualitatively valid when the PH_3 ligands and the vinyl groups were replaced by the commonly used PPh_3 ligands and phenyl groups,[67] respectively. Importantly, in the transmetalation with phenyl groups, the reaction from **S-3** was found to take place in one transition state instead of in two (i.e. **S-TS2** and **S-TS3**).

of water and bases of the strength of carbonates; and *iii)* the calculated rate for the reaction of the hydroxo complex with the neutral organoboron compound was several orders of magnitude faster than that for the reaction of halide complexes with the organoboronate species.

It should be noted, however, that the transmetalation reaction via the two proposed mechanisms (i.e. pathways A and B) leads to the formation of the same reaction intermediate (**S-3**, Figure 6.2). Thus, assuming that this species precedes the step with the highest energy barrier (**S-TS3**, Figure 6.2), it follows that the mechanism through which **S-3** is formed can be considered, to some extent, to be irrelevant.[†]

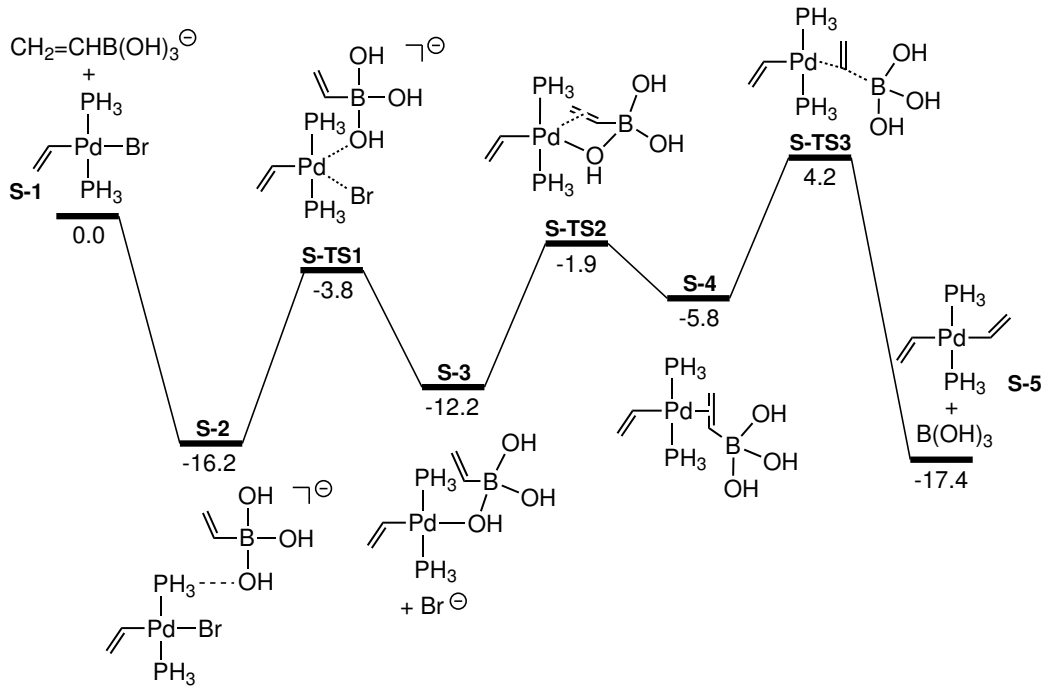

Figure 6.2: Energy profile for the transmetalation of *trans*-[Pd(CH_2=CH)$_2$(PH_3)$_2$] (**S-5**) with CH_2=CH-B(OH)$_2$ via the pathway A.[65]

Similarly to other cross-coupling reactions,[273,285,286] the steric and electronic effects induced by the ancillary ligands bound to the Pd catalyst on the Suzuki-Miyaura reaction has been one of the topics that has drawn more attention during the last years.[99] This interest mainly emerged from the improved efficiency and selectivity observed in Suzuki-Miyaura reactions with Pd catalysts possessing bulky and

[†]As we will see later, this was assumed in the asymmetric Suzuki-Miyaura reaction investigated in this thesis.

electron-rich phosphine ligands.[287] As commented in Chapter 1, the enhanced reactivity with this type of ligands is generally attributed to a combination of their electronic and steric properties that favor the stabilization of mono-ligated [PdL] intermediates, which are believed to actively participate in the catalytic cycle.[288,289] Consequently, the effect of the ligands coordinated to the Pd catalyst on the Suzuki-Miyaura reaction has been extensively investigated in the last years by several groups, including ours.†[66,79,290–292]

On the other hand, ligands bound to Pd catalysts are also of considerable importance because they can promote asymmetric catalytic transformations. In fact, one of the recent and growing interests in the Suzuki-Miyaura reaction has been the development of asymmetric versions for this reaction. In this context, the synthesis of axially chiral biaryls has attracted significant attention principally owing to their profound impact in organocatalysis[293,294] and their biological and technological applications.[295–297] However, it should be mentioned that despite the considerable advances that have been made since the pioneering works of Buchwald[298] and Cammidge,[299] the number of studies concerning asymmetric Suzuki-Miyaura cross-coupling to biaryls is still rather limited,[300–306] specially those including theoretical calculations, which are very rare.[307] Hence, on view of this, we decided to investigate computationally the asymmetric Suzuki-Miyaura reaction recently reported by Fernández and Lassaletta,[308] with the aim of providing a plausible explanation for the high yields and enantioselectivities observed therein. In particular, we focused our study on one of their reported examples for which an exceptional enantiomeric excess (% ee) and yield was obtained (see below).

In the following sections, a brief summary of the experimental work of Fernández and Lassaletta[308] will be presented, followed by the our theoretical results obtained on this study. It has to be mentioned, however, that this study in process of completion. Therefore, the theoretical results and conclusions presented in this chapter will be the ones obtained to date.

6.2 Experimental data

In 2004, the experimental group of professors Fernández and Lassaletta reported an asymmetric Diels-Alder reaction catalyzed by a [$Cu(OTf)_2$/(bis-hydrazone)] catalyst in which the C_2-symmetric dialkylamino groups, making rotations around N–N bonds inconsequential, were deemed responsible for the high enantioselectivities obtained.[309] Based on these results and experimental[310,311] and theoretical[312]

†If you are interested in further reading, a selection of the most relevant computational studies on this topic are discussed in the book chapter included in Appendix B.

precedents reported to that date for the use of diimine and bis-hydrazone ligands in Suzuki-Miyaura reactions, the authors decided to explore the use of bis-hydrazone ligands in the development of a new asymmetric version for this reaction. Thus, in 2008, after preliminary experiments testing different chiral bis-hydrazones ligands in catalysts of the type [$PdCl_2$(bis-hydrazone)], the authors reported that the use of (*S,S*)-2,5-diphenyl-pyrrolidine-derived glyoxal bis-hydrazone ligand in conjunction with Cs_2CO_3 as base and toluene as solvent, allows the asymmetric Suzuki-Miyaura coupling of a broad variety of substrates in high yields and enantioselectivities (Scheme 6.2).[308]

Scheme 6.2: Asymmetric Suzuki-Miyaura cross-coupling reactions.

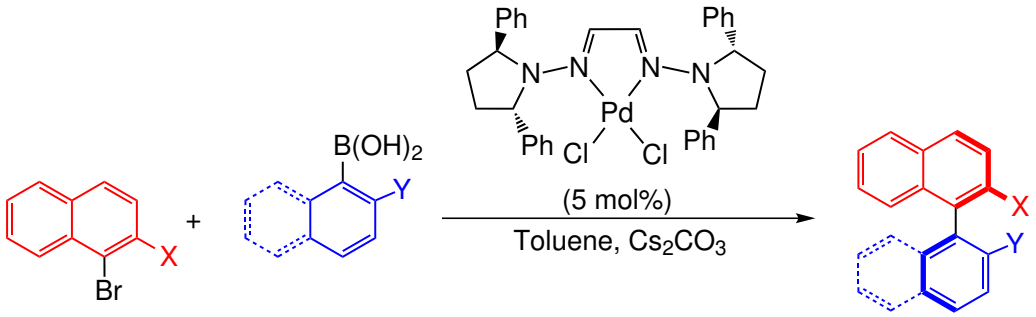

Additionally, in an attempt to rationalize the high enantioselectivities and the absolute configuration observed for all the reactions, the authors proposed four possible reaction pathways based on rational orientations that ligands can adopt in the species formed in the course of the reaction (Figure 6.3). So, in the oxidative addition step, two plausible species were considered to be generated: one with the X substituent of the organic halide pointing inside the page, and other with this group pointing outside (i.e. $\mathbf{I_1(A)}$ and $\mathbf{I_1(B)}$, respectively). Subsequently, each of these two species would undergo transmetalation resulting in two new intermediates: one with the Y substituent of the organoboron reagent pointing inside the page, and other with this group pointing outside (i.e. $\mathbf{I_2(A)}$**-syn** and $\mathbf{I_2(A)}$**-anti** in the case of the route A, and $\mathbf{I_2(B)}$**-anti** and $\mathbf{I_2(B)}$**-syn** in the case of the route B). Finally, each of these species would afford the coupled product with the corresponding (*R*)- or (*S*)-configuration by common reductive elimination. Among these four pathways, the authors proposed the one going through $\mathbf{I_2(A)}$**-anti** as the most favored on the basis of the supposed presence of a higher number of π-stacking interactions between ligands. Furthermore, according to the authors, the product derived from $\mathbf{I_2(A)}$**-anti** would be generated by reductive elimination with counterclockwise conrotatory Pd–C(aryl) bond rotations (favored against the opposite clockwise rotations for steric reasons), thus accounting

for the observed configuration in the final product (Figure 6.3).

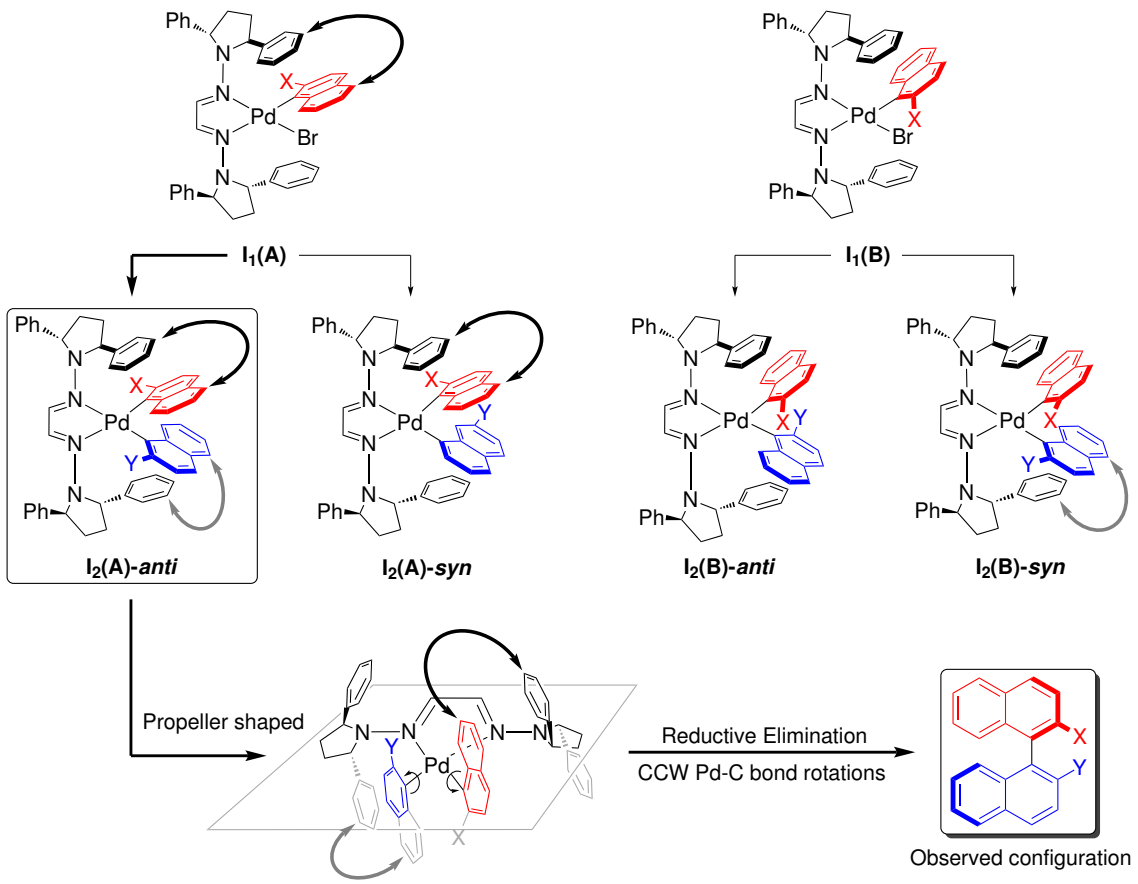

Figure 6.3: Oxidative addition and transmetalation intermediates proposed to account for the configuration observed in the final product. Curved arrows indicate stabilizing π-stacking interactions. The route proposed as the most plausible one is depicted with bold arrows.

Hence, prompted by these striking results, we decided to investigate theoretically the reported Suzuki-Miyaura coupling of 1-bromo-2-methylnaphthalene (Scheme 6.2, X = Me) with 1-naphthaleneboronic acid (Scheme 6.2, Y = H).[308] We selected this coupling in purpose as this is one of the cases with the highest yield and enantiomeric excess reported therein, and furthermore, is one of the less computationally demanding. In particular, when this coupling was carried out at room temperature, a 80% yield of the coupling (*R*)-product was obtained in 95% ee (Figure 6.4).[†]

[†]The same coupling was also carried out at 80 ºC affording the (*R*)-product at a higher yield (i.e. 98%) but with a lower ee (i.e. 90% (*R*)).

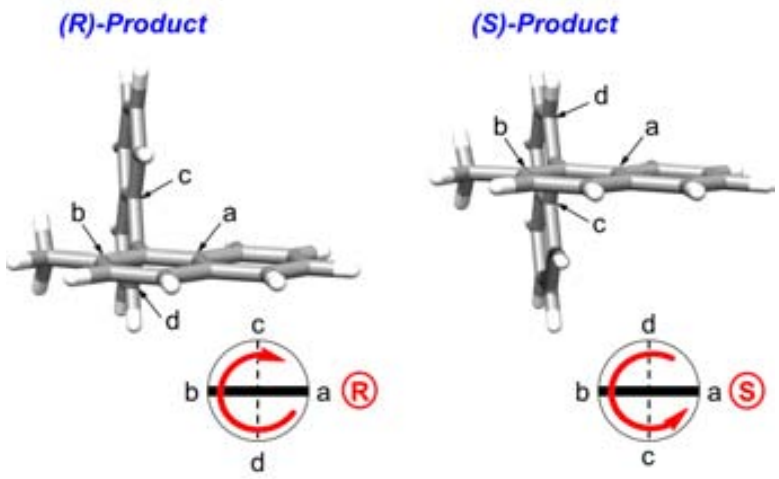

Figure 6.4: Application of the method of designation[313] of the absolute (*R*),(*S*)-configuration to the investigated coupling product.

As previously stated, the major objective of our ongoing theoretical study is to give an explanation for the high yields and enantioselectivities observed in the experiments. With this aim, the full catalytic cycle for the above mentioned coupling has been computed and the derived results analyzed. The computational details of this study and the results obtained so far, will be presented in the next sections.

6.3 Computational details

All the calculations presented in this study have been performed at the *DFT* level of theory by means of the dispersion-corrected *M06* functional[171] and using the *Gaussian09* program.[215] We chose this functional for calculations based on the satisfactory results that we obtained in the mechanistic study on the transmetalation step in the Negishi cross-coupling reaction,[70,71] and the good description of non-covalent interactions that this functional has shown to provide.[171] The latter, is particularly important in this study because this type of interactions (e.g. π-stacking) are very likely to be present in reactions involving biaryls. Actually, the experimental study[308] pointed out to these interactions as responsible for the high enantioselectivities and the absolute configuration observed.

Importantly, this study has been carried without modeling the catalyst and the reagents employed for the experiments (Figure 6.2, X = Me, Y = H). The B, C, and H atoms have been described using the standard 6-31G(d,p) basis set, while for the more electronegative O and N atoms the 6-31+G(d) basis set including diffuse functions

has been employed. On the other hand, for Pd and Br atoms the *SDD* effective core potential[269] and its associated double-ζ basis set has been adopted. Additionally, for Pd f-polarization functions have been also added (exponent = 1.472),[270] whereas for Br both d-polarization (exponent = 0.428) and p-diffuse (exponent = 0.0376) functions[272] have been added.

All the geometries of the reactants, products, and transition states shown in this study have been fully optimized without symmetry constraints. These structures have been further characterize as minima or saddle points by computing the corresponding harmonic force constants and vibrational frequencies at the optimized geometries. In particular, the former species have been confirmed by having a full set of real frequencies, and the latter by presenting a unique imaginary frequency and correlating the corresponding reactants and products.

Solvent effects (i.e. toluene, $\varepsilon = 2.3741$) have been introduced by means of a continuum model, the *SMD*[196] solvation model† implemented in *Gaussian09*, performing single point calculations at all the optimized gas phase geometries.

All the energies presented throughout this study correspond to Gibbs energies in toluene (ΔG_{solv}) at 298.15 K calculated by employing the following scheme:

$$\Delta G_{solv} = \Delta E_{solv} + (\Delta G_{gas} - \Delta E_{gas})$$

6.4 The oxidative addition step

The oxidative addition is the first step in the catalytic cycle and, accordingly, it was the first step that we analyzed. In the particular coupling under study, this reaction takes place between the complex [Pd(bis-hydrazone)] (**1**) and 1-bromo-2-methylnaphthalene (**2**) (Scheme 6.2, X = Me). As proposed in the experiments,[308] two different products can be envisaged in this process: one with the Me group of the organo halide **2** being above the plane defined by palladium and their bound atoms, and other with that group being below this plane (i.e. **OAA-I2** and **OAB-I2**, respectively,‡ in Figure 6.5). Therefore, it follows that there are two possible approaches of **2** to the starting Pd complex **1** (i.e. approach A and B, Figure 6.5), and consequently, two possible oxidative addition reactions. In view of this, and in order to further locate the corresponding transition states for these two processes, we started by calculating the intermediates prior to these reactions. Interestingly, for both approaches, two different η^2-coordination modes of **2** to the Pd complex **1**

†For further details on this model, see the last section of Chapter 2.

‡These species correspond to $\mathbf{I_1(A)}$ and $\mathbf{I_1(B)}$, respectively, in Figure 6.3.

were found, namely η^2-*a* and η^2-*j* (corresponding to **OAA-I1/OAB-I1** and **OAA-I1'/OAB-I1'**, respectively, in Figure 6.5).† The optimized structures for the reaction intermediates with these η^2-coordination modes show shorter Pd–C distances (with the carbon atoms involved in this coordination) for the η^2-*a* coordination regardless of the approach, which can be attributed to the electron-donating effect of the Me group and the less steric hindrance that **2** exerts to the ligands in **1** adopting this coordination. Conversely, the distances in the computed intermediates for the two approaches and presenting the same η^2-coordination have almost identical distances (with differences within 0.07 Å).

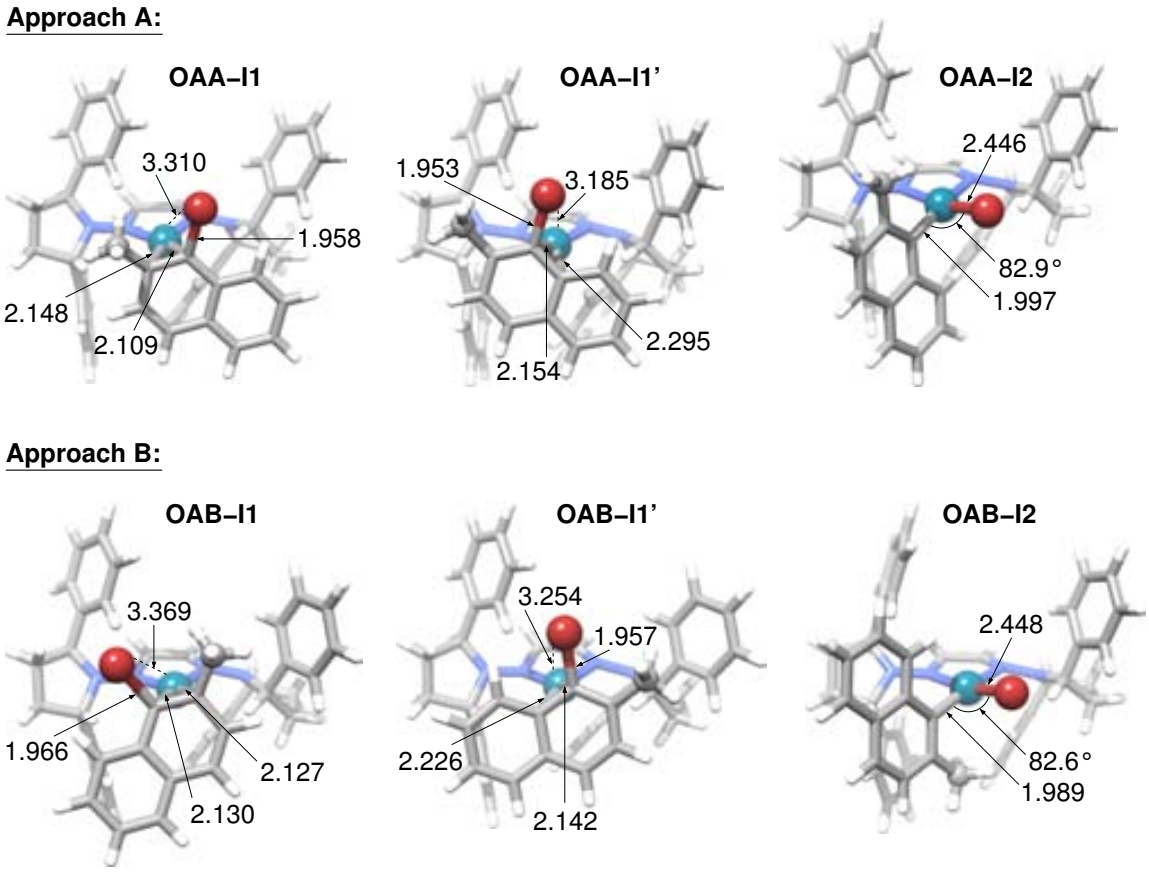

Figure 6.5: Optimized structures for the intermediates and products involved in the oxidative addition reactions through the two possible approaches. Only the Me group of **2** is represented in ball-and-stick for a better distinction between these two approaches. Relevant distances are shown in Å.

†The nomenclature adopted for these η^2-coordination modes is the one according to the *IUPAC* nomenclature for polycyclic aromatic hydrocarbons. For simplicity, we denoted the η^2-*j* coordination in the different intermediates shown in Figure 6.5 by adding a prime symbol (') to their names.

Subsequently, from the above optimized reaction intermediates, the corresponding transitions states for the oxidative addition reaction were computed (Figure 6.6).[†] As expected, all the located transitions states display a three-centered member ring formed between Pd, C_1 and Br atoms, and present an imaginary frequency that corresponds to the concerted cleavage of the C_1–Br bond and the coordination of **2** to **1** through only the C_1 atom. It should be noted that the optimized transition state structures for the oxidative addition through the approach B (**OAB-TS** and **OAB-TS'**, Figure 6.6) are practically identical (with differences in distances within 0.08 Å), which led us to think that there is only "one" transition state for each approach.[‡]

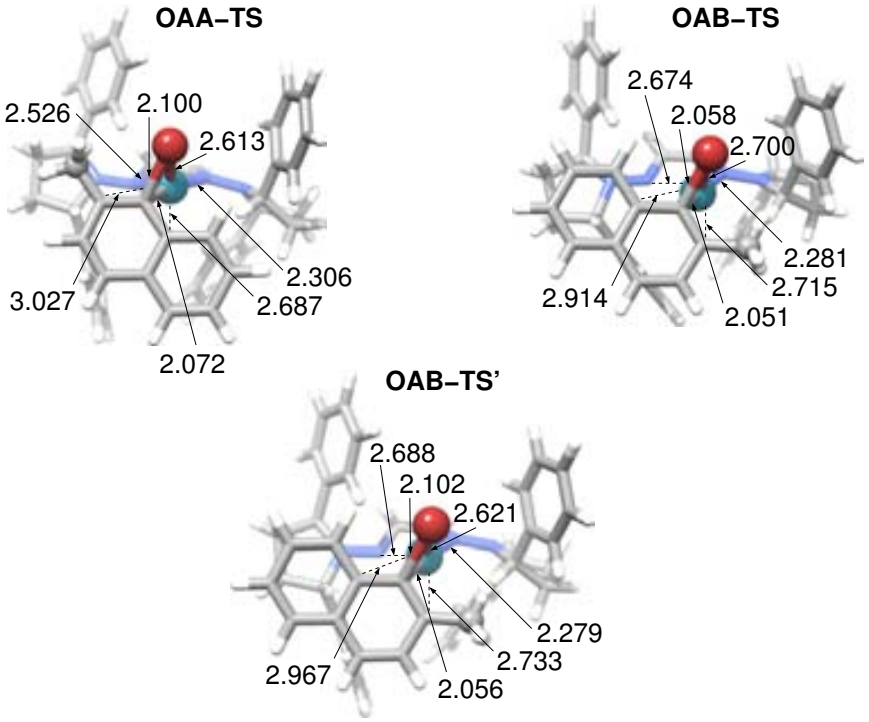

Figure 6.6: Optimized structures for the transition states involved in oxidative addition reactions through the two possible approaches. Only the Me group of **2** is represented in ball-and-stick for a better distinction between these two approaches. Relevant distances are shown in Å.

[†]The transition state starting from **OAA-I1'** could not be located. Additional calculations are currently underway.

[‡]Of course there may other transition states, but we think that they will probably correspond to transition states with different conformations of the ligands coordinated to Pd, as it is the case of **OAB-TS** and **OAB-TS'**.

The computation of the Gibbs energies in toluene for all the species involved in the oxidative addition step led to the Gibbs energy profile depicted in Figure 6.7. As far as the thermodynamics is concerned, the Gibbs energy profile show that both oxidative addition reactions through the two possible approaches are highly exergonic, being the product resulting from the approach B (**OAB-I2**) 1.6 kcal·mol^{-1} more stable than the one from A (**OAA-I2**). Furthermore, the calculated Gibbs energies for the intermediates previous to the oxidative addition transition states indicate that there is a clear preference for the η^2-*a* coordination mode, which can be rationalized with the stronger Pd–C interactions (with the carbon atoms involved in this coordination) due to the electron-donating effect of the Me group and the lower steric hindrance between **2** and the ligands bound to Pd in **1** with this coordination. On the other hand, from the kinetic point of view, the Gibbs energy profile shows that the transition state **OAB-TS'** is the one that has the lowest Gibbs energy, with a value even lower than the intermediate **OAB-I1'** and similar to **OAA-I1'**.

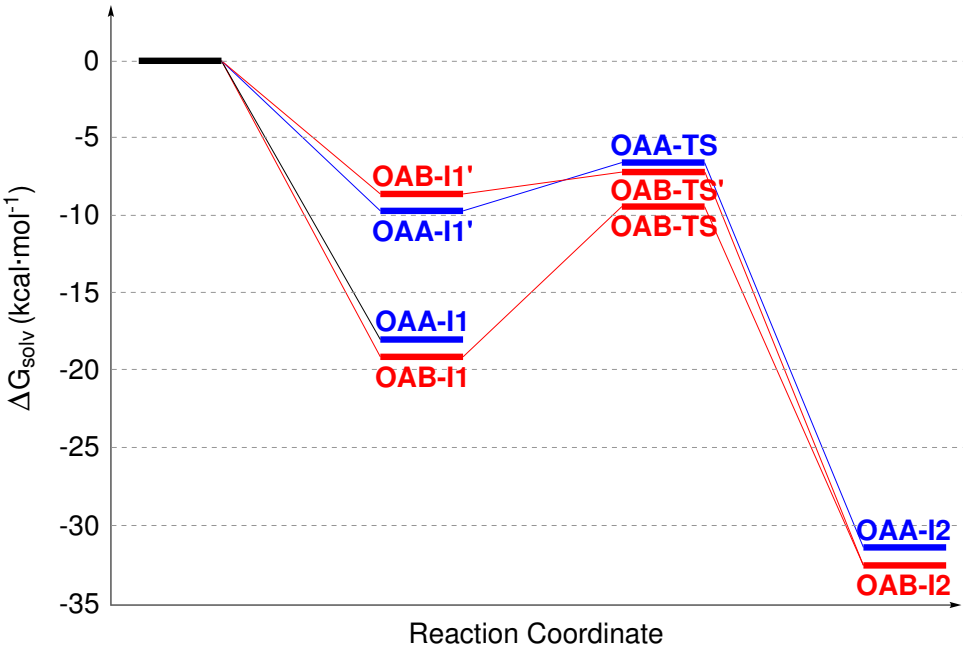

Figure 6.7: Gibbs energy profile in toluene (ΔG_{solv}, kcal·mol^{-1}) at 298 K for the two possible oxidative addition reactions of **2** to the palladium complex **1**. Approach A is shown in blue, whereas approach B is shown in red.

6.5 The transmetalation step

After the oxidative addition, the next step in the catalytic cycle is the transmetalation step. As we have seen in the introduction of this chapter, this step was recently investigated by our group[66] and, even though there is still some controversy over the role of the base, its reaction pathway is in general quite well understood. Thus, based on the generally accepted reaction mechanism (Figure 6.2), we next investigated the transmetalation reaction between the two oxidative addition products (i.e. **OAA-I2** and **OAB-I2**) and 1-naphthaleneboronic acid (**3**) (Scheme 6.2, Y = H).

According to the experimental work of Fernández and Lassaletta,[308] two transmetalation products for each oxidative addition product can be expected on the basis of the two possible orientations of the organic group of the organoboronic species. These two products, in our case (Figure 6.3, Y = H), correspond to the Pd complexes where the phenyl ring of naphthalene that is not coordinated to Pd (i.e. the "tail" of naphthalene) is pointing inside the plain of the page and outside the plain of the page. Consequently, there is a total of 4 possible routes for transmetalation. In order to keep the nomenclature for these routes consistent with the experimental work (Figure 6.3), we named *"anti"* those routes where the two tails of the naphthalenes are pointing to the opposite direction, and *"syn"* those routes where the two tails are pointing to the same direction. Thus, the name for the four transmetalation routes are: *A-anti*, *A-syn*, *B-anti*, and *B-syn*. In this chapter, since the reaction mechanism for the four routes is basically the same, only the one for the *B-anti* route will be described herein.

The computation of reaction pathway for the transmetalation through the route *B-anti* resulted in the Gibbs energy profile shown in Figure 6.8. The first intermediate in this profile is **TBa-I1**, which, as we previously explained, can be generated by either the substitution of the bromide by the organoboronate species (pathway A, Figure 6.1), or by the OH-for-bromide substitution and subsequent coordination of the neutral organoboron species to the OH ligand (pathway B, Figure 6.1). We also saw that recently some controversy has been stirred over which of these two processes is favored but that, in any case, they are not expected to contribute significantly to the observed reactivity as the step with the highest energy barrier corresponds to the cleavage of the C–B bond (**S-TS3**, Figure 6.2). Thus, in this work we decided to not study this step and focused our attention on investigating the transmetalation reaction from **TBa-I1**.

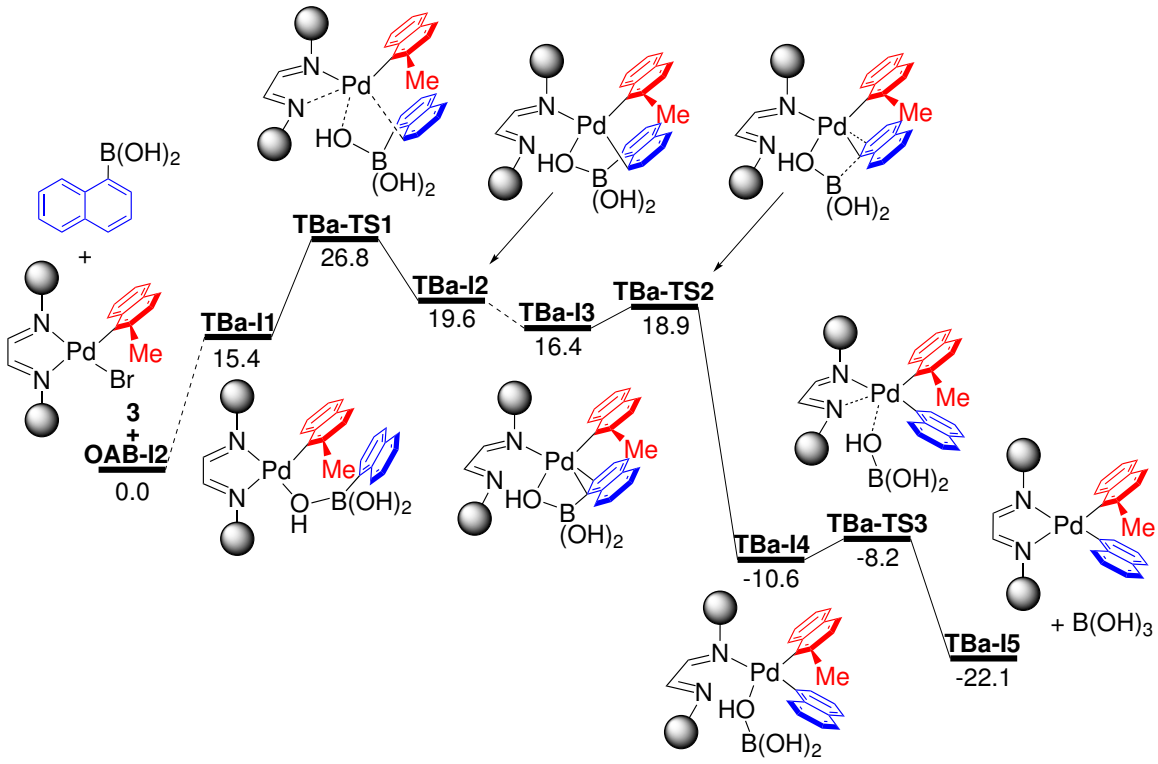

Figure 6.8: Gibbs energy profile in toluene (ΔG_{solv}, kcal·mol^{-1}) at 298 K for the transmetalation reaction through the pathway *B-anti*. Substituents in the bis-hydrazone ligand has been simplified for clarity.

According to the generally accepted mechanism for aryls,[67] once **TBa-I1** is formed, it undergoes transmetalation reaction trough a four-membered ring transition state in which the Pd–O and C–B bonds are broken at the same time that the Pd–C bond is formed. In our case, however, all the efforts devoted to locate and characterize such transition state were fruitless. Instead, we found the η^2-coordination of **3** to Pd and the substitution of one of the N ligands bound to Pd by one of the OH ligands of boron. The transition state for this process (**TBa-TS1**) requires a relative Gibbs energy barrier of 11.4 kcal·mol^{-1} and leads to the next intermediate **TBa-I2**, where **3** is coordinated to Pd in a η^2-*b* fashion (Figure 6.9). Then, from this species, in order to undergo transmetalation the change from the η^2-*b* to the η^2-*j* coordination mode is required.† The intermediate resulting from this η^2-coordination change is **TBa-I3** (Figure 6.9), from which the concerted cleavage of the C–B bond

†This does not happen in the cases in which the tail of **3** is below the plain defined by Pd and their coordinated ligands, as the η^2-coordination that results from **TBa-TS1** is already the appropriate η^2-*b* coordination required in **TBa-TS2**. Hence, in the *A-anti* and *B-syn* routes no coordination change is required and, accordingly, the transmetalation takes place directly from **TBa-I2** via the

and the formation of the Pd–C bond occurs with a low Gibbs energy barrier (2.5 kcal·mol^{-1}) via **TBa-TS2**. This transition state gives rise to **TBa-I4**, which affords the final product of the transmetalation reaction by the substitution of the borane by the N ligand through the transition state **TBa-TS3**. The Gibbs energy required for this last step is very low (1.6 kcal·mol^{-1}) and yields **TBa-I5**, where the two organic groups are in a *cis* disposition ready for the coupling by reductive elimination. The optimized structures for the most relevant species involved in the transmetalation step are shown in Figure 6.9.

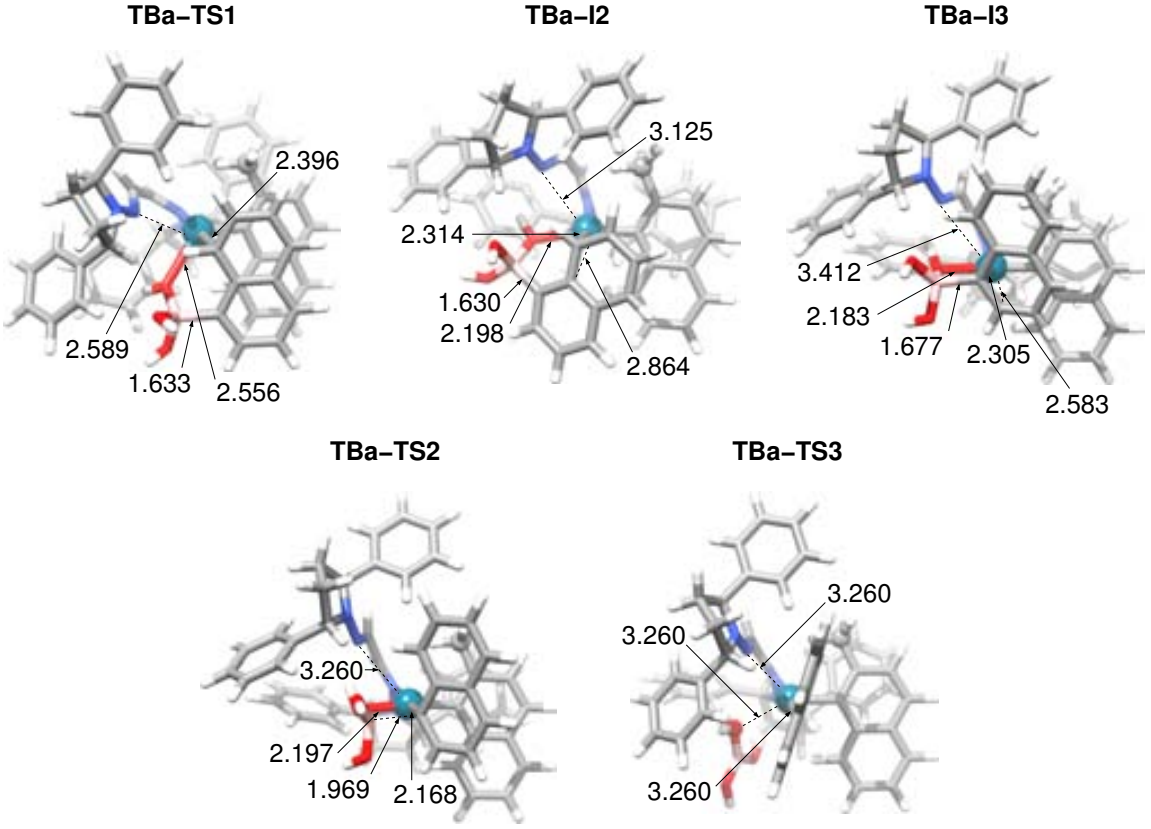

Figure 6.9: Optimized structures for the transition states involved in transmetalation reaction through the pathway B-anti. Only the Me group of **2** and the oxygen atom coordinated to Pd in **TBa-TS3** are represented in ball-and-stick for clarity. Relevant distances are shown in Å.

In summary, the calculated Gibbs energies depicted in Figure 6.8 shows that the transmetalation reaction is exergonic by 22.1 kcal·mol^{-1}. The highest energy point within the overall Gibbs energy profile is **TBa-TS1** (26.8 kcal·mol^{-1}), which

transition state **TBa-TS2**. In contrast, in the *A-syn* route the transmetalation occurs in the same way than in the *B-anti* route.

corresponds to the η^2-coordination of **3** to Pd and the concomitant substitution of one of the N ligands by one of the OH groups of boron (**TBa-TS1**, Figure 6.9). As expected, the computed transition states analogous to **TBa-TS1** in the alternative transmetalation routes resulted also to provide the highest Gibbs energy barriers. These values, as well as the Gibbs energies for the transition states corresponding to **TBa-TS2**, are collected in Table 6.1.

Table 6.1: Calculated Gibbs energy barriers in toluene (ΔG_{solv}, kcal·mol^{-1}) at 298 K for the transition states corresponding to **TBa-TS1** (i.e. **TS1**) and **TBa-TS2** (i.e. **TS2**) in the different transmetalation routes. The highest-energy transition states within these routes are shown in bold.

	Route A[a]		**Route B**	
	A-anti	**A-syn**	**B-anti**	**B-syn**
TS1	**23.9**	**26.2**	**26.8**	**26.8**
TS2	21.6	20.7	18.9	22.6

[a] These Gibbs energy barriers are relative to the separated oxidative addition product **OAA-I2** and **3**, which are 1.6 kcal·mol^{-1} less stable than the separated oxidative addition product **OAB-I2** and **3**.

As above mentioned, the step with the highest energy barrier in all the transmetalation routes is the one that involves the η^2-coordination of **3** to Pd and the substitution of one of the N ligands by one of the OH ligands of boron (**TS1**, Table 6.1). Consequently, the route *A-anti* that is the one that has the lowest energy for this step (23.9 kcal·mol^{-1}), is expected to be the more favorable route for transmetalation.

6.6 The reductive elimination step

The last step in the catalytic cycle and that leads to the final coupling product with the defined stereochemistry and the concomitant regeneration of the catalytic species, is the reductive elimination. Thus, for the sake of completeness, the reductive elimination reactions starting from the products obtained in the four analyzed transmetalation routes (Figure 6.10) were investigated. In particular, for each of these intermediates, the corresponding transition state and product involved in this process were computed.

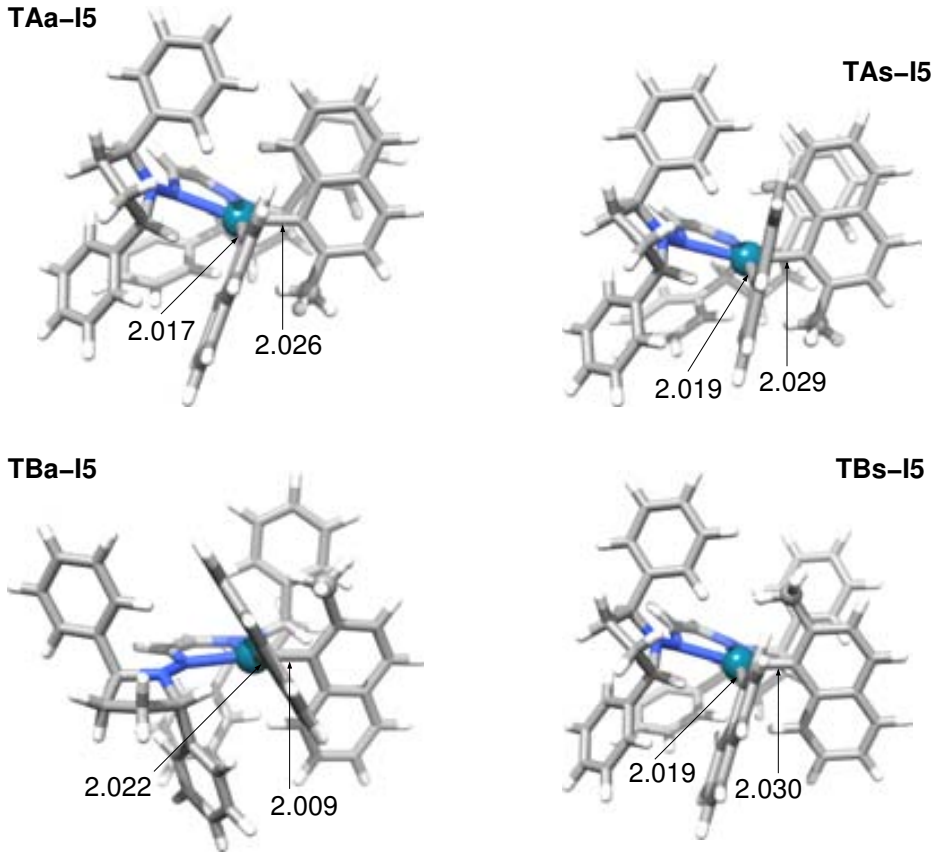

Figure 6.10: Optimized structures for the different intermediates previous to the reductive elimination reactions. Only the Me group of **2** is represented in ball-and-stick for a better distinction between the different intermediates. The letters "A" and "B" in the labels of the intermediates refer to the routes A and B, respectively, whereas "a" and "s" refers to -*anti* or -*syn*, respectively. Relevant distances are shown in Å.

As expected, in all the calculated transition states for the different reductive eliminations, the formation of a three-membered ring between Pd and the two carbon

atoms to be coupled, as well as an imaginary frequency according to this process, were found. The optimized transition state structure for the reductive elimination that provides the lowest Gibbs energy barrier (i.e route *A-syn*) is shown in Figure 6.11.

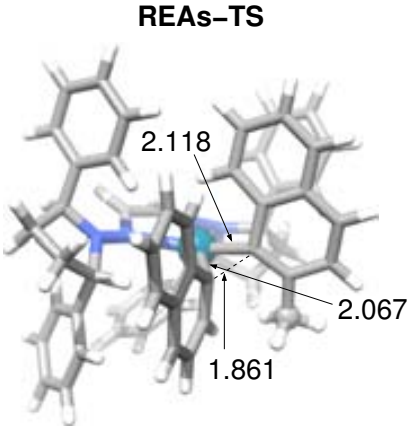

Figure 6.11: Optimized transition state structure for the reductive elimination reaction through the route *A-syn*. Only the Me group of **2** is represented in ball-and-stick for clarity. Relevant distances are shown in Å.

According to calculations, all the analyzed reductive eliminations have reasonable Gibbs energy barriers, with values ranging from 14.6 (i.e. *A-syn*) to 17.4 kcal·mol^{-1} (i.e. *B-syn*) (Table 6.2).

Table 6.2: Calculated Gibbs energy barriers in toluene (ΔG_{solv}, kcal·mol^{-1}) at 298 K for the different reductive elimination reactions. Gibbs energies are relative to the corresponding oxidative addition products. The stereochemistry of the product formed after reductive elimination is denoted in parenthesis.

Route A		**Route B**	
A-anti	**A-syn**	**B-anti**	**B-syn**
15.8 (*S*)	14.6 (*R*)	15.8 (*R*)	17.4 (*R*)

As stated in the beginning of this section, each of the transition states for the different routes leads to a coupled product with a defined stereochemistry. In particular, one of the routes (i.e. *A-anti*) results in the coupling product with an (*S*)-configuration, whereas the other three routes (i.e. *A-syn*, *B-anti* and *B-syn*) afford

the (*R*)-coupling product (Table 6.2). This distribution of products is completely unexpected, since, a priori, two routes should give the (*R*)-product, and two the (*S*)-product. Therefore, it follows that either the *B-anti* or the *B-syn* route should provide the (*S*)-product instead of the (*R*)-one. Of course, there exists a good explanation for this surprising distribution of products, that in fact, led us to reach one of the main conclusions of this study. This justification will be given in the following section.

6.7 Where is the enantioselectivity defined?

In the previous section we have seen that the reductive elimination is the step that regenerates the catalytic species and affords the final product with a defined (*R*)- or (*S*)-configuration. However, it does not necessarily imply that the stereochemistry of the product is defined in this last step. Actually, if one takes a look to the intermediates previous to reductive elimination (Figure 6.10), one could (in principle) predict the absolute configuration of the final product. For instance, in the case of the intermediate of the route *B-anti* (**TBa-I5**, Figure 6.10) the tail of **3** is rather twisted toward the left, which ends up defining the (*R*)-configuration observed after reductive elimination (Table 6.2). In contrast, if it were twisted toward the right, the C–C coupling from this intermediate would result in the (*S*)-product. Importantly, whether the tail of **3** will be right or left rotated will depend on its steric hindrance with the ligands coordinated to Pd. Consequently, the absolute (*R*)- or (*S*)-configuration of the coupling product will depend on steric effects (Figure 6.12).

In the case of **TBa-I5**, Figure 6.12 shows how the steric hindrance exerted by the Me group of **2** favors the rotation of the tail of **3** to the left, thus favoring the formation of the (*R*)-product. Similarly, in **TAa-I5**, the Me group of **2** also promotes the rotation of the tail of **3** to the left, and accordingly, the (*S*)-product is obtained. On the other hand, in **TAs-I5**, the Me group of **2** and the tail of **3** are oriented in opposite directions; therefore, the steric bulk of the Ph group of the bis-hydrazone ligand located above the plain defined by Pd and their coordinated ligands is now the responsible for the favored clockwise rotation of **3** and the subsequent formation of the (*R*)-product. Finally, in **TBs-I5**, as in **TAs-I5**, the Me group of **2** and the tail of **3** are pointing to opposite directions. However, in this case, the tail of **3** is now below the plain defined by Pd and their ligands, where instead of a Ph group we find a hydrogen atom.[†] Thus, the tail of **3** can, in principle, "freely" rotate both to the right or to the left resulting in both (*R*)- and (*S*)-products. However, the approach of **2** and **3** in order to locate the transition state for the reductive elimination led to the clockwise rotation of **3**, and consequently, the unexpected (*R*)-configuration of

[†]This is due to the C_2-symmetric structure of the bis-hydrazone ligand.

the product (Table 6.2).

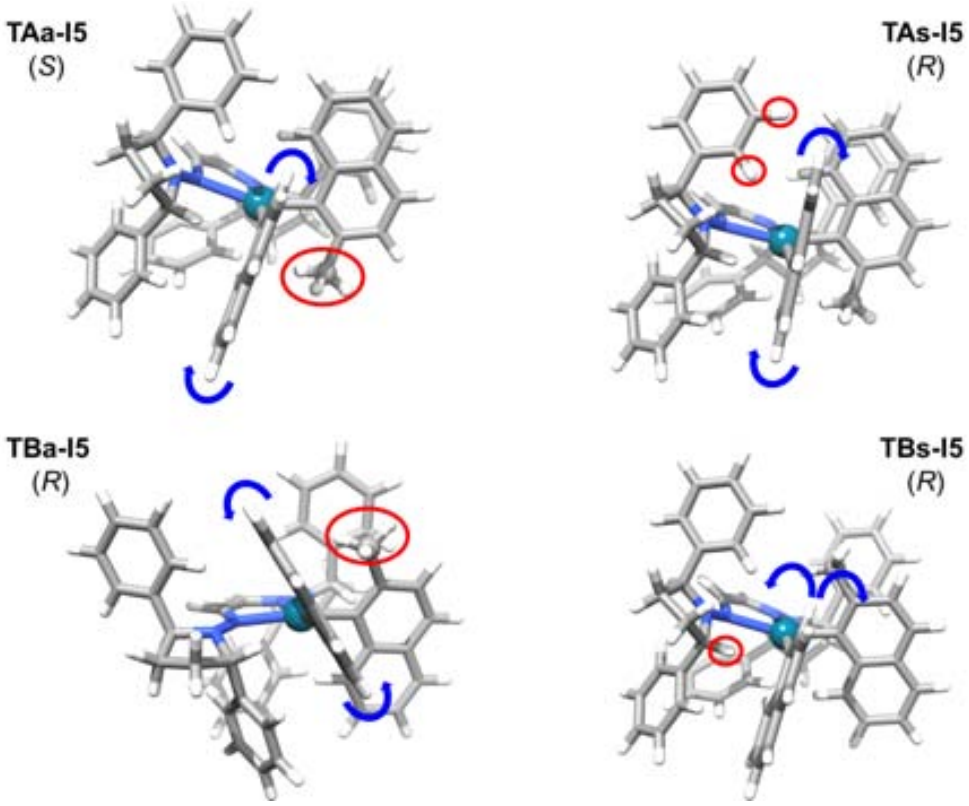

Figure 6.12: Representation of the steric interactions (in red) that govern the stereochemical outcome of the reductive elimination reaction from the intermediates obtained in the four transmetalation routes. Favored rotations of the tail of **3** are shown in blue. Only the Me group of **2** is represented in ball-and-stick for clarity.

Hence, we know now that the stereochemistry of the final product is predicted before the reductive elimination step. But, where is it exactly defined? In order to find the answer to this question we have to look back to the transmetalation step.

As shown in Figure 6.13, in the second intermediate of this step (**TBaI2**) the stereochemistry is clearly not defined yet, since **2** and **3** are parallel to one another. Thus, it necessarily has to be defined in the next step, **TBa-TS2**, where the Pd–C bond with **3** is formed and it can undergo either clockwise or counterclockwise rotations. This transition state, however, is not the one with the highest Gibbs energy barrier, which means that, even if after this step the stereochemical outcome of the route is defined, this transition state does not govern the absolute configuration observed in the reaction.

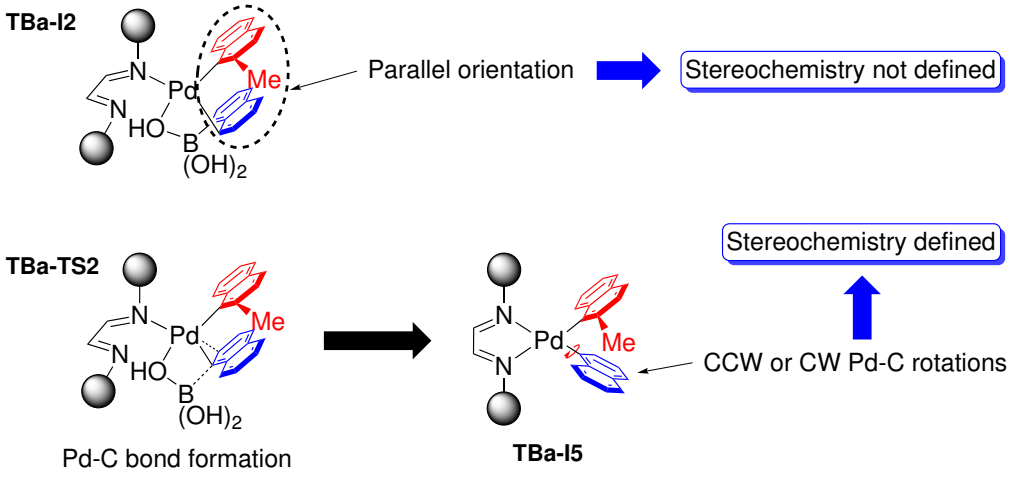

Figure 6.13: Optimized transition state structure for the reductive elimination reaction through the route *A-syn*.

In fact, the stereochemistry of the reaction will be dictated by the route with the lowest value for the highest Gibbs energy barrier (**TS1**, Table 6.1). Thus, according to this and the values collected in Table 6.1, the (*R*)- or (*S*)-configuration of the final product would be provided by the route *A-anti* (**TAa-TS1**). Consequently, the absolute configuration of the product observed in the experiments should be (*S*). Nevertheless, the product observed in the experiments has a (*R*)-configuration. For this discrepancy between theory and experiments there are two possible reasons: either calculations so far have not identified the real pathway, or at some point in the reaction the interconversion among the intermediates may take place giving rise to the product observed experimentally. In particular, one alternative for the first reason would be that the difference between the rates for the oxidative addition through the route B and A was enough to prevent the subsequent transmetalation reactions from the latter (i.e. *A-anti* and *A-syn* routes). In that case, the route B would be the only accessible route, which would be consistent with experiments as we have previously seen that (in principle) it only affords the (*R*)-product (Figure 6.12). On the other hand, an alternative for the second reason would be that the intermediate previous to reductive elimination in the route *A-anti* (**TAa-I5**, Figure 6.10) evolved to another intermediate that afforded the (*R*)-product with a lower energy barrier.[†] This interconversion would consist in the counterclockwise rotation of the tail of **3** from the left side of the Me group of **2** to the right side of this group. This alternative, in fact, is based on the behavior found for the *B-syn* route, where it seems that the

[†]Of course, this alternative would be valid only if the barrier for this interconversion and the subsequent reductive elimination from this intermediate were lower than the reductive elimination from **TAa-I5** (Table 6.2).

both (*R*)- and (*S*)-products could be obtained just by rotating the tail of **3**, and the recently reported study on a related asymmetric Suzuki-Miyaura coupling, where this alternative was deemed responsible for the observed stereochemistry.[307] These two alternatives are currently being investigated.

6.8 Conclusions

In this study, the full catalytic cycle for the recently reported asymmetric Suzuki-Miyaura coupling between 1-bromo-2-methylnaphthalene (**2**) and 1-naphthaleneboronic acid (**3**) catalyzed by a [Pd(bis-hydrazone)] (**1**) complex,[308] was theoretically investigated by means of *DFT* calculations. Importantly, the results derived from this study revealed that the transmetalation reaction does not occur in just one step, as it is generally believed, but occurs in three steps. This is owing to the relative lability of the bis-hydrazone ligand, which can easily dissociate one of the N atoms coordinated to the Pd catalyst. It is worth mentioning that, at the time we found this alternative mechanism for transmetalation, no evidence for it had been reported. Recently, however, this variant for the transmetalation mechanism has been reported for the Suzuki-Miyaura coupling catalyzed by a diimine chelated palladium complex.[283]

As suggested in the experimental work,[308] four different routes for the reaction leading to the final coupled product were analyzed (i.e. *A-anti*, *A-syn*, *B-anti*, *B-syn*). Furthermore, for each of them, the (*R*)- or (*S*)-configuration of the final product was also determined. Interestingly, theoretical calculations on these routes showed that their stereochemistry is not defined in the step with the highest Gibbs energy barrier (i.e. **TS1**). Moreover, calculations also showed that the (*R*)-configuration observed in the experiments can not be governed by this step, since the route with the lowest Gibbs energy for this step (i.e. *A-anti*) leads to the opposite configuration. The discrepancy between theory and experiments may be attributed to two different reasons: the first one is based on assuming that the rate for the oxidative addition via the route B is higher enough to neglect the oxidative addition through the route A; this would make the route B the only one available for transmetalation, which would result in the formation of the (*R*)-product in agreement with experiments. On the other hand, the second explanation can be based on considering the interconversion of the intermediate previous to the reductive elimination in the route *A-anti* (i.e. the one with the higher rate) into another intermediate that would afford the (*R*)-product. This type of interconversion, which entails a counterclockwise Pd–C bond rotation, has been also involved in a related Suzuki-Miyaura coupling as responsible for the observed stereochemistry.[307] We expect with the calculations that we are at present carrying out on these two alternatives to be able to rationalize the formation

of the (*R*)-product observed in the experiments.

"The whole of science is nothing more than a refinement of everyday thinking"

Albert Einstein

7

General conclusions

The specific conclusions for each of the cross-coupling reactions investigated in this thesis have been presented at the end of the corresponding chapter. Thus, only the general conclusions drawn from these studies will be summarized herein.

In the case of the Negishi reaction, the theoretical studies on the transmetalation reactions with ZnMeCl and $ZnMe_2$ showed the complexity of these processes and providing a detailed picture of their reaction mechanisms. In particular, for the transmetalation reaction with ZnMeCl, calculations warned on the many chances for the generation of new intermediates that would eventually afford homocoupling side products. On the other hand, the theoretical results derived from the study with $ZnMe_2$ proved the existence, operation and effects of competitive transmetalation pathways, some of which had not been invoked before, but that should be considered when planning or discussing Negishi syntheses.

For the copper-free Sonogashira reaction, the mechanistic study reported in this thesis revealed that, just like in other cross-coupling reactions (i.e. Stille, Negishi), there are several competing reaction pathways and a change on the reaction conditions (e.g. solvent, ligands, substrates, base) might favor one over the other ones.

Last but not least, theoretical calculations on the investigated asymmetric Suzuki-Miyaura coupling showed that the mechanism for the transmetalation step differs from the typical reaction pathway proposed in the literature. This is owing to the relative lability of the bis-hydrazone ligand, which can easy dissociate one of the N atoms directly coordinated to Pd. As far as the stereochemistry of the reaction is concerned, calculations so far do not provide an explanation for the high enantioselectivities observed in the experiments. Two possible reasons are: either the real pathway has not been identified, or an interconversion among the reaction intermediates takes place at some point in the reaction, thus giving rise to the product observed experimentally.

Overall, theoretical calculations have been used in this thesis to determine, elucidate, and propose reaction mechanisms for Pd-catalyzed cross-coupling reactions. In particular, they have allowed the characterization of reaction intermediates and transition states involved in these processes. Hence, we can conclude that the results presented in this thesis prove that the use of computational methods, namely *DFT* calculations, is a very useful tool for the study of reaction mechanisms of homogeneous catalytic reactions.

Bibliography

[1] Berzelius, J. J. *Annales chimie physiques,* **1836**, *61*, 146.

[2] Leicester, H. M.; Klickstein, H. S. In *Source Book in Chemistry 1400-1900;* Harvard University Press: Massachusetts, 1965; p 267.

[3] Arrhenius, S. *Zeit. Phys. Chem.* **1899**, *28*, 317.

[4] Rothenberg, G. *Catalysis: Concepts and Green Applications;* Wiley-VCH: Weinheim, 2008.

[5] Eyring, H. *J. Chem. Phys.* **1935**, *3*, 107.

[6] Evans, M. G.; Polanyi, M. *Trans. Faraday Soc.* **1935**, *31*, 875.

[7] Hartwig, J. *Organotransition Metal Chemistry: From Bonding to Catalysis;* University Science Books: California, 2010.

[8] Kozuch, S.; Shaik, S. *J. Am. Chem. Soc.* **2006**, *128*, 3355.

[9] Kozuch, S.; Shaik, S. *J. Phys. Chem. A,* **2008**, *112*, 6032.

[10] Uhe, A.; Kozuch, S.; Shaik, S. *J. Comput. Chem.* **2011**, *32*, 978.

[11] Kozuch, S.; Shaik, S. *Acc. Chem. Res.* **2011**, *44*, 101.

[12] *Transition Metals for Organic Synthesis*; 2nd ed.; Beller, M.; Bolm, C., Eds.; Wiley-VCH: Weinheim, 2004.

[13] *Metal-Catalyzed Cross-Coupling Reactions*; 2nd ed.; de Meijere, A.; Diedrich, F., Eds.; Wiley-VCH: Weinheim, 2004.

[14] *Cross-Coupling Reactions: A Practical Guide*; No. 219 in *Topics in Current Chemistry*, Miyaura, N., Eds.; Springer: Berlin, 2002.

[15] Buchwald, S. L. *(Ed.) Acc. Chem. Res.* **2008**, *41 (special issue)*, 1439.

[16] Tamao, K.; Hiyama, T.; Negishi, E.-I. *J. Organomet. Chem.* **2002**, *653 (special issue)*, 1.

[17] Phapale, V. B.; Cárdenas, D. J. *Chem. Soc. Rev.* **2009**, *38*, 1598.

[18] Nicolaou, K. C.; Bulger, P. G.; Sarlah, D. *Angew. Chem. Int. Ed.* **2005**, *44*, 4442.

[19] Negishi, E.-I.; Hu, Q.; Huang, Z.; Wang, G.; Yin, N. In *The Chemistry of Organozinc Compounds*; Rappoport, Z. Z.; Marek, I., Eds.; John Wiley & Sons, Ltd: England, 2006; pp 457–553.

[20] Kosugi, M.; Sasazawa, K.; Shimizu, Y.; Migita, T. *Chem. Lett.* **1977**, *3*, 301.

[21] Stille, J. K. *Angew. Chem. Int. Ed.* **1986**, *25*, 508.

[22] Espinet, P.; Echavarren, A. M. *Angew. Chem. Int. Ed.* **2004**, *43*, 4704.

[23] Miyaura, N.; Yamada, K.; Suzuki, A. *Tetrahedron Lett.* **1979**, *20*, 3437.

[24] Miyaura, N.; Suzuki, A. *Chem. Rev.* **1995**, *95*, 2457.

[25] Negishi, E.-I.; King, A. O.; Okukado, N. *J. Org. Chem.* **1977**, *42*, 1821.

[26] Nicolaou, K. C.; Sorensen, E. J. In *Classics in Total Synthesis;* VCH: New York, 1996; Chapter 31.

[27] Chemler, S. R.; Trauner, D.; Danishefsky, S. J. *Angew. Chem. Int. Ed.* **2001**, *40*, 4544.

[28] Negishi, E.-I. *Bull. Chem. Soc. Jpn.* **2007**, *80*, 233.

[29] Anderson, B.; Becke, L.; Booher, R.; Flaugh, M.; Harn, N.; Kress, T.; Varie, D.; Wepsiec, J. *J. Org. Chem.* **1997**, *62*, 8634.

[30] Rouhi, A. M. *Chem. & Eng. News,* **2004**, *82*, 49.

[31] Zapf, A.; Beller, M. *Top. Catal.* **2002**, *19*, 101.

[32] Corbet, J. P.; Mignani, G. *Chem. Rev.* **2006**, *106*, 2651.

[33] Zapf, A.; Beller, M. In *Handbook of Organopalladium Chemistry for Organic Synthesis*; Negishi, E.-I., Eds.; Wiley: New York, 2002; Vol. 1.

[34] Blaser, H. U.; Indolese, A.; Naud, F.; Nettekoven, U.; Schnyder, A. *Adv. Synth. Catal.* **2004**, *346*, 1583.

[35] Tamura, M.; Kochi, J. *J. Am. Chem. Soc.* **1971**, *93*, 1483.

[36] Tamura, M.; Kochi, J. *J. Am. Chem. Soc.* **1971**, *93*, 1485.

[37] Tamura, M.; Kochi, J. K. *J. Organomet. Chem.* **1972**, *42*, 205.

[38] Ishiyama, T.; Abe, S.; Miyaura, N.; Suzuki, A. *Chem. Lett.* **1992**, 691.

[39] Devasagayaraj, A.; Studemann, T.; Knochel, P. *Angew. Chem. Int. Ed.* **1996**, *34*, 2723.

[40] Giovannini, R.; Studemann, T.; Dussin, G.; Knochel, P. *Angew. Chem. Int. Ed.* **1998**, *37*, 2387.

[41] Giovannini, R.; Studemann, T.; Devasagayaraj, A.; Dussin, G.; Knochel, P. *J. Org. Chem.* **1999**, *64*, 3544.

[42] Jensen, A. E.; Knochel, P. *J. Org. Chem.* **2002**, *67*, 79.

[43] Frisch, A. C.; Beller, M. *Angew. Chem. Int. Ed.* **2005**, *44*, 674.

[44] Littke, A. F.; Fu, G. C. *Angew. Chem. Int. Ed.* **2002**, *41*, 4176.

[45] Wolfe, J. P.; Singer, R. A.; Yang, B. H.; Buchwald, S. L. *J. Am. Chem. Soc.* **1999**, *121*, 9550.

[46] Zapf, A.; Ehrentraut, A.; Beller, M. *Angew. Chem. Int. Ed.* **2000**, *39*, 4153.

[47] Fleckenstein, C. A.; Plenio, H. *Chem. Soc. Rev.* **2010**, *39*, 694.

[48] Kantchev, E. A. B.; O'Brien, C. J.; Organ, M. G. *Angew. Chem. Int. Ed.* **2007**, *46*, 2768.

[49] Marion, N.; Nolan, S. P. *Acc. Chem. Res.* **2008**, *41*, 1440.

[50] Amatore, C.; Jutand, A. *Acc. Chem. Res.* **2000**, *33*, 314.

[51] Galardon, E.; Ramdeehul, S.; Brown, J. M.; Cowley, A.; Hii, K. K. M.; Jutand, A. *Angew. Chem. Int. Ed.* **2002**, *41*, 1760.

[52] Hartwig, J. F. *Inorg. Chem.* **2007**, *46*, 1936.

[53] Yandulov, D. V.; Tran, N. T. *J. Am. Chem. Soc.* **2007**, *129*, 1342.

[54] Senn, H. M.; Ziegler, T. *Organometallics,* **2004**, *23*, 2980.

[55] Goossen, L. J.; Koley, D.; Hermann, H. L.; Thiel, W. *Organometallics,* **2005**, *24*, 2398.

[56] Pérez-Rodríguez, M.; Braga, A. A. C.; García-Melchor, M.; Pérez-Temprano, M. H.; Casares, J. A.; Ujaque, G.; Lera, de A. R.; Álvarez, R.; Maseras, F.; Espinet, P. *J. Am. Chem. Soc.* **2009**, *131*, 3650.

[57] Xue, L.; Lin, Z. *Chem. Soc. Rev.* **2010**, *39*, 1692.

[58] Casado, A. L.; Espinet, P. *J. Am. Chem. Soc.* **1998**, *120*, 8978.

[59] Goossen, L. J.; Koley, D.; Hermann, H. L.; Thiel, W. *J. Am. Chem. Soc.* **2005**, *127*, 11102.

[60] Sicre, C.; Braga, A. A. C.; Maseras, F.; Cid, M. M. *Tetrahedron,* **2008**, *64*, 7437.

[61] Liu, Q.; Lan, Y.; Liu, J.; Li, G.; Wu, Y.-D.; ; Lei, A. *J. Am. Chem. Soc.* **2009**, *131*, 10201.

[62] Casares, J. A.; Espinet, P.; Fuentes, B.; Salas, G. *J. Am. Chem. Soc.* **2007**, *129*, 3508.

[63] Álvarez, R.; Faza, O. N.; López, C. S.; Lera, de A. R. *Org. Lett.* **2006**, *8*, 35.

[64] Amatore, C.; Jutand, A.; Le Duc, G. *Chem. Eur. J.* **2011**, *17*, 2492.

[65] Braga, A. A. C.; Morgon, N. H.; Ujaque, G.; Maseras, F. *J. Am. Chem. Soc.* **2005**, *127*, 9298.

[66] Braga, A. A. C.; Ujaque, G.; Maseras, F. *Organometallics,* **2006**, *25*, 3647.

[67] Braga, A. A. C.; Morgon, N. H.; Ujaque, G.; Lledós, A.; Maseras, F. *J. Organomet. Chem.* **2006**, *691*, 4459.

[68] Nova, A.; Ujaque, G.; Maseras, F.; Lledós, A.; Espinet, P. *J. Am. Chem. Soc.* **2006**, *128*, 14571.

[69] Pérez-Temprano, M. H.; Nova, A.; Casares, J. A.; Espinet, P. *J. Am. Chem. Soc.* **2008**, *130*, 10518.

[70] Fuentes, B.; García-Melchor, M.; Lledós, A.; Maseras, F.; Casares, J. A.; Ujaque, G.; Espinet, P. *Chem. Eur. J.* **2010**, *16*, 8596.

[71] García-Melchor, M.; Fuentes, B.; Lledós, A.; Casares, J. A.; Ujaque, G.; Espinet, P. *J. Am. Chem. Soc.* **2011**, *133*, 13519.

[72] García-Melchor, M.; Pacheco, M. C.; Nájera, C.; Lledós, A.; Ujaque, G. *ACS Catal.* **2012**, *2*, 135.

[73] Noell, J. O.; Hay, P. J. *J. Am. Chem. Soc.* **1982**, *104*, 4578.

[74] Low, J. J.; Goddard, W. A. *J. Am. Chem. Soc.* **1984**, *106*, 6928.

[75] Obara, S.; Kitaura, K.; Morokuma, K. *J. Am. Chem. Soc.* **1984**, *106*, 7482.

[76] Bickelhaupt, F. M.; Ziegler, T.; Schleyer, P. V. R. *Organometallics,* **1995**, *14*, 2288.

[77] Ahlquist, M.; Norrby, P. O. *Organometallics,* **2007**, *26*, 550.

[78] Li, Z.; Fu, Y.; Guo, Q.-X.; Liu, L. *Organometallics,* **2008**, *27*, 4043.

[79] Jover, J.; Fey, N.; Purdie, M.; Lloyd-Jones, G. C.; Harvey, J. N. *J. Mol. Catal. A,* **2010**, *324*, 39.

[80] Schoenebeck, F.; Houk, K. N. *J. Am. Chem. Soc.* **2010**, *132*, 2496.

[81] Stille, J. K.; Lau, K. S. Y. *Acc. Chem. Res.* **1997**, *10*, 434.

[82] Casado, A. L.; Casares, J. A.; Espinet, P. *Inorg. Chem.* **1998**, *37*, 4154.

[83] Netherton, M. R.; Fu, G. C. *Angew. Chem. Int. Ed.* **2002**, *41*, 3910.

[84] Hills, I. D.; Netherton, M. R.; Fu, G. C. *Angew. Chem. Int. Ed.* **2003**, *42*, 5749.

[85] Gourlaouen, C.; Ujaque, G.; Lledós, A.; Medio-Simón, M.; Asensio, G.; Maseras, F. *J. Org. Chem.* **2009**, *74*, 4049.

[86] Crabtree, R. H. *The Organometallic Chemistry of the Transition Metals*; 3rd ed. John Wiley-Interscience: New York, 2001.

[87] Lappert, M.; Lednor, P. *Adv. Organomet. Chem.* **1976**, *14*, 345.

[88] Kurosawa, H.; Ogoshi, S.; Kawasaki, Y.; Murai, S.; Miyoshi, M.; Ikeda, I. *J. Am. Chem. Soc.* **1990**, *112*, 2813.

[89] Kurosawa, H.; Kajimaru, H.; Ogoshi, S.; Yoneda, H.; Miki, K.; Kasai, N.; Murai, S.; Ikeda, I. *J. Am. Chem. Soc.* **1992**, *114*, 8417.

[90] Amatore, C.; Jutand, A. *J. Organomet. Chem.* **1999**, *576*, 254.

[91] Kozuch, S.; Amatore, C.; Jutand, A.; Shaik, S. *Organometallics,* **2005**, *24*, 2319.

[92] Diefenbach, A.; de Jong, G. T.; Bickelhaupt, F. M. *J. Chem. Theory Comput.* **2005**, *1*, 286.

[93] Ariafard, A.; Lin, Z. *Organometallics,* **2006**, *25*, 4030.

[94] Hartwig, J. F.; Paul, F. *J. Am. Chem. Soc.* **1995**, *117*, 5373.

[95] Ahlquist, M.; Fristrup, P.; Tanner, D.; Norrby, P. O. *Organometallics,* **2006**, *25*, 2066.

[96] Lam, K. C.; Marder, T. B.; Lin, Z. Y. *Organometallics,* **2007**, *26*, 758.

[97] Barrios-Landeros, F.; Carrow, B. P.; Hartwig, J. F. *J. Am. Chem. Soc.* **2009**, *131*, 8141.

[98] McMullin, C. L.; Jover, J.; Harvey, J. N.; Fey, N. *Dalton Trans.* **2010**, *39*, 10833.

[99] García-Melchor, M.; Ujaque, G.; Maseras, F.; Lledós, A. In *Phosphorus Compounds: Advanced Tools in Catalysis and Material Sciences*; Peruzzini, M.; Gonsalvi, L., Eds.; Springer: Berlin, 2011; Vol. 37; Chapter 3, pp 57–84.

[100] Farina, V. In *Comprehensive Organometallic Chemistry II*; Abel, E. W.; Stone, F.; Wilkinson, G.; Hegedus, L. S., Eds.; Elsevier: Oxford, 1995; Vol. 12; Chapter 3.4.

[101] Osakada, K. In *Fundamentals of Molecular Catalysis*; *Current Methods in Inorganic Chemistry*, Kurosawa, H.; Yamamoto, A., Eds.; Elsevier: Amsterdam, 2003; Chapter 5.

[102] Marshall, J. A. *Chem. Rev.* **2000**, *100*, 3163.

[103] Pérez-Temprano, M. H.; Gallego, A. M.; Casares, J. A.; Espinet, P. *Organometallics,* **2011**, *30*, 611.

[104] Tatsumi, K.; Hoffmann, R.; Yamamoto, A.; Stille, J. K. *Bull. Chem. Soc. Jpn.* **1981**, *54*, 1857.

[105] Low, J. J.; Goddard, W. A. *J. Am. Chem. Soc.* **1986**, *108*, 6115.

[106] Low, J. J.; Goddard, W. A. *Organometallics,* **1986**, *5*, 609.

[107] Ananikov, V. P.; Musaev, D. G.; Morokuma, K. *J. Am. Chem. Soc.* **2002**, *124*, 2839.

[108] Ananikov, V. P.; Musaev, D. G.; Morokuma, K. *Organometallics,* **2005**, *24*, 715.

[109] Ananikov, V. P.; Musaev, D. G.; Morokuma, K. *Eur. J. Inorg. Chem.* **2007**, 5390.

[110] Zuidema, E.; van Leeuwen, P. W. N. M.; Bo, C. *Organometallics,* **2005**, *24*, 3703.

[111] Ariafard, A.; Yates, B. F. *J. Organomet. Chem.* **2009**, *694*, 2075.

[112] Ziegler, T.; Rauk, A. *Theor. Chim. Acta.* **1977**, *46*, 1.

[113] Bickelhaupt, F. M. *J. Comput. Chem.* **1999**, *20*, 114.

[114] Negishi, E.-I.; Takahashi, T.; Akiyoshi, K. *J. Organomet. Chem.* **1987**, *334*, 181.

[115] Pérez-Rodríguez, M.; Braga, A. A. C.; Lera, de A. R.; Maseras, F.; Álvarez, R.; Espinet, P. *Organometallics,* **2010**, *29*, 4983.

[116] Méndez, M.; Cuerva, J. M.; Gómez-Bengoa, E.; Cárdenas, D. J.; Echavarren, A. M. *Chem. Eur. J.* **2002**, *8*, 3620.

[117] Heisenberg, W. *Zeitschrift für Physik A Hadrons and Nuclei,* **1927**, *43*, 172.

[118] Gasser, R. P. H.; Richards, W. G. *An Introduction to Statistical Thermodynamics;* World Scientific Publishing: London, 1995.

[119] McQuarrie, D. A. *Statistical Mechanics;* University Science Books: California, 2000.

[120] Atkins, P.; de Paula, J. *Physical Chemistry*; 9th ed. W. H. Freeman & Co.: New York, 2010; Vol. 2.

[121] Zhou, H.-X.; Gilson, M. K. *Chem. Rev.* **2009**, *109*, 4092.

[122] Spickermann, C. *Entropies of Condensed Phases and Complex Systems: A first Principles Approach;* Springer: Berlin, 2011.

[123] Tamura, H.; Yamazaki, H.; Sato, H.; Sakaki, S. *J. Am. Chem. Soc.* **2003**, *125*, 16114.

[124] Sakaki, S.; Takayama, T.; Sumimoto, M.; Sugimoto, M. *J. Am. Chem. Soc.* **2004**, *126*, 3332.

[125] Sumimoto, M.; Iwane, N.; Takahama, T.; Sakaki, S. *J. Am. Chem. Soc.* **2004**, *126*, 10457.

[126] Cooper, J.; Ziegler, T. *Inorg. Chem.* **2002**, *41*, 6614.

[127] Zhu, H.; Ziegler, T. *J. Organomet. Chem.* **2006**, *691*, 4486.

[128] Zhu, H.; Ziegler, T. *Organometallics,* **2008**, *27*, 1743.

[129] Wertz, D. H. *J. Am. Chem. Soc.* **1980**, *102*, 5316.

[130] Martin, R. L.; Hay, P. J.; Pratt, L. R. *J. Phys. Chem. A,* **1998**, *102*, 3565.

[131] Hohenberg, P.; Kohn, W. *Phys. Rev. B,* **1964**, *136*, 864.

[132] Thomas, L. H. *Proc. Camb. Phil. Soc.* **1927**, *23*, 542.

[133] Fermi, E. *Rend. Accad. Lincei.* **1927**, *6*, 602.

[134] Dirac, P. A. M. *Proc. Camb. Phil. Soc.* **1930**, *26*, 376.

[135] Kohn, W.; Sham, L. J. *Phys. Rev. A,* **1965**, *140*, 1133.

[136] Genesis, 28:11-19.

[137] Ceperley, D. M.; Alder, B. J. *Phys. Rev. Lett.* **1980**, *45*, 566.

[138] Vosko, S. J.; Wilk, L.; Nusair, M. *Can. J. Phys.* **1980**, *58*, 1200.

[139] Becke, A. D. *Phys. Rev. A,* **1988**, *38*, 3098.

[140] Perdew, J. P. In *Electronic Structure of Solids*; Ziesche, P.; Eschrig, H., Eds.; Akademie Verlag: Berlin, 1991.

[141] Perdew, J. P.; Chevary, J. A.; Vosko, S. H.; Jackson, K. A.; Pederson, M. R.; Singh, D. J.; Fiolhais, C. *Phys. Rev. B,* **1992**, *46*, 6671. Erratum: *Phys. Rev. B,* **1993**, *48*, 4978.

[142] Perdew, J. P.; Burke, K.; Wang, Y. *Phys. Rev. B,* **1996**, *54*, 16533.

[143] Burke, K.; Perdew, J. P.; Wang, Y. In *Electronic Density Functional Theory. Recent Progress and New Directions*; Dobson, J. F.; Vignale, G.; Das, M. P., Eds.; Plenum Press: New York, 1998.

[144] Handy, N. C.; Cohen, A. J. *Mol. Phys.* **2001**, *99*, 403.

[145] Hoe, W.-M.; Cohen, A.; Handy, N. C. *Chem. Phys. Lett.* **2001**, *341*, 319.

[146] Adamo, C.; Barone, V. *J. Chem. Phys.* **1998**, *108*, 664.

[147] Becke, A. D. *J. Chem. Phys.* **1986**, *84*, 4524.

[148] Perdew, J. P. *Phys. Rev. B,* **1986**, *33*, 8822.

[149] Perdew, J. P.; Burke, K.; Ernzerhof, M. *Phys. Rev. Lett.* **1996**, *77*, 3865. Erratum: *Phys. Rev. Lett.* **1997**, *78*, 1396.

[150] Lee, C.; Yang, W.; Parr, R. G. *Phys. Rev. B,* **1988**, *37*, 785.

[151] Perdew, J. P.; Kurth, S.; Zupan, A.; Blaha, P. *Phys. Rev. Lett.* **1999**, *82*, 2544.

[152] Schmider, H. L.; Becke, A. D. *J. Chem. Phys.* **1998**, *108*, 9624.

[153] Tao, J. M.; Perdew, J. P.; Staroverov, V. N.; Scuseria, G. E. *Phys. Rev. Lett.* **2003**, *91*, 146401.

[154] Van Voorhis, T.; Scuseria, G. E. *J. Chem. Phys.* **1998**, *109*, 400.

[155] Rey, J.; Savin, A. *Int. J. Quantum Chem.* **1998**, *69*, 581.

[156] Krieger, J. B.; Chen, J. Q.; Iafrate, G. J.; Savin, A. In *Electron Correlations and Materials Properties*; Gonis, A.; Kioussis, N.; Ciftan, M., Eds.; Kluwer Academic: New York, 1999; pp 463–477.

[157] Krieger, J. B.; Chen, J. Q.; Kurth, S. In *Density Functional Theory and its Application to Materials*; van Doren, V.; van Alsenoy, C.; Geerlings, P., Eds.; A.I.P.: New York, 2001; Vol. 577; pp 48–69.

[158] Toulouse, J.; Savin, A.; Adamo, C. *J. Chem. Phys.* **2002**, *117*, 10465.

[159] Becke, A. D. *J. Chem. Phys.* **1993**, *98*, 1372.

[160] Poater, J.; Solà, M.; Rimola, A.; Rodríguez-Santiago, L.; Sodupe, M. *J. Phys. Chem. A,* **2004**, *108*, 6072.

[161] Georgieva, I.; Trendafilova, N.; Rodríguez-Santiago, L.; Sodupe, M. *J. Phys. Chem. A,* **2005**, *109*, 5668.

[162] Rimola, A.; Rodríguez-Santiago, L.; Sodupe, M. *J. Phys. Chem. B,* **2006**, *110*, 24189.

[163] Rimola, A.; Constantino, E.; Rodríguez-Santiago, L.; Sodupe, M. *J. Phys. Chem. A,* **2008**, *112*, 3444.

[164] Becke, A. D. *J. Chem. Phys.* **1993**, *98*, 5648.

[165] Stephens, P. J.; Devlin, F. J.; Chabalowski, C. F.; Frisch, M. J. *J. Phys. Chem.* **1994**, *98*, 11623.

[166] Gonzales, J. M.; Cox III, R. S.; Brown, S. T.; Allen, W. D.; Schaefer III, H. F. *J. Phys. Chem. A,* **2001**, *105*, 11327.

[167] Zhao, Y.; Truhlar, D. G. *Acc. Chem. Res.* **2007**, *41*, 157.

[168] Zhao, Y.; Schultz, N. E.; Truhlar, D. G. *J. Chem. Phys.* **2005**, *123*, 161103.

[169] Zhao, Y.; Schultz, N. E.; Truhlar, D. G. *J. Chem. Theory Comput.* **2006**, *2*, 364.

[170] Zhao, Y.; Truhlar, D. G. *Acc. Chem. Res.* **2008**, *41*, 157.

[171] Zhao, Y.; Truhlar, D. G. *Theor. Chem. Acc.* **2008**, *120*, 215.

[172] Zhao, Y.; Truhlar, D. G. *J. Chem. Phys.* **2006**, *125*, 194101.

[173] Zhao, Y.; Truhlar, D. G. *J. Phys. Chem. A,* **2006**, *110*, 13126.

[174] Zhao, Y.; Truhlar, D. G. *J. Chem. Theory Comput.* **2008**, *4*, 1849.

[175] Peverati, R.; Zhao, Y.; Truhlar, D. G. *J. Phys. Chem. Lett.* **2011**, *2*, 2810.

[176] Grimme, S. *J. Comput. Chem.* **2004**, *25*, 1463.

[177] Sato, T.; Tsuneda, T.; Hirao, K. *Mol. Phys.* **2005**, *103*, 1151.

[178] Von Lilienfeld, O. A.; Tavernelli, I.; Röthlisberger, U.; Sebastiani, D. *Phys. Rev. Lett.* **2004**, *93*, 153004.

[179] Sun, Y. Y.; Kim, Y.-H.; Lee, K.; Zhang, S. B. *J. Chem. Phys.* **2008**, *129*, 154102.

[180] Grimme, S. *J. Comput. Chem.* **2006**, *27*, 1787.

[181] Grimme, S.; Antony, J.; Ehrlich, S.; Krieg, H. *J. Chem. Phys.* **2010**, *132*, 154104.

[182] Grimme, S.; Ehrlich, S.; Goerigk, L. *J. Comput. Chem.* **2011**, *32*, 1456.

[183] Langreth, D. C.; Perdew, J. P. *Phys. Rev. B,* **1980**, *21*, 5469.

[184] Pitarke, J. M.; Eguiluz, A. G. *Phys. Rev. B,* **2001**, *63*, 045116.

[185] Furche, F. *Phys. Rev. B,* **2001**, *64*, 195120.

[186] Fuchs, M.; Gonze, X. *Phys. Rev. B,* **2002**, *65*, 235109.

[187] Yan, Z.; Perdew, J. P.; Kurth, S. *Phys. Rev. B,* **2000**, *61*, 16430.

[188] Lein, M.; Gross, E. K. U.; Perdew, J. P. *Phys. Rev. B,* **2000**, *61*, 13431.

[189] Seidl, M.; Perdew, J. P.; Kurth, S. *Phys. Rev. Lett.* **2000**, *84*, 5070.

[190] Szabo, A.; Ostlund, N. S. *Modern Quantum Chemistry;* Dover Publications, INC.: New York, 1996.

[191] Jensen, F. *Introduction to Computational Chemistry;* John Wiley & Sons: England, 1999.

[192] Andrés, J.; Bertran, J. In *Química Teórica y Computacional*; Andrés, J.; Bertran, J., Eds.; Publicacions de la Universitat de Jaume I: Castelló de la Plana, 2000; Vol. 2.

[193] Perdew, J. P.; Zunger, A. *Phys. Rev. B,* **1981**, *23*, 5048.

[194] Tomasi, J.; Persico, M. *Chem. Rev.* **1994**, *94*, 2027.

[195] Miertus, S.; Scrocco, E.; Tomasi, J. *J. Chem. Phys.* **1981**, *55*, 117.

[196] Marenich, A. V.; Cramer, C. J.; Truhlar, D. G. *J. Phys. Chem. B,* **2009**, *113*, 6378.

[197] Foresman, J. B.; Keith, T. A.; Wiberg, K. B.; Snoonian, J.; Frisch, M. J. *J. Phys. Chem.* **1996**, *100*, 16098.

[198] Negishi, E.-I. *Acc. Chem. Res.* **1982**, *15*, 340.

[199] Knochel, P.; Singer, R. D. *Chem. Rev.* **1993**, *93*, 2117.

[200] Rouhi, A. M. *Chem. & Eng. News,* **2004**, *82*, 49.

[201] King, A. O.; Yasuda, N. *Organometallics in Process Chemistry*; Vol. 6 of *Topics in Organometallic Chemistry;* Springer: Berlin, 2004; pp 205–245.

[202] Hirashima, S.; Aoyagi, S.; Kibayashi, C. *J. Am. Chem. Soc.* **1999**, *121*, 9873.

[203] Wipf, P.; Lim, S. *J. Am. Chem. Soc.* **1995**, *117*, 558.

[204] Álvarez, R.; Pérez, M.; Faza, O. N.; Lera, de A. R. *Organometallics,* **2008**, *27*, 3378.

[205] Álvarez, R.; Faza, O. N.; Lera, de A. R.; Cárdenas, D. J. *Adv. Synth. Catal.* **2007**, *349*, 887.

[206] Carrow, B. P.; Hartwig, J. F. *J. Am. Chem. Soc.* **2011**, *133*, 2116.

[207] Urkalan, K.; Sigman, M. S. *J. Am. Chem. Soc.* **2009**, *131*, 18042.

[208] Howell, G. P.; Minnaard, A. J.; Feringa, B. L. *Org. Biomol. Chem.* **2006**, *4*, 1278.

[209] Jin, L.; Zhao, Y.; Zhu, L.; Zhang, H.; Lei, A. *Adv. Synth. Catal.* **2009**, *351*, 630.

[210] Chen, M.; Zheng, X.; Li, W.; He, J.; Lei, A. *J. Am. Chem. Soc.* **2010**, *132*, 4101.

[211] Van Asselt, R.; Elsevier, C. J. *Organometallics,* **1994**, *13*, 1972.

[212] Chass, G. A.; O'Brien, C. J.; Hadei, N.; Kantchev, E. A. B.; Mu, W.-H.; Fang, D.-C.; Hopkinson, A. C.; Csizmadia, I. G.; Organ, M. G. *Chem. Eur. J.* **2009**, *15*, 4281.

[213] Ribagnac, P.; Blug, M.; Villa-Uribe, J.; Le Goff, X.-F.; Gosmini, C.; Mézailles, N. *Chem. Eur. J.* **2011**, *17*, 14389.

[214] Mendes, P. *Comput. Appl. Biosci.* **1993**, *9*, 563.

[215] Frisch, M. J.; Trucks, G. W.; Schlegel, H. B.; Scuseria, G. E.; Robb, M. A.; Cheeseman, J. R.; Scalmani, G.; Barone, V.; Mennucci, B.; Petersson, G. A.; Nakatsuji, H.; Caricato, M.; Li, X.; Hratchian, H. P.; Izmaylov, A. F.; Bloino, J.; Zheng, G.; Sonnenberg, J. L.; Hada, M.; Ehara, M.; Toyota, K.; Fukuda, R.; Hasegawa, J.; Ishida, M.; Nakajima, T.; Honda, Y.; Kitao, O.; Nakai, H.; Vreven, T.; Montgomery, Jr., J. A.; Peralta, J. E.; Ogliaro, F.; Bearpark, M.; Heyd, J. J.; Brothers, E.; Kudin, K. N.; Staroverov, V. N.; Kobayashi, R.; Normand, J.; Raghavachari, K.; Rendell, A.; Burant, J. C.; Iyengar, S. S.; Tomasi, J.; Cossi, M.; Rega, N.; Millam, J. M.; Klene, M.; Knox, J. E.; Cross, J. B.; Bakken, V.; Adamo, C.; Jaramillo, J.; Gomperts, R.; Stratmann, R. E.; Yazyev, O.; Austin, A. J.; Cammi, R.; Pomelli, C.; Ochterski, J. W.; Martin, R. L.; Morokuma, K.; Zakrzewski, V. G.; Voth, G. A.; Salvador, P.; Dannenberg, J. J.; Dapprich, S.; Daniels, A. D.; Farkas, Ö. ; Foresman, J. B.; Ortiz, J. V.; Cioslowski, J.; Fox, D. J., Gaussian 09, Revision A.1, Gaussian, Inc., Wallingford, CT, 2009.

[216] Weidenbruch, M.; Herrndorf, M.; Schäfer, A.; Pohl, S.; Saak, W. *J. Organomet. Chem.* **1989**, *361*, 139.

[217] Hay, P. J.; Wadt, W. R. *J. Chem. Phys.* **1985**, *82*, 270.

[218] Hay, P. J.; Wadt, W. R. *J. Chem. Phys.* **1985**, *82*, 299.

[219] Godbout, N.; Salahub, D. R.; Andzelm, J.; Wimmer, E. *Can. J. Chem.* **1992**, *70*, 560.

[220] Schäfer, A.; Huber, C.; Ahlrichs, R. *J. Chem. Phys.* **1994**, *100*, 5829.

[221] Álvarez, R.; Lera, de A. R.; Aurrecoechea, J. M.; Durana, A. *Organometallics,* **2007**, *26*, 2799.

[222] Spielvogel, D. J.; Davis, W. M.; Buchwald, S. L. *Organometallics,* **2002**, *21*, 3833.

[223] Spielvogel, D. J.; Buchwald, S. L. *J. Am. Chem. Soc.* **2002**, *124*, 3500.

[224] Anderson, T. J.; Vicic, D. A. *Organometallics,* **2004**, *23*, 623.

[225] Sonogashira, K. *J. Organomet. Chem.* **2002**, *653*, 46.

[226] Negishi, E.-I.; Anastasia, L. *Chem. Rev.* **2003**, *103*, 1979.

[227] Tykwinski, R. R. *Angew. Chem. Int. Ed.* **2003**, *42*, 1566.

[228] Chinchilla, R.; Nájera, C. *Chem. Rev.* **2007**, *107*, 874.

[229] Chinchilla, R.; Nájera, C. *Chem. Soc. Rev.* **2011**, *40*, 5084.

[230] Bunz, U. H. F. *Chem. Rev.* **2000**, *100*, 1605.

[231] Müller, T. J.; D'Souza, D. M. *Pure Appl. Chem.* **2008**, *80*, 609.

[232] Schiedel, M. S.; Briehn, C. A.; Bäuerle, P. *J. Organomet. Chem.* **2002**, *653*, 200.

[233] Hortholary, C.; Coudret, C. *J. Org. Chem.* **2003**, *68*, 2167.

[234] Torborg, C.; Beller, M. *Adv. Synth. Catal.* **2009**, *351*, 3027.

[235] Dieck, H. A.; Heck, F. R. *J. Organomet. Chem.* **1975**, *93*, 259.

[236] Cassar, L. *J. Organomet. Chem.* **1975**, *93*, 253.

[237] Kotora, M.; Takahashi, T. In *Handbook of Organopalladium Chemistry for Organic Synthesis*; Negishi, E.-I.; de Meijere, A., Eds.; Wiley-Interscience: New York, 2002; p 973.

[238] Bräse, S.; de Meijere, A. In *Handbook of Organopalladium Chemistry for Organic Synthesis*; Negishi, E.-I.; de Meijere, A., Eds.; Wiley-Interscience: New York, 2002; p 1133.

[239] Sonogashira, K.; Tohda, Y.; Hagihara, N. *Tetrahedron Lett.* **1975**, 4467.

[240] Ljungdahl, T.; Pettersson, K.; Albinsson, B.; Mårtensson, J. *J. Org. Chem.* **2006**, *71*, 1677.

[241] Gelman, D.; Buchwald, S. L. *Angew. Chem. Int. Ed.* **2003**, *42*, 5993.

[242] Siemsen, P.; Livingston, R. C.; Diederich, F. *Angew. Chem. Int. Ed.* **2000**, *39*, 2633.

[243] Fukuyama, T.; Shinmen, M.; Nishitani, S.; Sato, M.; Ryu, I. *Org. Lett.* **2002**, *4*, 1691.

[244] Soheili, A.; Albaneze-Walker, J.; Murry, J. A.; Dormer, P. G.; Hughes, D. L. *Org. Lett.* **2003**, *5*, 4191.

[245] Nájera, C.; Gil-Moltó, J.; Karlström, S.; Falvello, L. R. *Org. Lett.* **2003**, *5*, 1451.

[246] Rau, S.; Lamm, K.; Görls, H.; Schöffel, J.; Walther, D. *J. Organomet. Chem.* **2004**, *689*, 3582.

[247] Li, J.-H.; Zhang, X.-D.; Xie, Y.-X. *Eur. J. Org. Chem.* **2005**, 4256.

[248] Gil-Moltó, J.; Nájera, C. *Eur. J. Org. Chem.* **2005**, 4073.

[249] Yi, C.; Hua, R. *Catal. Commun.* **2006**, *7*, 377.

[250] Galdino de Lima, P.; Antunes, O. A. C. *Tetrahedron Lett.* **2008**, *49*, 2506.

[251] Komáromi, A.; Tolnai, G.; Novák, Z. *Tetrahedron Lett.* **2008**, *49*, 7294.

[252] Alonso, D. A.; Nájera, C.; Pacheco, M. C. *Tetrahedron Lett.* **2002**, *43*, 9365.

[253] Cheng, J.; Sun, Y.-H.; Wang, F.; Guo, M.-J.; Xu, J.-H.; Pan, Y.; Zhang, Z.-G. *J. Org. Chem.* **2004**, *69*, 5428.

[254] Ruiz, J.; Cutillas, N.; López, F.; López, G.; Bautista, D. *Organometallics,* **2006**, *25*, 5768.

[255] Komáromi, A.; Novák, Z. *Chem. Commun.* **2008**, 4968.

[256] John, A.; Shaikh, M. M.; Ghosh, P. *Dalton Trans.* **2009**, 10581.

[257] Torborg, C.; Huang, J.; Schulz, T.; Schäffner, B.; Zapf, A.; Spannenberg, A.; Börner, A.; Beller, M. *Chem. Eur. J.* **2009**, *15*, 1329.

[258] Liang, B.; Dai, M.-J.; Chen, J.-H.; Yang, Z. *J. Org. Chem.* **2005**, *70*, 391.

[259] Li, J.-H.; Liang, Y.; Xie, Y.-X. *J. Org. Chem.* **2005**, *70*, 4393.

[260] Carpita, A.; Ribecai, A. *Tetrahedron Lett.* **2009**, *50*, 204.

[261] Urgaonkar, S.; Verkade, J. G. *J. Org. Chem.* **2004**, *69*, 5752.

[262] Liang, Y.; Xie, Y.-X.; Li, J.-H. *J. Org. Chem.* **2006**, *71*, 379.

[263] Amatore, C.; Bensalem, S.; Ghalem, S.; Jutand, A.; Medjour, Y. *Eur. J. Org. Chem.* **2004**, 366.

[264] Tougerti, A.; Negri, S.; Jutand, A. *Chem. Eur. J.* **2007**, *13*, 666.

[265] Ljungdahl, T.; Bennur, T.; Dallas, A.; Emtenas, H.; Mårtensson, J. *Organometallics,* **2008**, *27*, 2490.

[266] Chen, L.-P.; Hong, S.-G.; Hou, H.-Q. *Chin. J. Struct. Chem.* **2008**, *27*, 1404.

[267] Sikk, L.; Tammiku-Taul, J.; Burk, P. *Organometallics,* **2011**, *30*, 5656.

[268] Frisch, M. J.; Trucks, G. W.; Schlegel, H. B.; Scuseria, G. E.; Robb, M. A.; Cheeseman, J. R.; Montgomery, Jr., J. A.; Vreven, T.; Kudin, K. N.; Burant, J. C.; Millam, J. M.; Iyengar, S. S.; Tomasi, J.; Barone, V.; Mennucci, B.; Cossi, M.; Scalmani, G.; Rega, N.; Petersson, G. A.; Nakatsuji, H.; Hada, M.; Ehara, M.; Toyota, K.; Fukuda, R.; Hasegawa, J.; Ishida, M.; Nakajima, T.; Honda, Y.; Kitao, O.; Nakai, H.; Klene, M.; Li, X.; Knox, J. E.; Hratchian, H. P.; Cross, J. B.; Bakken, V.; Adamo, C.; Jaramillo, J.; Gomperts, R.; Stratmann, R. E.; Yazyev, O.; Austin, A. J.; Cammi, R.; Pomelli, C.; Ochterski, J. W.; Ayala, P. Y.; Morokuma, K.; Voth, G. A.; Salvador, P.; Dannenberg, J. J.; Zakrzewski, V. G.; Dapprich, S.; Daniels, A. D.; Strain, M. C.; Farkas, O.; Malick, D. K.; Rabuck, A. D.; Raghavachari, K.; Foresman, J. B.; Ortiz, J. V.; Cui, Q.; Baboul, A. G.; Clifford, S.; Cioslowski, J.; Stefanov, B. B.; Liu, G.; Liashenko, A.; Piskorz, P.; Komaromi, I.; Martin, R. L.; Fox, D. J.; Keith, T.; Al-Laham, M. A.; Peng, C. Y.; Nanayakkara, A.; Challacombe, M.; Gill, P. M. W.; Johnson, B.; Chen, W.; Wong, M. W.; Gonzalez, C.; Pople, J. A., Gaussian 03, Revision E.01, Gaussian, Inc., Wallingford, CT, 2004.

[269] Andrae, D.; Häussermann, U.; Dolg, M.; Stoll, H.; Preuss, H. *Theor. Chim. Acta.* **1990**, *77*, 123.

[270] Ehlers, A. W.; Bohme, M.; Dapprich, S.; Gobbi, A.; Hollwarth, A.; Jonas, V.; Kohler, K. F.; Stegmann, R.; Veldkamp, A.; Frenking, G. *Chem. Phys. Lett.* **1993**, *208*, 111.

[271] Hollwarth, A.; Bohme, M.; Dapprich, S.; Ehlers, A. W.; Gobbi, A.; Jonas, V.; Kohler, K. F.; Stegmann, R.; Veldkamp, A.; Frenking, G. *Chem. Phys. Lett.* **1993**, *208*, 237.

[272] Check, C. E.; Faust, T. O.; Bailey, J. M.; Wright, B. J.; Gilbert, T. M.; Sunderlin, L. S. *J. Phys. Chem. A,* **2001**, *105*, 8111.

[273] Ariafard, A.; Yates, B. F. *J. Am. Chem. Soc.* **2009**, *131*, 13981.

[274] Thaler, T.; Haag, B.; Gavryushin, A.; Schober, K.; Hartmann, E.; Gschwind, R. M.; Zipse, H.; Mayer, P.; Knochel, P. *Nature Chem.* **2010**, *2*, 125.

[275] Besora, M.; Braga, A. A. C.; Ujaque, G.; Maseras, F.; Lledós, A. *Theor. Chem. Acc.* **2011**, *128*, 639.

[276] Casado, A. L.; Espinet, P. *Organometallics,* **1998**, *17*, 954.

[277] Suzuki, A.; Yamamoto, Y. *Chem. Lett.* **2011**, *40*, 894.

[278] Myers, A. G.; Tom, N. J.; Fraley, M. E.; Cohen, S. B.; Madar, D. J. *J. Am. Chem. Soc.* **1997**, *119*, 6072.

[279] Suzuki, A. *J. Organomet. Chem.* **1999**, *576*, 147.

[280] Kotha, S.; Lahiri, K.; Kashinath, D. *Tetrahedron,* **2002**, *58*, 9633.

[281] Garg, N. K.; Caspi, D. D.; Stoltz, B. M. *J. Am. Chem. Soc.* **2004**, *126*, 9552.

[282] Suzuki, A. *Angew. Chem. Int. Ed.* **2011**, *50*, 6723.

[283] Weng, C.-M.; Hong, F.-E. *Dalton Trans.* **2011**, *40*, 6458.

[284] Quasdorf, K. W.; Antoft-Finch, A.; Liu, P.; Silberstein, A. L.; Komaromi, A.; Blackburn, T.; Ramgren, S. D.; Houk, K. N.; Snieckus, V.; Garg, N. K. *J. Am. Chem. Soc.* **2011**, *133*, 6352.

[285] Ariafard, A.; Lin, Z.; Fairlamb, I. J. S. *Organometallics,* **2006**, *25*, 5788.

[286] Krasovskiy, A.; Lipshutz, B. H. *Org. Lett.* **2011**, *13*, 3818.

[287] Martín, R.; Buchwald, S. L. *Acc. Chem. Res.* **2008**, *41*, 1461.

[288] Christmann, U.; Vilar, R. *Angew. Chem. Int. Ed.* **2005**, *44*, 366.

[289] Fleckenstein, C. A.; Plenio, H. *Chem. Soc. Rev.* **2010**, *39*, 694.

[290] Goossen, L. J.; Koley, D.; Hermann, H. L.; Thiel, W. *Organometallics,* **2006**, *25*, 54.

[291] Joshaghani, M.; Faramarzi, E.; Rafiee, E.; Daryanavard, M.; Xiao, J.; Baillie, C. *J. Mol. Catal. A: Chem.* **2006**, *259*, 35.

[292] Kozuch, S.; Martin, J. M. *ACS Catal.* **2011**, *1*, 246.

[293] Brunel, J. M. *Chem. Rev.* **2005**, *105*, 857.

[294] Berthod, M.; Mignani, G.; Woodward, G.; Lemaire, M. *Chem. Rev.* **2005**, *105*, 1801.

[295] Kozlowski, M. C.; Morgan, B. J.; Linton, E. C. *Chem. Soc. Rev.* **2009**, *38*, 3193.

[296] Zehm, D.; Fudickar, W.; Hans, M.; Schilde, U.; Kelling, A.; Linker, T. *Chem. Eur. J.* **2008**, *14*, 11429.

[297] Ma1, B.; Zeng1, F.; Zheng, F.; Wu, S. *Chem. Eur. J.* **2011**, *17*, 14844.

[298] Yin, J.; Buchwald, S. L. *J. Am. Chem. Soc.* **2000**, *122*, 12051.

[299] Cammidge, A. N.; Crépy, K. V. L. *Chem. Commun.* **2000**, 1723.

[300] Jensen, J. F.; Johannsen, M. *Org. Lett.* **2003**, *5*, 3025.

[301] Mikami, K.; Miyamoto, T.; Hatano, M. *Chem. Commun.* **2004**, 2082.

[302] Colobert, F.; Valdivia, V.; Choppin, S.; Leroux, F. R.; Fernández, I.; Álvarez, E.; Khiar, N. *Org. Lett.* **2009**, *11*, 5130.

[303] Debono, N.; Labande, A.; Manoury, E.; Daran, J.-C.; Poli, R. *Organometallics,* **2010**, *29*, 1879.

[304] Lee, J. C. H.; McDonald, R.; Hall, D. G. *Nature Chem.* **2011**, *3*, 894 .

[305] Kamei, T.; Sato, A. H.; Iwasawa, T. *Tetrahedron Lett.* **2011**, *52*, 2638.

[306] Yamamoto, T.; Akai, Y.; Nagata, Y.; Suginome, M. *Angew. Chem. Int. Ed.* **2011**, *50*, 8844.

[307] Shen, X.; Jones, G. O.; Watson, D. A.; Bhayana, B.; Buchwald, S. L. *J. Am. Chem. Soc.* **2010**, *132*, 11278.

[308] Bermejo, A.; Ros, A.; Fernández, R.; Lassaletta, J. M. *J. Am. Chem. Soc.* **2008**, *130*, 15798.

[309] Lassaletta, J. M.; Alcarazo, M.; Fernández, R. *Chem. Commun.* **2004**, 298.

[310] Grasa, G. A.; Hillier, A. C.; Nolan, S. P. *Org. Lett.* **2001**, *3*, 1077.

[311] Mino, T.; Shirae, Y.; Sakamoto, M.; Fujita, T. *J. Org. Chem.* **2005**, *70*, 2191.

[312] Huang, Y.-L.; Weng, C.-M.; Hong, F.-E. *Chem. Eur. J.* **2008**, *14*, 4426.

[313] Wang, C.; Wu, W. *J. Chem. Educ.* **2011**, *88*, 299.

A

Appendix A: Published articles on the topics included in this Ph.D. Thesis

A.1 Article I:

Palladium Round Trip in the Negishi Coupling of *trans*-[PdMeCl($PMePh_2$)$_2$] with ZnMeCl: An Experimental and DFT Study of the Transmetalation Step

Fuentes, B.; **García-Melchor, M.**; Lledós, A.; Maseras, F.; Casares, J. A.; Ujaque, G.; Espinet, P. *Chem. Eur. J.* **2010**, *16*, 8596-8599.

CHEMISTRY
A EUROPEAN JOURNAL

DOI: 10.1002/chem.201001332

Palladium Round Trip in the Negishi Coupling of *trans*-[PdMeCl(PMePh$_2$)$_2$] with ZnMeCl: An Experimental and DFT Study of the Transmetalation Step

Beatriz Fuentes,[a] Max García-Melchor,[b] Agustí Lledós,[b] Feliu Maseras,[b, c] Juan A. Casares,*[a] Gregori Ujaque,*[b] and Pablo Espinet*[a]

Compared with the detailed mechanistic knowledge of the Stille reaction,[1] little is known about the Negishi reaction.[2,3] Recently, we experimentally uncovered the complicated behavior of the transmetalation of *trans*-[PdRfCl(PPh$_3$)$_2$] (Rf = 3,5-dichloro-2,4,6-trifluorophenyl) with ZnMe$_2$ or ZnMeCl, showing that each methylating reagent afforded stereoselectively a different isomer (*trans* or *cis*, respectively) of the coupling intermediate [PdRfMe(PPh$_3$)$_2$].[4] Moreover, the study revealed the occurrence of undesired transmetalations, such as those shown in Scheme 1, which could eventually produce homocoupling products; the corresponding undesired intermediates were detected and identified by NMR spectroscopy techniques.

The formation of undesired intermediates in related reactions with aryl zinc derivatives was later observed by Lei et al.[5]

Herein, we report an experimental mechanistic study of the reaction of *trans*-[PdClMe(PMePh$_2$)$_2$] (**1**) with

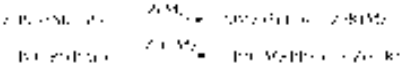

Scheme 1.

[a] B. Fuentes, Dr. J. A. Casares, Prof. P. Espinet
IU CINQUIMA/Química Inorgánica
Facultad de CienciasUniversidad de Valladolid
47071 Valladolid (Spain)
Fax: (+34) 983423231/(+34) 983186336
E-mail: casares@qi.uva.es
espinet@qi.uva.es

[b] M. García-Melchor, Prof. A. Lledós, Prof. F. Maseras, Dr. G. Ujaque
Química Física, Edifici C.n, Universitat Autònoma de Barcelona
08193 Bellaterra, Catalonia (Spain)
Fax: (+34) 935812920
E-mail: gregori@klingon.uab.es

[c] Prof. F. Maseras
Institute of Chemical Research of Catalonia (ICIQ)
Av. Països Catalans, 16, 43007 Tarragona, Catalonia (Spain)

Supporting information for this article is available on the WWW under http://dx.doi.org/10.1002/chem.201001332.

ZnMeCl,[6] which affords the first experimental determination of thermodynamic parameters of a Negishi transmetalation. This is complemented with a theoretical DFT study, which provides a detailed view of the reaction pathway, consistent with the experimental parameters.

The reactions of **1** with ZnMeCl were carried out (with one exception) in 1:20 ratio, simulating catalytic conditions with 5% Pd, in THF at different temperatures.

At room temperature, the only product observed was *cis*-[PdMe$_2$(PMePh$_2$)$_2$] (**2**), in equilibrium with the starting material **1**. In these conditions, complex **2** undergoes slow decomposition (reductive elimination) to give ethane.[7,8]

When the reaction was monitored by ^{31}P NMR spectroscopy at 223 K (Figure 1a), the coupling rate to give ethane became negligible and the formation of *trans*-[PdMe$_2$(PMePh$_2$)$_2$] (**3**), as well as *cis*-[PdMe$_2$(PMePh$_2$)$_2$] (**2**), was observed. The *trans* isomer **3** seemed to be formed first and then disappeared. The same reaction, carried out at 203 K in 1:1 ratio to get a slower rate of transformation, confirmed that **3** is formed noticeably faster than **2** (Figure 1b). Thus, the observation of the *cis* isomer at room temperature is deceptive for the stereoselectivity of the transmetalation. Snapshots of two moments of the transmetalation reaction at 203 K, as seen by ^{31}P NMR spectroscopy, are shown in Figure 1c.

The behavior of **3** is typical of a kinetic product of noticeably lower stability than the thermodynamic product (**2**): eventually it disappears from observation as the reaction proceeds and gets closer to the equilibrium concentrations, where the concentration of **3** is very small. In effect, during the progress of the reaction at 223 K (Figure 1a), the concentration of **2** increases continuously; in contrast, a small accumulation of **3** is produced initially and then its concentration decreases, so that in 300 min **3** has practically disappeared. After about 10 h at 223 K, the system has reached equilibrium between the starting complex **1** and the final thermodynamic product **2** ($[\mathbf{1}] = 5.8\times10^{-3}$ mol l^{-1}, $[\mathbf{2}] = 4.4\times10^{-3}$ mol l^{-1}, and $K_{eq} = 2.0\times10^{-2}$); the concentration of **3** is below the limit of NMR observation.

COMMUNICATION

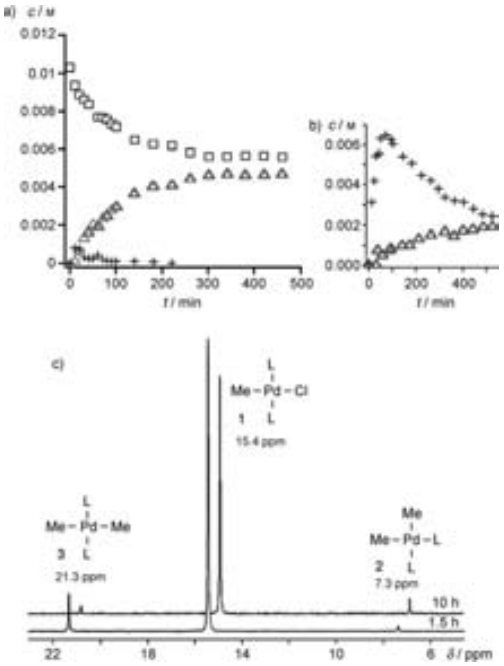

Figure 1. Concentration versus time data, obtained by ^{31}P NMR spectroscopy, for the reaction of **1** (□) with ZnMeCl in different conditions: a) ratio 1:20, in THF at 223 K. Starting conditions: [Pd] = 0.01 M; [ZnMeCl] = 0.20 M; b) ratio 1:1, in THF at 203 K (**1** is not depicted because its abundance is above the values represented in the ordinate axis). △: **2**, +: **3**. Starting conditions: [Pd] = 0.056 M; [ZnMeCl] = 0.056 M; c) ^{31}P NMR spectra of the transmetalation reaction at 203 K, showing the evolution with time of the signals of **1**, **2**, and **3**.

In contrast to the transient existence of **3** in the transmetalation experiments (in fact **3** could not be observed in the experiments at room temperature), *trans*-[$PdMe_2(PMePh_2)_2$] (**3**) as an isolated compound (prepared by an independent method)[8] is fairly stable: it takes 10 h in THF at 273 K for about half of it to isomerize to **2**, whereas at 223 K the **3** to **2** isomerization rate is negligible. On the other hand, the addition of $ZnCl_2$ to a solution of **3** in THF, at 223 K, produces the instantaneous and complete transformation of **3** to **1**. In the same conditions (addition of $ZnCl_2$), compound **2** is also transformed into **1** until equilibrium is reached. In other words, the transmetalations between **1** and ZnMeCl to give **2** or **3** are quickly reversible. These experiments support the interpretation of the observations shown in Figure 1 that in Negishi conditions there should be a fast isomerization between **3** and **2** by fast retrotransmetalations to **1**, in spite of the fact that direct isomerization is slow.[9]

The measured concentration versus time data of the experiments depicted in Figure 1 were fitted to the kinetic model shown in Figure 2,[10] and the transmetalation and retrotransmetalation rates at 223 K were calculated. From these rates, the relative ΔG_{223} values for **1**, **2**, **3**, and for the transition states were obtained (for details see the Supporting Information). These thermodynamic parameters are plotted in Figure 2. Similar parameters ($\Delta G^{\ddagger}_{203}(Ts_{\mathbf{1\text{-}2}}) = 15.6$ kcal mol^{-1}; $\Delta G^{\ddagger}_{203}(Ts_{\mathbf{1\text{-}3}}) = 14.3$ kcal mol^{-1}) were obtained at 203 K. The values obtained indicate that the transmetalation of **1** to **3** is about 5–10 times faster than the transmetalation of **1** to **2**; the retrotransmetalations from **3** or **2** to **1** are still faster. At the same temperatures, the coupling rate for **2** to give ethane is negligible.

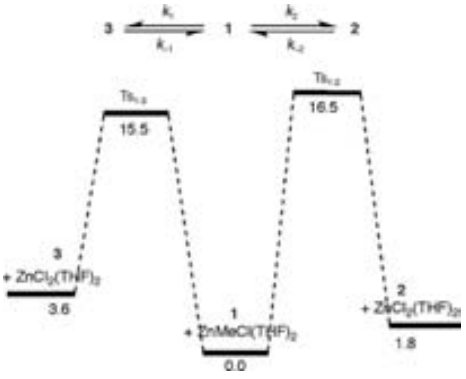

Figure 2. Kinetic model (top) and experimental $\Delta G^{\ddagger}$ profile (bottom) (kcal mol^{-1}, in THF at 223 K) of the reaction. k_1 and k_2 are the transmetalation rate constants, whereas k_{-1} and k_{-2} are the retrotransmetalation rate constants. Ts = transition state.

These quantitative results support the mechanism shown in Scheme 2. The transmetalation follows two competitive pathways: One, producing **3**, is kinetically preferred, but is unproductive for coupling. The other, about one order of magnitude slower, affords **2** from which coupling will eventually take place, although at a much slower rate. The rate of direct *cis–trans* isomerization (very slow even at room temperature) is negligible compared with the indirect isomerization by retrotransmetalation to **1**, catalyzed by the

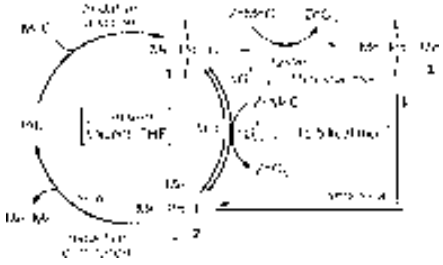

Scheme 2. Simplified reaction mechanism of the Negishi coupling.

CHEMISTRY
A EUROPEAN JOURNAL

$ZnCl_2$ formed in the reaction. Thus, the slowness of the reductive elimination of **2** allows many **1**–**2** and **1**–**3** round trips to occur before the irreversible coupling takes place.

Having the experimental thermodynamic parameters in hand, we performed DFT calculations by means of the Truhlar's M06 functional to uncover the features of the transition states and other mechanistic details. There are two recent theoretical studies on Negishi reactions,[5,11] but they are on special Pd complexes that cannot give rise to *cis*/*trans* isomers, as observed here. One of the studies uses a chelating ligand, in which *cis*–*trans* isomerism is excluded; the other is on a tricoordinated complex with a bulky ligand, again excluding isomers. Hence, none of them could account for our experimental observation of two competing transmetalation products. Moreover, the two studies have overlooked the usual tetrahedral coordination of Zn, using instead linearly coordinated Zn species. This neglect of the coordination ability of the solvent gives birth to some intermediates that might perhaps exist in vacuum, but are unrealistic in coordinating solvents.

Our theoretical DFT study was undertaken by using the real molecules and realistic tetrahedral Zn species coordinated with THF;[12] moreover, the calculations were fitted to the same temperature of the experimental kinetic study (223 K). Two low-energy, concerted transmetalation pathways were found, leading to the kinetic product **3** (concerted *trans* (CT) transmetalation, Figure 3, lower ΔG^{+}) and the thermodynamic one **2** (concerted *cis* (CC) transmetalation, Figure 4, higher ΔG^{+}), respectively. The reaction starts by ligand substitution on Zn, which involves THF displacement

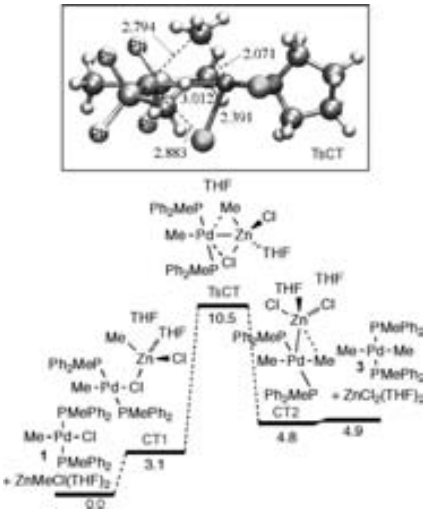

Figure 3. Energy profile for the concerted transmetalation to form the *trans* product, showing ΔG_{solv} values obtained at 223 K (a color version of the drawing of the TsCT geometry can be found in the Supporting Information).

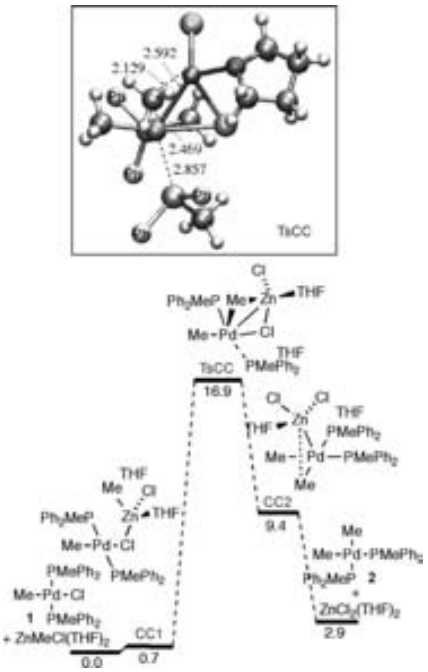

Figure 4. Energy profile for the concerted transmetalation to form the *cis* product showing the ΔG_{solv} values obtained at 223 K (a color version of the drawing of the TsCC geometry can be found in the Supporting Information).

by the Cl atom of **1**. Each possible conformation of this intermediate leads to a different transition state. Both transmetalations involve the formation of cyclic transition states [Pd(μ-Cl)(μ-Me)Zn], which are very reminiscent of the cyclic mechanism proposed for the Stille reaction.[1,9,14,15] However, a distinct feature found in the theoretical study of the Negishi transmetalation and absent in the Stille reaction is the existence, in both transition states and in some intermediates, of Pd···Zn bond interactions between the electron-rich Pd center and the fairly positive Zn center.[13] These interactions are deemed responsible for the remarkably low energy of the transmetalation barriers with organozinc compounds as nucleophiles, compared with the noticeably higher barriers for organotin compounds.

The experimental evidence and the theoretical calculations presented herein consistently support the fast reversibility of the transmetalation reactions of Pd complexes with Zn alkyl reagents. Based on these kinetic observations, a new possibility for the formation of undesired homocoupling products can be envisaged for a catalyzed coupling $R^1X + R^2ZnCl$ (or $R^2{}_2Zn$), in addition to the undesired transmetalations already discussed in above. Since the transmetalations and their reverse processes are much faster than the

reductive elimination from **2**, the **2**–**1**–**3** round trip will take place many times before coupling occurs. Consequently, for the general case of reactions [PdR^{1}ClL$_2$] with ZnR^{2}Cl, there are statistically many chances for new intermediates [PdR^{2}ClL$_2$] and ZnR^{1}Cl to be formed through undesired retrotransmetalations from the initial intermediate [PdR^{1}R^{2}L$_2$], eventually leading to R^1–R^1 and R^2–R^2 homocoupling side products. In fact, the compounds [PdMe$_2$(PPh$_3$)$_2$] and ZnRfCl, reported to be formed in the reaction of [PdRfCl(PPh$_3$)$_2$] with ZnMeCl,[4] are undesired retrotransmetalation products (Scheme 3). Of course the mistaken retrotransmetalation products can, in turn, enter the cycle, further complicating the problem.

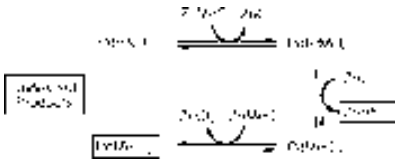

Scheme 3. Formation of side products (in black boxes) from undesired retrotransmetalations.

Side products of undesired retrotransmetalations have also been observed in Stille reactions (e.g., formation of SnRfBu$_3$ from Sn(CH=CH$_2$)Bu$_3$ and BrRf),[16] and are expected for other metal-catalyzed couplings whenever the retrotransmetalation is faster than the reductive elimination step. It is worth recalling that complexes [PdR^{1}R^{2}L$_2$] can also undergo uncatalyzed rearrangements by R exchange,[17] or isomerize through a gold-catalyzed process.[18] However, these reactions take usually place at a much slower rate than the transmetalations observed herein and do not seem to be an effective source of complications in Pd-catalyzed C–C heterocoupling reactions.

Experimental Section

Kinetic studies: A solution of palladium complex (5.15×10^{-3} mmol) in THF (0.30 mL) was prepared in an NMR tube and cooled to −78 °C. A precooled solution of ZnMeCl in THF (0.09 mL 1.14 M, 0.103 mmol) was added, plus cold THF to make 0.50 mL of final volume. The sample was placed into thermostated NMR spectrometer at 223 or 203 K. The kinetic experiments were followed by ^{31}P NMR spectroscopy and concentration–time data were acquired by integration of the ^{31}P NMR signals.

Acknowledgements

We thank financial support by Ministerio de Ciencia y Tecnología (CTQ2007-67411/BQU, CTQ2008-06866-CO2–01, CTQ2008-06866-CO2-02), Consolider Ingenio 2010 (CSD2006-0003, CSD2007-00006) and by Junta de Castilla y León (VA044A07 and GR169) and studentships to B.F. (MCyT) and M.G.-M. (UAB PIF).

Keywords: C–C coupling · density functional calculations · homogeneous catalysis · kinetics · Negishi coupling

[1] P. Espinet, A. M. Echavarren, *Angew. Chem.* **2004**, *116*, 4808–4839; *Angew. Chem. Int. Ed.* **2004**, *43*, 4704–4734.
[2] a) *Handbook of Organopalladium Chemistry for Organic Synthesis, Vol. 1* (Ed.: E. Negishi), Wiley-Interscience, New York, **2002**, Part I-II; b) E. Negishi, X. Zeng, Z. Tan, M. Qian, Q. Hu, Z. Huang, *Metal-Catalyzed Cross-Coupling Reactions* (Eds.: by A. de Meijere, F. Diederich), Wiley-VCH, Weinheim, **2004**, Chapter 15.
[3] a) J. Zhou, G. C. Fu, *J. Am. Chem. Soc.* **2003**, *125*, 12527–12530; b) J. Zhou, G. C. Fu, *J. Am. Chem. Soc.* **2003**, *125*, 14726–14727; c) Z. Tan, E. Negishi, *Angew. Chem.* **2006**, *118*, 776–779; *Angew. Chem. Int. Ed.* **2006**, *45*, 762–765; d) G. D. Jones, J. L. Martin, C. McFarland, O. R. Allen, R. E. Hall, A. D. Haley, R. J. Bandon, T. Konovalova, P. J. Desrochers, P. Pulay, D. A. Vicic, *J. Am. Chem. Soc.* **2006**, *128*, 13175–13183; e) G. D. Jones, C. McFarland, T. J. Anderson, D. A. Vicic, *Chem. Commun.* **2005**, 4211–4213.
[4] J. A. Casares, P. Espinet, B. Fuentes, G. Salas, *J. Am. Chem. Soc.* **2007**, *129*, 3508–3509.
[5] Q. Liu, Y. Lan, J. Liu, G. Li, Y. D. Wu, A. Lei, *J. Am. Chem. Soc.* **2009**, *131*, 10201–10210.
[6] *trans*-[PdClMe(PMePh$_2$)$_2$] (**1**) was chosen as the starting product for transmetalation because it is the stable isomer in THF. We checked experimentally that the oxidative addition of MeI to [Pd(PMePh$_2$)$_4$] in THF affords directly *trans*-[PdIMe(PMePh$_2$)$_2$] at 203 K. It is known that different oxidative addition mechanisms of alkyl halides are operational depending on the solvent and the halide, which affects the enantioselectivity of this step and the stereochemistry (*cis* or *trans*) of the kinetic product; however, in all experimental cases using alkyl halides in polar solvents the product observed is the *trans* isomer regardless of the enantioselectivity, showing that the *cis*-to-*trans* isomerization, if needed, is extremely fast, most likely faster than transmetalation.
[7] A. Gillie, J. K. Stille, *J. Am. Chem. Soc.* **1980**, *102*, 4933–4941.
[8] a) F. Ozawa, T. Ito, Y. Nakamura, A. Yamamoto, *Bull. Chem. Soc. Jpn.* **1981**, *54*, 1868–1880; b) F. Ozawa, K. Kurihara, T. Yamamoto, A. Yamamoto, *J. Organomet. Chem.* **1985**, *279*, 233–243.
[9] For retro-transmetalation we mean the reverse of the transmetalation reaction. For a study of the retro-transmetalation in a Stille reaction see: M. H. Pérez-Temprano, A. Nova, J. A. Casares, P. Espinet, *J. Am. Chem. Soc.* **2008**, *130*, 10518–10519.
[10] The multivariable adjust program Gepasi was used: a) P. Mendes, *Comput. Appl. Biosci.* **1993**, *9*, 563–571.
[11] G. A. Chass, C. J. O'Brien, N. Hadei, E. A. B. Kantchev, W-H. Mu, D.-C. Fang, A. C. Hopkinson, I. G. Csizmadia, M. G. Organ, *Chem. Eur. J.* **2009**, *15*, 4281–4288.
[12] M. Weidenbruch, M. Herrndorf, A. Schafer, S. Pohl, W. Saak, *J. Organomet. Chem.* **1989**, *361*, 139–145.
[13] This kind of interaction was initially proposed by calculation in the context the propargylation of aldehydes: R. Álvarez, A. R. de Lera, J. M. Aurrecoechea, D. Aritz, *Organometallics* **2007**, *26*, 2799–2802.
[14] A. L. Casado, P. Espinet, *J. Am. Chem. Soc.* **1998**, *120*, 8978–8985.
[15] A. Nova, G. Ujaque, F. Maseras, A. Lledós, P. Espinet, *J. Am. Chem. Soc.* **2006**, *128*, 14571–14578.
[16] A. L. Casado, P. Espinet, A. M. Gallego, *J. Am. Chem. Soc.* **2000**, *122*, 11771–11782.
[17] A. L. Casado, J. A. Casares, P. Espinet, *Organometallics* **1998**, *17*, 5416–5423.
[18] A. L. Casado, P. Espinet, *Organometallics* **1999**, *18*, 3677–3683.

Received: February 4, 2010
Published online: July 7, 2010

A.2 Article II:

Cationic Intermediates in the Pd-Catalyzed Negishi Coupling. Kinetic and Density Functional Theory Study of Alternative Transmetalation Pathways in the Me-Me Coupling of $ZnMe_2$ and *trans*-[$PdMeCl(PMePh_2)_2$]

García-Melchor, M.; Fuentes, B.; Lledós, A.; Casares, J. A.; Ujaque, G.; Espinet, P. *J. Am. Chem. Soc.* **2011**, *133*, 13519-13526.

JACS
JOURNAL OF THE AMERICAN CHEMICAL SOCIETY
ARTICLE
pubs.acs.org/JACS

Cationic Intermediates in the Pd-Catalyzed Negishi Coupling. Kinetic and Density Functional Theory Study of Alternative Transmetalation Pathways in the Me−Me Coupling of $ZnMe_2$ and *trans*-[$PdMeCl(PMePh_2)_2$]

Max García-Melchor,[†] Beatriz Fuentes,[‡] Agustí Lledós,[†] Juan A. Casares,*[,‡] Gregori Ujaque,*[,†] and Pablo Espinet*[,‡]

[†]Química Física, Edifici C.n., Universitat Autònoma de Barcelona, E-08193 Bellaterra, Catalonia, Spain

[‡]IU CINQUIMA/Química Inorgánica, Facultad de Ciencias, Universidad de Valladolid, E-47071 Valladolid, Spain

Supporting Information

ABSTRACT: The complexity of the transmetalation step in a Pd-catalyzed Negishi reaction has been investigated by combining experiment and theoretical calculations. The reaction between *trans*-[$PdMeCl(PMePh_2)_2$] and $ZnMe_2$ in THF as solvent was analyzed. The results reveal some unexpected and relevant mechanistic aspects not observed for ZnMeCl as nucleophile. The operative reaction mechanism is not the same when the reaction is carried out in the presence or in the absence of an excess of phosphine in the medium. In the absence of added phosphine an ionic intermediate with THF as ligand ($[PdMe(PMePh_2)_2(THF)]^+$) opens ionic transmetalation pathways. In contrast, an excess of phosphine retards the reaction because of the formation of a very stable cationic complex with three phosphines ($[PdMe(PMePh_2)_3]^+$) that sequesters the catalyst. These ionic intermediates had never been observed or proposed in palladium Negishi systems and warn on the possible detrimental effect of an excess of good ligand (as $PMePh_2$) for the process. In contrast, the ionic pathways via cationic complexes with one solvent (or a weak ligand) can be noticeably faster and provide a more rapid reaction than the concerted pathways via neutral intermediates. Theoretical calculations on the real molecules reproduce well the experimental rate trends observed for the different mechanistic pathways.

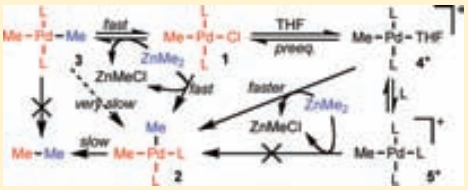

INTRODUCTION

The Negishi reaction is a wide scope most reliable cross-coupling process that can be applied to every possible combination of carbon type (sp, sp^2, or sp^3), and tolerates many different functions in the reagents.[1−3] The reaction can be carried out using either ZnR_2 or ZnRX as the nucleophile, and the more accessible reagent is usually chosen. While the choice of organozinc does not seem to alter the cross coupling products in the Negishi coupling, the rate and mechanism of the transmetalation step might be affected. However, very little is known about this transmetalation, compared to the transmetalation mechanisms in the Stille[4−8] or Suzuki[9−12] reactions, in spite of the fact that the transmetalation between organozinc and palladium complexes is also involved in other synthetically useful processes such as the hydroalkylation of styrenes,[13] the asymmetric allylation of aryl aldehydes,[14] the coupling of propargylic benzoates and aldehydes,[15] or the double-transmetalation oxidative cross-coupling reaction.[16]

In an initial mechanistic work on the Negishi reaction we met a remarkable behavior in the transmetalation of *trans*-[$PdRfCl(PPh_3)_2$] (Rf = 3,5-dichloro-2,4,6-trifluorophenyl) with $ZnMe_2$ or with ZnMeCl: apparently each methylating reagent afforded a different isomer (*trans* or *cis*, respectively) of the coupling intermediate [$PdRfMe(PPh_3)_2$].[17] The study revealed also the existence of secondary undesired transmetalations (methyl by aryl exchanges, eqs 1 and 2), which could eventually produce homocoupling products. The same phenomenon had been noted by van Asselt and Elsevier,[18] and after our report was also observed by A. Lei et al. on related reactions with aryl zinc derivatives.[19]

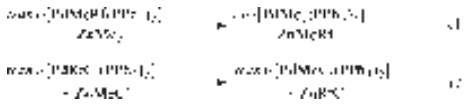

Recently, we have published kinetic experimental and theoretical studies of the transmetalation between ZnMeCl and *trans*-[$PdMeCl(PMePh_2)_2$].[20] That study showed that the

Received: May 9, 2011
Published: July 27, 2011

Journal of the American Chemical Society ARTICLE

Scheme 1. Simplified Reaction Mechanism of the Negishi Coupling with ZnMeCl

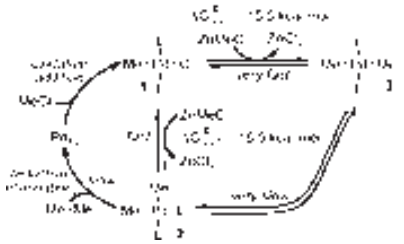

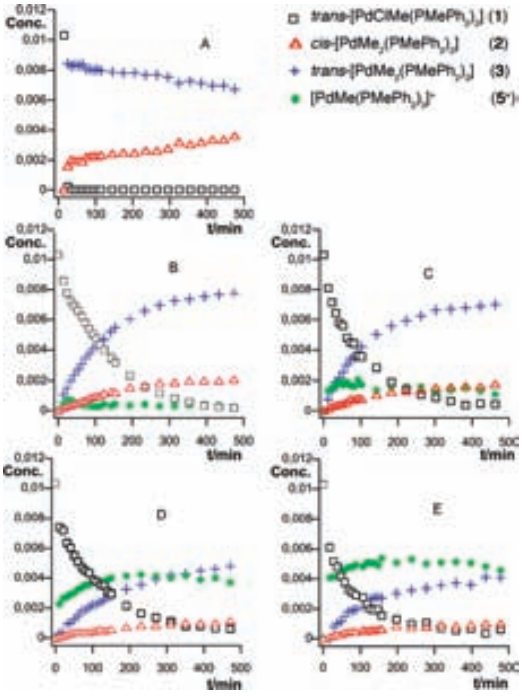

Figure 1. Concentration/time data, obtained by ^{31}P NMR, for the reaction of *trans*-[PdMeCl($PMePh_2$)$_2$] (**1**) with $ZnMe_2$ in THF at 203 K. Starting conditions: $[\mathbf{1}]_0 = 1.0 \times 10^{-2}$ M, $[ZnMe_2]_0 = 0.21$ M. Added phosphine: (**A**) $[PMePh_2] = 0$ M, (**B**) $[PMePh_2] = 6.0 \times 10^{-4}$ M, (**C**) $[PMePh_2] = 2.0 \times 10^{-3}$ M, (**D**) $[PMePh_2] = 5.0 \times 10^{-3}$ M, (**E**) $[PMePh_2] = 1.0 \times 10^{-2}$ M.

reagents (ZnMeCl + *trans*-[PdMeCl($PMePh_2$)$_2$] (**1**)) are more stable than the products ($ZnCl_2$ + *cis*-[$PdMe_2$($PMePh_2$)$_2$] (**2**)), and the latter are more stable than the alternative products ($ZnCl_2$ + *trans*-[$PdMe_2$($PMePh_2$)$_2$] (**3**)). The Gibbs energy differences are such that, in catalytic conditions (using a large excess of ZnMeCl), the equilibria are shifted toward the most stable products $ZnCl_2$ + *cis*-[$PdMe_2$($PMePh_2$)$_2$], but the kinetics of the reactions favor the faster formation of *trans*-[$PdMe_2$-($PMePh_2$)$_2$], which is seen to appear and then fade out in favor of

Scheme 2

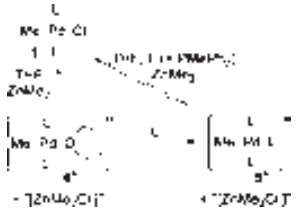

the more stable *cis*-[$PdMe_2$($PMePh_2$)$_2$]. It was demonstrated that the latter transformation is not a direct *trans*/*cis* isomerization, which is slow, but occurs *via* retrotransmetalation to the initial reagents followed by transmetalation to *cis*-[$PdMe_2$-($PMePh_2$)$_2$].[21] The catalytic cycle in Scheme 1 summarizes those results. No other Pd complex was observed in that study.[20]

In this paper we study the transmetalation using $ZnMe_2$ as the transmetalating nucleophile. *A priori* only minor differences with the results with ZnMeCl were expected. However, this study has revealed unknown and unexpected aspects of the Negishi process.

RESULTS AND DISCUSSION

1. Experimental Studies. The reaction of **1** with $ZnMe_2$ (1:20 ratio simulating catalytic conditions with 5% Pd, in THF at room temperature) gives *cis*-[$PdMe_2$($PMePh_2$)$_2$] (**2**) as the only observable product. In these conditions complex **2** slowly decomposes to give the Negishi coupling product ethane.[22,23] This behavior is in coincidence with the synthetic results observed using ZnMeCl at room temperature.[20] However, important mechanistic differences between the two Zn reagents were observed when the reactions were monitored by ^{31}P NMR at 203 K (at which temperature the coupling rate to give ethane is negligible), with and without added phosphine (Figure 1).

1.1. Occurrence of Cationic Pd Species. The first unexpected observation (Figure 1A) was that the rate of consumption of *trans*-[PdMeCl($PMePh_2$)$_2$] (**1**) with $ZnMe_2$ seemed too high, compared to our previous study with ZnMeCl,[20] even considering that $ZnMe_2$ is a stronger nucleophile than ZnMeCl and some rate acceleration was to be expected. Addition of a small amount of $PMePh_2$ markedly decreased the rate of consumption (Figure 1B), bringing the reaction rate into the range convenient for kinetic studies by ^{31}P NMR. Interestingly, further increases in $PMePh_2$ concentration affected only slightly the rate of consumption (Figure 1C−E) and the profiles of the other curves in the graphics (these are discussed later). This behavior suggests the existence, in the initial conditions of reaction **1A**, of a minute proportion of a nonobserved catalytic intermediate that opens a much faster reaction pathway; this intermediate would be quenched by addition of just a small amount of phosphine. A most plausible intermediate is the cation *trans*-[PdMe-($PMePh_2$)$_2$(THF)]$^+$ (THF = tetrahydrofuran, **4**$^+$), formed in the presence of a large amount of $ZnMe_2$ acting as Cl^- scavenger (Scheme 2). As a precedent for this proposal, the role of $ZnBr_2$ as a Lewis acid, facilitating halide abstraction from Ni complexes, was hypothesized by Buchwald et al.,[24] who found an accelerating effect of $ZnBr_2$ as cocatalyst in a process of enantioselective α-arylation of α-substituted γ-butyrolactones requiring a step of

 dx.doi.org/10.1021/ja204256x |*J. Am. Chem. Soc.* 2011, 133, 13519–13526

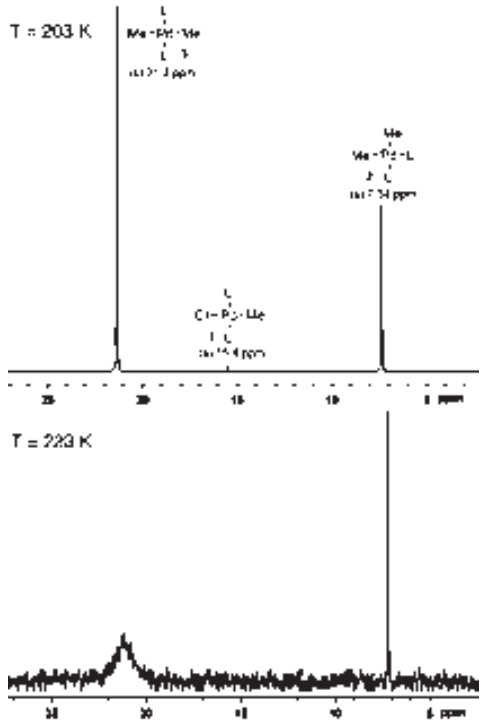

Figure 2. ^{31}P NMR of a mixture of **1**, $ZnMe_2$, and $PMePh_2$ in THF at 203 and 223 K, after 15 min, close to the end of the transmetalation. Starting conditions: $[\mathbf{1}]_0 = 0.033$ M, $[ZnMe_2]_0 = 0.16$ M, $[PMePh_2] = 0.008$ M. The coalescence of the signals at 223 K is due to exchange of coordinated and uncoordinated phosphine. The signal of the free phosphine appears at −29.5 ppm at 203 K, and is not observed at 223 K.

halide abstraction from [(*S*)-BINAP]Ni(Ar)(X), and also by Majundar and Cheng in the Ni(II)/Zn-mediated chemoselective arylation of aromatic aldehydes.[25] Actually, the formation of [Ni(η^3-Bz)(diphosphine)][$ZnBr_3$(THF)] complexes from [Ni(σ-Bz)Br(diphosphine)] and $ZnBr_2$ in THF has been reported by Anderson and Vicic.[26]

To the best of our knowledge this instrumental effect of $ZnMe_2$ acting as Cl^- scavenger has never been observed nor proposed in palladium Negishi systems where, probably due to the different hardness of the metal center, the behavior is somewhat different from nickel. A THF complex similar to $\mathbf{4}^+$, *trans*-[Pd(C_6F_5)-(PPh_3)$_2$(THF)](OTf), in equilibrium with *trans*-[Pd(C_6F_5)-(OTf)(PPh_3)$_2$] in THF,[6,7] has been reported, but TfO^- is a very good leaving ligand. Moreover, treating *trans*-[PdMeCl-($PMePh_2$)$_2$] in THF solution at −20 °C with $AgBF_4$, to force the extraction of Cl^- (see Supporting Information for details), [PdMe($PMePh_2$)$_2$(THF)](BF_4) ($\mathbf{4}\cdot BF_4$) is formed quantitatively. When the counteranion is Cl^- an equilibrium between *trans*-[PdMeCl($PMePh_2$)$_2$] and *trans*-[PdMeCl($PMePh_2$)$_2$(THF)]$^+$ ($\mathbf{4}^+$) seems to be established to a small extent, but only in the presence of $ZnMe_2$ as Cl^- acceptor. This accelerating effect was not detected in the reactions where the reagent was the better acceptor ZnMeCl,[20] but this has some logic: intermediate $\mathbf{4}^+$ would not be formed in solutions very rich in species containing terminal chloro donor atoms, which will coordinate palladium in preference to THF.[27]

The proposal of intermediate $\mathbf{4}^+$ was reinforced by the observation of a cationic complex ($\mathbf{5}^+$ in Scheme 2) when $PMePh_2$ was added (Figure 1B−E). It was identified as [PdMe($PMePh_2$)$_3$]$^+$ by comparison with an authentic sample prepared independently (eq 3).

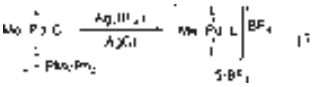

The observation of $\mathbf{5}^+$, in variable concentration depending on the amount of phosphine added, confirms unequivocally that, in the presence of added phosphine, a second cationic species, this time observable, is made available from the very beginning of the reaction, opening a plausible additional alternative transmetalation pathway. In summary, depending on the reaction conditions the transmetalation could take place on **1**, on $\mathbf{4}^+$, or on $\mathbf{5}^+$ (Scheme 2). It looks that the reaction via $\mathbf{4}^+$ is faster than on **1**, while the presence of $\mathbf{5}^+$ does not accelerate the transmetalation.

1.2. Kinetic Studies of the Transmetalation with $ZnMe_2$, without Added $PMePh_2$. The high transmetalation rate observed in Figure 1A (no added $PMePh_2$) leads to the complete transformation of the starting complex *trans*-[PdMeCl($PMePh_2$)$_2$] (**1**) into a mixture of the transmetalated products *trans*- and *cis*-[$PdMe_2$($PMePh_2$)$_2$] (**3** and **2**, respectively) where the *trans* isomer is very major. This takes place in about one minute, which is very fast considering that the working temperature is 203 K. Then a very slow isomerization of **3** to **2** follows.

1.3. Kinetic Studies of the Transmetalation with $ZnMe_2$ and Added $PMePh_2$. In order to observe the products involved in catalysis, these reactions were carried out at 203 K to quench the fast exchange of coordinated and uncoordinated phosphine that already occurs at 223 K (Figure 2).

The reactions in the presence of added $PMePh_2$ (Figure 1B−D) show the fast formation of the cationic species $\mathbf{5}^+$, and a much slower rate of transmetalation than without added phosphine, in agreement with the absence of $\mathbf{4}^+$. The graphics show that, as usual, *trans* isomer **3** is formed faster than *cis* isomer **2**. In order to decide whether the transmetalation takes place on **1**, on $\mathbf{5}^+$, or competitively on both species, the experimental data collection was fitted to two kinetic models: (a) supposing that the transmetalation operates only on the neutral complexes **1** (eqs 4 and 5); and (b) considering also the competitive transmetalation operating on the cationic complex [PdMe($PMePh_2$)$_3$]$^+$ ($\mathbf{5}^+$) (eqs 6 and 7). The results are given in Tables 1 and 2. The fitting using model b affords negligible values for k^+_3; thus, the competitive transmetalation pathway *via* the trisphosphine cationic complex $\mathbf{5}^+$ can be discarded. Consistently, almost identical values are obtained for k_3 and for k_4 in models a and b. The two rate constants, with average values $k_3 \approx 2.8 \times 10^{-2}$ min^{-1}, and $k_4 \approx 6.2 \times 10^{-3}$, differ in less than 1 order of magnitude.

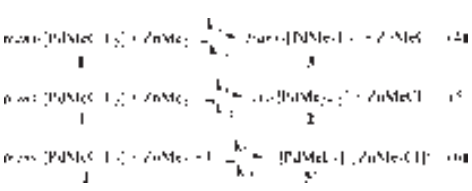

Journal of the American Chemical Society ARTICLE

Table 1. Rate Constants (min^{-1} mol^{-1}L) and $\Delta G^{\ddagger}$ values (kcal mol^{-1}) at 203 K, Using Model A[a]

% added $PMePh_2$	k_3[b]	$\Delta G_3^{\ddagger}$	k_4	$\Delta G_4^{\ddagger}$
6	$3.0(\pm0.1) \times 10^{-2}$	14.80 (±0.07)	$7.5(\pm0.2) \times 10^{-3}$	15.36 (±0.08)
20	$3.3(\pm0.1) \times 10^{-2}$	14.77 (±0.07)	$7.7(\pm0.2) \times 10^{-3}$	15.37 (±0.08)
50	$1.9(\pm0.1) \times 10^{-2}$	14.99 (±0.08)	$4.1(\pm0.1) \times 10^{-3}$	15.61 (±0.08)
100	$2.2(\pm0.1) \times 10^{-2}$	14.93 (±0.08)	$5(\pm1) \times 10^{-3}$	15.53 (±0.08)

[a] Sandström, J. *Dynamic NMR Spectroscopy*; Academic Press: London, 1982. The fittings were made using the values $k_5 = 9.8$ min^{-1} mol^{-1}L; $k_{-5} = 0.002$ min^{-1} mol^{-1} L for the formation of 5^+ (eq 6). These were determined in the experiment in Figure 1E, where the experimental values to be measured for formation of 5^+ are larger, and hence more reliable. This also applies to Table 2. [b] Standard deviations in parentheses.

Table 2. Rate Constants at 203 K, Using Model *b*[a]

(%) added $PMePh_2$	k_3 (min^{-1} mol^{-1} L)	k_4 (min^{-1} mol^{-1} L)	k^+_3 (min^{-1})
6	$3(\pm>3) \times 10^{-2}$	$8(\pm>8) \times 10^{-3}$	$2(\pm>2) \times 10^{-16}$
20	$3.4(\pm1) \times 10^{-2}$	$8(\pm2) \times 10^{-3}$	$1(\pm>1) \times 10^{-4}$
50	$2.7(\pm2) \times 10^{-2}$	$4(\pm1.6) \times 10^{-3}$	$3(\pm>3) \times 10^{-15}$
100	$2(\pm>2) \times 10^{-2}$	$6(\pm>6) \times 10^{-3}$	$2(\pm>2) \times 10^{-16}$

[a] See note text in Table 1. Standard deviations in parentheses.

In summary, the experimental results show the following: (1) In the absence of added phosphine the observed rate is unusually fast for the transmetalation that should take place on *trans*-[PdMeCl($PMePh_2$)$_2$],[28] and this suggests that it must be going through a nonobserved cationic intermediate $\mathbf{4}^+$. This proposal is later supported by DFT calculations. (2) In the presence of some added phosphine the reactions go *via* *trans*-[PdMeCl($PMePh_2$)$_2$]. The presence of a new cationic intermediate $\mathbf{5}^+$ is kinetically of little relevance (except for the detrimental effect associated to the percentage of Pd scavenging), indicating that it is not an intermediate toward a faster reaction pathway. (3) At variance with the system using ZnMeCl, where the reaction equilibrium is displaced toward the reagents (**1** + ZnMeCl, see Figure 1),[20] in the system **1** + $ZnMe_2$ the reaction is displaced toward the products (**2** + ZnMeCl, and **3** + ZnMeCl), reflecting the higher nucleophilicity of $ZnMe_2$. Methyl for chloride exchange is an exergonic process for $ZnMe_2$ and an endergonic one for ZnMeCl, reflecting the relative stability of the Zn complexes. Since it is already known that **2** is about 2 kcal mol^{-1} more stable than **3**,[20] it follows that the reaction equilibrium with $ZnMe_2$ is strongly displaced toward **2**. (4) The transmetalation to *trans* (**3**) is clearly faster than the transmetalation to *cis* (**2**), in coincidence with the reaction with ZnMeCl.[20] (5) The subsequent isomerization of **3** to **2** is much slower than in the reaction with ZnMeCl. This was expected from our previous study, which showed that the rate of the *trans*/*cis* uncatalyzed isomerization is negligible at low temperatures, while the isomerization *via* retrotransmetalation to *trans*-[PdMeCl($PMePh_2$)$_2$] is catalyzed by the presence of $ZnCl_2$ and, less efficiently, by ZnMeCl.[20] Additional experiments (at 223 K, in order to increase the isomerization rates) show that $ZnMe_2$ does not catalyze the isomerization: after 13 h at 223 K a solution 0.01 M of **3** and 0.21 M of $ZnMe_2$ contains only 1% of the *cis* isomer **2**; in contrast, the same experiment performed with ZnMeCl gives, after 10 min, a mixture of about 25% *cis*-[$PdMe_2$($PMePh_2$)$_2$] and 75% *trans*-[PdMeCl(PPh_2Me)$_2$], reaching equilibrium (**1**:**2** ≈ 43:57) in 200 min.

2. DFT Studies of the Transmetalation. In order to support the proposals based on the experimental data and obtain a more detailed picture of the transmetalation process, all the proposed transmetalation pathways were computationally investigated by density functional theory (DFT) calculations using the M06 dispersion-corrected functional, which has been shown to provide good results for both organometallic systems and noncovalent interactions.[29] The theoretical calculations were performed on the very catalyst used for the experiments (i.e., with the real ligands). The solvent, THF, was introduced by a discrete-continuum model: two THF molecules were explicitly included in the calculations as potential ligands, and the effect of the bulk solvent was taken into account with a continuum model ($\varepsilon = 7.4257$). This methodology allowed us to consider tetrahedral Zn species coordinated with THF along the studied pathways, rather than the unrealistic linear dicoordinated Zn species often used that lead to calculated species of unlikely existence in THF solution.[30] Gibbs energies in THF solution (ΔG_{THF}) were calculated adding the gas-phase Gibbs energy corrections of the solute to the energies in solution. All the energies collected in the text are ΔG_{THF}, calculated at 203 K for further approximation to the experimental conditions.[31] With these DFT calculations we expected to reproduce the trends of energy barriers found experimentally,[32] which are the following: ionic to *trans* ($PMePh_2$) > concerted to *cis* > concerted to *trans* > ionic to *trans* (THF).

2.1. Ionic Mechanism via an Undetectable Cationic Intermediate [PdMe($PMePh_2$)$_2$(THF)]$^+$ ($\mathbf{4}^+$). The experimental studies suggest the formation of an undetected cationic intermediate [PdMe($PMePh_2$)$_2$(THF)]$^+$ ($\mathbf{4}^+$) (with [$ZnMe_2Cl$(THF)]$^-$ as the counterion), which is the one undergoing the fastest transmetalation process. The computational analysis of a plausible transmetalation *via* $\mathbf{4}^+$ afforded the reaction profile and optimized transition state structures shown in Figure 3. The reaction pathway starts with a chloride abstraction from the initial Pd complex (**1**), assisted by a THF molecule and $ZnMe_2$ (which is in large excess). This results in the formation of **IT2** (corresponding to the proposed intermediate $\mathbf{4}^+$ in the experimental nomenclature) through the transition state **TsIT1**.[33] Interestingly, the position of **IT2** in the Gibbs energy profile is 5.3 kcal mol^{-1} higher than the initial reactants, which makes its observation by NMR extremely unlikely.[34] Subsequently, the transmetalation takes place from **IT2** *via* **TsIT2**, yielding the last intermediate **IT3**. The latter transition state has the highest energy value (10.3 kcal mol^{-1}) within the overall reaction profile thus becoming the rate-determining step.

2.2. Concerted Mechanisms. The only operative transmetalation pathways for the transmetalation reaction with ZnMeCl involve concerted Cl for Me exchanges.[20] A similar concerted mechanism

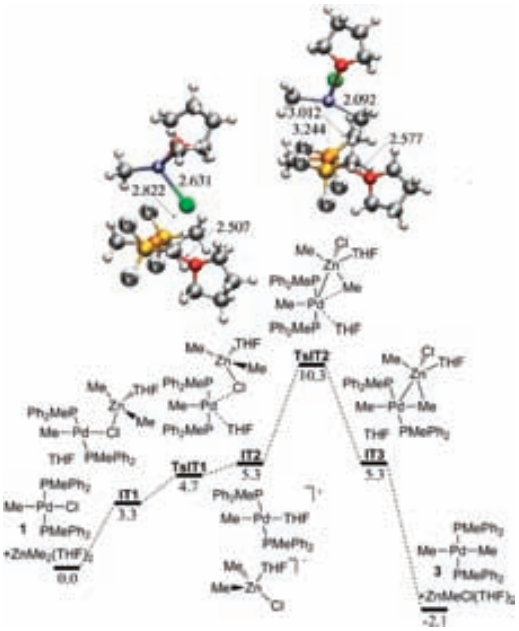

Figure 3. Gibbs energy profile in THF (in kcal mol^{-1}) calculated for the transmetalation to the trans product (**3**) via Pd ionic intermediate with THF. The optimized structures for the transition states **TsIT1** (left) and **TsIT2** (right) are shown. Phenyl rings simplified for clarity.

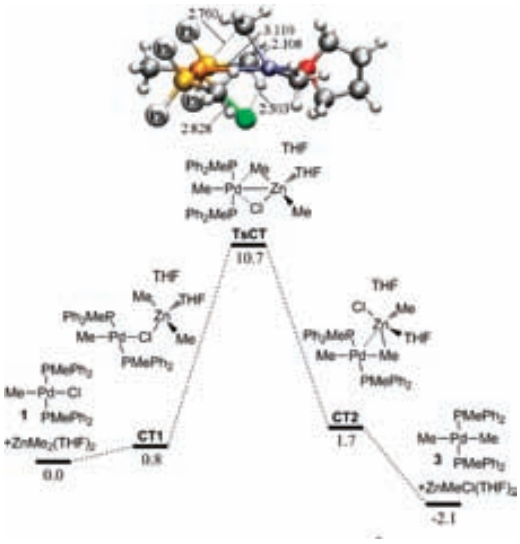

Figure 4. Gibbs energy profile in THF (in kcal mol^{-1}) calculated for the concerted transmetalation to the *trans* product (**3**). The optimized structure for the transition state **TsCT** is shown. Phenyl rings simplified for clarity.

was found for $ZnMe_2$. Figures 4 and 5 depict the Gibbs energy profiles of the concerted transmetalation pathways on *trans*-$[PdMeCl(PMePh_2)_2]$ (**1**) to *trans*- and *cis*-$[PdMe_2(PMePh_2)_2]$, respectively. Both mechanisms share the initial dissociation of a THF molecule from the Zn reagent with concomitant chloride coordination to Zn, yielding intermediates **CT1** and **CC1**, respectively.[35] The concerted transmetalation to the *trans* product **3** (Figure 4) takes place through one transition state (**TsCT**), with an energy barrier of 10.7 kcal mol^{-1}. At variance, the transmetalation to *cis* product **2** (Figure 5) displays two transition states of almost identical energy (**TsCC1** =11.5; **TsCC2** = 11.8 kcal mol^{-1}). **TsCC1** corresponds to the substitution of the phosphine ligand by a methyl group from the Zn reactant, giving rise to a high energy intermediate **CC2**, unobservable by NMR. In **TsCC2**, the phosphine ligand replaces the chloride group, which ends up bound to Zn.

From the calculated barriers, the concerted transmetalation to *trans* is slower than the transmetalation through the ionic intermediate $\mathbf{4}^+$, and faster than the concerted transmetalation to *cis*. On the other hand, the *cis* isomer **2** is 2.3 kcal mol^{-1} more stable than the *trans* isomer **3**.

2.3. Ionic Mechanism via a Detected Cationic Intermediate $[PdMe(PMePh_2)_3]^+$ ($\mathbf{5}^+$). Finally, in order to unravel the observed decrease of the reaction rates for the transmetalation process with added phosphine, and further support the observation of the species $[PdMe(PMePh_2)_3]^+[ZnMe_2Cl(THF)]^-$ ($\mathbf{5}^+$), we computed the transmetalation pathway *via* this species (Figure 6). The pathway is analogous to that going through $\mathbf{4}^+$, but very different energies are involved. The calculations indicate that intermediate **IT2** (corresponding to $\mathbf{5}^+$ in the experimental nomenclature) is very stable, as expected from its NMR observation. For the ionic pathway through $\mathbf{5}^+$ the calculated transmetalation barrier **TsIT2** increases to 15.5 kcal mol^{-1}. This is more than 3 kcal mol^{-1} higher than that calculated for the concerted processes (11.8−10.7 kcal mol^{-1}, see above), which in terms of reaction rates means more than 3 orders of magnitude slower. In other words, this pathway is clearly the most disfavored one for the Negishi transmetalation studied, in agreement with the experimental observations.

3. Comparing Theoretical and Experimental Results. The number of computational studies of transition metal catalyzed reactions has increased exponentially in recent years,[36] but only rarely are experimental energy values (especially transition barriers) available for direct comparison with the theoretical results. When they are, it is found that the quantitative matching is not always as good as hoped.[37−39] It has been stated that, at present, it cannot be excluded that good matches stem from error cancellation of different contributions to the calculated values.[38]

The experimental ΔG values derived from the kinetic experimental studies are estimated to have an error of ±0.08 kcal mol^{-1}.[40] Aiming at obtaining theoretical results to compare with the experimental values, we have used in this paper an optimum chemical model for calculations. The reactant molecules were not substituted by a simplified model: the complete catalyst with the real ligands and realistic tetracoordinated Zn species including explicitly solvent molecules were used. Moreover, a well balanced computational cost/quality method was selected by using a dispersion-corrected functional with a large basis set and including a discrete + continuum solvent scheme (the new implemented SMD solvation model) in the calculations.

Simplified experimental profiles for the concerted transmetalations to *trans* and to *cis* using $ZnMe_2$ are plotted in black in Figure 7. The values for the concerted mechanisms are the quantitative kinetic results, whereas for the ionic mechanisms the

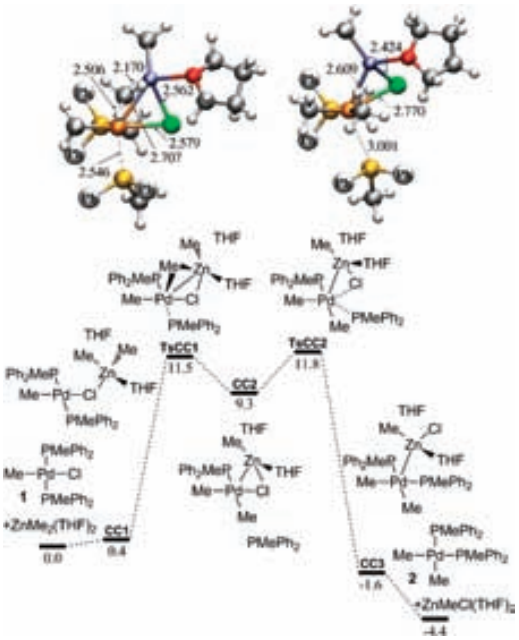

Figure 5. Gibbs energy profile in THF (in kcal mol^{-1}) calculated for the concerted transmetalation to the *cis* product (**2**). The optimized structures of the transition states **TsCC1** (left) and **TsCC2** (right) are shown.

Figure 6. Gibbs energy profile in THF (in kcal mol^{-1}) calculated for the transmetalation to the *trans* product (**3**) via ionic intermediate with $PMePh_2$. Gibbs energies are given in kcal mol^{-1}. Phenyl rings simplified for clarity.

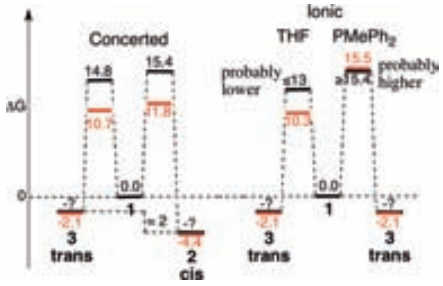

Figure 7. Comparison, for the reactions with $ZnMe_2$, of the relative Gibbs energy values at 203 K (kcal mol^{-1}) of the rate determining transition states and the products. Experimental values in black, calculated values in red.

Scheme 3. Simplified Reaction Mechanism of the Negishi Coupling with $ZnMe_2$

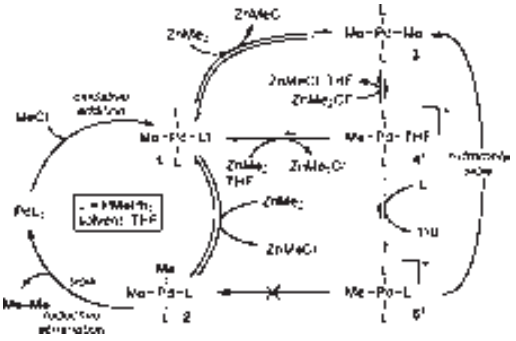

values plotted are the estimated maximum (for L = THF) or minimum (for L = $PMePh_2$) value compatible with the experimental observations. The data in red correspond to the computationally obtained values. First of all, it is worth noting that the calculations reproduce qualitatively the experimental observations. From the kinetic point of view, the order of the energy barriers for the transmetalation process through the different pathways is as follows: ionic to *trans* ($PMePh_2$) > concerted to *cis* > concerted to *trans* > ionic to *trans* (THF). As far the thermodynamics is concerned, the order of stability of the reagents and products in equilibrium (as represented by the Pd complex contained in the corresponding combination of compounds) is **2** (*cis*) > **3** (*trans*) > **1**.

From a strictly quantitative perspective, we can compare theoretical and experimental values only for the concerted mechanisms, for which we have specific experimental values (for the ionic mechanisms specific values could not be obtained from experiments, and only lower (for $\mathbf{4}^+$) or higher (for $\mathbf{5}^+$) limits can be estimated). On the basis of these results it seems that our theoretical calculations underestimate the reaction barriers by about 4 kcal mol^{-1}. However, the calculations nicely reproduce the energy difference between both concerted mechanisms (the difference is 0.6 kcal mol^{-1} for the experimental values and 1.1 kcal mol^{-1} for the theoretical values), which is important, and sufficient in this case to compare reaction rates and elucidate which

Journal of the American Chemical Society ARTICLE

pathway is preferred. On the other hand, the relative stability for the products **2** and **3** could not be experimentally quantified in this paper, but we had determined in a previous study that **2** is about 2.0 kcal mol^{-1} more stable than **3**.[20] In this study the calculated difference is 2.3 kcal mol^{-1}, which is a very satisfactory fit with the experiment.

CONCLUSIONS

The experimental study of the transmetalation step in a Pd-catalyzed Negishi reaction to produce Me−Me coupling using $ZnMe_2$, in THF as solvent, shows that in all cases the reactions are faster than with ZnMeCl. The concerted transmetalation to *trans* is faster than the transmetalation to *cis*, and the *trans*-to-*cis* isomerization (which is required to produce the coupling product) is slower than in the case of ZnMeCl as nucleophile, because $ZnMe_2$ is not a good isomerization catalyst.

Particularly interesting is the observation that, in addition to the expected concerted pathways previously found for ZnMeCl as nucleophile, alternative ionic mechanisms can operate, through ionic intermediates $[PdMe(PMePh_2)_2L]^+[ZnMe_2Cl(THF)]^-$ (L = THF, $PMePh_2$). For L = THF this pathway is faster than the concerted mechanisms, while for L = $PMePh_2$ this pathway is much slower than the concerted mechanisms; in fact, the corresponding intermediate $[PdMe(PMePh_2)_3]^+$ becomes a trap of part of the Pd catalyst. The observation of these ionic intermediates warns on the possible detrimental effect of using excess of good ligands (as $PMePh_2$) in the Negishi process, but is also suggestive of the possibility to use solvents or weak ligands more coordinating than THF in order to promote the existence, in higher concentration than for THF, of ionic intermediates that could still produce further acceleration of the transmetalation step. All these conclusions are summarized in Scheme 3.

Concerning the DFT results, the theoretically calculated free energy values reproduce fairly well the experimental trends (which depend on the differences of calculated values for several pathways). Nevertheless, in spite of all the computational efforts, the calculated values do not match the experimental ones. In fact, matching experimental relative Gibbs energies in solution with theoretical calculations for a complex multistep reaction system like ours is, particularly regarding Gibbs activation barriers, a harsh work, even using good chemical and methodological models. There is still a long way in front before such accuracy is reached. In particular, the computation of entropic contributions in solution and the description of the solvent effects require further improvements.[41] Any progress in this problem will need more interactive work where experiments and calculations are put and discussed together.

Finally, following the suggestion of a reviewer, it is worth putting into perspective the significance of this work. It provides proof of the existence, operation, and effects of competitive transmetalation pathways, some of which had not been invoked before but should be considered from now on when planning or discussing Negishi syntheses. The basic transmetalation scheme proposed here is expected not to change dramatically for reactions involving aryls instead of Me, although obviously the specific values and energetic barriers determining the fastest pathway will depend on each change in the reacting system (R, X, ligands, solvent). For instance, the RX reagent in a general synthesis could probably be ArX (X = Br, I or OAc, OTs, etc.) rather than MeCl, and afford as starting point for transmetalation $[PdArXL_2]$, or $[PdArL_2(solvent)]^+X^-$ in the case of weakly coordinating anions; the latter groups will undoubtedly propitiate ionic transmetalation mechanisms. In reactions with aryls, a less donating Ar group on Pd, instead of Me, is expected to be somewhat less prone to produce ionic species, whereas heavier halogens will propitiate ionic Pd intermediates better than Cl. Concerning solvents, those more coordinating solvents than THF will also be more favorable for ionic mechanisms. All these circumstances can now be considered, in the framework of our reaction scheme of competitive pathways, when planning new synthesis.

It is worth recalling that this study concerns the transmetalation step only. The oxidative addition or the reductive elimination steps are required for a successful cross coupling, but can turn out to be rate determining. This should not be overlooked.[42]

ASSOCIATED CONTENT

Supporting Information. Details of experimental studies, computational details, relative energies for all the computed structures, optimized structures, and absolute energies in gas phase and in solution. This material is available free of charge via the Internet at http://pubs.acs.org.

AUTHOR INFORMATION

Corresponding Authors
casares@qi.uva.es; gregori@klingon.uab.es; espinet@qi.uva.es

ACKNOWLEDGMENT

We thank the Ministerio de Ciencia y Tecnología (CTQ2010-18901, CTQ2008-06866-CO2-01), Consolider Ingenio 2010 (CSD2006-0003, CSD2007-00006), and the Junta de Castilla y León (VA373A11-2 and VA281A11-2) for financial support, and for studentships to M.G.-M. (UAB PIF) and B.F. (MCyT).

REFERENCES

(1) For reviews see: (a) Negishi, E. *Bull. Chem. Soc. Jpn.* **2007**, *80*, 233–257. (b) Negishi, E.; Hu, Q.; Huang, Z.; Qian, M.; Wang, G. *Aldrichimica Acta* **2005**, *38*, 71–87. (c) Phapale, V. B.; Cárdenas, D. J. *Chem. Soc. Rev.* **2009**, *38*, 1598–1607.

(2) (a) *Handbook of Organopalladium Chemistry for Organic Synthesis*, Vol. 1, part III; Negishi, E., Ed; Wiley-Interscience: New York, 2002. (b) Negishi, E.; Zeng, X.; Tan, Z.; Qian, M.; Hu, Q.; Huang, Z. In *Metal-Catalyzed Cross-Coupling Reactions*; de Meijere, A., Diederich, F., Eds.; Wiley-VCH: New York, 2004; Chapter 15.

(3) (a) Zhou, J.; Fu, G. C. *J. Am. Chem. Soc.* **2003**, *125*, 12527–12530. (b) Zhou, J.; Fu, G. C. *J. Am. Chem. Soc.* **2003**, *125*, 14726–14727. (c) Tan, Z.; Negishi, E. *Angew. Chem., Int. Ed.* **2006**, *45*, 762–765. (d) Jones, G. D.; Martin, J. L.; McFarland, C.; Allen, O. R.; Hall, R. E.; Haley, A. D.; Bandon, R. J.; Konovalova, T.; Desrochers, P. J.; Pulay, P.; Vicic, D. A. *J. Am. Chem. Soc.* **2006**, *128*, 13175–13183. (e) Jones, G. D.; McFarland, C.; Anderson, T. J.; Vicic, D. A. *Chem. Commun.* **2005**, 4211–4213.

(4) Espinet, P.; Echavarren, A. M. *Angew. Chem., Int. Ed.* **2004**, *43*, 4704–4734.

(5) Casado, A. L.; Espinet, P. *J. Am. Chem. Soc.* **1998**, *120*, 8978–8985.

(6) Casado, A. L.; Espinet, P.; Gallego, A. M. *J. Am. Chem. Soc.* **2000**, *122*, 11771–11782.

(7) Nova, A.; Ujaque, G.; Maseras, F.; Lledós, A.; Espinet, P. *J. Am. Chem. Soc.* **2006**, *128*, 14571–14578.

(8) Pérez-Temprano, M. H.; Gallego, A. M.; Casares, J. A.; Espinet, P. *Organometallics* **2011**, *30*, 611–617.

(9) Goossen, L. J.; Koley, D.; Hermann, H. L.; Thiel, W. *J. Am. Chem. Soc.* **2005**, *127*, 11102–11114.

(10) Braga, A. A. C.; Morgon, N. H.; Ujaque, G.; Maseras, F. *J. Am. Chem. Soc.* **2005**, *127*, 9298–9307.
(11) Braga, A. A. C.; Ujaque, G.; Maseras, F. *Organometallics* **2006**, *25*, 3647–3658.
(12) Jover, J.; Fey, N.; Purdie, M.; Lloyd-Jones, G. C.; Harvey, J. N. *J. Mol. Catal. A: Chem.* **2010**, *324*, 39–47.
(13) Urkalan, K. B.; Sigman, M. S. *J. Am. Chem. Soc.* **2009**, *131*, 18042–18043.
(14) Howell, G. P.; Minnaard, A. J.; Feringa, B. L. *Org. Biomol. Chem.* **2006**, *4*, 1278–1283.
(15) Marshall, J. A. *Chem. Rev.* **2000**, *100*, 3163–3185.
(16) (a) Jin, L.; Zhao, Y.; Zhu, L.; Zhang, H.; Lei, A. *Adv. Synth. Catal.* **2009**, *351*, 630–634. (b) Chen, M.; Zheng, X.; Li, W.; He, J.; Lei, A. *J. Am. Chem. Soc.* **2010**, *132*, 4101–4103.
(17) Casares, J. A.; Espinet, P.; Fuentes, B.; Salas, G. *J. Am. Chem. Soc.* **2007**, *129*, 3508–3509.
(18) van Asselt, R.; Elsevier, C. J. *Organometallics* **1994**, *13*, 1972–1980.
(19) Liu, Q.; Lan, Y.; Liu, J.; Li, G.; Wu, Y. D.; Lei, A. *J. Am. Chem. Soc.* **2009**, *131*, 10201–10210.
(20) Fuentes, B.; García-Melchor, M.; Casares, J. A.; Ujaque, G.; Lledós, A.; Maseras, F.; Espinet, P. *Chem.—Eur. J.* **2010**, *16*, 8596–8599.
(21) By "retrotransmetalation" we mean the reverse of the transmetalation reaction. See: Pérez-Temprano, M. H.; Nova, A.; Casares, J. A.; Espinet, P. *J. Am. Chem. Soc.* **2008**, *130*, 10518–10519.
(22) Gillie, A.; Stille, J. K. *J. Am. Chem. Soc.* **1980**, *102*, 4933–4941.
(23) (a) Ozawa, F.; Ito, T.; Nakamura, Y.; Yamamoto, A. *Bull. Chem. Soc. Jpn.* **1981**, *54*, 1868–1880. (b) Ozawa, F.; Kurihara, K.; Yamamoto, T.; Yamamoto, A. *J. Organomet. Chem.* **1985**, *279*, 233–243.
(24) (a) Spielvogel, D. J.; Davis, W. M.; Buchwald, S. L. *Organometallics* **2002**, *21*, 3833–3836. (b) Spielvogel, D. J.; Buchwald, S. L. *J. Am. Chem. Soc.* **2002**, *124*, 3500–3501.
(25) Majumdar, K. K.; Cheng, C.-H. *Org. Lett.* **2000**, *15*, 2295–2298.
(26) Anderson, T. J.; Vicic, D. A. *Organometallics* **2004**, *23*, 623–625.
(27) The exact structure of the anion represented as "[$ZnMe_2Cl^-$]" in Scheme 2 was not determined, but it is very reasonable to assume a chloro-bridged dimeric structure $[Me_2Zn(\mu\text{-}Cl)_2ZnMe_2]^{2-}$, which satisfies a tetrahedral coordination for Zn. This anion is not good at coordinating, and THF can compete for the vacant Pd site. In contrast, if $[ClMeZn(\mu\text{-}Cl)_2ZnMeCl]^{2-}$ is formed by Cl^- abstraction when using ZnMeCl, the anionic dimer produced contains terminal chlorides that will still be better coordinating than THF, and will occupy the Pd site forming Pd−Cl−Zn bridges.
(28) Although the kinetic data for this process are not so good, we estimate that the value of $\Delta G^{\ddagger}_{transmetal}$ for the reaction via $\mathbf{4}^+$ should be at most 13.6 kcal mol^{-1} to the *trans* and 14.6 kcal mol^{-1} to the *cis*, or lower.
(29) Zhao, Y.; Truhlar, D. G. *Theor. Chem. Acc.* **2008**, *120*, 215–241.
(30) Weidenbruch, M.; Herrndorf, M.; Schafer, A.; Pohl, S.; Saak, W. *J. Organomet. Chem.* **1989**, *361*, 139–145.
(31) For further computational details, see Supporting Information.
(32) As discussed below, because of the difficult treatment of noncovalent interactions, matching quantitative values in transition metal containing molecules is unlikely.
(33) This transition state **TsIT1** appears 0.6 kcal mol^{-1} lower in energy than the following intermediate **IT2** in the Gibbs energy surface, indicating a very easy backward process to regenerate the reactants.
(34) A Gibbs energy difference larger than 3 kcal mol^{-1} compared to the starting materials should be sufficient to make its equilibrium concentration low enough to be nonobservable by NMR.
(35) The very small energy difference between these two intermediates (0.4 kcal mol^{-1}) is due to the different conformations of the tetrahedral Zn.
(36) Sakaki, S.; Ohnishi, Y.-Y.; Sato, H. *Chem. Rec.* **2010**, *10*, 29–45.
(37) Bartlett, K. L.; Goldberg, K. I.; Borden, W. T. *J. Am. Chem. Soc.* **2000**, *122*, 1456–1465.
(38) Sieffert, N.; Bühl, M. *Inorg. Chem.* **2009**, *48*, 4622–4624.
(39) (a) Zhao, Y.; Truhlar, D. G. *Org. Lett.* **2007**, *9*, 1967–1970. (b) Zhao, Y.; Truhlar, D. G. *J. Chem. Theory Comput.* **2009**, *5*, 324–333.
(40) At 203 K, assuming as safe estimations 10% error in the rate constant and 1 degree in the determination of *T*, the error in ΔG is only 0.08 kcal mol^{-1}.
(41) (a) Harvey, J. N. *Faraday Discuss.* **2010**, *145*, 487–505. (b) McMullin, C. L.; Jover, J.; Harvey, J. N.; Fey, N. *Dalton Trans.* **2010**, *39*, 10833–10836.
(42) For oxidative addition, see refs 4 and 5; for concurrence of competitive pathways and the occasional need of isomerization, see reference 8; for C−C coupling, see: Pérez-Rodríguez, M.; Braga, A. A. C.; García-Melchor, M.; Pérez-Temprano, M. H.; Casares, J. A.; Ujaque, G.; de Lera, A. R.; Álvarez, R.; Maseras, F.; Espinet, P. *J. Am. Chem. Soc.* **2009**, *131*, 3650–3657.

A.3 Article III:

Mechanistic Exploration of the Pd-Catalyzed Copper-Free Sonogashira Reaction

García-Melchor, M.; Pacheco, M. C.; Nájera, C.; Lledós, A.; Ujaque, G. *ACS Catal.* **2012**, *2*, 135-144.

ACS Catalysis

Research Article

pubs.acs.org/acscatalysis

Mechanistic Exploration of the Pd-Catalyzed Copper-Free Sonogashira Reaction

Max García-Melchor,[†] María C. Pacheco,[‡] Carmen Nájera,*[,‡] Agustí Lledós,*[,†] and Gregori Ujaque*[,†]

[†]Departament de Química, Edifici Cn, Universitat Autònoma de Barcelona, E-08193 Cerdanyola del Vallès, Catalonia, Spain

[‡]Departamento de Química Orgánica, Universidad de Alicante, Apartado 99, E-03080 Alicante, Spain

Supporting Information

ABSTRACT: The reaction mechanism for the Pd-catalyzed Cu-free Sonogashira reaction is analyzed by means of density functional theory (DFT) calculations on a model system. The most common routes proposed in the literature for this reaction, namely, the carbopalladation and deprotonation, are considered. In agreement with experiment, calculations clearly demonstrate that the carbopalladation route can be discarded. For the case of the deprotonation route, however, the reaction pathway may take place via several alternatives; calculations suggest that all of them are feasible. Moreover, an additional pathway where the halide is initially replaced by the base in the coordination sphere of the catalyst is found to be also competitive. The effects of the alkyne's substituents on the reaction are also analyzed by a combined computational and experimental work. Theoretical results suggest that these effects are rather small, and they are confirmed by experiments.

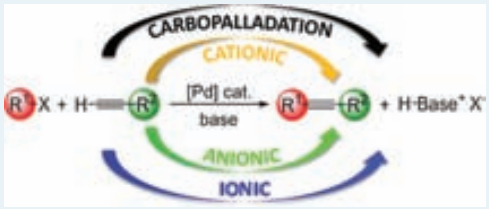

KEYWORDS: *cross-coupling reactions, Sonogashira reaction, DFT calculations, palladium, alkynes*

1. INTRODUCTION

The palladium-catalyzed Sonogashira reaction is one of the most important and widely used methods for preparing arylacetylenes and conjugated enynes,[1−6] which are precursors for natural products, pharmaceuticals, and materials with specialized optical and electronic properties.[6−12] The general Sonogashira protocol for the coupling of terminal alkynes with aryl or alkenyl halides (or triflates) usually involves an organic solvent, a Pd(0)/Cu(I) catalytic system, and at least a stoichiometric amount of a base (Scheme 1).[13] The presence

Scheme 1. General Pd-Catalyzed Sonogashira Reaction

of a copper(I) salt as cocatalyst in the typical Sonogashira reaction is generally believed to facilitate the reaction by the in situ generation of copper acetylide. However, the addition of this copper(I) salt under the reaction conditions entails some drawbacks,[14,15] mainly the induction of the so-called Glaser-type oxidative homocoupling of the terminal alkyne to yield the diyne.[16,17] Aiming at the suppression of the formation of this byproduct, many efforts have been devoted to develop reaction procedures working in the absence of copper salts.[18−26] All these copper-free strategies are commonly known as copper-free Sonogashira reaction. Unfortunately, this copper-free variant frequently requires the use of an excess of amine (often even acting as solvent), which proves detrimental to the environmental and economical advantages of this methodology. To avoid that, several modifications of the original Sonogashira reaction have been recently reported including amine-free, ligand-free, and solvent-free conditions.[27−37] All these modifications, however, are based on assumptions about a hypothetical reaction mechanism, since very little is known about the mechanism of the Sonogashira reaction, specially for the copper-free variant.

Two different mechanisms have been proposed for the copper-free Sonogashira reaction (Figure 1): the *deprotonation*[19] and *carbopalladation*[38] mechanisms. Both mechanisms share the initial oxidative addition of the organohalide R^1-X to the $PdL_2(0)$ complex giving the intermediate **1** and the subsequent ligand by alkyne substitution from this species, which results in the formation of complex **2**. At this point, the two reaction mechanisms differ in the next steps leading to the final coupled product. More specifically, in the case of the deprotonation mechanism (Figure 1, left) the deprotonation of the alkyne and the coordination of the ligand L take place from **2** yielding a square planar Pd complex with the two organic groups in cis disposition, from which the coupled product is expelled by reductive elimination. Alternatively, in the carbopalladation mechanism (Figure 1, right) complex **2** undergoes addition of the organic group R^1 to the terminal

Received: October 11, 2011
Revised: November 23, 2011

   dx.doi.org/10.1021/cs200526x | ACS Catal. 2012, 2, 135−144

ACS Catalysis Research Article

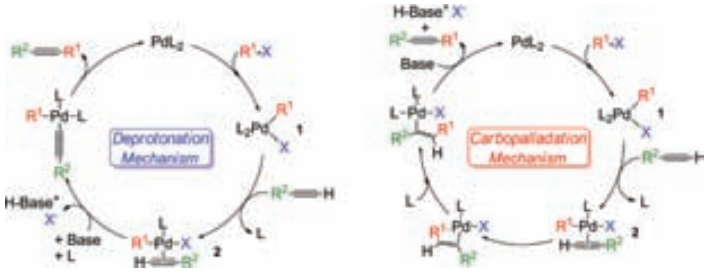

Figure 1. Proposed reaction mechanisms for the copper-free Sonogashira reaction: *deprotonation* (left)[19] and *carbopalladation* (right)[38] mechanisms.

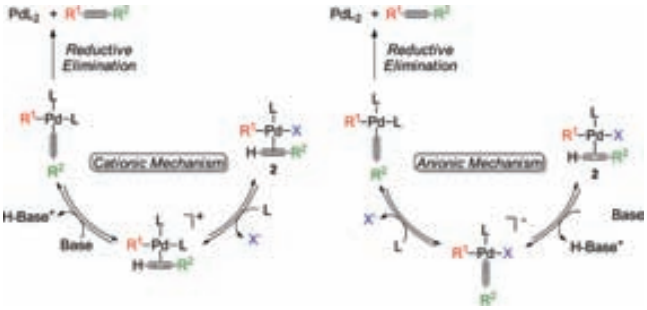

Figure 2. *Cationic* (left) and *anionic* (right) alternatives for the deprotonation mechanism.

Scheme 2. Copper-Free Sonogashira Reaction between Several 4-Substituted Phenylacetylenes and Iodobenzene

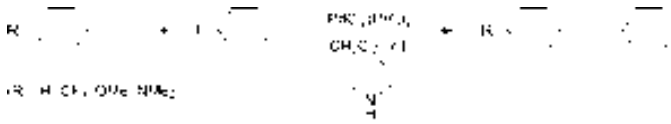

alkyne, followed by the coordination of the ligand L and subsequent base-mediated reductive elimination.

Over the past years, these two mechanisms have been somewhat discussed in the literature, but the mechanism that operates in the copper-free Sonogashira reaction remains still unclear. In fact, up to date, the reported experimental and theoretical mechanistic studies on this process have been rather scarce. Among the experimental ones, one must mention the ones reported by Jutand et al.[39,40] and Mårtensson et al.[41] On one hand, Jutand et al. by means of a thoughtful work shed light on the decelerating effect of alkynes in the oxidative addition step and suggested that amines might have multiple roles in the reaction mechanism. On the other hand, Mårtensson et al.[41] demonstrated with a simple though clever experiment that the carbopalladation mechanism can be discarded, and they proposed two alternative routes for the deprotonation pathway. These two variants of the deprotonation, labeled by the authors as *cationic* and *anionic mechanisms*, only differ in the order of the steps (Figure 2). The cationic mechanism (Figure 2, left) involves the L-X ligand substitution in **2** giving rise to the cationic Pd complex *cis*-$[Pd(R^1)(alkyne)(L)_2]^+$, which undergoes deprotonation of the alkyne by an external base and subsequent reductive elimination. In contrast, in the anionic mechanism (Figure 2, right) the deprotonation of the alkyne occurs first resulting in the anionic complex *cis*-$[Pd(R^1)(acetylide)(X)(L)]^-$, in which the L-X ligand substitution takes place followed by the reductive elimination step. According to Mårtensson et al.,[41] the cationic and the anionic alternatives can be favored depending on the electronic nature of the substituents directly attached to the terminal alkynes. Particularly, the authors suggest that alkynes bearing electron withdrawing groups (EWG) may favor the anionic mechanism whereas alkynes bearing electron donating groups (EDG) may favor the cationic pathway.

As far as the theoretical studies on the reaction mechanism are concerned, to the best of our knowledge, there are those reported by Chen et al.[42] where they considered the halide (Br^-) as the species accepting the proton from the alkyne and by Sikk et al.[43] where a reaction mechanism for the process was analyzed; the latter paper appeared during the revision process of this work. In spite of the importance of the Sonogashira reaction, there is a lack of deep understanding of the reaction mechanism.

The purpose of this work is to evaluate the reaction mechanisms proposed in the literature and possible alternative pathways using a general model of the typical Pd-catalyzed copper-free Sonogashira reaction. To this end, the Gibbs energy profiles of the different mechanistic proposals have been obtained by Density Functional Theory (DFT) calculations. An additional objective of this work is to analyze the effect of the electronic nature of the alkyne's substituents over all the

dx.doi.org/10.1021/cs200526x | *ACS Catal.* 2012, 2, 135–144

studied reaction pathways. This feature for a set of substituents has been investigated by combining theory and experiment.

2. RESULTS AND DISCUSSION

2.1. Selection of the Model. For the analysis of the general reaction mechanism we selected a set of model molecules to obtain a general overview on the process. Hence, phenylacetylene and iodobenzene species were selected as models for the coupling organic reactants, pyrrolidine as base, and dichloromethane (DCM) as solvent. For the additional analysis of the effect of the alkyne's substituents, several 4-substituted phenylacetylenes (R = H, CF_3, OMe, NMe_2) were considered (Scheme 2). As far as the catalyst is concerned, all the calculations were performed using $Pd(PH_3)_2$ as a model for the catalyst. Because of the increase of computational power, this model used to be considered too small, and catalysts with bigger phosphine ligands used to be calculated. Nevertheless, we have selected this model on purpose for this study for the following reasons: (a) as we have recently shown, conformational diversity may introduce significant errors in the calculations of the energy profiles (with modifications in energy barriers higher than 10 kcal·mol^{-1} depending on the phosphines),[44] (b) regarding the electronic properties of the phosphine, PH_3 can be considered as a neutral one, (c) and in terms of computational requirements it is by far the less demanding one. The main objective of the present work is to map the potential energy surface by analyzing all the reasonable reaction profiles. Thus, we think the present model covers most of the general features of the reaction system, apart from the steric effects that should be evaluated for the particular system studied. Full computational details are provided in the Computational Details section.

The oxidative addition of PhI to $[Pd(PH_3)_2]$ is the first step of the reaction giving rise to the *cis*-$[Pd(Ph)(I)(PH_3)_2]$ complex. The calculated energy barrier for this process is rather low, 17.0 kcal·mol^{-1}, as expected for aryl iodides. The subsequent cis-to-trans isomerization is known to take place following different pathways,[45] but in any case it is an easy process.[46] Thus, we focus on analyzing the reaction process starting from the *trans*-$[Pd(Ph)(I)(PH_3)_2]$ (**1**) complex.

2.2. Copper-Free Sonogashira Reaction via a Carbopalladation Mechanism. Despite that Mårtensson et al.[41] experimentally showed that the carbopalladation mechanism can not be operative, to have a comprehensive mechanistic understanding of the reaction we investigated this mechanism together with the deprotonation mechanism including their cationic and anionic alternatives.

The theoretical investigation of the copper-free Sonogashira reaction with phenylacetylene as a model substrate (R = H) through a carbopalladation mechanism afforded the reaction profile shown in Figure 3. As previously mentioned, the carbopalladation and the deprotonation mechanisms share the initial substitution of a phosphine ligand by the alkyne, which leads to the formation of a common intermediate (**2**). The calculation of the associative substitution indicate that this is an endergonic process by 13.5 kcal·mol^{-1} with an energy barrier of 23.0 kcal·mol^{-1}. Once complex **2** is formed, the carbopalladation reaction occurs through the transition state **C-TS1** resulting in the intermediate **C-1** with a relative energy barrier of 14.2 kcal·mol^{-1}. Subsequently, this intermediate evolves with a low energy barrier (6.4 kcal·mol^{-1}) to the very stable intermediate **C-2** (Figure 4) by coordination of a phosphine ligand via **C-TS2**. Finally, the alkenyl moiety in **C-2** is

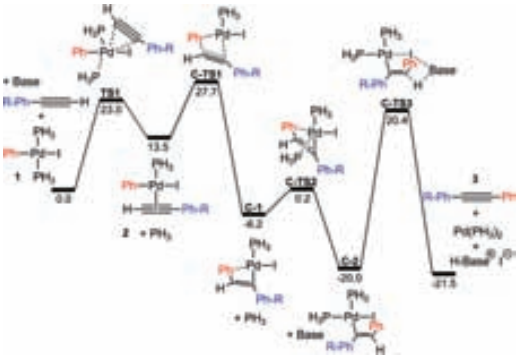

Figure 3. Gibbs energy profile in DCM (ΔG_{DCM}, kcal·mol^{-1}) at 298 K for the carbopalladation mechanism with R = H, and Base = pyrrolidine.

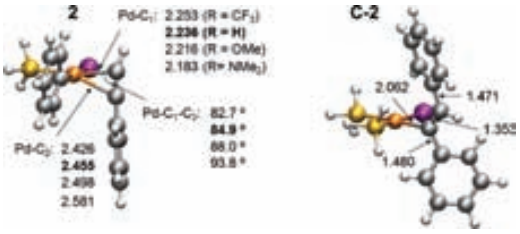

Figure 4. Optimized structures for intermediates **2** and **C-2** with phenylacetylene (R = H). Distances (shown in Å) and angles in complex **2** with the other R groups are also shown.

deprotonated by an external base through the transition state **C-TS3** yielding the final coupled product (**3**) and the regeneration of the catalyst. This last step has the highest energy barrier in the overall energy profile (40.4 kcal·mol^{-1}), which can be attributed to the high stability of **C-2** and the difficulty that the deprotonation of a double bond entails (high energy of **C-TS3**). As a result, this step has the highest energy barrier in the carbopalladation mechanism with phenylacetylene (R = H).

Overall, the reaction is exergonic by 21.5 kcal·mol^{-1}, but the carbopalladation mechanism has a very high energy barrier (40.4 kcal·mol^{-1}), making it unfeasible for the copper-free Sonogashira reaction. The occurrence of a very stable intermediate placed 20 kcal·mol^{-1} below reactants and the necessity of overcoming a barrier of about 40 kcal·mol^{-1} are responsible for the unsuitability of the carbopalladation mechanism. This theoretical finding agrees with the experimental observation of Mårtensson et al.[41] that a complex analogue to **C-2** synthesized through an alternative route does not afford the coupled product under the Sonogashira reaction conditions.

As far as the effect of the electronic nature of the R substituents of the alkyne is concerned, the Gibbs energy profiles for the Sonogashira reaction with several 4-substituted phenylacetylenes (R = CF_3, OMe, NMe_2) through a carbopalladation mechanism were also computed (Table 1).

As shown in Table 1, the influence of the substituent on the reaction energy is rather low: the reaction is highly exergonic with all the substituents by around 21 kcal·mol^{-1}. The most

dx.doi.org/10.1021/cs200526x | ACS Catal. 2012, 2, 135–144

Table 1. Relative Gibbs Energies in DCM (ΔG_{DCM}, kcal·mol^{-1}) at 298 K for the Carbopalladation Mechanism with the Different 4-Substituted Phenylacetylenes (R = H, CF_3, OMe, NMe_2)

species	R = H	R = CF_3	R = OMe	R = NMe_2
1 + Base + alkyne	0.0	0.0	0.0	0.0
TS1	23.0	24.8	22.9	20.6
2 + PH_3	13.5	15.9	12.7	9.9
C-TS1	27.7	28.3	27.5	26.7
C-1	−6.2	−7.1	−5.7	−5.4
C-TS2	0.2	−1.8	0.2	−0.1
C-2	−20.0	−21.5	−19.5	−19.8
C-TS3	20.4	19.4	21.3	21.2
3 + $[Pd(PH_3)_2]$ + H-Base$^+$ I^-	−21.5	−21.6	−21.3	−21.4

important effect of the different R groups is in the step common to all the mechanisms, which is the coordination of the alkyne to the palladium complex **1** to yield complex **2**. However, this is not the rate-determining step in the carbopalladation mechanism. The calculated energy barrier for this step (Table 1, **TS1**) decreases in the order: R = CF_3 > H > OMe > NMe_2, which correlates with the higher electron donor ability of the R groups, and consequently, with the higher donor ability of the alkyne. This higher donor ability of the alkyne with EDGs is responsible for the higher stability of the corresponding complexes **2**, which feature shorter Pd−C_1 distances and higher Pd−C_1−C_2 angles with these substituents (Figure 4).

Similarly to the case with R = H, the deprotonation of the alkene moiety in **C-2** with the other R groups has the highest energy barrier in the overall reaction pathway, with values ranging from 40.4 to 41.0 kcal·mol^{-1} (Table 1). Thus, for these substituted phenylacetylenes the carbopalladation mechanism is also too energy-demanding to be operative under the reaction conditions, which agrees again with the experimental findings of Mårtensson et al.[41]

2.3. Copper-Free Sonogashira Reaction via a Deprotonation Mechanism. The copper-free Sonogashira reaction through a deprotonation mechanism was also investigated. As mentioned in the introduction, for this mechanism two different alternatives have been proposed, namely the *cationic* and the *anionic* mechanisms (Figure 2).[41]

2.3.1. Copper-Free Sonogashira Reaction via a Cationic Mechanism. The cationic mechanism differs from the anionic mechanism by the order in which the deprotonation and substitution steps occur (Figure 2). The computed Gibbs energy profile for the copper-free Sonogashira reaction with phenylacetylene (R = H) through a cationic mechanism is shown in Figure 5. In contrast to the carbopalladation mechanism, once complex **2** is formed, the substitution of the iodide by the phosphine ligand takes place giving rise to the ion-pair (**DC-1**) formed between the cationic Pd complex and the iodide with a relative energy barrier of 14.0 kcal·mol^{-1} (**DC-TS1**). Then, from this species the deprotonation of the alkyne by the external base occurs (**DC-TS2**, 25.9 kcal·mol^{-1}) yielding the intermediate **RE-1**, where the two organic groups are in a cis configuration. Finally, **RE-1** undergoes reductive elimination via **RE-TS1** (17.9 kcal·mol^{-1}) resulting in the final product (**3**) and the regeneration of the catalyst. In the overall energy profile, the highest global energy barrier corresponds to the iodide-by-phosphine ligand substitution via **DC-TS1** (27.5 kcal·mol^{-1}).

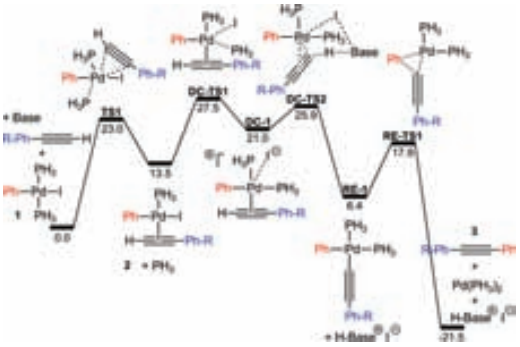

Figure 5. Gibbs energy profile in DCM (ΔG_{DCM}, kcal·mol^{-1}) at 298 K for the cationic mechanism with R = H, and Base = pyrrolidine.

The Gibbs energy profiles for the Sonogashira reaction via the cationic mechanism with the other 4-substituted phenylacetylenes (R = CF_3, OMe, NMe_2) were also computed (Table 2). Interestingly, the energy of the transition state for the substitution of the iodide by the phosphine ligand (the energy difference between **DC-TS1** and **1**) with the different R groups increases in the order R = NMe_2 < OMe < H < CF_3. However, the relative energy barrier for this step (the energy difference between **DC-TS1** and **2**) is practically the same for all the R groups (the highest energy difference between the R groups is 0.8 kcal·mol^{-1}), which indicates that the different stability of intermediates **2** is responsible for the differences in the global energy barriers. On the other hand, Table 2 shows that the deprotonation of the alkyne in **DC-1** through **DC-TS2** follows a similar trend as the iodide-for-phosphine substitution step (NMe_2 < OMe < CF_3 < H). In this case, however, the overall energy barrier range (the energy differences between **DC-TS2** and **DC-1**) is slightly higher (the lowest energy difference between the R groups is 1.4 kcal·mol^{-1}). More specifically, the relative energy barriers for the deprotonation step increase in the following order: CF_3 < OMe ≈ H < NMe_2. This trend can be rationalized: the presence of a EWG (i.e., R = CF_3) in the alkyne makes its proton more acidic and thus, the relative energy barrier for this step decreases. Conversely, the presence of an EDG (i.e., R = NMe_2) makes the proton of the alkyne less acidic, which increases the relative energy barrier. The cases with the model substituent (i.e., R = H) and the moderate EDG

Table 2. Relative Gibbs Energies in DCM (ΔG_{DCM}, kcal·mol^{-1}) at 298 K for the Cationic Mechanism with the Different 4-Substituted Phenylacetylenes (R = H, CF_3, OMe, NMe_2)

species	R = H	R = CF_3	R = OMe	R = NMe_2
1 + Base + alkyne	0.0	0.0	0.0	0.0
TS1	23.0	24.8	22.9	20.6
2 + PH_3	13.5	15.9	12.7	9.9
DC-TS1	27.5	29.1	26.4	23.7
DC-1	21.0	22.2	20.6	16.1
DC-TS2	25.9	25.5	25.3	21.5
RE-1	6.4	4.3	7.1	6.8
RE-TS1	17.9	15.5	18.8	18.8
3 + $[Pd(PH_3)_2]$ + H-Base$^+$ I^-	−21.5	−21.6	−21.3	−21.4

dx.doi.org/10.1021/cs200526x | *ACS Catal.* 2012, 2, 135–144

(i.e., R = OMe) have similar energy barriers and lie in between the other R groups.

Similarly to the reaction with phenylacetylene (R = H), the highest energy point in the overall energy profile regardless of the R groups corresponds to the substitution of the iodide by the phosphine ligand (**DC-TS1**); therefore this step has also the highest energy barrier for all these R groups. Moreover, these calculated energy barriers are lower for EDGs than for EWGs indicating that the more EDG the faster the process via this cationic mechanism should be.

2.3.2. Copper-free Sonogashira Reaction via an Anionic Mechanism. In the anionic mechanism the steps of the deprotonation mechanism take place in reverse order compared to the cationic mechanism. Thus, in the anionic mechanism the deprotonation of the alkyne by the external base from complex **2** occurs first, followed by the iodide-for-phosphine substitution. The Gibbs energy profile of the Sonogashira reaction with phenylacetylene (R = H) through the anionic mechanism is shown in Figure 6.

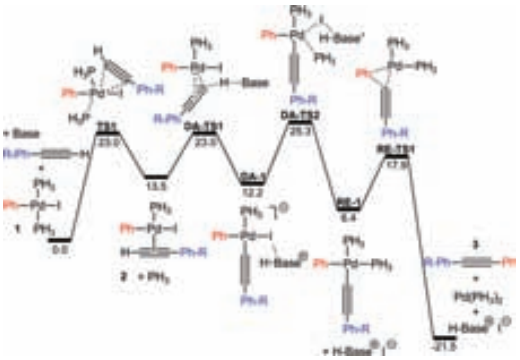

Figure 6. Gibbs energy profile in DCM (ΔG_{DCM}, kcal·mol^{-1}) at 298 K for the anionic mechanism with R = H, and Base = pyrrolidine.

The deprotonation of the alkyne by the external base in complex **2** occurs through the transition state **DA-TS1** (23.0 kcal·mol^{-1}) and leads to the formation of the ion-pair (**DA-1**) formed between the anionic Pd complex and the protonated base. Subsequently, this species evolves to intermediate **RE-1** by an iodide-by-phosphine substitution via **DA-TS2**. This step corresponds to the highest transition state within the energy profile (2.3 kcal·mol^{-1} higher than **DA-TS1** and **TS1**). Finally, **RE-1** undergoes reductive elimination giving rise to the coupling product and regenerating the catalyst.

The relative Gibbs energy values for the other 4-substituted phenylacetylenes (R = CF_3, OMe, NMe_2) were also computed and are summarized in Table 3. For all the 4-substituted phenylacetylenes, Table 3 shows that the highest energy barrier corresponds to the substitution of the iodide by the phosphine ligand via **DA-TS2**, indicating that this step, like with R = H, is rate limiting in the anionic mechanism. Moreover, the small energy differences between the transition states **DA-TS2** (all of them within 1 kcal·mol^{-1}) suggest that the electronic nature of the R groups may not have a significant effect over the reaction rates through this mechanism.

2.3.3. Cationic Mechanism versus Anionic Mechanism. According to calculations, in both cationic and anionic mechanisms the highest energy barrier corresponds to the

Table 3. Relative Gibbs Energies in DCM (ΔG_{DCM}, kcal·mol^{-1}) at 298 K for the Anionic Mechanism with the Different 4-Substituted Phenylacetylenes (R = H, CF_3, OMe, NMe_2)

species	R = H	R = CF_3	R = OMe	R = NMe_2
1 + Base + alkyne	0.0	0.0	0.0	0.0
TS1	23.0	24.8	22.9	20.6
2 + PH_3	13.5	15.9	12.7	9.9
DA-TS1	23.0	23.1	22.3	19.3
DA-1	12.2	10.8	12.3	12.5
DA-TS2	25.3	24.6	25.8	25.6
RE-1	6.4	4.3	7.1	6.8
RE-TS1	17.9	15.5	18.8	18.8
3 + [Pd(PH_3)$_2$] + H-Base$^+$ I$^-$	−21.5	−21.6	−21.3	−21.4

substitution of the iodide by the phosphine ligand. However, depending on the mechanism this substitution takes place either before (i.e., the cationic mechanism) or after (i.e., the anionic mechanism) the deprotonation of the alkyne. More specifically, in the case of the cationic mechanism this substitution takes place in complex **2** via **DC-TS1** (Figure 5), whereas in the anionic mechanism it occurs in **DA-1** via **DA-TS2** (Figure 6). The computed global Gibbs energy barriers for these processes with all the 4-substituted phenylacetylenes (Table 4) show that both mechanisms are feasible. Importantly,

Table 4. Global Gibbs Energy Barriers in DCM (ΔG_{DCM}, kcal·mol^{-1}) at 298 K for the Cationic and Anionic Mechanisms with the Different 4-Substituted Phenylacetylenes (R = H, CF_3, OMe, NMe_2)

	global Gibbs energy barriers[a]	
substituent	cationic mechanism	anionic mechanism
R = CF_3	29.1	**24.6**
R = H	27.5	**25.3**
R = OMe	26.4	**25.8**
R = NMe_2	**23.7**	25.6

[a]The Gibbs energy barriers for the lowest-energy deprotonation pathways with the different R groups are in bold.

these values also suggest that depending on the electronic nature of the R group there might be a change in the reaction mechanism. In particular, with both the highly electron withdrawing group R = CF_3 and the model substituent R = H, the anionic mechanism is favored compared to the cationic mechanism by 4.5 and 2.2 kcal·mol^{-1}, respectively. On the other hand, with the moderate electron donating group R = OMe this energy difference becomes smaller (0.6 kcal·mol^{-1}) but still in favor of the anionic mechanism. Finally, with the highly electron donating group R = NMe_2 this energy difference is reversed favoring the cationic mechanism by 1.9 kcal·mol^{-1}.

This predicted change in the reaction mechanism can be rationalized as follows: the first step in the cationic mechanism yields intermediate **2** (Figure 5). As previously stated, in the case of EWGs (i.e., R = CF_3, H) or moderate EDGs (i.e., R = OMe) this species is less stable than with highly EDGs (i.e., R = NMe_2) (the energy difference range from 2.8 kcal·mol^{-1} to 6.0 kcal·mol^{-1}). Thus, EWGs groups cause higher energy barriers because the following iodide-by-phosphine substitution step has a very similar relative energy barrier for all the R groups. In contrast, the first step in the anionic mechanism from complex

dx.doi.org/10.1021/cs200526x | ACS Catal. 2012, 2, 135–144

2 gives the intermediate **DA-1** (Figure 6). In this case, the anionic charge on the Pd complex is better stabilized with EWGs, which offsets the energy gain in complex **2** with the highly EDGs and leads to lower energy barriers compared to the cationic mechanism. This results in a preference for the anionic mechanism with EWGs (i.e., R = CF_3, H) or moderate EDGs (i.e., R = OMe) and a preference for the cationic mechanism with highly EDGs (i.e., R = NMe_2).

2.4. Alternative Mechanism: The Ionic Mechanism. Recently, some of us reported a combined experimental and theoretical study on the transmetalation step in a Negishi cross-coupling reaction[47] in which we demonstrated that an external coordinating ligand (i.e., $PMePh_2$, THF) can easily replace the chloride from the complex *trans*-[PdMeCl$(PMePh_2)_2$] (complex analogue to **1**). The reaction mechanism involving this step was labeled as *ionic mechanism*. The role of additional ligands has been also shown to be important in related Sonogashira processes.[48,49] On the basis of these results and that the coordination of the alkyne requires a considerably high energy barrier (higher than 20 kcal·mol^{-1}), we computed an alternative mechanism for the Sonogashira reaction that we also named *ionic mechanism* because of its similarities with the one reported for the Negishi coupling.[47] The computed Gibbs energy reaction profile via this mechanism with phenylacetylene (R = H) is shown in Figure 7.

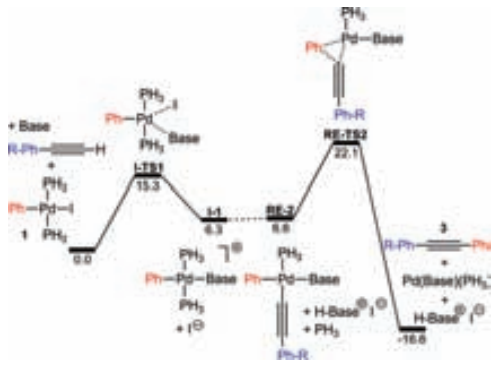

Figure 7. Gibbs energy profile in DCM (ΔG_{DCM}, kcal·mol^{-1}) at 298 K for the ionic mechanism with R = H, and Base = pyrrolidine.

In contrast to the cationic and anionic mechanisms, where the iodide is always expelled after the coordination of the alkyne, in the ionic mechanism it is replaced by the base in the first step. This process occurs through the transition state **I-TS1** and results in the formation of the cationic Pd complex **I-1**. Importantly, the energy barrier required for this process is 15.3 kcal·mol^{-1}, which is much lower (it is at least 5 kcal·mol^{-1} lower) than the energy required for the coordination of the alkyne to **1** via **TS1**. At this point, and on the basis that the reaction is carried out with an excess of base, we considered that the corresponding phenylacetylide may be present in solution as a result of the acid–base reaction. According to calculations, the phenylacetylide can replace one of the phosphine ligands in **I-1** with a barrierless process.[50] This process without energy barrier affords the isoenergetic species **RE-2**, which directly evolves to the desired alkyne (**3**) by common reductive elimination via **RE-TS2** (22.1 kcal·mol^{-1}).[51−54] The relative Gibbs energies for the reactions with the other 4-substituted phenylacetylenes through this ionic mechanism are collected in Table 5.

Table 5. Relative Gibbs Energies in DCM (ΔG_{DCM}, kcal·mol^{-1}) at 298 K for the Ionic Mechanism with the Different 4-Substituted Phenylacetylenes (R = H, CF_3, OMe, NMe_2)

species	R = H	R = CF_3	R = OMe	R = NMe_2
1 + Base + alkyne	0.0	0.0	0.0	0.0
I-TS1	15.3	15.3	15.3	15.3
I-1	6.3	6.3	6.3	6.3
RE-2	6.6	3.5	6.0	6.4
RE-TS2	22.1	18.5	22.6	21.8
3 + [Pd(base)(PH_3)] + H-Base$^+$ I^-	−16.6	−16.7	−16.4	−16.5

As shown in Table 5, the highest energy barrier corresponds to the reductive elimination step from complex **RE-2**. The calculated energy barriers for this process with the different R groups range from 18.5 (R = CF_3) to 22.6 kcal·mol^{-1} (R = OMe), which indicates that this ionic mechanism might be competitive with the cationic and anionic mechanisms. Interestingly, the reaction rate through this ionic mechanism depends on the concentration of acetylide present in solution, which is also directly linked to the concentration of the base. In other words, this mechanism depends on the base[55] and the acidity of the proton of the alkyne, which at the same time depends on the electron withdrawing ability of the R group coordinated to the alkyne. Thus, the reaction through this mechanism is expected to be faster when alkynes bearing EWGs are used.

2.5. Effect of the R Substituents on R-C_6H_4–C≡C–H from Experiments. Theoretical calculations demonstrate that the carbopalladation mechanism is not operating under the reaction conditions. Furthermore, calculations also show that the other three investigated mechanisms (i.e., cationic, anionic, and ionic mechanisms) may have competitive rates. Thus, a change on the reaction conditions (i.e., solvent, ligands, substrates, base, etc.) might favor one or another mechanism.

Regarding the effect of the R groups, the theoretical results show relatively small energy differences in the activation energies for the Sonogashira reactions with the different 4-substituted phenylacetylenes (Tables 4 and 5). At this point, we decided to carry out experimental copper-free Sonogashira reactions of 1-fluoro-4-iodobenzene with the 4-substituted phenylacetylenes used for the computational study for comparison. These couplings were performed in dichloromethane with $PdCl_2(PPh_3)_2$ (2 mol %) as catalyst and pyrrolidine as base at room temperature and under Ar atmosphere. In these reactions, the values of conversion (%) of the desired alkyne **3** versus time were obtained by monitoring the reactions by ^{19}F NMR spectroscopy (Figure 8).

The conversion/time data plotted in Figure 8 show that the reaction rate increases with the electron withdrawing ability of the R group (R = NMe_2 < OMe < H ≈ CF_3). Thus, according to experiments, the more acidic the proton of the alkyne is, the higher the reaction rate is; this experimental trend is supported by the ionic mechanism. Notice that if we compare the ratio of conversion of **3** after 1 h for the fastest (R = CF_3) and the slowest (R = NMe_2) reaction, it is 5:1.[56] In terms of activation energies this ratio corresponds to an energy difference lower

dx.doi.org/10.1021/cs200526x | *ACS Catal.* 2012, 2, 135–144

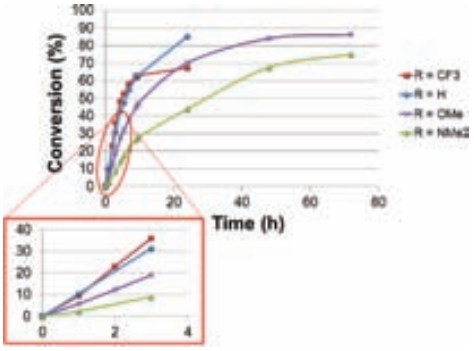

Figure 8. Conversion/time data, obtained by ^{19}F NMR, for the Sonogashira reaction with the analyzed 4-substituted phenylacetylenes (R = H, CF_3, OMe, NMe_2).

than 1 kcal·mol^{-1}, which means that the activation energies for the different R groups are very similar, in agreement with theoretical calculations. According to these results there is not a clear preference for either the deprotonation or the ionic mechanism. Thus, the precise mechanism for a coupling reaction need to be evaluated in detail for each particular case, and competitive mechanisms may take place together. The analysis on a model system for the Suzuki cross-coupling reaction gave rise to similar conclusions regarding the operative reaction mechanism.[45]

3. CONCLUSIONS

The reaction mechanism for the copper-free Sonogashira reaction between iodobenzene and several 4-substituted phenylacetylenes (R = H, CF_3, OMe, NMe_2) was investigated. To the best of our knowledge, this is the first theoretical study that investigates all the reported mechanistic proposals for the copper-free Sonogashira reaction. The theoretical results show that the carbopalladation mechanism has a very high energy barrier, which indicates that this mechanism is not operating under the reaction conditions. For the proposed cationic and the anionic alternatives in the deprotonation mechanism,[41] the calculated Gibbs energy barriers indicate that both mechanisms are feasible. Moreover, calculations predict that one or the other reaction mechanism is favored depending on the electronic nature of the R group coordinated to the alkyne. Thus, EWGs (R = CF_3, H) or moderate EDGs (R = OMe) might favor an anionic mechanism, whereas highly EDGs (R = NMe_2) might favor a cationic mechanism. These differences can be attributed to the different stability of the intermediates that precede the highest energy barrier; the relative intermediate stabilities depend on the R group. These results are in agreement with the reported experimental work of Mårtensson et al.[41]

The presence of an excess of a coordinating ligand like pyrrolidine, the base, and the presence of phenylacetylide opens a new reaction pathway for the copper-free Sonogashira reaction: the ionic mechanism. In this mechanism the base substitutes the halide and helps in forming acetylide species. The theoretical results for this mechanism show that it is competitive with the analyzed cationic and anionic mechanisms and that it may lead to higher reaction rates with alkynes bearing EWGs, which agrees with experiments. Overall, these results suggest that in the copper-free Sonogashira reaction, like in other cross-coupling reactions (i.e., Stille, Negishi), there are several reaction pathways that may have competitive rates, and a change on the reaction conditions (i.e., solvent, ligands, substrates, base, etc.) might favor one over the other reaction mechanisms. Thus, a detailed study of a specific reaction is required to assess which mechanism is favored on a particular system. The present study on a general model of Pd-catalyzed copper-free Sonogashira reaction has mapped out the reaction scenario, and shows the complexity of this process.

4. COMPUTATIONAL DETAILS

All calculations were performed at DFT level by means of the hybrid Becke3LYP[57,58] functional as implemented in Gaussian03 program package.[59] Pd and I atoms were described using the Stuttgart-Dresden (SDD) effective core potential[60] for the inner electrons and its associated double-ζ basis set for the outer ones. Additionally, for these atoms f-polarization (exponent 1.472)[61] and d-polarization (exponent 0.289)[62] shells were added, respectively. In the case of I atoms diffuse functions were also added (exponent 0.0308).[63] For the C, P, H atoms and the N atoms the 6-31G(d,p) and the 6-31+g(d) basis sets were used, respectively. Such a computational level has been widely employed in theoretical studies on related cross-coupling reactions providing good results.[46,64−69] The structures of the reactants, intermediates, and transition states were fully optimized without any symmetry constraint. During these optimizations, no artifactual interactions involving hydrogens of the PH_3 model phosphine were detected. Harmonic force constants were computed at the optimized geometries to characterize the stationary points as minima or saddle points. The latter were confirmed by having one imaginary frequency in the Hessian matrix and correlating the corresponding reactants and products. The entropic contributions were evaluated at a pressure of 382 atm to model the changes in entropy for a condensed phase.[70,71] Solvent effects (CH_2Cl_2, ε = 8.930) were introduced through single point calculations at optimized gas-phase geometries for all the minima and transition states by means of a continuum method, the PCM approach[72] implemented in Gaussian03. Moreover, the default cavity model was modified by adding individual spheres to the hydrogen atoms directly linked to the alkyne and to the nitrogen atom of the pyrrolidine molecule, using the keyword SPHEREONH. The relative Gibbs energies in dichloromethane shown throughout this present work (ΔG_{DCM}) were obtained by employing the following scheme: $\Delta G_{DCM} = \Delta E_{DCM} + (\Delta G_{gas} - \Delta E_{gas})$.

5. EXPERIMENTAL DETAILS

General Procedures. All the reagents and dry solvents were obtained from commercial sources. Flash chromatography was performed on silica gel 60 (0.040−0.063 mm). Thin layer chromatography was performed on precoated silica gel plates and the spots were visualized under UV light (λ = 254 nm). Mp were determined on a hot stage apparatus. Gas chromatographic analyses were performed on an instrument equipped with a fused silica capillary column. IR data (only the structurally most important peaks are listed) were collected on a FT spectrophotometer in cm^{-1}. ^1H NMR spectra were recorded at 300 MHz. Chemical shifts are reported in ppm using tetramethylsilane (TMS, 0.00 ppm) as internal standard. ^{13}C NMR spectra were recorded at 75 MHz. ^{19}F NMR spectra

dx.doi.org/10.1021/cs200526x | ACS Catal. 2012, 2, 135−144

were recorded at 282.1 MHz with $CFCl_3$ as the internal reference. Low-resolution electron impact (EI) mass spectra were obtained on a GC-MS spectrometer at 70 eV. High resolution mass spectra were performed at the MS service of the University of Alicante. Solid products were recrystallized in hexane/Et_2O unless otherwise stated, and melting points were not corrected. All reactions were carried out under an argon atmosphere in dried glassware. The products 1-fluoro-4-(phenylethynyl)benzene (**3a**), 1-fluoro-4-{[4-(trifluoromethyl)-phenyl]ethynyl}benzene (**3b**), and 1-fluoro-4-[(4-methoxyphenyl)ethynyl]benzene (**3c**) have been previously reported.

Preparation of Alkynes 3. To a stirred solution of $PdCl_2(PPh_3)_2$ (7.0 mg, 0.01 mmol, 2 mol % Pd) in dry CH_2Cl_2 (1 mL, 0.5 M) was added 1-fluoro-4-iodobenzene (58 μL, 0.5 mmol), alkyne (0.55 mmol), and pyrrolidine (84 μL, 1 mmol) at room temperature under an argon atmosphere. Stirring was continued at room temperature for 10−30 h. The reaction mixture was then quenched with H_2O (4 mL). The mixture was extracted with EtOAc (3 × 6 mL). The organic layer was dried over $MgSO_4$, followed by removal of the solvent at reduced pressure. The resulting crude was purified by silica gel column chromatography.

1-Fluoro-4-(phenylethynyl)benzene (3a).[73]

Pale yellow solid; mp 109−111 °C (Lit. 108−109 °C); ^{1}H NMR ($CDCl_3$) δ 7.00−7.06 (m, 2H), 7.30−7.37 (m, 3H), 7.47−7.54 (m, 4H); ^{13}C NMR ($CDCl_3$) δ 82.3, 89.0, 115.6 (d, J = 21.9 Hz), 119.3 (d, J = 3.4 Hz), 123.1, 128.30, 128.34, 131.5, 133.4 (d, J = 8.3 Hz), 162.5 (d, J = 247.9 Hz); ^{19}F NMR (282.1 MHz, $CDCl_3$) δ −111.5; IR (ν, cm^{-1}) 1594, 1509 (Ar); MS (GC-MS, EI): m/z 196 (M, 100%), 194 (M-2, 13%).

1-Fluoro-4-{[4-(trifluoromethyl)phenyl]ethynyl]}-benzene (3b).[74]

Colorless solid; mp 75−77 °C; ^{1}H NMR (300 MHz, $CDCl_3$) δ 7.01−7.09 (m, 2H), 7.48−7.55 (m, 2H), 7.59 (bs, 4H); ^{13}C NMR (75 MHz, $CDCl_3$) δ 87.7, 90.6, 115.8 (d, J = 22.1 Hz), 118.7 (d, J = 3.4 Hz), 123.9 (q, J = 270.3 Hz), 125.3 (q, J = 3.6 Hz), 126.9, 130.0 (q, J = 32.5 Hz), 131.7, 133.7 (d, J = 8.4 Hz), 162.8 (d, J = 248.9 Hz); ^{19}F NMR (282.1 MHz, $CDCl_3$) δ −110.4, −63.3; IR (ν, cm^{-1}) 2223 (C≡C), 1597, 1501 (Ar); MS (GC-MS, EI): m/z 264 (M, 100%), 263 (M-1, 16%), 245 (M-19, 11%).

1-Fluoro-4-[(4-methoxyphenyl)ethynyl]benzene (3c).[75]

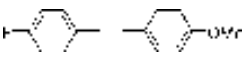

Pale yellow solid {it is a mixture 9:1 of desired product and diyne [1,4-bis(4-methoxyphenyl)buta-1,3-diyne]}; mp 90−92 °C (mixture); ^{1}H NMR (300 MHz, $CDCl_3$) δ 3.80 (s, 3H), 6.82−6.89 (m, 2H), 6.98−7.05 (m, 2H), 7.43−7.50 (m, 4H); ^{13}C NMR (75 MHz, $CDCl_3$) δ 55.2, 86.9, 89.0, 114.0, 115.1, 115.5 (d, J = 21.9 Hz), 119.6 (d, J = 3.5 Hz), 133.0, 133.2 (d, J = 8.2 Hz), 159.6, 162.2 (d, J = 247.4 Hz); ^{19}F NMR (282.1 MHz, $CDCl_3$) δ −112.1; IR (ν, cm^{-1}) 2838, 2217 (C≡C), 1903, 1596, 1509 (Ar); MS (GC-MS, EI): m/z 226 (M, 100%), 211 (M-15, 49%), 183 (36).

4-[(4-Fluorophenyl)ethynyl]-*N*,*N*-dimethylaniline (3d).

Pale brown solid; mp 135−137 °C; ^{1}H NMR (300 MHz, $CDCl_3$) δ 2.96 (bs, 6H), 6.58−6.69 (m, 2H), 6.96−7.04 (m, 2H), 7.35−7.50 (m, 4H); ^{13}C NMR (75 MHz, $CDCl_3$) δ 40.1, 86.2, 90.2, 109.7, 111.8, 115.4 (d, J = 21.8 Hz), 120.2 (d, J = 3.4 Hz), 132.6, 133.0 (d, J = 8.1 Hz), 150.1, 162.0 (d, J = 246.7 Hz); ^{19}F NMR (282.1 MHz, $CDCl_3$) δ −112.8; IR (ν, cm^{-1}) 2210 (C≡C), 1609, 1500 (Ar); MS (GC-MS, EI): m/z 240 (M+1, 17%), 239 (M, 100%), 238 (M−1, 56%), 223 (17), 194 (10), 119 (13); HRMS (ESI): m/z 239.1131, calcd. for $C_{16}H_{14}FN$: 239.1110.

Kinetics of the Copper-Free Sonogashira Reaction. ^{19}F NMR Decoupled Studies. To a solution of $PdCl_2(PPh_3)_2$ (7.0 mg, 0.01 mmol, 2 mol % Pd) in $CDCl_3$ (3 mL) was added a solution of 1-fluoro-4-iodobenzene (58 μL, 0.5 mmol), alkyne (0.5 mmol), and pyrrolidine (251 μL, 3 mmol) in $CDCl_3$ (2 mL) at room temperature under an argon atmosphere. The reaction mixture was stirred mechanically for 30 s. After 10 min, an aliquot of 0.7 mL was removed, and the reaction process was monitored by ^{19}F NMR decoupled studies.

■ ASSOCIATED CONTENT

Supporting Information

Cartesian coordinates and absolute energies for all computed structures and spectra and kinetic data of the synthesized alkynes **3**. This material is available free of charge via the Internet at http://pubs.acs.org.

■ AUTHOR INFORMATION

Corresponding Author

*E-mail: cnajera@ua.es (C.N.), agusti@klingon.uab.es (A.L.), gregori@klingon.uab.es (G.U.).

Funding

We thank the Ministerio de Ciencia e Innovación (MICINN) (Projects FEDER-CTQ2007-62771/BQU, CTQ2008-06866-C02-01, CTQ2010-20387, CTQ2011-23336 and ORFEO Consolider Ingenio 2010 CSD2007-00006), the Generalitat Valenciana (PROMETEO/2009/038), the Generalitat de Catalunya (2009/SGR/68), and the University of Alicante for financial support, and the Universitat Autònoma de Barcelona for the scholarship to M.G.-M. (UAB PIF). M.P. thanks the MICINN for financial support under the JdC program. We are also grateful to CESCA for generous allocation of computer time.

■ REFERENCES

(1) For reviews, see: Sonogashira, K. *J. Organomet. Chem.* **2002**, *653*, 46 , and refs 2−6.
(2) Negishi, E.-I.; Anastasia, L. *Chem. Rev.* **2003**, *103*, 1979.
(3) Tykwinski, R. R. *Angew. Chem., Int. Ed.* **2003**, *42*, 1566.
(4) Chinchilla, R.; Nájera, C. *Chem. Rev.* **2007**, *107*, 874.
(5) Chinchilla, R.; Nájera, C. *Chem. Soc. Rev.* **2011**, *40*, 5084.
(6) Bunz, U. H. F. *Chem. Rev.* **2000**, *100*, 1605.
(7) Nicolaou, K. C.; Bulger, P. G.; Sarlah, D. *Angew. Chem., Int. Ed.* **2005**, *44*, 4442.
(8) Müller, T. J. J.; D'Souza, D. M. *Pure Appl. Chem.* **2008**, *80*, 609.

(9) Shiedel, M.-S.; Briehn, C. A.; Bäuerle, P. *J. Organomet. Chem.* **2002**, *653*, 200.
(10) Hortholary, C.; Coudret, C. *J. Org. Chem.* **2003**, *68*, 2167.
(11) Zapf, A.; Beller, M. *Top. Catal.* **2002**, *19*, 101.
(12) Torborg, C.; Beller, M. *Adv. Synth. Catal.* **2009**, *351*, 3027.
(13) Sonogashira, K.; Tohda, Y.; Hagihara, N. *Tetrahedron Lett.* **1975**, *16*, 4467.
(14) Ljungdahl, T.; Pettersson, K.; Albinsson, B.; Mårtensson, J. *J. Org. Chem.* **2006**, *71*, 1677.
(15) Gelman, D.; Buchwald, S. L. *Angew. Chem., Int. Ed.* **2003**, *42*, 5993.
(16) Kotora, M.; Takahashi, T. In *Handbook of Organopalladium Chemistry for Organic Synthesis*; Negishi, E.-I., de Meijere, A., Eds.; Wiley-Interscience: New York, 2002; p 973.
(17) Siemsen, P.; Livingston, R. C.; Diederich, F. *Angew. Chem., Int. Ed.* **2000**, *39*, 2632.
(18) For selected papers on Pd-catalyzed Sonogashira reactions under Cu-free conditions, see: Fukuyama, T.; Shinmen, M.; Nishitani, S.; Sato, M.; Ryu, I. *Org. Lett.* **2002**, *4*, 1691 , and refs 19−26.
(19) Soheili, A.; Albaneze-Walker, J.; Murry, J. A.; Dormer, P. G.; Hughes, D. L. *Org. Lett.* **2003**, *5*, 4191.
(20) Nájera, C.; Gil-Moltó, J.; Karlström, S.; Falvello, L. R. *Org. Lett.* **2003**, *5*, 1451.
(21) Rau, S.; Lamm, K.; Görls, H.; Schöffel, J.; Walther, D. *J. Organomet. Chem.* **2004**, *689*, 3582.
(22) Li, J.-H.; Zhang, X.-D.; Xie, Y.-X. *Eur. J. Org. Chem.* **2005**, 4256.
(23) Gil-Moltó, J.; Nájera, C. *Eur. J. Org. Chem.* **2005**, 4073.
(24) Yi, C.; Hua, R. *Catal. Commun.* **2006**, *7*, 377.
(25) Galdino de Lima, P.; Antunes, O. A. C. *Tetrahedron Lett.* **2008**, *49*, 2506.
(26) Komáromi, A.; Tolnai, G. L.; Novák, Z. *Tetrahedron Lett.* **2008**, *49*, 7294.
(27) For selected papers on Sonogashira reactions under both Cu-free and amine-free conditions, see: Alonso, D. A.; Nájera, C.; Pacheco, M. C. *Tetrahedron Lett.* **2002**, *43*, 9365 , and refs 28−32.
(28) Cheng, J.; Sun, Y.; Wang, F.; Guo, M.; Xu, J.-H.; Pan, Y.; Zhang, Z. *J. Org. Chem.* **2004**, *69*, 5428.
(29) Ruiz, J.; Cutillas, N.; López, F.; López, G.; Bautista, D. *Organometallics* **2006**, *25*, 5768.
(30) Komáromi, A.; Novák, Z. *Chem. Commun.* **2008**, 4968.
(31) John, A.; Shaikh, M. M.; Gosh, P. *Dalton Trans.* **2009**, 10581.
(32) Torborg, C.; Huang, J.; Schulz, T.; Schäffner, B.; Zapf, A.; Spannenberg, A.; Börner, A.; Beller, M. *Chem.—Eur. J.* **2009**, *15*, 1329.
(33) For selected papers on Sonogashira reactions under both Cu-free and ligand-free conditions, see: Liang, B.; Dai, M.; Chen, J.; Yang, Z. *J. Org. Chem.* **2005**, *70*, 391 , and reference 34.
(34) Li, J.-H.; Liang, Y.; Xie, Y.-X. *J. Org. Chem.* **2005**, *70*, 4393.
(35) For a paper on a Sonogashira reaction under both Cu-free and solvent-free conditions, see: Carpita, A.; Ribecai, A. *Tetrahedron Lett.* **2009**, *50*, 204.
(36) For a paper on a Sonogashira reaction under Cu-free, amine-free and ligand-free conditions, see: Urgaonkar, S.; Verkade, J. G. *J. Org. Chem.* **2004**, *69*, 5752.
(37) For a paper on a Sonogashira reaction under Cu-free, amine-free and solvent-free conditions, see: Liang, Y.; Xie, Y.-X.; Li, J.-H. *J. Org. Chem.* **2006**, *71*, 379.
(38) Heck, F.; Dieck, H. A. *J. Organomet. Chem.* **1975**, *93*, 259.
(39) Amatore, C.; Bensalem, S.; Ghalem, S.; Jutand, A.; Medjour, Y. *Eur. J. Org. Chem.* **2004**, 366.
(40) Tougerti, A.; Negri, S.; Jutand, A. *Chem.—Eur. J.* **2007**, *13*, 666.
(41) Ljungdahl, T.; Bennur, T.; Dallas, A.; Emtenäs, H.; Mårtensson, J. *Organometallics* **2008**, *27*, 2490.
(42) Chen, L.-P.; Hong, S.-G.; Huo, H.-Q. *Chin. J. Struct. Chem.* **2008**, *27*, 1404.
(43) Sikk, L.; Tammiku-Taul, J.; Burk, P. *Organometallics* **2011**, *30*, 5656.
(44) Besora, M.; Braga, A. A. C.; Ujaque, G.; Maseras, F.; Lledós, A. *Theor. Chem. Acc.* **2011**, *128*, 639.
(45) Braga, A. A. C.; Ujaque, G.; Maseras, F. *Organometallics* **2006**, *25*, 3647.
(46) Casado, A. L.; Espinet, P. *Organometallics* **1998**, *17*, 954.
(47) García-Melchor, M.; Fuentes, B.; Lledós, A.; Casares, J. A.; Ujaque, G.; Espinet, P. *J. Am. Chem. Soc.* **2011**, *133*, 13519.
(48) Beaupérin, M.; Fayad, E.; Amardeil, R.; Cattey, H.; Richard, P.; Brandès, S.; Meunier, P.; Hierso., J.-C. *Organometallics* **2008**, *27*, 1506.
(49) Beaupérin, M.; Job, A.; Cattey, H.; Royer, S.; Meunier, P.; Hierso., J.-C. *Organometallics* **2010**, *29*, 2815.
(50) This was also confirmed by optimizing the full system in dichloromethane starting with the phenylacetylide at 4 Å far from the cationic complex **I-1**.
(51) Theoretical calculation of the TOF using the scheme developed by Kozuch et al. by means of the AUTOF program shows that the ratio between the anionic and the ionic mechanisms is 2:1 for R = H. This result indicates that both mechanisms are competitive. See refs 52−54.
(52) Kozuch, S.; Shaik, S. *J. Am. Chem. Soc.* **2006**, *128*, 3355.
(53) Kozuch, S.; Shaik, S. *J. Phys. Chem. A* **2008**, *112*, 6032.
(54) Uhe, A.; Kozuch, S.; Shaik, S. *J. Comput. Chem.* **2011**, *32*, 978.
(55) The 2:1 ratio between the base and the alkyne in this ionic mechanism is compatible with the reaction conditions used in experimental kinetic studies, where 6 equiv of base are employed (see Experimental Details section).
(56) For the conversion/time data of the reactions with the different 4-substituted phenylacetylenes, see Supporting Information.
(57) Becke, A. D. *J. Chem. Phys.* **1993**, *98*, 5648.
(58) Lee, C.; Yang, W.; Parr, R. G. *Phys. Rev.* **1988**, *B37*, 785.
(59) Frisch, M. J.; Trucks, G. W.; Schlegel, H. B.; Scuseria, G. E.; Robb, M. A.; Cheese-man, J. R.; Montgomery, J. A., Jr.; Vreven, T.; Kudin, K. N.; Burant, J. C.; Millam, J. M.; Iyengar, S. S.; Tomasi, J.; Barone, V.; Mennucci, B.; Cossi, M.; Scalmani, G.; Rega, N.; Petersson, G. A.; Nakatsuji, H.; Hada, M.; Ehara, M.; Toyota, K.; Fukuda, R.; Hasegawa, J.; Ishida, M.; Nakajima, T.; Honda, Y.; Kitao, O.; Nakai, H.; Klene, M.; Li, X.; Knox, J. E.; Hratchian, H. P.; Cross, J. B.; Bakken, V.; Adamo, C.; Jaramillo, J.; Gomperts, R.; Stratmann, R. E.; Yazyev, O.; Austin, A. J.; Cammi, R.; Pomelli, C.; Ochterski, J. W.; Ayala, P. Y.; Morokuma, K.; Voth, G. A.; Salvador, P.; Dannenberg, J. J.; Zakrzewski, V. G.; Dapprich, S.; Daniels, A. D.; Strain, M. C.; Farkas, O.; Malick, D. K.; Rabuck, A. D.; Raghavachari, K.; Foresman, J. B.; Ortiz, J. V.; Cui, Q.; Baboul, A. G.; Clifford, S.; Cioslowski, J.; Stefanov, B. B.; Liu, G.; Liashenko, A.; Piskorz, P.; Komaromi, I.; Martin, R. L.; Fox, D. J.; Keith, T.; Al-Laham, M. A.; Peng, C. Y.; Nanayakkara, A.; Challacombe, M.; Gill, P. M. W.; Johnson, B.; Chen, W.; Wong, M. W.; Gonzalez, C.; Pople, J. A. *Gaussian 03*, Revision E.01; Gaussian, Inc.: Wallingford, CT, 2004.
(60) Andrae, D.; Häussermann, U.; Dolg, M.; Stoll, H.; Preuss, H. *Theor. Chim. Acta.* **1990**, *77*, 123.
(61) Ehlers, A. W.; Böhme, M.; Dapprich, S.; Gobbi, A.; Höllwarth, A.; Jonas, V.; Köhler, K. F.; Stegmann, R.; Veldkamp, A.; Frenking, G. *Chem. Phys. Lett.* **1993**, *208*, 111.
(62) Höllwarth, A.; Böhme, M.; Dapprich, S.; Ehlers, A. W.; Gobbi, A.; Jonas, V.; Köhler, K. F.; Stegmann, R.; Veldkamp, A.; Frenking, G. *Chem. Phys. Lett.* **1993**, *208*, 237.
(63) Check, C. E.; Faust, T. O.; Bailey, J. M.; Wright, B. J.; Gilbert, T. M.; Sunderlin, L. S. *J. Phys. Chem. A* **2001**, *105*, 8111.
(64) Nova, A.; Ujaque, G.; Maseras, F.; Lledós, A.; Espinet, P. *J. Am. Chem. Soc.* **2006**, *128*, 14571.
(65) Álvarez, R.; Pérez, M.; Faza, O. N.; de Lera, A. R. *Organometallics* **2008**, *27*, 3378.
(66) Ariafard, A.; Yates, B. F. *J. Am. Chem. Soc.* **2009**, *131*, 13981.
(67) Pérez-Rodríguez, M.; Braga, A. A. C.; García-Melchor, M.; Pérez-Temprano, M. H.; Casares, J. A.; Ujaque, G.; de Lera, A. R.; Álvarez, R.; Maseras, F.; Espinet, P. *J. Am. Chem. Soc.* **2009**, *131*, 3650.
(68) Pérez-Rodríguez, M.; Braga, A. A. C.; de Lera, A. R.; Maseras, F.; Álvarez, R.; Espinet, P. *Organometallics* **2010**, *29*, 4983.
(69) Thaler, T.; Haag, B.; Gavryushin, A.; Schober, K.; Hartmann, E.; Gschwind, R. M.; Zipse, H.; Mayer, P.; Knochel, P. *Nat. Chem.* **2010**, *2*, 125.

(70) Following the argument in: Martin, R. L.; Hay, P. J.; Pratt, L. R. *J. Phys. Chem. A* **1998**, *102*, 3565 , and its application in reference 71.
(71) Sieffert, N.; Bühl, M. *J. Am. Chem. Soc.* **2010**, *132*, 8056.
(72) Miertus, S.; Scrocco, E.; Tomasi, J. *J. Chem. Phys.* **1981**, *55*, 117.
(73) Mao, J.; Xie, G.; Wu, M.; Guo, J.; Ji, S. *Adv. Synth. Catal.* **2008**, *350*, 2477.
(74) Wan, Z.; Jones, C. D.; Mitchell, D.; Pu, J. Y.; Zang, T. Y. *J. Org. Chem.* **2006**, *71*, 826.
(75) Polshettiwar, V.; Nadagouda, M. N.; Varma, R. S. *Chem. Commun.* **2008**, 6318.

dx.doi.org/10.1021/cs200526x | *ACS Catal.* 2012, 2, 135−144

B

Appendix B: Published articles on related topics that are not included in this Ph.D. Thesis

B.1 Article IV:

C-C Reductive Elimination in Palladium Complexes, and the Role of Coupling Additives. A DFT Study Supported by Experiment

Pérez-Rodríguez, M.; Braga, A. A. C.; **García-Melchor, M.**; Pérez-Temprano, M. H.; Casares, J. A.; Ujaque, G.; de Lera, A. R.; Álvarez, R.; Maseras, F.; Espinet, P. *J. Am. Chem. Soc.* **2009**, *131*, 3650-3657.

J|A|C|S
ARTICLES

Published on Web 02/20/2009

C−C Reductive Elimination in Palladium Complexes, and the Role of Coupling Additives. A DFT Study Supported by Experiment

Martín Pérez-Rodríguez,[†] Ataualpa A. C. Braga,[||] Max Garcia-Melchor,[‡] Mónica H. Pérez-Temprano,[§] Juan A. Casares,[§] Gregori Ujaque,[‡] Angel R. de Lera,[†] Rosana Álvarez,*[,†] Feliu Maseras,*[,‡,||] and Pablo Espinet*[,§]

Departamento de Química Orgánica, Facultad de Química, Universidade de Vigo, Lagoas-Marcosende s/n, 36310 Vigo, Galicia, Spain, Institute of Chemical Research of Catalonia (ICIQ), Av. Països Catalans, 16, 43007 Tarragona, Catalonia, Spain, Unitat de Química Física, Edifici Cn, Universitat Autònoma de Barcelona, 08193 Bellaterra, Catalonia, Spain, and IUCINQUIMA/Química Inorgánica, Facultad de Ciencias, Universidad de Valladolid, 47071 Valladolid, Castilla y León, Spain

Received October 11, 2008; E-mail: rar@uvigo.es; fmaseras@iciq.es; espinet@qi.uva.es

Abstract: A DFT study of R−R reductive elimination (R = Me, Ph, vinyl) in plausible intermediates of Pd-catalyzed processes is reported. These include the square-planar tetracoordinated systems *cis*-[$PdR_2(PMe_3)_2$] themselves, possible intermediates *cis*-[$PdR_2(PMe_3)L$] formed in solution or upon addition of coupling promoters (L = acetonitrile, ethylene, maleic anhydride (ma)), and tricoordinated intermediates *cis*-[$PdR_2(PMe_3)$] (represented as L = empty). The activation energy ranges from 0.6 to 28.6 kcal/mol in the gas phase, increasing in the order vinyl−vinyl < Ph−Ph < Me−Me, depending on R, and ma < "empty" < ethylene < $PMe_3 \approx$ MeCN, depending on L. The effect of added olefins was studied for a series of olefins, providing the following order of activation energy: *p*-benzoquinone < ma < *trans*-1,2-dicyanoethylene < 3,5-dimethylcyclopent-1-ene < 2,5-dihydrofuran < ethylene < *trans*-2-butene. Comparison of the calculated energies with experimental data for the coupling of *cis*-[$PdMe_2(PPh_3)_2$] in the presence of additives (PPh_3, *p*-benzoquinone, ma, *trans*-1,2-dicyanoethylene, 2,5-dihydrofuran, and 1-hexene) reveals that: (1) There is no universal coupling mechanism. (2) The coupling mechanism calculated for *cis*-[$PdMe_2(PMe_3)_2$] is direct, but PPh_3 retards the coupling for *cis*-[$PdMe_2(PPh_3)_2$], and DFT calculations support a switch of the coupling mechanism to dissociative for PPh_3. (3) Additives that would provide intermediates with coupling activation energies higher than a dissociative mechanism (e.g., common olefins) produce no effect on coupling. (4) Olefins with electron-withdrawing substituents facilitate the coupling through *cis*-[$PdMe_2(PR_3)$(olefin)] intermediates with much lower activation energies than the starting complex or a tricoordinated intermediate. Practical consequences are discussed.

Introduction

The field of transition metal-catalyzed C−C and C−Het coupling processes[1−3] has witnessed an explosion of empirical research aimed at the promotion of otherwise difficult reactions. Notable among those are the C−C coupling of aryl chlorides with a variety of organometallic partners (B, Sn, Mg, or Zn nucleophiles),[4,5] and the formation of C−Het (N, O, S) bonds.[6,7] Hartwig has nicely summarized the experimental results accumulated in the past decade or so and discussed the role of each partner (reactive ligands and ancillary ligands, electronic, and steric effects) on the coupling rate and efficiency.[8] One interesting conclusion is that C−C and C−Het couplings can be discussed under very similar schemes. Novel bulky phosphines[9,10] and carbene ligands[11] have been instrumental to facilitate these processes. The role of solvents and additives has been investigated.[4] Kinetic analysis of the processes, isolation of reaction intermediates, monitoring of the evolution of these species,[4,12,13] and computational studies[14−17] have corroborated or modified mechanistic proposals, or suggested stimulating

[†] Universidade de Vigo.
[||] ICIQ.
[‡] Universitat Autònoma de Barcelona.
[§] Universidad de Valladolid.

(1) Brown, J. M.; Cooley, N. A. *Chem. Rev.* **1988**, *88*, 1031–1046.
(2) Ozawa, F. Reductive Elimination. In *Fundamentals of Molecular Catalysis*; Kurosawa, H., Yamamoto, A., Eds.; Elsevier: New York, 2003; Vol. 3, pp 479−511.
(3) (a) de Meijere, A.; Diederich, F.; *Metal Catalyzed Cross-Coupling Reactions*, 2nd ed.; John Wiley & Sons: New York, 2004. (b) Tamao, K.; Miyaura, N. *Cross-Coupling Reactions; Topics in Current Chemistry*; Springer: Berlin, 2002; Vol. 219. (c) Ziegler, T. *Chem. Rev.* **1991**, *91*, 651–667.
(4) Espinet, P.; Echavarren, A. M. *Angew. Chem., Int. Ed.* **2004**, *43*, 4704–4734.
(5) Littke, A. F.; Fu, G. C. *Angew. Chem., Int. Ed.* **2002**, *41*, 4177–4211.
(6) Hartwig, J. F. *Acc. Chem. Res.* **1998**, *31*, 852–860.
(7) Hartwig, J. F. *Angew. Chem., Int. Ed.* **1998**, *37*, 2046–2067.
(8) Hartwig, J. F. *Inorg. Chem.* **2007**, *46*, 1936–1947.
(9) Littke, A. F.; Fu, G. C. *Angew. Chem., Int. Ed.* **1998**, *37*, 3387–3388.
(10) Barder, T. E.; Walker, S. D.; Martinelli, J. R.; Buchwald, S. L. *J. Am. Chem. Soc.* **2005**, *127*, 4685–4696.
(11) Herrmann, W. A. *Angew. Chem., Int. Ed.* **2002**, *41*, 1290–1309.

10.1021/ja808036j CCC: $40.75

alternative mechanistic views. Nowadays, the excessively schematic mechanisms of metal-catalyzed cross-coupling reactions are being revisited, and more detailed and complex views are replacing the traditional beliefs.

Recent results show that each of the main steps in the catalytic cycle of Pd-catalyzed coupling reactions (oxidative addition, transmetalation, isomerization, and reductive elimination) can be rate determining, depending on the reagents, the ligands, the solvent, and the additives.[4] Often taken for granted, the final C−C or C−Het coupling is critical for the success of the reaction, as the other steps are frequently reversible,[13] and it is the irreversible reductive elimination that must pull the catalytic cycle forward. Since the early theoretical works of Tatsumi, Hoffmann, Yamamoto and Stille,[18] and Low and Goddard,[19] the reductive elimination step had received scant attention, but recently Ananikov, Musaev, and Morokuma carried out extensive studies on the C−C reductive elimination, in the gas phase, of the most common types of coupling partners in square-planar *cis*-[MRR′$(PH_3)_2$] complexes (R or R′ = methyl, vinyl, phenyl, alkynyl; M = Pd, Pt).[20] Moreover, Bo et al. studied the effect of the bite angle of chelating diphosphines on the formation of C−C and C−O bonds.[21] The feasibility of Ar−F elimination from Pd(II) has been theoretically assessed and then experimentally addressed.[22] Finally, during the development of the present study, Ananikov, Musaev, and Morokuma published a theoretical investigation of the reductive elimination from square planar and T-shaped Pd species with phosphines of different bulkiness.[23] Despite these recent contributions, the theoretical description of the reductive elimination step is still rather incomplete. For instance, the role of additives, solvents, or other ligands present in solution is not well understood, and the feasibility under experimental circumstances of the species proposed in-silico has not been experimentally tested. This article reports theoretical results on *cis*-[$PdMe_2(PMe_3)$L] systems that model some C−C coupling conditions, which are then compared to experimental results on *cis*-[$PdMe_2(PPh_3)_2$] + L systems.

Computational Models

The models chosen, *cis*-[PdRR(PMe_3)(L)] (R = Me, vinyl, and Ph) complexes, represent, depending on L, plausible coupling intermediates formed in the presence of solvents, ligands, or coupling additives. The ancillary ligand PMe_3 was chosen as a more realistic phosphine model than PH_3. Nonsymmetrical complexes (PdRR′L_2) were spared because it has been shown that their computed activation energies are roughly the average between those of their symmetrical counterparts;[20] note, however, that experimental evidence shows that coupling rates are faster for PdRR′L_2 than for PdR_2L_2 or PdR'_2L_2.[8] The following L ligands were used: (i) L = PMe_3 gives square-planar tetracoordinated complexes *cis*-[$MR_2(PMe_3)_2$]; (ii) L = MeCN models σ-donor coordinating solvents of moderate donating ability; (iii) L = ethylene represents π-coordinating molecules present in solution in cross-coupling reactions involving vinyl, allyl, and other C=C containing moieties,[24] for example, the starting electrophile or the coupling product; (iv) L = ma (maleic anhydride, an electron-withdrawing olefin) was included due to reports showing that electron-withdrawing olefins are additives that promote the reductive elimination step;[25] and (v) finally, L = "empty position" represents tricoordinated T-shaped *cis*-[$PdR_2(PR_3)$] complexes with only one ancillary phosphine ligand, suggested by kinetic studies to be coupling intermediates in some cases.[10,18,26] Evidence for the formation of monophosphine complexes with one bulky phosphine as the only ancillary ligand includes crystal structures of apparently tricoordinated complexes, in which Pd turns out to be stabilized by weak agostic interactions,[27,28] and also true T-shaped complexes.[28] A theoretical study of the factors making T-shaped palladium complexes more accessible has appeared very recently.[29]

As this work was progressing, the experimental tests in parallel to the initial calculations pushed us to extend the models to gain insight on the effect of olefins. On the other hand, a study dealing with case (v) appeared, which covered some aspects pursued in this chapter of our study.[23] Our data on case (v) are still needed in the context of our discussion, but, for the sake of page economy, only the novel aspects of tricoordinated intermediates will be dealt with in the text, while more information is given in the Supporting Information.

Scheme 1

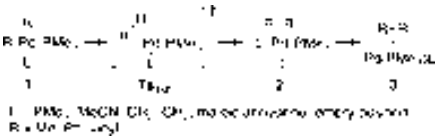

Results and Discussion

Overall Reaction Profile. The reductive elimination process shows four significant stages in the reaction profile (Scheme 1):[19−21,23] (i) the cis reactant species, **1**; (ii) the transition state $\mathbf{TS_{1-2}}$; (iii) an intermediate adduct, **2**, with the R−R coupling product weakly bound to the metal center; and (iv) the coupling product already separated from the Pd(0) complex (stage **3**). Each stage was computed for all R and L combinations (R =

(12) Casares, J. A.; Espinet, P.; Fuentes, B.; Salas, G. *J. Am. Chem. Soc.* **2007**, *129*, 3508–3509.
(13) Pérez-Temprano, M. H.; Nova, A.; Casares, J. A.; Espinet, P. *J. Am. Chem. Soc.* **2008**, *130*, 10518–10520.
(14) Niu, S.; Hall, M. B. *Chem. Rev.* **2000**, *100*, 353–405.
(15) Goossen, L. J.; Koley, D.; Hermann, H. L.; Thiel, W. *J. Am. Chem. Soc.* **2005**, *127*, 11102–11114.
(16) (a) Braga, A. A. C.; Morgon, N. H.; Ujaque, G.; Maseras, F. *J. Am. Chem. Soc.* **2005**, *127*, 9298–9307. (b) Nova, A.; Ujaque, G.; Maseras, F.; Lledos, A.; Espinet, P. *J. Am. Chem. Soc.* **2006**, *128*, 14571–14578. (c) Braga, A. A. C.; Ujaque, G.; Maseras, F. *Organometallics* **2006**, *25*, 3647–3658.
(17) (a) Alvarez, R.; Faza, O. N.; López, C. S.; de Lera, A. R. *Org. Lett.* **2006**, *8*, 35–38. (b) Álvarez, R.; Faza, O. N.; de Lera, A. R.; Cárdenas, D. J. *Adv. Synth. Catal.* **2007**, *349*, 887. (c) Alvarez, R.; Pérez, M.; Faza, O. N.; de Lera, A. R. *Organometallics* **2008**, *27*, 3378–3389.
(18) Tatsumi, K.; Hoffmann, R.; Yamamoto, A.; Stille, J. K. *Bull. Chem. Soc. Jpn.* **1981**, *54*, 1857–1867.
(19) (a) Low, J. J.; Goddard, W. A. *Organometallics* **1986**, *5*, 609–622. (b) Low, J. J.; Goddard, W. A. *J. Am. Chem. Soc.* **1986**, *108*, 6115–6128.
(20) Ananikov, V. P.; Musaev, D. G.; Morokuma, K. *Organometallics* **2005**, *24*, 715–723.
(21) Zuidema, E.; Van Leeuwen, P. W. N. M.; Bo, C. *Organometallics* **2005**, *24*, 3703–3710.
(22) Yandulov, D. V.; Tran, N. T. *J. Am. Chem. Soc.* **2007**, *129*, 1342–1358.
(23) Ananikov, V. P.; Musaev, D. G.; Morokuma, K. *Eur. J. Inorg. Chem.* **2007**, 5390–5399.
(24) Albéniz, A. C.; Espinet, P.; Martín-Ruiz, B. *Chem.-Eur. J.* **2001**, *7*, 2481–2489.
(25) (a) Goliaszewski, A.; Schwartz, J. *J. Am. Chem. Soc.* **1984**, *106*, 5028–5030. (b) Goliaszewski, A.; Schwartz, J. *Tetrahedron Lett.* **1985**, *26*, 5779–5789. (c) Kluwer, A. M.; Elsevier, C. J.; Bühl, M.; Lutz, M.; Spek, A. L. *Angew. Chem., Int. Ed.* **2003**, *42*, 3501–3504. (d) Sustmann, R.; Lau, J. *Chem. Ber.* **1986**, *119*, 2531–2541.
(26) Louie, J.; Hartwig, J. F. *J. Am. Chem. Soc.* **1995**, *117*, 11598–11599.
(27) (a) Stambuli, J. P.; Buhl, M.; Hartwig, J. F. *J. Am. Chem. Soc.* **2002**, *124*, 9346–9347. (b) Stambuli, J. P.; Incarvito, C. D.; Buhl, M.; Hartwig, J. F. *J. Am. Chem. Soc.* **2004**, *126*, 1184–1194.
(28) Yamashita, M.; Hartwig, J. F. *J. Am. Chem. Soc.* **2004**, *126*, 5344–5345.
(29) Moncho, S.; Ujaque, G.; Lledós, A.; Espinet, P. *Chem.-Eur. J.* **2008**, *14*, 8986–8994.

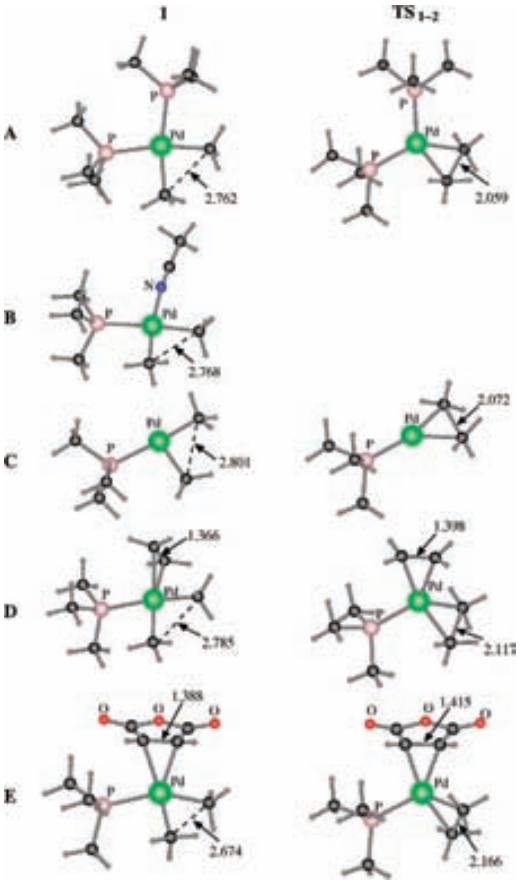

Figure 1. Optimized geometry of the reactant **1** and the transition state $\mathbf{TS_{1-2}}$ for the reductive elimination of ethane. (A) L = PMe_3; (B) L = MeCN; (C) L = empty; (D) L = CH_2CH_2; (E) L = ma. Relevant selected distances (Å) are shown.

Me, Ph, vinyl; L = empty position, ethylene, PMe_3, ma, MeCN). Details of the 60 computed geometries, tables of selected geometrical parameters, and a discussion of the geometrical changes along the reductive elimination are given as Supporting Information.

The structures of the reactants and the transition states are shown in Figure 1 for R = Me (for the other R groups the coordination geometries are similar). Fairly symmetrical concomitant shortening of the C−C distance and elongation of the Pd−C distances is observed as the reactants evolve to their transition states. For L = empty, the coupling is direct. For L ≠ empty, the calculation predicts also direct coupling, now in the tricoordinated complex. As an exception (not found in any of the published studies), for R = Me and L = MeCN a stepwise mechanism is predicted, initiated by MeCN dissociation and followed by coupling in the resulting tricoordinated complex. It makes sense that the case of a dissociative coupling is found in the calculation for the combination of the strongest R σ-donor (Me) with MeCN, which is a weak donor, non π-acceptor ligand.

Influence of the R Group on the Energy Barrier. Table 1 gathers $\Delta G^{\ddagger}$ data calculated for the 15 reductive eliminations

Table 1. Thermodynamic Data ($\Delta G^{\ddagger}$ in kcal/mol, Relative to Reactant **1**) for the Reductive Elimination of R−R Starting from the *cis*-[$PdR_2(PMe_3)(L)$] Complexes

R	L	$\mathbf{TS_{1-2}}$[a]	**2**[a]	**3**[a]
Me	ma	8.6	−43.0	−49.3
	empty	13.2	−19.9	−25.6
	CH_2CH_2	21.7	−34.8	−43.7
	MeCN	27.0[b]	−32.9	−37.8
	PMe_3	28.6	−35.0	−43.1
Ph	ma	2.9	−46.4	−50.7
	empty	4.9	−33.3	−27.2
	CH_2CH_2	11.3	−30.9	−43.7
	MeCN	13.2	−31.2	−36.1
	PMe_3	12.8	−33.9	−41.9
vinyl	ma	0.6	−56.2	−51.9
	empty	4.9	−39.9	−24.9
	CH_2CH_2	8.9	−43.0	−43.3
	MeCN	11.9	−32.6	−35.6
	PMe_3	11.5	−36.1	−40.1

[a] In gas phase. Values in acetonitrile including solvation energies using a continuum model are given in the Supporting Information. [b] This value corresponds to the overall energy barrier for the stepwise mechanism (see text).

from *cis*-[$PdR_2(PMe_3)L$]. The trend of computed barriers is $Csp^3-Csp^3 > C_{Ar}-C_{Ar} > Csp^2-Csp^2$ for any series with an identical L ligand (occasional exceptions within the error of calculation are found for very similar values of $C_{Ar}-C_{Ar}$ and Csp^2-Csp^2 data). This and the trends in bond angles and lengths (Supporting Information) are in coincidence with the sequences reported for *cis*-[$PdR_2(PH_3)_2$] complexes.[20]

In general, the structures where Me−Me elimination occurs deviate from planarity, and the corresponding transition states $\mathbf{TS_{1-2}}$ show distorted tetrahedral structures around the metal. In contrast, the complexes with Ph or vinyl groups feature almost planar $\mathbf{TS_{1-2}}$ structures. The higher directionality of the M−C(sp^3) bond, its weaker M−C bond dissociation energy, and a larger influence of steric effects have been deemed responsible for these structural differences.[20] Whereas the activation energies reported for PH_3 complexes are about 4 times lower for the Csp^2-Csp^2 relative to the Csp^3-Csp^3 bond formation,[20] the differences calculated for the bulkier PMe_3 ligand are significantly smaller (2.5-fold at most). This could be due to a destabilization of the reactants **1** for R = Me, arising from the higher crowding with PMe_3 as compared to PH_3, which could attenuate the differences in energy for higher absolute values. All of the coupling processes are strongly exothermic, which makes the C−C coupling irreversible. Values differing by as much as 25 kcal/mol are computed for eliminations starting from tricoordinated Pd versus tetracoordinated Pd complexes. For the latter, the more exothermic reductive eliminations for each R are those with ma as auxiliary ligand, followed by those with ethylene, phosphine, and acetonitrile. The significance of these thermodynamic results should not be overemphasized, however, as its connection to the experimental conditions is not straightforward. Considering, for instance, a catalytic process in the presence of excess PMe_3 as auxiliary ligand and with ma as coupling promoter, the most likely Pd(II) species in solution preceding the coupling will be [$PdR_2(PMe_3)_2$], in equilibrium with minute amounts of a [$PdR_2(PMe_3)$(ma)] intermediate, due to the fact that PMe_3 is a much better ligand toward Pd(II) than is ma. On the other hand, coordination of the strongly acceptor ma is much better in the

Scheme 2

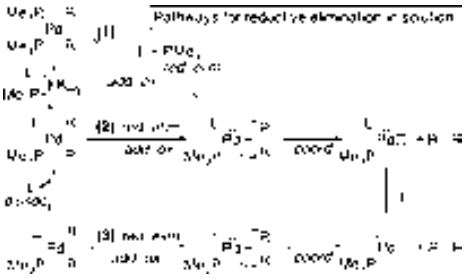

reduced Pd(0) complex $[Pd(PMe_3)_2(ma)]$.[30] Consequently, the thermodynamic balance for the experimental reductive elimination might well correspond to a process going from $PdR_2(PMe_3)_2$ + ma to $Pd(PMe_3)_2(ma)$ + R−R, rather than any of the direct coupling models studied here.

The activation barriers calculated are much higher for R = Me than for R = Ph or vinyl, both in vacuum and in continuum MeCN solution. The values for the coupling of Csp^3 centers are so high in some cases (e.g., ca. 28.6 kcal/mol when L = PMe_3) that this step becomes a likely candidate to be rate determining in a cycle. In other words, failures in coupling alkyl organometallics with alkyl halides or pseudohalides should not be attributed cursorily to the oxidative addition or the transmetalation step. For R = Ph and vinyl, the activation barriers are smaller and likely less critical for synthetic purposes. It is worth mentioning that a continuum solvent correction (see Supporting Information) increases more the calculated barriers for R = vinyl, making vinyl and phenyl barriers similar.

Very interestingly, Table 1 reveals that the influence of R is not necessarily prevailing over other factors, and can be overcome if different L ligands are used to couple different R groups (i.e., *cis*-$[PdR_2(PMe_3)L]$ versus *cis*-$[PdR'_2(PMe_3)L']$). In other words, the nature of L is extremely important.

Influence of the L Group on the Coupling Barrier. This factor has not been theoretically considered in the literature. In an experimental reaction using phosphines as the initial ligands, the model complexes studied here could be interconnected by ligand-substitution or ligand-dissociation equilibria (Scheme 2).[31] The reductive elimination would take place from tetracoordinated (pathways 1 and 2) or tricoordinated (pathway 3) complexes and should be the microscopic reverse of the oxidative addition of a nonpolar C−C bond. The latter is believed to follow a concerted mechanism,[2] where the oxidative addition is the result of a side-on coordination of the single bond to the metal; σ-donation from the R−R σ bonding orbital plus back-donation from the metal to the R−R σ^* antibonding orbital will eventually break the R−R bond. In fact, the geometries observed for the transition states $\mathbf{TS_{1-2}}$, which are very symmetric for R = phenyl and vinyl, and less so but still fairly symmetric for R = Me, support this mechanism.

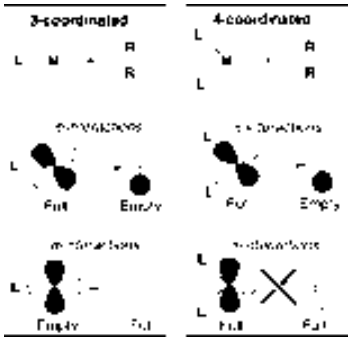

Figure 2. Key orbital interactions in the transition state for reductive elimination from tricoordinated complexes (left) and tetracoordinated complexes (right).

The $\mathbf{Ts_{1-2}}$ values in Table 1 indicate that, for each R group considered, the activation energy for different L ligands decreases in the order MeCN ≈ PMe_3 > CH_2CH_2 > "empty" > ma. The range of energy values is large, and larger for the complexes with R = Me reflecting the higher absolute values involved in the reductive elimination of this group. Synthetic interest is usually to favor the coupling, and we will discuss in the following sections the reasons why the cases of L = empty and L = ma are particularly favorable.

The geometry of the C−Pd−C triangle is relatively similar for all of the computed tetracoordinated transition states, but the reductive elimination from tricoordinated complexes (the case L = empty) is different from the others, as this is the only case where the bond is formed in a position trans to the phosphine ligand (Figure 1). The qualitative difference in reductive elimination from tetracoordinated or from tricoordinated complexes has been previously noted and analyzed using simple extended Hückel descriptions,[18,32] and by DFT calculations in a recent study.[23] Those computational studies and ours show that the reductive elimination is easier for the tricoordinated systems. This lower reductive elimination barrier in tricoordinated systems (L = "empty") can be explained considering the orbital interactions shown in Figure 2. The key factor is the different occupation of the σ_M orbital for 3-coordinated and 4-coordinated d^8 complexes in the corresponding symmetry.[33] Whereas for both types of complex the interactions roughly corresponding to π-symmetry are bonding, those roughly corresponding to σ-symmetry are repulsive for the two interacting full orbitals in the 4-coordinated system, but bonding for the empty−full interaction in the 3-coordinated system. This orbital diagram also explains the fact that the forming C−C bond is placed trans to the phosphine in the tricoordinated system. It follows as well from this diagram that any external

(30) Espinet, P.; Albéniz, A. C. In *Comprehensive Organometallic Chemistry*; Mingos, D. M. P., Crabtree, R. H., Canty, A., Eds.; Elsevier: Oxford, 2007; Vol. 8, pp 317−332.

(31) In principle, these equilibria could be analyzed theoretically from the computed ligand dissociation energies, collected in Table SI4 of the Supporting Information, but estimation of these specific equilibrium constants with the computational methods applied is troublesome. In fact, the two magnitudes reported, potential energy and free energy, present sharply different values, with differences around 16 kcal/mol. This discrepancy proves the importance of entropic corrections in these bimolecular processes. Unfortunately, in our computational approach, these particular terms are estimated through assumption of ideal gas behavior of the molecules, which is obviously not the optimal choice for systems in solution. Moreover, experimental reactions can be carried out in solvents of very different polarity. Thus, rather than focusing on the intrinsically inaccurate estimation of these equilibrium constants, we decided to analyze the trends in the computed activation barriers associated with the different ligands, where entropic contributions are less critical.

(32) Tatsumi, K.; Nakamura, A.; Komiya, S.; Yamamoto, A.; Yamamoto, T. *J. Am. Chem. Soc.* **1984**, *16*, 8181–8188.

(33) Jean, Y. *Molecular Orbitals of Transition Metal Complexes*; Oxford University Press: London, 2005.

factor withdrawing density from the σ_M orbital in a 4-coordinated molecule will lower the barrier for reductive elimination in tetracoordinated compounds.

The low barrier associated with the tricoordinated system has important mechanistic implications. If there is a weak ligand, or if the crowding in the tetracoordinated complex is high, tricoordination will be more easily accessible,[29] and it may be energetically more efficient for the system to release one ligand and undergo reductive elimination from the tricoordinated species (pathway 3 in Scheme 2). In fact, this is what we find in our calculations for *cis*-[$PdMe_2(PMe_3)$(NCMe)], and in our experiments for *cis*-[$PdMe_2(PPh_3)_2$] (see later). Dissociative coupling might be fairly general for reasonably hindered compounds.

For the cases found to couple directly in *cis*-[$PdMe_2(PMe_3)$L], the trend PMe_3 > CH_2CH_2 > ma confirms that the barrier decreases with the π-acceptor ability of L. As discussed above, the more π-acceptor the ligand, the lower should be the coupling barrier because they draw electron density away from the σ_M and this orbital is antibonding in the transition state. Consistently, ethylene is a better π-acceptor than is PMe_3 and produces a lower coupling barrier. The barrier for ma is even lower because it is a much stronger π-acceptor,[34,35] to the point that the coupling is calculated to be easier for the tetracoordinated complex with ma than for the tricoordinated species (for R = Me, $\Delta G^{\ddagger}$ is 21.7 for L = ethylene, 13.2 kcal/mol for the tricoordinated species, and 8.6 kcal/mol for L = ma).

Electronic and Structural Factors in Olefins. The structures of the reactant **1** and the transition state $\mathbf{TS_{1-2}}$, for ethylene and ma (Figure 1), show that for ethylene the olefin rotates from a perpendicular to an "in-plane" coordination during the reaction, whereas ma is coordinated in-plane already in the reactant. The olefin orientation is defined by the Pd−P−X−C_{olefin} dihedral angle, where X is the midpoint of the C=C bond. In the reactant, the dihedral angle is 89.0° for ethylene, but only 9.0° for MA. In the transition state, however, the double bond is practically in the metal plane in both cases (dihedral values of 0.1° for CH_2CH_2, and 6.5° for ma). To examine this matter, additional systems with the ligands *trans*-2-butene, fumaronitrile (*trans*-1,2-dicyanoethylene), 3,5-dimethylcyclopent-1-ene, and 2,5-dihydrofuran were studied. Fumaronitrile was chosen as a strong π-accepting olefin with no hindrance to perpendicular coordination; 3,5-dimethylcyclopent-1-ene is a conjugated cyclic olefin with expectedly medium π-acceptor properties; 2,5-dihydrofuran is a cyclic olefin structurally very similar to ma, but without electron-withdrawing substituents; and *trans*-2-butene is sterically similar to *trans*-1,2-dicyanoethylene, but lacks strong electron-withdrawing substituents. Only the reactant and the transition state with R = Me were computed for these systems. The key results are summarized in Figure 3 for the geometries, and in Table 2 for the computed energy barriers.

The computed geometries show that, for the transition state, the torsion angle is always close to 0°, regardless of the structure aspect of the olefin. The in-plane arrangement observed for $\mathbf{TS_{1-2}}$ is also observed in the final Pd(0) product (stage **3**) and in the structures found experimentally for [PdL_2(olefin)] complexes.[30] Along with an incipient Me−Me bond (compare C−C distances of about 2.8 Å in the Pd(II) reactants **1** with 2.1−2.2 Å in $\mathbf{TS_{1-2}}$ and 1.54 Å for a C−C single bond), the transition states show a clear elongation (about 0.03−0.04 Å) of the coordinated C=C double bond, reflecting the increased electron

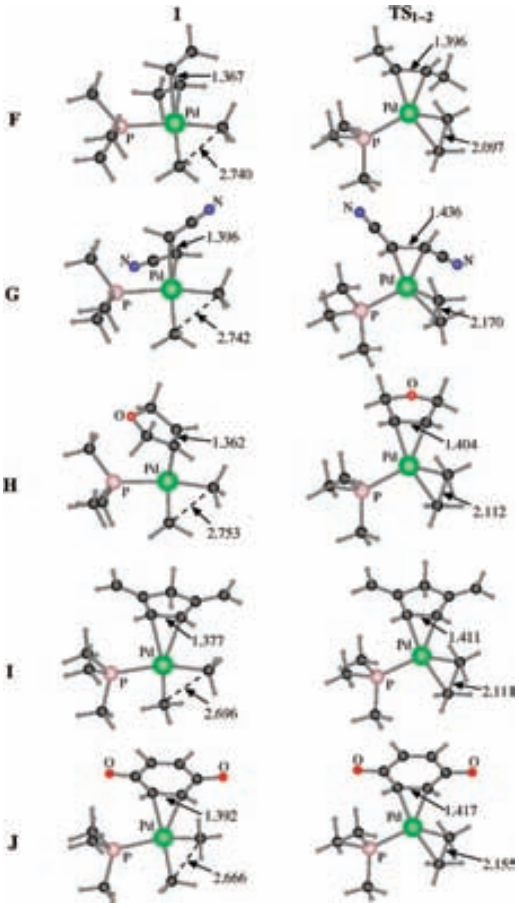

Figure 3. Optimized geometry of the reactant **1** and the transition state $\mathbf{TS_{1-2}}$ for additional olefins with different steric and electronic features. (F) L = *trans*-2-butene; (G) L = *trans*-1,2-dicyanoethylene; (H) 2,5-dihydrofuran; (I) L = 3,5-dimethylencyclopent-1-ene; (J) L = *p*-benzoquinone. Relevant selected distances (in Å) are shown.

Table 2. Computed Energy Barrier ($\Delta G^{\ddagger}$, kcal/mol) and Orientation (deg) of Olefin for the Reductive Elimination of Me−Me Starting from the *cis*-[$PdMe_2(PMe_3)$(L)] Complexes

entry	L	$\Delta G^{\ddagger}$	P−Pd−X−C_{olef} (**1**)	P−Pd−X−C_{olef} ($\mathbf{TS_{1-2}}$)
1	*trans*-2-butene	23.0	65.1	4.2
2	ethylene	21.7	89.0	0.1
3	2,5-dihydrofuran	19.8	88.3	−0.4
4	3,5-dimethylcyclopent-1-ene	15.9	13.5	−0.4
5	*trans*-1,2-dicyanoethylene	10.0	71.7	6.0
6	maleic anhydride	8.6	9.0	6.5
7	*p*-benzoquinone	5.9	10.9	−2.4
8	empty	13.2		

(34) Albéniz, A. C.; Espinet, P.; Pérez-Mateo, A.; Nova, A.; Ujaque, G. *Organometallics* **2006**, *25*, 1293–1297.

(35) The ma ligand is a very strong π-acceptor, to the point that the oxidation level of its formally Pd(0) complexes must be relatively high. This is shown, for instance, by the fact that these complexes are air stable and difficult to oxidize (see refs 30 and 33). It looks reasonable that, as the reductive elimination progresses, the overall π-acceptance will increase more steeply for ma than for other poorer π-acceptors, making this lowering of the barrier particularly effective.

back-donation to the olefin π^* orbitals. This supports the qualitative orbital diagram proposed in Figure 2, which predicts strong electronic preference for the in-plane arrangement in $\mathbf{TS_{1-2}}$.

There is no general preferred arrangement of the olefin for the reactants **1**. Angles spanning the whole range 0−90° are found, apparently not related to the π-acceptor strength of the olefin. Typically, simple olefins coordinate to Pd(II) with the double bond roughly perpendicular to the coordination plane (entry 2), or making a somewhat smaller angle to minimize interligand repulsion (entries 1 and 5). It would appear that for cyclic-planar olefins the in-plane coordination is favored (entries 4, 6, and 7), but this is not the case of 2,5-dihydrofuran (entry 3). Inspection of the calculated structures suggests that often there are only minor differences (1−3 kcal/mol) for alternative arrangements and in many cases the minimum might be dictated by subtle steric repulsions. Hence, although one could wonder whether the in-plane coordination of the double bond "prepares" the reactant for reductive elimination, in fact there is no conclusive support for this (nor against) in Table 2.[36]

There is, however, a clear relationship with the electronic effect of the olefin substituents. Comparing for instance entries 1, 2, and 5, the substituents have only a small effect on the structure, which should hardly affect the energy barrier, and the sequence of $\Delta G^{\ddagger}$ observed (*trans*-2-butene > CH_2CH_2 > *trans*-1,2-dicyanoethylene) corresponds to the increase of electron withdrawal (or decrease of electron donation) of the substituents. This electronic effect is expected to be smaller for the reactant, where the π back-donation ability of Pd(II) is modest,[37] than for the transition state, which is very much stabilized by electron withdrawal from the antibonding orbital σ_M (Figure 2). Replacement of H by Me (entry 1 vs 2) brings about only a minor increase in activation barrier of 1.3 kcal/mol, while the inclusion of strong π-acceptor substituents (C≡N or C═O) produces a substantial lowering of the barrier. The differences of 13 kcal/mol between *trans*-2-butene and fumaronitrile (entries 1 and 5), and 11.2 kcal/mol between 2,5-dihydrofuran and maleic anhydride (entries 3 and 6), clearly reflect the enormous importance of the π-acceptor ability of L on the reductive elimination process. Dimethylcyclopent-1-ene (entry 4), a less strong acceptor olefin, produces intermediate values. The optimal effects are achieved for maleic anhydride and *p*-benzoquinone (entries 6 and 7), which appear very good choices as coupling additives. Very interestingly, these and the fumaronitrile (entries 5−7) provide a lower coupling barrier on the tetracoordinated complex than the barrier for the tricoordinated (entry 8).

(36) An additional set of calculations we carried out to check whether the energy barrier to olefin rotation could be relevant to the overall kinetics. In these calculations, collected in the Supporting Information (Figure SI5), we found two local minima for *cis*-[$PdMe_2(PMe_3)(H_2C{=}CH_2)$]. The most stable one is the out-of-plane species reported in the text; a secondary in-plane species is 4.7 kcal/mol higher in energy. The transition state between these two minima is only 1.2 kcal/mol above the least stable minimum, indicative of a fast process at room temperature.

(37) The filled d orbitals in square-planar Pd(II) complexes are very stable, and this reduces their involvement in back donation. This can be noted, for instance, in the fact that Pd(II)–carbene bonds show typical single bond distances. See some X-ray structures in: (a) Albéniz, A. C.; Espinet, P.; Manrique, R.; Pérez-Mateo, A. *Angew. Chem., Int. Ed.* **2002**, *41*, 2363–2366. (b) Albéniz, A. C.; Espinet, P.; Manrique, R.; Pérez-Mateo, A. *Chem.-Eur. J.* **2005**, *11*, 1565–1573. (c) Albéniz, A. C.; Espinet, P.; Pérez-Mateo, A. *Organometallics* **2006**, *25*, 1293–1297.

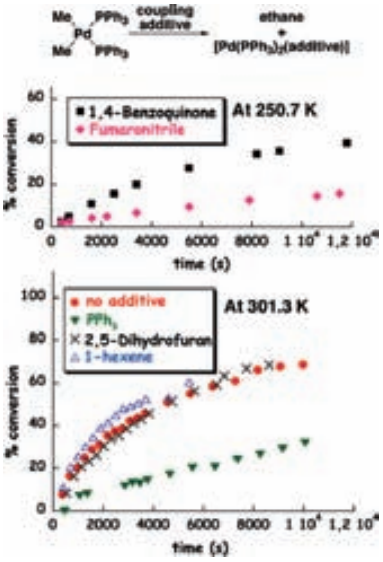

Figure 4. Coupling conversion of [$PdMe_2(PPh_3)_2$] (**4**) in acetone-d_6 in the presence of additives. Upper plot is at 250.7 K, for the fast reactions; for the rest, no conversion is observed at this temperature. Lower plot is at 301.3 K, for the fast reactions; the conversion for fumaronitrile or *p*-benzoquinone at this temperature is 100% in the first measurement and is not plotted.

Experimental Studies on the System *cis*-[$PdMe_2(PPh_3)_2$] + Additive. The computational results above indicate clearly which features in L should favor the reductive elimination in complexes *cis*-[$PdR_2(PR'_3)L$]. It is difficult, however, to find in the literature quantitative experimental support for these predictions, as in operational catalytic systems the *cis*-[$PdR_2(PR'_3)L$] intermediates should be non observable. We decided to study the systems *cis*-[$PdMe_2(PPh_3)_2$] (**4**) + additive (additive = PPh_3, ma, *p*-benzoquinone, fumaronitrile, dihydrofuran, 1-hexene) in acetone-d_6.[38] Three circumstances in the real system differ from the theoretical conditions. First, the experimental phosphine used is somewhat bulkier and less basic. Second, in the experimental system, the corresponding complexes **1**, where the calculation starts, must be formed in solution (except for L = PPh_3) by dissociation (for L = empty) or by ligand substitution (Scheme 2), which means that not only the $\mathbf{TS_{1-2}}$ but also the preequilibrium constant that determines the concentration of **1** will influence the coupling rate observed. Finally, the experimental reactions are studied in acetone-d_6, which is a hard coordinating solvent. In other words, the experimental study deals with a related but not identical process, shown on top of Figure 4.

The experiments with maleic anhydride revealed the formation of ethane and methane, the latter associated with Pd−Me acidolysis by maleic acid produced by the water contamination of the acetone-d_6 (Scheme 3). At low temperature, the formation of the corresponding Pd(0) and Pd(II) products was confirmed. Thus, although ma induces very fast coupling (comparable to

(38) PPh_3 was used instead of the PMe_3 used for calculations, due to its much easier handling. The choice turned out to be fortunate, and PPh_3 produced a range of coupling rates that could be monitored by ^1H NMR. Moreover, it contributed to reveal the importance of the steric effect of the phosphine.

Scheme 3

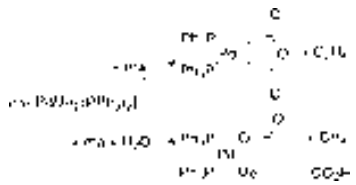

Table 3. Experiments at ca. 300 K

additive	concentration/10^{-3} mmol	temperature/K	$[4]_o/10^{-3}$ mmol
none		301.6	1.06
PPh_3	1.02	301.6	1.06
fumaronitrile	3.28	301.0	1.06
p-benzoquinone	3.40	301.3	1.06
maleic anhydride	3.12	301.3	1.06
2,5-dihydrofuran	3.10	301.3	1.06
1-hexene	3.12	301.1	1.06

Table 4. Experiments at ca. 250 K

additive	concentration/10^{-3} mmol	temperature/K	$[4]_o/10^{-4}$ mmol
fumaronitrile	3.14	250.7	5.90
p-benzoquinone	3.09	250.7	5.90
maleic anhydride	3.11	250.7	5.90

p-benzoquinone), the actual rate could not be properly quantified. In a practical sense, ma looks to be a problematic coupling additive in reactions where complete dryness cannot be guaranteed.

For the other additives, the experimental results show a clear division. The strongly π-acceptor olefins produce a dramatic acceleration of the coupling, somewhat larger for the cyclic olefin *p*-benzoquinone. The common olefins do not produce any significant effect (the differences are within experimental error) on the coupling rate shown by *cis*-$[PdMe_2(PPh_3)_2]$ alone. Finally, the addition of PPh_3 brings about retardation of the coupling, which is an indication of prior dissociation of phosphine before coupling takes place on a tricoordinated complex. This latter result is in contrast with our calculation for *cis*-$[PdMe_2(PMe_3)_2]$, where coupling occurs in the tetracoordinated complex. Hence, the electronic and steric differences between PPh_3 and PMe_3 turn out to be mechanistically decisive, as dissociation becomes more accessible for the bulkier phosphine. In fact, DFT calculations for the dissociation process of *cis*-$[PdMe_2(PR_3)_2]$ into *cis*-$[PdMe_2(PR_3)]$ and PR_3 afford markedly different values: ΔE 12.1 kcal mol for R = Ph, versus 21.7 kcal mol for R = Me, which makes a considerable difference of 9.6 kcal mol, and clearly supports easier dissociation for R = Ph.[39] The entropic contributions, difficult to compute accurately, would further weigh in favor of a dissociative mechanism.[40] Experimental retardation of coupling had been reported for *cis*-$[PdMe_2(PPh_2Me)_2]$ upon addition of PPh_2Me,[18,41] in DMF or THF, whereas coupling in tetracoordinated complexes was calculated for complexes with PH_3.[20] On the other hand, a dissociative mechanism was calculated here for *cis*-$[PdMe_2(PMe_3)(NCMe)]$. Thus, the interpretation of the rest of our calculated (with PMe_3) and experimental (with PPh_3) data has to be made in the light of this propensity to dissociation observed for the complexes with bulkier phosphines or with weaker L ligands.

Whereas the values in Table 2 predict a graduation of coupling activation energy from *cis*-$[PdMe_2(PMe_3)(olefin)]$ for common olefins (entries 1−3), the experiments show no difference for the coupling of *cis*-$[PdMe_2(PPh_3)_2]$ upon addition of olefin, whether linear (1-hexene) or cyclic (dihydrofuran). In these cases, the formation of small amounts in equilibrium of a putative *cis*-$[PdMe_2(PPh_3)(olefin)]$ is kinetically insignificant,[42] and the coupling occurs via dissociation to the tricoordinated $[PdMe_2(PPh_3)]$ (path 3 in Scheme 2). As the replacement of PMe_3 by an olefin is even less favorable than that of PPh_3, it can be extrapolated that the addition of common olefins to promote the coupling in *cis*-$[PdMe_2(PMe_3)_2]$ should also be ineffective, regardless of the theoretical prediction that a *cis*-$[PdMe_2(PMe_3)(olefin)]$ intermediate would couple more easily than *cis*-$[PdMe_2(PMe_3)_2]$, because that intermediate is not expected to form in kinetically significant amounts.

In contrast, the dramatic activating effect observed experimentally for π-acceptor olefins (Figure 4) indicates that, in these cases of considerably lower coupling barrier, the formation of a small proportion of intermediate *cis*-$[PdMe_2(PPh_3)(acceptor\ olefin)]$ becomes kinetically decisive, and these olefins drive the reaction through pathway 2 in Scheme 2. In this respect, it is interesting to note that the recent use of chelating ligands providing P and electron-deficient olefin coordinating ends, $P(acceptor\ olefin)R_2$, has led to a dramatic improvement in efficiency of $C(sp^3)-C(sp^3)$ and $C(sp^3)-C(sp^2)$ couplings in Suzuki and Negishi reactions.[43] Obviously, the chelate effect helps to increase the stability and concentration of a coupling active intermediate *cis*-$[PdR'R''(P(acceptor\ olefin)R_2)]$, and likely that of the corresponding transition state.

Conclusions

The C−C coupling in *cis*-$[PdR_2(PR'_3)_2]$ complexes can occur directly, or on tetracoordinated intermediates *cis*-$[PdR_2(PR'_3)L]$ formed upon addition of an additive L, or on tricoordinated intermediate $[PdR_2(PR'_3)]$ formed by phosphine dissociation. The size and nature of the R group and the phosphine, as well as the coordinating features of L, have a determinant influence on the coupling mechanism. The ancillary ligands used in catalysis can be critical to the feasibility of a catalytic cycle.

In difficult couplings, the addition of olefins with electron-withdrawing substituents as coupling promoters can be decisive for the success of the coupling, as the formation of a coupling

(39) See also refs 23 and 29.

(40) Calculated free energy values are $\Delta G = -6.4$ kcal mol for R = Ph versus 5.5 kcal mol for R = Me. The trend in computed free energies thus confirms the easier dissociation for PPh_3. The absolute free energy values should not be taken, however, as quantitatively correct. In fact, if these values were quantitatively correct, the complex with PPh_3 should be observed as fully dissociated. Even if dissociation was only 1%, the dissociated species should be detected (by NMR at 250 K). This is not the case, suggesting that *cis*-$[PdMe_2(PPh_3)_2]$:$[PdMe_2(PPh_3)] \geq 100{:}1$, wherefrom $\Delta G_{eq.dis.}$ (250 K) ≥ 2.3 kcal mol for R = Ph. It is well known that entropic contributions for bimolecular processes are overestimated in this type of calculations.

(41) Guillie, A.; Stille, J. K. *J. Am. Chem. Soc.* **1980**, *102*, 4933–4941.

(42) There are two reasons for this: (a) Assuming that the order of activation energy found for PMe_3 complexes is maintained for PPh_3 complexes, coupling is faster in the tricoordinated intermediate formed by PPh_3 dissociation than in the tetracoordinated complex formed with a common olefin (roughly speaking, ligands in entries 1−4 of Table 2). (b) In energetically limiting cases, it would help to lack of effect that the amount of a putative tetracoordinated intermediate with coordinated olefin is probably insignificant.

(43) (a) Williams, D. B. G.; Shaw, M. L. *Tetrahedron* **2007**, *63*, 1624–1629. (b) Luo, X.; Zhang, H.; Duan, H.; Liu, Q.; Zhu, L.; Zhang, T.; Lei, A. *Org. Lett.* **2007**, *9*, 4571–4574.

intermediate *cis*-[$PdMe_2(PR_3)$(acceptor olefin)] can reduce the coupling barrier up to 15 kcal/mol (higher concentration of this kind of active intermediate can be favored using phosphine-olefin chelating ligands). It should be noted, however, that olefins with electron-withdrawing substituents disfavor the subsequent oxidative addition and could render this step rate determining in the cycle.[44] Hence, a tradeoff between the two effects of acceptor olefins should be reached in each case.

Bulkier phosphines help to access to lower energy dissociative couplings. Because coupling on a tricoordinated complex has lower activation energy than most couplings on a tetracoordinated complex, the use of bulky phosphines that facilitate ligand dissociation favors a faster coupling. Furthermore, when the coupling takes place on tricoordinated intermediates, the more difficult alkyl−alkyl couplings come closer in activation energy to the easier phenyl−phenyl or vinyl−vinyl couplings. Hence, the positive effect of bulky ancillary ligands is particularly important for the case of alkyl−alkyl coupling.

Interestingly, the calculations suggest and the experiment shows that in cases where a low coupling barrier is operating via a tricoordinated intermediate (e.g., with bulky phosphines), the addition of small electron-deficient olefins able to coordinate can still help very noticeably to further accelerate the coupling rate (e.g., 7.3 kcal/mol reduction of the coupling barrier is observed in Table 2 comparing entries 8 and 7), forming a *cis*-[PdR_2(bulky phosphine)(acceptor olefin)] intermediate with even lower activation energy. In summary, this study explains the effect of potentially coordinating additives on the reductive elimination and opens the path for the experimental design of more efficient catalytic systems.

Experimental Section

Kinetic Study of the Reductive Elimination. The kinetic experiments were monitored by ^{1}H NMR at 400 MHz. NMR tubes (5 mm) were charged with the corresponding olefin. Next, the tubes were cooled at −78 °C, and a solution of *cis*-$[PdMe_2(PPh_3)_2]$[45] (**4**) in acetone-d_6 was added (0.7 mL). The tubes were placed into a thermostated probe. Concentration−time data were then acquired from ^{1}H integration of signals of **4**. The experimental data are collected in Tables 3 and 4. The exact temperature was calibrated with an ethylene glycol standard for Table 3, and with a methanol standard for Table 4.

Acknowledgment. We thank the Spanish Ministerio de Educación y Ciencia (INTECAT Consolider Ingenio-2010 (CSD2006-0003), and Consolider Ingenio 2010 (CSD2007-00006); SAF07-63880, FEDER; CTQ2005-09000-CO2-01; CTQ2005-09000-CO2-02; CTQ2007-67411/BQU; CTQ2008-06647-C02-01/BQU; "Juan de la Cierva" contract to A.A.C.B.; studentship to M.H.P-T.); the Xunta de Galicia (Parga Pondal Contract to M.P.-R.); the Catalan DURSI through project 2005SGR00715; the Junta de Castilla y León (Projects VA044A07 and GR169); the UAB for a PIF studentship to M.G-M.; and the ICIQ foundation for financial support. We also thank CESGA and CESCA for generous allocation of computational resources.

Supporting Information Available: Computational methods. Complete computational data and discussion for the complexes with R = Me, Ph, and vinyl and L = PMe_3, MeCN, empty, CH_2CH_2, ma. Computational data for the complexes with R = Me and L = *trans*-2-butene, 2,5-dihydrofuran, 3,5-dimethyl-cyclopent-1-ene, *trans*-1,2-dicyanoethylene, *p*-benzoquinone. Data for the ligand dissociation from *cis*-$[PdMe_2(PPh_3)_2]$ and *cis*-$[PdMe_2(PMe_3)L]$, and for the olefin rotation in *cis*-$[PdMe_2(PMe_3)(H_2C{=}CH_2)]$. This material is available free of charge via the Internet at http://pubs.acs.org.

JA808036J

(44) Fairlamb, I. J. S.; Kapdi, A. R.; Lee, A. F.; McGlacken, G. P.; Weissburger, F.; de Vries, A. H. M.; Schmieder-van de Vondervoort, L. *Chem.-Eur. J.* **2006**, *12*, 8750–8761, and references therein.

(45) Byers, P. K.; Canty, A. J.; Jin, H.; Kruis, D.; Markies, B. A.; Boersma, J.; van Koten, G. *Inorg. Synth.* **1998**, *32*, 170.

B.2 Article V:

Mechanistic Analysis of Iridium(III) Catalyzed Direct sp^2 C-H Arylations: A DFT Study

García-Melchor, M.; Gorelsky, S. I.; Woo, T. K. *Chem. Eur. J.* **2011**, *17*, 13847-13853.

CHEMISTRY
A EUROPEAN JOURNAL

has been widely implicated as being operative. However, for the Ir^{III}-catalyzed reaction an electrophilic metalation mechanism, (S_EAr) was proposed. To our knowledge, no computational studies on Ir^{III}-catalyzed cross-coupling direct arylation have been reported to date. Previously published computational studies on Ir^{III}-catalyzed C–H activation concern either other reaction types[14] or noncatalytic processes with different Ir-based complexes.[15] An understanding of the underlying mechanism of Ir-catalyzed direct arylation is crucial for further optimization and development of this chemistry. We use density functional theory (DFT) calculations to investigate the reaction mechanism of the Ir^{III}-catalyzed direct arylation of several heteroarenes, reported by Itami and coworkers[11b] with a purpose of gaining better understanding of C–H bond activation by Ir^{III} in comparison to Pd^{II}.

Results and Discussion

The C–H activation process in the reaction of PhI with benzene (**1**) and heteroarenes **2**–**4** (Scheme 1) was evaluated with quantum chemical calculations at the B3LYP[16]/TZVP[17] level of theory (full details are provided in the Computational Methods section). The main mechanisms proposed for the direct C–H arylation step are (Scheme 2): 1) oxidative addition of Ar–H to the metal, 2) CMD mechanism, and 3) electrophilic aromatic substitution. Electrophilic metalation–deprotonation (EMD), the mechanism that lies in between CMD and S_EAr, has been also suggested.[7k] While discussed for reactions with Pd^{II} catalysts, the oxidative addition mechanism for Ir^{III} is not feasible as it requires generation of a highly unfavorable Ir^{V} intermediate. Thus, the oxidative addition mechanism has not been explored further. The S_EAr mechanism consists in a two-step process: first, a metal–carbon bond is formed resulting in a stable Wheland intermediate, second, C–H bond cleavage occurs with the concomitant proton transfer to the base. On the other hand, the CMD mechanism is a process in which formation of the metal–carbon bond and the proton abstraction from the C–H bond occur simultaneously; thus, the CMD reaction pathway may involve only a weak π-complex intermediate before the CMD transition state. We first examine the nature of the active species. We considered Ir^{III} complexes that could be generated after the oxidative addition of PhI to the starting Ir^{I} complex [Ir(cod)(py)-(PMe_3)](PF_6). In Itami's original work, it was speculated that the catalysis was initiated by oxidative addition of an iodoarene to the Ir^{I} complex to yield a $[Ar–Ir^{III}–I]^+$ intermediate, which was followed by abstraction of the iodide by the Ag_2CO_3 to generate a dicationic $[Ar–Ir^{III}]^{2+}$ active species. In the nonpolar solvent such as *m*-xylene it can be expected that the formation of such cationic species will be unfavorable. Given that previous computational and experimental studies have shown that under the reaction conditions[11b] the base anionic ligand (that is carbonate) is coordinated to the metal center[12a,d] it is more plausible that a neutral Ir^{III}-carbonate complex is involved as the active species. To examine this we have evaluated the Gibbs free energies of formation of potential dicationic Ir^{III} intermediates from the corresponding neutral species. As anticipated, all such species were found to be highly unfavorable in nonpolar solvents.[18] Since a cationic active species is unlikely, we have explored the stability of several neutral 4-, 5-, and 6-coordinate Ir^{III} complexes as potential active species. These are depicted in Figure 1. The species with the lowest Gibbs free energy are the 6-coordinate Ir^{III} complexes. However, the CMD reactivity starting from these complexes requires the carbonate ligand to change from κ^2-binding to κ^1-binding in order to generate a vacant site for the incoming heteroarene. The calculations indicate that this is a highly endergonic process (34.5 kcal mol^{-1} for **C6-py** with L = py and 32.7 kcal mol^{-1} for **C6-py** with L = PMe_3). Hence, the 6-coordinate Ir^{III} species are unlikely to be catalytic species. Among the 5-coordinate Ir^{III} complexes, the trigonal bipyramidal (tbp) structures were all found to be unstable and any attempts to locate stable minima resulted in square-based pyramid-like (*sbp-like*) geometries where one of the oxygens from the carbonate ligand occupies the axial position. Among the five-coordinate Ir^{III} complexes, **C5-Ph** has the lowest Gibbs free energy and, therefore, its energy was taken as a reference. The order in the stability of the Ir^{III} complexes with the sbp geometry (**C5-Ph** > **C5-PMe$_3$** > **C5-py**) can be explained by the *trans* effect of these ligands (Ph > PMe_3 > py), since it is known[19] that for complexes with sbp geometries, the axial position is occupied by the ligand with the strongest *trans* effect. Finally, the 4-coordinate Ir^{III} complex, **C4**, was examined and found to be a high-energy species (+18.2 kcal mol^{-1} relative to **C5-Ph**) due to the low coordination number of the central atom. To elucidate if the CMD or S_EAr mechanism was operative, the CMD mechanism was first examined with the various arenes, **1**–**4**, and following this, the potential energy surface was further examined to identify how concerted the calculated reaction pathway is, and if Wheland intermediates could be located. The CMD transition states for the C–H

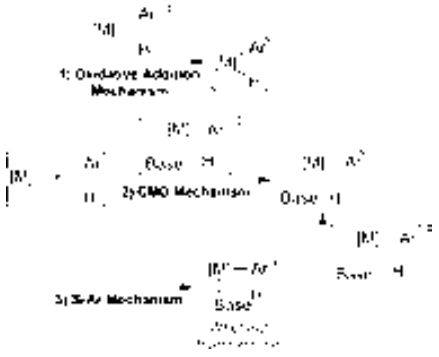

Scheme 2. Reaction mechanisms relevant for metal-catalyzed C–H bond activation.

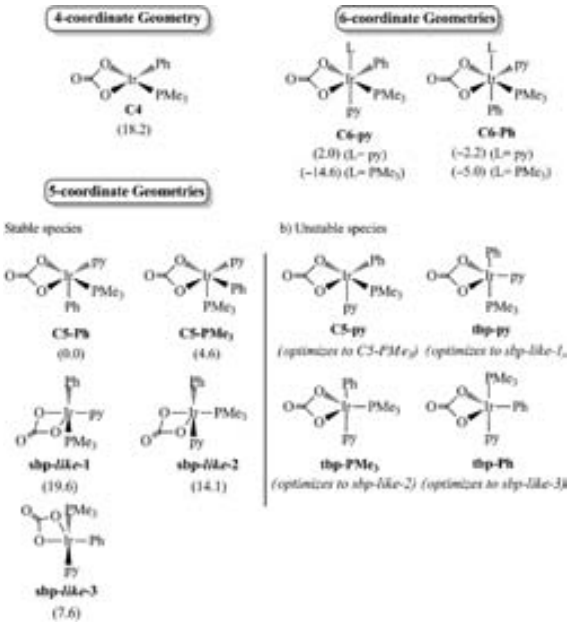

Figure 1. Possible Ir^{III} catalytic species and their relative free energies in gas phase at 298 K (ΔG_g, kcal mol^{-1}).[18] The energies are given relative to the energy of the **C5-Ph** complex.

activation process starting from the 5- and 4-coordinate species shown in Figure 1 were calculated with benzene as a model C–H sp^2 substrate. The CMD reaction pathway starting from the tetracoordinate Ir^{III} species can be ruled out based on the fact that the corresponding CMD TS has very high energy ($\Delta G^{+}_{s} = 58.2$ kcal mol^{-1}). Among the reaction pathways involving the different 5-coordinate sbp Ir^{III} complexes, the pathway through **C5-py-TS** was found to have the lowest energy barrier with $\Delta G^{+}_{s} = 39.4$ kcal mol^{-1}. This transition state, **C5-py-TS**, is shown in Figure 2. Interestingly, the **C5-py-TS** transition state structure is derived from a 5-coordinate sbp structure **C5-py** that is not a stable minimum on the PES and attempts to optimize a **C5-py** structure without the benzene moiety complexed resulted in the sbp structure **C5-PMe$_3$**. With the incoming benzene molecule weakly coordinated, a stable intermediate with the C5-py ligand arrangement does form, and is shown in Figure 2 as **C5-py-I1**. This implies that the coordination of the benzene moiety facilitates the formation of the intermediate **C5-py-I1**. Thus, the lowest energy CMD reaction pathway proceeds through a transition state **C5-py-TS**, in which the base 5-coordinate sbp Ir^{III} complex itself is not stable. This was confirmed by an intrinsic reaction coordinate (IRC) calculation from **C5-py-TS** and subsequent optimization of the isolated Ir^{III} complex. Importantly, the optimized structure of the weak adduct **C5-py-I1** reveals that the Ir–$C_{(arene)}$ bond length is fairly large (2.574 Å) and the NPA-derived charge buildup on the arene fragment is small (+0.226 a.u.). These two observations indicate that **C5-py-I1** is not a Wheland intermediate in which a strong Ir–$C_{(arene)}$ interaction with the bond order approaching 1 and a formal +1 charge on the arene are expected. Other attempts to locate an energy minimum structure that resembles the Wheland intermediate resulted in structure going to **C5-py-I1**. The benzene adducts formed from the other five-coordinate Ir^{III} complexes (Figure 1) show even larger Ir–$C_{(arene)}$ distances (due to the stronger *trans* effect of the PMe_3 and Ph groups in the axial position compared to the py ligand). With the CMD reaction pathway established for benzene, transition states analogous to **C5-py-TS** were calculated for the reactions involving the heteroarene substrates, **2**–**4**

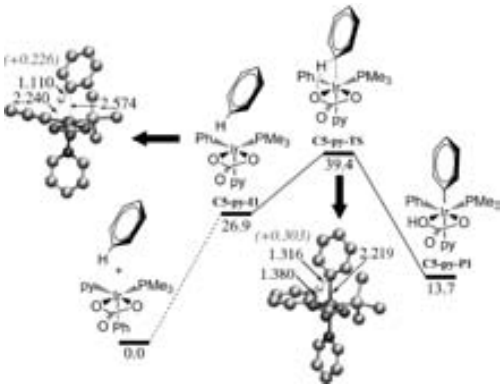

Figure 2. Gibbs free energy profile (ΔG_s, kcal mol^{-1}) of the CMD reaction pathway for C–H bond cleavage of benzene catalyzed by [Ir(Ph)-(PMe_3)(py)(CO_3)] in toluene solution at 298 K. Hydrogen atoms not involved in the C–H activation step are not shown for clarity. The NPA-derived charges[20,21] of the ArH fragment in the π-complex intermediate and the CMD TS structure are shown in parenthesis.

(Scheme 1). The structures of the lowest-energy transition states with these substrates, **TS-2** to **TS-4**, as well as the structures for the CMD reaction intermediates, **I2** to **I4**, are

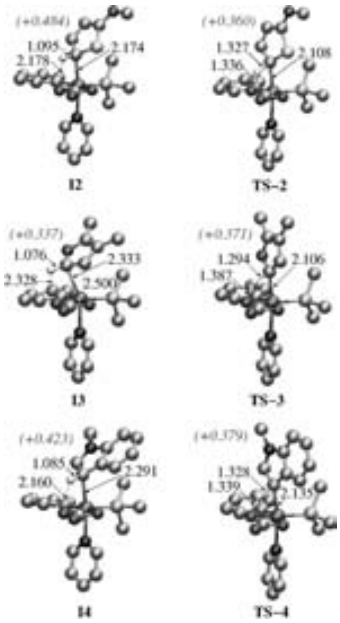

Figure 3. Optimized structures of the reaction intermediates **(I2-I4)** that precede the lowest-energy CMD transition states (**TS-2**,**3**,**4**) with substrates **2**–**4**. Only hydrogen atoms that are involved in the C–H activation step are shown, for clarity. The NPA-derived charges[20,21] of the ArH fragments are shown in parenthesis.

shown in Figure 3. The CMD transition states have an octahedral geometry for the Ir^{III} and the C–H bond of the arene occupies the vacant 6th position. In these transition states the carbonate ligand that acts as a base for proton abstraction from the C–H bond remains bound in a κ^2-fashion. This is in contrast to the corresponding Pd^{II} CMD transition states where the acetate ligand is bound to Pd^{II} as a monodentate ligand.[12d] This can be rationalized as follows: in the CMD transition states with Pd^{II} as a central atom, a coordination site for the incoming substrate is needed and therefore the acetate ligand has to undergo a change in the coordination mode. In the CMD transition states with Ir^{III} as a central atom, the vacant position for the heteroarene is already available in the pentacoordinate species, hence the carbonate ligand remains coordinated to Ir^{III} in a κ^2-mode. Intermediates **I2**–**I4** (Figure 3) that precede the lowest-energy CMD transition states can be classified as η^1-C complexes. In these complexes, the Ir–$C_{(arene)}$ distances are fairly large, with **I2** possessing the shortest Ir–$C_{(arene)}$ distance of 2.174 Å and the positive charges on the arene fragments, also shown in Figure 3, are not as large as expected for the Wheland structures. The computed free energy barriers for substrates **1**–**4** through the CMD mechanism are found to be consistent with the experimental regioselectivity as shown by the free energy barriers provided in Figure 4. More specifically, furans and thiophenes exhibit an α-arylation site preference, whereas for indoles the preferred arylation site is the C3 position, as was found experimentally.[11b] Additionally, our calculated kinetic isotope effect (KIE) for the reaction also agrees with the experiments. Specifically, we determined a KIE of 3.2 at 433 K for both substrate **2** and 2-deuterothiophene (C_4H_3DS), which compares well to the KIE of 1.9 determined experimentally[11b] for the same substrates. Itami and co-workers determined the kinetic isotope effect (KIE) for the reaction to be 1.9 for at 433 K[11]. The NPA-derived charges[20,21] on the metal atom and the arene fragments (Table 1) and the metal–$C_{(arene)}$ bond order (Table 2) in the

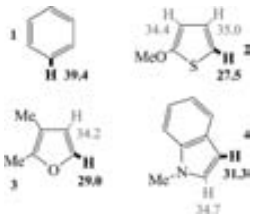

Figure 4. Lowest Gibbs free energy barriers (ΔG^{+}_{s}, kcal mol^{-1}) for direct arylation with the Ir^{III} catalyst via the CMD pathway in toluene solution at 298 K. C–H bonds shown in bold indicate the arylation sites experimentally observed.

Table 1. Distortion/interaction energies (kcal mol^{-1}), NPA-derived charges (a.u.), and C–H_{ArH} bond lengths (Å) for the lowest-energy CMD transition states for Ir and Pd direct arylation catalysts.

Catalyst Metal	Arene	ΔE^{+}[a]	E_{dist} (ArH)	E_{dist} (ML)[b]	E_{int}[c]	q(ArH)[d,e]	q(M)[f]	q(M)[g]	d(C–H_{ArH})
Ir	1	24.2	31.3	29.8	−36.9	+0.303	+0.432	+0.050	1.32
Pd[h]	1	25.1	44.6	15.8	−35.3	+0.056	+0.497	+0.274	1.44
Ir	2	11.2	35.3	31.3	−55.4	+0.360	+0.436	+0.020	1.33
Pd[h]	2	14.0	42.4	18.5	−46.9	+0.088	+0.506	+0.267	1.43
Ir	3	14.2	34.0	30.5	−50.3	+0.371	+0.434	+0.010	1.29
Pd[h]	3	15.4	44.6	18.3	−47.5	+0.101	+0.506	+0.260	1.44
Ir	4	13.4	37.1	31.8	−55.5	+0.379	+0.437	+0.035	1.33
Pd[h]	4	17.3	46.1	19.0	−47.7	+0.122	+0.508	+0.262	1.44

[a] The energy relative to the sum of the energies of the isolated arene and the Ir^{III} complex with the Ph ligand in axial position (Figure 1, **C5**–**Ph**). [b] The distortion energy of the metal–ligand fragment ([Ir(Ph)(py)-(PMe_3)(CO_3)] in the case of Ir^{III} and [Pd(Ph)(PMe_3)(OAc)] in the case of Pd^{II}. [c] The computed BSSE in the interaction energies for Ir CMD TSs were in the 3.9–4.6 kcal mol^{-1} range.[18] [d] NPA-derived charge of the ArH fragment in the CMD TS. [e] The NBO implementation[20] where valence p orbitals of the metal atom are included in the Rydberg shell indicate smaller positive charge build-up on the ArH fragment (−0.010, +0.017, +0.031, +0.052 a.u. for Pd-catalyzed TS with **1**, **2**, **3**, and **4**, respectively). [f] NPA-derived charge of the metal atom in the ML fragment of the CMD TS structure before the electronic interaction with the ArH fragment is "turned on". [g] NPA-derived charge of the metal atom in the CMD TS. [h] Direct C–H arylation of benzene catalyzed by [Pd(Ph)(PMe_3)(OAc)].[12d]

Table 2. Wiberg metal–carbon (ArH) and oxygen(base)–hydrogen bond orders (derived in the NAO basis) for the lowest-energy CMD transition states for Ir^{III} and Pd^{II} direct arylation catalysts.

Catalyst Metal	Arene	BO ($O-H_{ArH}$)[a]	BO ($M-C_{ArH}$)[b]
Ir	1	0.25	0.51
Pd[c]	1	0.38	0.36
Ir	2	0.28	0.63
Pd[c]	2	0.39	0.40
Ir	3	0.25	0.62
Pd[c]	3	0.39	0.42
Ir	4	0.27	0.61
Pd[c]	4	0.39	0.42

[a] Oxygen(base)–hydrogen(ArH) bond order in the CMD TS. [b] Metal–carbon(ArH) bond order in the CMD TS. [c] Direct C–H arylation of benzene catalyzed by $[Pd(Ph)(PMe_3)(OAc)]$.[12d]

CMD transition states with the Ir^{III} catalyst indicate that these structures feature stronger metal–carbon interactions than the corresponding structures with the Pd^{II} catalyst. At the same time, the O–H bond orders are weaker in the Ir^{III} structures as compared with the Pd^{II} structures (Table 2). This indicates that the Ir^{III}-catalyzed CMD process is less concerted than the Pd^{II}-catalyzed process, in which the metal–carbon and proton–oxygen bonds are formed to the same extent. This difference between Ir^{III} and Pd^{II} CMD structures explains stronger positive charge buildup on the arene fragments in the Ir^{III} transition states (Table 1): while the formation of the metal–carbon covalent bond involves the charge donation from the arene π orbitals to the empty acceptor orbital (the LUMO of the metal fragment) on the metal atom, the formation of the O–H bond involves the charge donation from the base (carbonate/acetate) to the unoccupied σ^* orbital of the C–H bond under the cleavage (Figure 5). When the formations of the O–H and metal–C bonds are concerted (Pd^{II}-catalyzed CMD process), the charge donation from the arene fragment to the metal are compensated by the charge donation from the base to the arene and, thus, the arene fragment exhibits only a small charge buildup. When the formation of the metal–C bond is ahead of the formation of the O–H bond (Ir^{III}-catalyzed CMD process), the charge donation from the arene fragment to the metal are not compensated by the charge donation from the base to the arene and, thus, the arene fragment now exhibits significant positive charge. Finally, in order to identify contributions to the CMD pathway barriers for the different arenes, an activation-strain analysis was performed[22] where contributions to the CMD energy barriers were evaluated. The distortion energy, E_{dist}, is defined as the energy associated with the geometric distortion of the Ir^{III} catalyst and the arene from the isolated species to their "strained" geometries in the transition state. The energy gain arising from the catalyst and the arene electronically interacting with each other in the transition state structure is termed the interaction energy (E_{int}). E_{int} and E_{dist} are represented in Figure 6, and the values for the lowest-energy transition states involving substrates **1**–**4** are given in Table 1. Table 1 also includes distortion and interaction energies for the Pd^{II} catalyst $[Pd(Ph)(PMe_3)(OAc)]$ with substrates **1**–**4**, for comparison.[12d] For both the Ir^{III} and Pd^{II} catalysts, Table 1 shows that the CMD barriers involving benzene are about 10 kcal mol^{-1} higher than the heteroarene substrates **2**–**4**. This is not surprising as benzene does not have any activated C–H bonds. Heteroarenes **2**–**4** (π-electron rich arenes) have significantly more negative interaction energies, E_{int}, compared to benzene due to higher nucleophilicity of the carbon atoms in these substrates. The CMD barriers for the heteroarenes with the Ir^{III} catalyst are predicted to be slightly lower than that with the Pd^{II} catalyst (Table 1), and the arylation regioselectivity is also preserved. The CMD transition states with Ir^{III} have distortion energies for the arene fragment that are 7 to 13 kcal mol^{-1} lower than those with Pd^{II}. This difference originates from the fact that the transition states with the Ir^{III} catalyst have the geometries with the less elongated C–H bonds (being cleaved) than the transition states with the Pd catalyst (Table 1). On the other hand, the CMD transition states with Ir^{III} have distortion energies for the metal fragment that are 12 to 14 kcal mol^{-1} higher than the Pd^{II} catalyst. This can be ra-

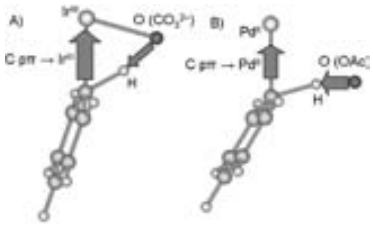

Figure 5. Schematic representation of the donor-acceptor interactions for the CMD transition states with a) Ir^{III}-carbonate and b) Pd^{II}-acetate catalysts. The arrows indicate charge donation from the arene to the metal and from the base (carbonate/acetate) to the arene fragment. Arrow size indicates the relative magnitude of charge transfer interactions.

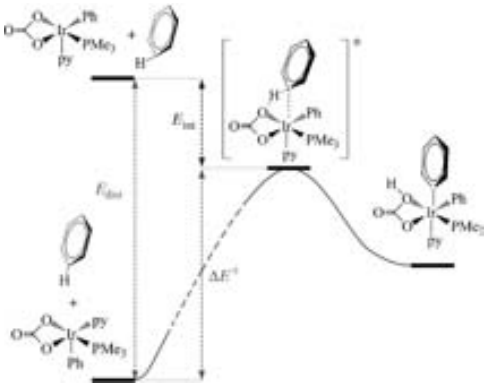

Figure 6. Schematic representation of the activation-strain analysis for the CMD transition state structures with the Ir^{III} catalyst.

tionalized with the higher energetic cost that is needed for distorting the pentacoordinate Ir^{III} species compared with tetracoordinate Pd^{II} species. However, this higher distortion energy of the metal fragment is more than offset by lower ArH distortion energies and higher interaction energies E_{int} with the Ir^{III} catalyst as compared with the Pd^{II} catalyst. The latter can be attributed to higher Lewis acidity of Ir^{III} that leads to stronger metal–carbon interactions in Ir^{III} CMD TS structures compared to the Pd^{II} CMD TS structures. Considering the recent report from Hartwig and co-workers[7k] that the arylpalladium(II) carboxylate complex without the phosphine ligand undergoes the C–H cleavage step of C_6H_6 with a lower CMD barrier than arylpalladium(II) carboxylate complex with the phosphine ligand, it appears that higher Lewis acidity of the metal site, both Pd^{II} and Ir^{III}, in the arylation catalyst can be a critical parameter for turning on the cleavage of the C–H bonds.

Conclusion

The direct arylation reaction of benzene and various heteroarenes catalyzed by a Ir^{III}-based catalyst was investigated by DFT calculations. This reaction is controlled by the metalation–deprotonation pathway, rather than the S_EAr mechanism as suggested previously.[11b] Wheland intermediates, which are part of the S_EAr mechanism, could not be located. The CMD mechanism and the corresponding activation barriers at different C–H bonds account for the regioselectivity experimentally observed. For the model substrate (that is, benzene), the ligand with the lowest *trans* effect in the axial position provides the lowest energy barrier for the C–H activation process. Hence, the use of ligands with lower *trans* effect may be beneficial for lowering the activation energy for the CMD process. The results for Ir^{III}-catalyzed C–H arylation were also compared to the Pd^{II} analogues. The CMD transition states with the Ir^{III} catalyst show stronger metal–carbon and weaker base–proton interactions indicating stronger electrophilic character in C–H bond activation with Ir^{III} catalysts. To our knowledge, this is the first mechanistic study on a direct arylation reaction catalyzed by Ir-based catalysts. Thus, it provides new and valuable information for the better understanding of direct C–H arylation using the different transition metal catalysts and for the further optimization of this important class of reactions.

Computational Methods

Density functional theory (DFT) calculations were performed with the Gaussian 03 program package[23] using the B3LYP[16] exchange correlation functional. The PCy_3 ligand in the catalyst used in the work of Itami and co-workers[11b] was modeled as the PMe_3 ligand. The LANL2DZ effective core potential[24] with an extra *f*-polarization (exponent 0.938) shell was used as a basis set for Ir.[25] The all-electron DZVP basis set[26] was used for Pd. For all the other atoms (H, C, N, O, P, S) the TZVP[17] basis set was used. Geometries were fully optimized without symmetry constraints . Harmonic frequency calculations were performed for all reported structures to determine the nature of the stationary points and to calculate vibrational zero-point energy corrections and Gibbs free energies (ΔG_g). Solvent effects were introduced through single point calculations at optimized gas-phase geometries for all the minima and transition states by means the PCM model[27] implemented in Gaussian 03 (ΔE_s). The solvent *m*-xylene ($\varepsilon = 2.37$) was substituted by toluene ($\varepsilon = 2.38$) as it is a parameterized solvent with similar polarity. For the hydrogen atoms involved in the C–H bond cleavage step, the keyword SPHEREONH was used in order to place individual spheres on them. The relative Gibbs energies in solution shown throughout this present work (ΔG_s) were obtained by employing the following scheme: $\Delta G_s = \Delta E_s + (\Delta G_g - \Delta E_g)$. Atomic charges and Wiberg bond orders were evaluated by using the natural population analysis (NPA)[20,21] as implemented in the Gaussian 09 program package.[28] The basis set superposition errors were computed for the interaction energies using the counterpoise method.[29,30]

Acknowledgements

We thank Universitat Autònoma de Barcelona for a PIF scholarship to MGM, and the Generalitat de Catalunya for the 2009-BE1–00326 travel scholarship to MGM. We would like to thank the NSERC and the Canada Research Chair Program for financial support. We are also grateful to CFI, the Ontario Innovation Trust, and IBM Canada for providing computing resources.

[1] G. W. Bemis, M. A. Murcko, *J. Med. Chem.* **1996**, *39*, 2887.
[2] For reviews: a) K. C. Nicolaou, P. G. Bulger, D. Sarlah, *Angew. Chem.* **2005**, *117*, 4516; *Angew. Chem. Int. Ed.* **2005**, *44*, 4442; b) J. S. Carey, D. Laffan, C. Thomson, M. T. Williams, *Org. Biomol. Chem.* **2006**, *4*, 2337; c) D. S. Surry, S. L. Buchwald, *Angew. Chem.* **2008**, *120*, 6438; *Angew. Chem. Int. Ed.* **2008**, *47*, 6338.
[3] *Metal-Catalyzed Cross-Coupling Reactions*, 2nd ed. (Eds.: A. de Meijere, F. Diederich), Wiley-VCH, Weinheim, **2004**.
[4] *Handbook of Organopalladium Chemistry for Organic Synthesis, Vols. 1 and 2* (Eds.: E.-I. Negishi, A. de Meijere), Wiley, New York, **2002**.
[5] For an illustrative review on aryl–aryl bond formation, see: J. Hassan, M. Sevignon, C. Gozzi, E. Shulz, M. Lemaire, *Chem. Rev.* **2002**, *102*, 1359.
[6] For recent reviews on C–H bond arylation of arenes, see: a) L.-C. Campeau, K. Fagnou, *Chem. Commun.* **2006**, 1253; b) D. Alberico, M. E. Scott, M. Lautens, *Chem. Rev.* **2007**, *107*, 174; c) I. J. S. Fairlamb, *Chem. Soc., Rev.* **2007**, *36*, 1036; d) B.-J. Li, S.-D. Yang, Z.-J. Shi, *Synlett* **2008**, 949–957; e) G. P. Chiusoli, M. Catellani, M. Costa, E. Motti, N. Della Ca′, G. Maestri, *Coord. Chem. Rev.* **2010**, *254*, 456.
[7] a) A. Mori, A. Sekiguchi, K. Masui, T. Shimada, M. Horie, K. Osakada, M. Kawamoto, T. Ikeda, *J. Am. Chem. Soc.* **2003**, *125*, 1700; b) B. S. Lane, M. A. Brown, D. Sames, *J. Am. Chem. Soc.* **2005**, *127*, 8050; c) J.-P. Leclerc, K. Fagnou, *Angew. Chem.* **2006**, *118*, 7945; *Angew. Chem. Int. Ed.* **2006**, *45*, 7781; d) L.-C. Campeau, M. Parisien, A. Jean, K. Fagnou, *J. Am. Chem. Soc.* **2006**, *128*, 581; e) N. Lebrasseur, I. Larrosa, *J. Am. Chem. Soc.* **2008**, *130*, 2926; f) L.-C. Campeau, M. Bertrand-Laperle, J.-P. Leclerc, E. Villemure, S. I. Gorelsky, K. Fagnou, *J. Am. Chem. Soc.* **2008**, *130*, 3276; g) S. Yanagisawa, K. Ueda, H. Sekizawa, K. Itami, *J. Am. Chem. Soc.* **2009**, *131*, 14622; h) K. Ueda, S. Yanagisawa, J. Yamaguchi, K. Itami, *Angew. Chem.* **2010**, *122*, 9130; *Angew. Chem. Int. Ed.* **2010**, *49*, 8946; i) J. M. Joo, B. B. Toure, D. Sames, *J. Org. Chem.* **2010**, *75*, 4911; j) D. Lapointe, T. Markiewicz, C. J. Whipp, A. Toderian, K. Fagnou, *J. Org. Chem.* **2011**, *76*, 749; k) Y. Tan, J. F. Hartwig, *J. Am. Chem. Soc.* **2011**, *133*, 3308.
[8] a) R. B. Bedford, S. J. Coles, M. B. Hursthouse, M. E. Limmert, *Angew. Chem.* **2003**, *115*, 116; *Angew. Chem. Int. Ed.* **2003**, *42*, 112;

b) J. C. Lewis, S. H. Wiedemann, R. G. Bergman, J. A. Ellman, *Org. Lett.* **2004**, *6*, 35; c) X. Wang, B. S. Lane, D. Sames, *J. Am. Chem. Soc.* **2005**, *127*, 4996; d) S. Yanagisawa, T. Sudo, R. Noyori, K. Itami, *J. Am. Chem. Soc.* **2006**, *128*, 11748; e) X. Zhao, Z. Yu, *J. Am. Chem. Soc.* **2008**, *130*, 8136.

[9] a) L. Ackermann, A. Althammer, R. Born, *Angew. Chem.* **2006**, *118*, 2681; *Angew. Chem. Int. Ed.* **2006**, *45*, 2619; b) I. Özdemir, S. Demir, B. Cetinkaya, C. Gourlaouen, F. Maseras, C. Bruneau, P. H. Dixneuf, *J. Am. Chem. Soc.* **2008**, *130*, 1156.

[10] H.-Q. Do, O. Daugulis, *J. Am. Chem. Soc.* **2008**, *130*, 1128.

[11] a) K. Fujita, M. Nonogawa, R. Yamaguchi, *Chem. Commun.* **2004**, 1926; b) B. Join, T. Yamamoto, K. Itami, *Angew. Chem.* **2009**, *121*, 3698; *Angew. Chem. Int. Ed.* **2009**, *48*, 3644.

[12] a) M. Lafrance, C. N. Rowley, T. K. Woo, K. Fagnou, *J. Am. Chem. Soc.* **2006**, *128*, 8754; b) D. Garcia-Cuadrado, A. A. C. Braga, F. Maseras, A. M. Echavarren, *J. Am. Chem. Soc.* **2006**, *128*, 1066; c) D. Garcia-Cuadrado, P. de Mendoza, A. A. C. Braga, F. Maseras, A. M. Echavarren, *J. Am. Chem. Soc.* **2007**, *129*, 6880; d) S. I. Gorelsky, D. Lapointe, K. Fagnou, *J. Am. Chem. Soc.* **2008**, *130*, 10848; e) H.-Y. Sun, S. I. Gorelsky, D. R. Stuart, L.-C. Campeau, K. Fagnou, *J. Org. Chem.* **2010**, *75*, 8180.

[13] In Ru-catalyzed arylations: L. Ackermann, R. Vicente, A. Althammer, *Org. Lett.* **2008**, *10*, 2299. For its involvement in Pd cyclometalation reactions, see: D. L. Davies, S. M. A. Donald, S. A. MacGregor, *J. Am. Chem. Soc.* **2005**, *127*, 13754.

[14] In Ir cyclometalation reactions: a) D. L. Davies, S. M. A. Donald, O. Al-Duaij, S. A. MacGregor, M. Polleth, *J. Am. Chem. Soc.* **2006**, *128*, 4210; b) Y. Boutadla, D. L. Davies, S. A. MacGregor, A. I. Poblador-Bahamonde, *Dalton Trans.* **2009**, 5887.

[15] For C–H activation with Ir, see: a) J. Oxgaard, W. J. Tenn, R. J. Nielsen, R. A. Periana, W. A. Goddard, *Organometallics* **2007**, *26*, 1565; b) D. H. Ess, S. M. Bischof, J. Oxgaard, R. A. Periana, W. A. Goddard, *Organometallics* **2008**, *27*, 6440; c) S. M. Bischof, D. H. Ess, S. K. Meier, J. Oxgaard, R. J. Nielsen, G. Bhalla, W. A. Goddard, R. A. Periana, *Organometallics* **2010**, *29*, 742.

[16] a) A. D. Becke, *J. Chem. Phys.* **1993**, *98*, 5648; b) C. Lee, W. Yang, R. G. Parr, *Phys. Rev. B* **1988**, *37*, 785.

[17] A. Schäfer, C. Huber, R. Ahlrichs, *J. Chem. Phys.* **1994**, *100*, 5829.

[18] For further details on these calculations see the Supporting Information.

[19] A. R. Rossi, R. Hoffmann, *Inorg. Chem.* **1975**, *14*, 365.

[20] A. E. Reed, R. B. Weinstock, F. Weinhold, *J. Chem. Phys.* **1985**, *83*, 735.

[21] a) F. Maseras, K. Morokuma, *Chem. Phys. Lett.* **1992**, *195*, 500; b) C. R. Landis, F. Weinhold, *J. Comput. Chem.* **2007**, *28*, 198.

[22] For recent examples of this type of analysis, see Ref. [12d] and: C. Y. Legault, Y. Garcia, C. A. Merlic, K. N. Houk, *J. Am. Chem. Soc.* **2007**, *129*, 12664.

[23] Gaussian 03, Revision C.02, M. J. Frisch, G. W. Trucks, H. B. Schlegel, G. E. Scuseria, M. A. Robb, J. R. Cheeseman, J. A. Montgomery, Jr., T. Vreven, K. N. Kudin, J. C. Burant, J. M. Millam, S. S. Iyengar, J. Tomasi, V. Barone, B. Mennucci, M. Cossi, G. Scalmani, N. Rega, G. A. Petersson, H. Nakatsuji, M. Hada, M. Ehara, K. Toyota, R. Fukuda, J. Hasegawa, M. Ishida, T. Nakajima, Y. Honda, O. Kitao, H. Nakai, M. Klene, X. Li, J. E. Knox, H. P. Hratchian, J. B. Cross, V. Bakken, C. Adamo, J. Jaramillo, R. Gomperts, R. E. Stratmann, O. Yazyev, A. J. Austin, R. Cammi, C. Pomelli, J. W. Ochterski, P. Y. Ayala, K. Morokuma, G. A. Voth, P. Salvador, J. J. Dannenberg, V. G. Zakrzewski, S. Dapprich, A. D. Daniels, M. C. Strain, O. Farkas, D. K. Malick, A. D. Rabuck, K. Raghavachari, J. B. Foresman, J. V. Ortiz, Q. Cui, A. G. Baboul, S. Clifford, J. Cioslowski, B. B. Stefanov, G. Liu, A. Liashenko, P. Piskorz, I. Komaromi, R. L. Martin, D. J. Fox, T. Keith, M. A. Al-Laham, C. Y. Peng, A. Nanayakkara, M. Challacombe, P. M. W. Gill, B. Johnson, W. Chen, M. W. Wong, C. Gonzalez, J. A. Pople, Gaussian, Inc., Wallingford CT, **2004**.

[24] a) P. J. Hay, W. R. Wadt, *J. Chem. Phys.* **1985**, *82*, 270; b) P. J. Hay, W. R. Wadt, *J. Chem. Phys.* **1985**, *82*, 299.

[25] A. W. Ehlers, M. Böhme, S. Dapprich, A. Gobbi, A. Höllwarth, V. Jonas, K. F. Köhler, R. Stegmann, A. Veldkamp, G. Frenking, *Chem. Phys. Lett.* **1993**, *208*, 111.

[26] N. Godbout, D. R. Salahub, J. Andzelm, E. Wimmer, *Can. J. Chem.* **1992**, *70*, 560.

[27] S. Miertuš, E. Scrocco, J. Tomasi, *Chem. Phys.* **1981**, *55*, 117.

[28] Gaussian 09, Revision A.1, M. J. Frisch, G. W. Trucks, H. B. Schlegel, G. E. Scuseria, M. A. Robb, J. R. Cheeseman, G. Scalmani, V. Barone, B. Mennucci, G. A. Petersson, H. Nakatsuji, M. Caricato, X. Li, H. P. Hratchian, A. F. Izmaylov, J. Bloino, G. Zheng, J. L. Sonnenberg, M. Hada, M. Ehara, K. Toyota, R. Fukuda, J. Hasegawa, M. Ishida, T. Nakajima, Y. Honda, O. Kitao, H. Nakai, T. Vreven, J. A. Montgomery, Jr., J. E. Peralta, F. Ogliaro, M. Bearpark, J. J. Heyd, E. Brothers, K. N. Kudin, V. N. Staroverov, R. Kobayashi, J. Normand, K. Raghavachari, A. Rendell, J. C. Burant, S. S. Iyengar, J. Tomasi, M. Cossi, N. Rega, J. M. Millam, M. Klene, J. E. Knox, J. B. Cross, V. Bakken, C. Adamo, J. Jaramillo, R. Gomperts, R. E. Stratmann, O. Yazyev, A. J. Austin, R. Cammi, C. Pomelli, J. W. Ochterski, R. L. Martin, K. Morokuma, V. G. Zakrzewski, G. A. Voth, P. Salvador, J. J. Dannenberg, S. Dapprich, A. D. Daniels, Ö. Farkas, J. B. Foresman, J. V. Ortiz, J. Cioslowski, D. J. Fox, Gaussian, Inc., Wallingford CT, **2009**.

[29] S. F. Boys, F. Bernardi, *Mol. Phys.* **1970**, *19*, 553.

[30] S. Simon, M. Duran, J. J. Dannenberg, *J. Chem. Phys.* **1996**, *105*, 11024.

Received: May 18, 2011
Revised: August 19, 2011
Published online: October 27, 2011

B.3 Article VI:

Theoretical Evaluation of Phosphine Effects in Cross-Coupling Reactions

García-Melchor, M.; Ujaque, G.; Maseras, F.; Lledós, A. In *Phosphorus Compounds: Advanced Tools in Catalysis and Material Sciences*; Peruzzini, M., Gonsalvi, L., Eds.; Springer: Berlin, 2011; Vol. 37; Chapter 3, pp 57-84.

Chapter 3
Theoretical Evaluation of Phosphine Effects in Cross-Coupling Reactions

Max García-Melchor, Gregori Ujaque, Feliu Maseras and Agustí Lledós

Abstract Cross-coupling reactions are one of the most useful reactions in organic synthesis. Among all the transition metal complexes developed as catalysts for this reaction those based on Pd are by far the most utilized ones. The most common stoichiometry of this family of catalyst is PdL_2 with L = phosphine ligands. The effects of the phosphine ligands on the reaction mechanism evaluated by means of theoretical calculations are reviewed in these lines. How the nature of the phosphine ligand affects each of the elementary processes involved in a cross-coupling reaction, namely oxidative addition, transmetalation and reductive elimination will be exposed separately. The transmetalation process has its own particular mechanistic details depending on the cross-coupling reaction; those for the Suzuki–Miyaura and Stille reactions will be described here. The dichotomy between the monophosphine and bisphosphine reaction pathways will be also discussed.

3.1 Introduction

During the last decades the design of new and more efficient transition metal catalysts has become of major importance in organometallic chemistry and homogenous catalysis [1, 2]. In this research field, the change of the ligands coordinated to

M. García-Melchor · G. Ujaque · F. Maseras · A. Lledós (✉)
Departament de Química, Edifici Cn, Universitat Autònoma de Barcelona, 08193 Bellaterra, Catalonia, Spain
e-mail: agusti@klingon.uab.es

F. Maseras
Institute of Chemical Research of Catalonia (ICIQ), Av. Països Catalans, 16, 43007 Tarragona, Catalonia, Spain

M. Peruzzini and L. Gonsalvi (eds.), *Phosphorus Compounds*, Catalysis by Metal Complexes, 37, DOI: 10.1007/978-90-481-3817-3_3,

the metal center modifying their properties has emerged as an elegant and useful alternative for that purpose [3–10]. Particularly, phosphorus compounds with the general structure PA_3 (A = R, X, NR_2, OR) or asymmetric substitution patterns PA_2A', $PAA'A''$ are a milestone, since the steric and electronic properties of the catalyst can be modified or fine-tuned by introducing different substituents on the phosphorus donor atom. These changes in the catalyst properties may modify its reactivity and therefore, the catalytic activity of that transition metal complex. For this reason, it is not surprising that steric and electronic parameters of an immense variety of phosphorus compounds have been analyzed in the literature [5–10].

In the last years, due to the growth in the development of new technologies and more powerful computers, theoretical calculations started to become more relevant in the design of new transition metal catalysts. In particular, the contributions from computational methods have enabled not only the better understanding of catalytic reactions, but in some cases the possibility to predict and suggest new transition metal complexes as more efficient catalysts [11, 12]. Thus, theoretical methods provide a big support to experimental techniques, besides being less expensive and more sustainable, which nowadays is a concern within the Chemist community.

Due to the limitations in computational resources, most of the initial computational studies of catalytic reactions were performed by quantum mechanic (QM) calculations, modeling the substituents on the phosphorus atom. Among all the models, PH_3 was the earliest and most widely used, and was shown to give acceptable results in many cases [13, 14]. However, with the appearance of more powerful computers the calculation of catalytic systems with the real phosphine ligands has been achieved, initially with hybrid methods like quantum mechanics/molecular mechanics (QM/MM) [15–19], and afterwards with full QM calculations [20, 21]. Thus, at present, the computation of catalytic systems with simplified phosphines is particularly useful when exploring multiple reaction pathways (qualitative studies), but care is needed when quantitative information for a particular system is required.

In this current chapter, we will focus on how transition metal catalysts containing phosphine ligands have been computationally treated and which is the effect of these ligands on their catalytic activity. Particularly, computational studies concerning one of the most important transformations in organometallic chemistry will be reviewed: The palladium-catalyzed C–C Cross-Coupling reactions.

3.2 Overview of C–C Cross-Coupling Reactions

The catalyzed C–C cross-coupling reactions have become increasingly important in modern organic synthesis and in organometallic chemistry during the last decades. A huge variety of complex compounds can be synthesized from readily accessible reactants [22–25]. These reactions consist in the carbon–carbon bond formation between an organic electrophile R-X and an organometallic nucleophile R-m in the presence of a catalyst [M] (Fig. 3.1). The catalysts most broadly used are the transition metal complexes from groups 8–10, especially Ni [26] and Pd [27, 28].

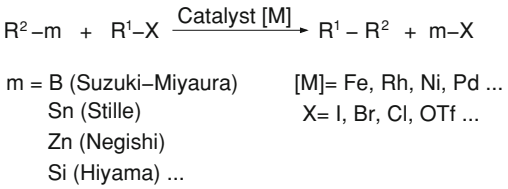

Fig. 3.1 General scheme for C–C cross-coupling reactions

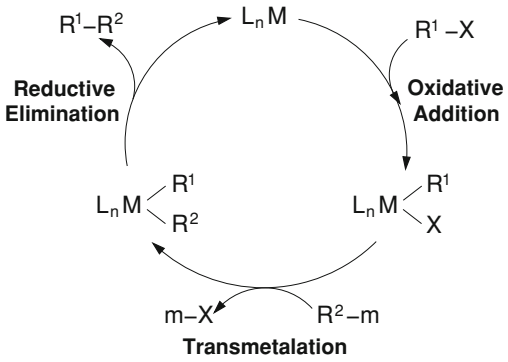

Fig. 3.2 General catalytic cycle for C–C cross-coupling reactions

Cross-coupling reactions can be classified depending on the metal or semimetal present in the nucleophile. For instance, Stille reaction [29, 30] is tin-mediated, Suzuki–Miyaura [31, 32] boron-mediated, Negishi [33, 34] zinc-mediated, etc. In general, these reactions follow a general accepted reaction pathway that consists of three steps (Fig. 3.2) [35]: (1) *oxidative addition* or insertion of the low valent transition metal into the electrophilic carbon-heteroatom bond, (2) *transmetalation* or displacement of a heteroatom leaving group by the nucleophile, and finally, (3) *Reductive elimination* to form the new C–C bond with the concomitant regeneration of the catalyst. The former and the latter steps are common to all cross-coupling reactions and have been studied in some depth both by experimental [36–39] and computational [40–42] methods. Hence, the mechanisms for these two steps are quite well understood. In contrast, the various cross-coupling reactions differ in the nucleophile used for transmetalation and, consequently, in the transmetalation step. In addition, experimental evidence for this process is particularly difficult to obtain due to the complexity that involves the isolation and characterization of key intermediates. Thus, it is not surprising that the mechanistic studies concerning this step are scarce [43–45] or even for some cross-coupling reactions it still remains unknown.

Initially, cross-coupling reactions had the important limitation that only aryl bromides and iodides could be employed as substrates. However, as aryl chlorides are more profusely available and in general are less expensive than their bromide and iodide analogs, many efforts to find a solution on that issue have been made since then [46]. In this way, important advances for the past few years are mainly

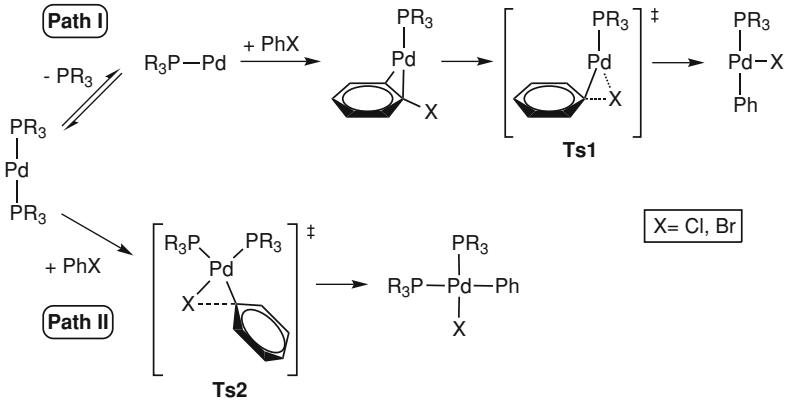

Fig. 3.3 Reaction mechanisms for the oxidative addition of PhX to $[Pd(PR_3)_2]$ [53]

due to the development of new transition metal complexes containing electron rich and bulky ligands (mostly phosphines [47–49], but also carbenes [50, 51]).

In the following sections, we will review some of the most relevant computational mechanistic studies on the three steps of some Pd-catalyzed C–C cross-coupling reactions and how the phosphine ligands coordinated to the transition metal center affect the catalyst reactivity within these steps. Most of the results reported have been obtained using the Density Functional Theory (DFT) with the hybrid functional B3LYP, although other functionals as B3PW91 have been also employed.

3.3 Phosphine Effects in Oxidative Addition

Oxidative addition constitutes the first step in cross-coupling reactions and it has drawn enough attention since it has been suggested to be rate-limiting step in some reactions, particularly when X = Cl. Even though this process has been investigated in some depth during the last years [37, 40–42] there are still some aspects that are not completely fully understood, such as the enhanced reactivity of transition metal complexes containing electron-rich and bulky ligands. This enhanced reactivity has been attributed to the formation of monoligated [ML] species which can undergo oxidative addition more rapidly than the corresponding bis-ligated ones $[ML_2]$ [52]. In order to shed light on this issue, Liu et al. recently reported a computational study in which the oxidative addition of aryl halides PhX to $Pd(PR_3)_2$ (R = Me, Et, *i*-Pr, *t*-Bu, Ph) was investigated at the Density Functional Theory (DFT) level [53]. In particular, the mechanisms for the oxidative addition reaction through both palladium complexes with one and two coordinated phosphine ligands were evaluated (Fig. 3.3). Geometry optimizations were performed by means of the B3PW91 functional and subsequently, single-point calculations were carried out at the PBEPBE level.

Path I involves dissociation of one phosphine ligand from the initial complex [Pd(PR_3)$_2$] followed by the coordination of PhX to form the complex [Pd(η^2-PhX)PR_3]. Afterwards, this last complex undergoes oxidative addition through **Ts1** resulting in the tricoordinated complex [Pd(PR_3)(Ph)X]. In contrast, Path II involves the direct oxidative addition to the initial Pd complex via the bisphosphine transition state **Ts2** to form *cis*-[Pd(PR_3)$_2$(Ph)X].

According to the results obtained by Liu et al. for the oxidative addition of PhCl to [Pd(PR_3)$_2$], a preference for the monophosphine pathway (Path I) was showed for all the analyzed PR_3 ligands (R = Me, Et, *i*-Pr, *t*-Bu, Ph) with energy differences ranging from 2.0 (R = Me) to 14.1 kcal/mol (R = *i*-Pr). Besides, the oxidative addition through Path II was found to be higher in energy, and even in the case of R = *t*-Bu, no transition state **Ts2** could be located. In the latter case, all the attempts to find the corresponding transition state always led to the substitution of one phosphine ligand by PhCl. The transition state for this substitution was located, but it resulted to be higher in energy compared to dissociation of one phosphine ligand via Path I (ca. 24 kcal/mol higher). The computational study reported by Liu was also extended to bromines for some PR_3 compounds.

Interestingly, among the different PR_3 ligands analyzed by Liu et al., no significant differences were found in the computed free-energy barriers for the oxidative addition of PhCl to the monophosphine species [Pd(PR_3)] (i.e. less than 2 kcal/mol); this indicates that this reaction is nearly independent of the organic group R. Conversely, a significant difference was found for the dissociation energy of one phosphine ligand from the initial Pd complex. Specifically, the computed dissociation energies for the different PR_3 ligands followed the order: R = Me > Et > PPh_3 > *i*-Pr > *t*-Bu with energy values ranging from 26.0 (R = Me) to 19.4 kcal/mol (R = *t*-Bu). This energy difference to generate the monophosphine Pd species was proposed by the authors to govern the different reactivity of the distinct PR_3 ligands in the oxidative addition process. In particular, the authors attributed the unique capability of P(*t*-Bu)$_3$ of accomplishing cross-coupling of inactivated aryl chlorides to that energy difference. Similar conclusions have been also reported by Ariafard and Yates in a very recent computational study with palladium catalysts containing the ligands L = P(*t*-Bu)$_3$, PPh_3 and PMe_3 [54].

More recently, Hartwig et al. reported an exhaustive kinetic study [55] parallel to that previously reported by Liu et al. Therein, the oxidative addition of aryl halides PhX (X = I, Br, Cl) to the complexes PdL_2 (L = P(*t*-Bu)$_3$, 1-AdP(*t*-Bu)$_2$ (1-Ad = 1-adamantyl), CyP(*t*-Bu)$_2$, and PCy_3) was examined. The aim of their work was to analyze the steric effects of the ligands on the coordination number of the species that undergo oxidative addition, and to determine whether the halide present in the PhX plays a role or not, in this step. For this investigation, three potential mechanisms for the oxidative addition reaction were considered (Fig. 3.4). The pathways A and C correspond to the same reaction pathways that Liu et al. previously examined in their work (Path II and Path I, respectively) [53] while pathway B assumes an oxidative addition from a monophosphine species generated via associative displacement of the ligand by the haloarene.

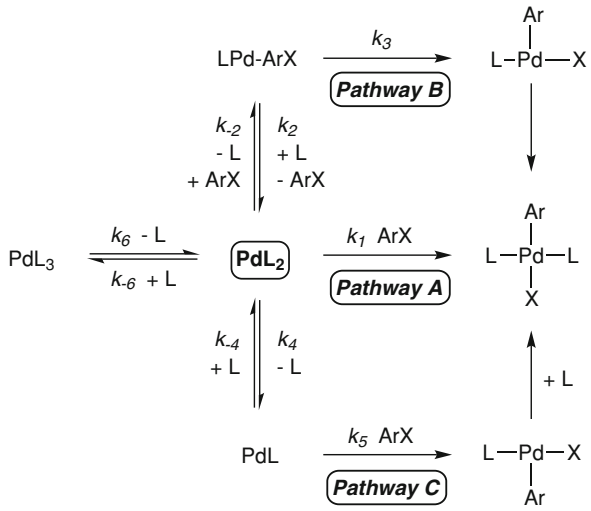

Fig. 3.4 Scheme of the three proposed mechanisms for the oxidative addition of ArX to [PdL_2] [55]

The kinetic results obtained by Hartwig et al. revealed that the rate constants for the oxidative addition reaction depend more on the identity of the halide than on the steric bulk of the ligand. All the reactions with iodoarenes were found to occur by rate-determining reaction involving a bisphosphine complex, whereas all the reactions with chloroarenes occur by rate-determining reaction with a monophosphine complex. Particularly, the reactions with iodoarenes follow the pathway B,[1] whereas the reactions with chloroarenes follow the dissociative pathway C. Further, the authors proposed that iodoarenes react with the bisphosphine complexes via an irreversible process because they are softer and more reactive than the other haloarenes. In contrast, in the case of chloroarenes they suggested that the generation of the more reactive monophosphine species is required because they are poorer ligands and necessitate a more reactive intermediate to cleave the less reactive C–Cl bond. These conclusions are in agreement with the recently reported low energy barriers for oxidative addition of chloroarenes to monophosphine Pd(0) species and high energy barriers for oxidative addition of chloroarenes to bisphosphine Pd(0) [42, 56].

As far as the bromoarenes are concerned, the oxidative addition to Pd complexes containing the ligands L = 1-AdP(*t*-Bu)$_2$ and L = CyP(*t*-Bu)$_2$ appeared to occur by two competitive paths involving rate-determining reactions of bisphosphine complexes to give rise to monophosphine intermediates (i.e. pathway B and pathway C). Besides, the oxidative addition to Pd complexes with the ligand

[1] For Pd complexes containing the ligand L = PCy_3, Hartwig et al. concluded that the reaction would take place from Pd(PCy_3)$_3$ (the major species under reaction conditions) via reversible dissociation of one phosphine ligand to generate the Pd(PCy_3)$_2$ species. Then, this species would react irreversibly with PhI. However, the mechanism for this reaction could not be confirmed whether it would occur through either the pathway A or the pathway B.

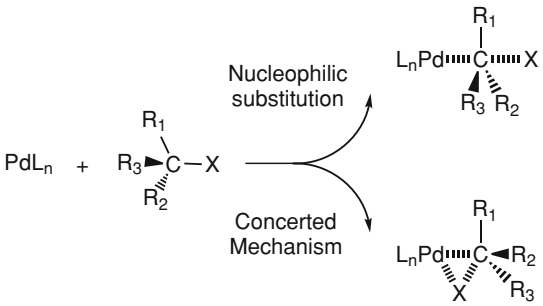

Fig. 3.5 Mechanisms proposed for the oxidative addition reaction

L = PCy_3 was consistent with both the pathway A and B, and so, no distinction between this two paths could be done.

More recently, the effect of the phosphine ligands L = PMe_3, $P(CF_3)_3$, PPh_3 and $P(t\text{-Bu})_3$ within the full catalytic cycle of Suzuki cross-coupling reaction was computationally analyzed by Harvey et al. [57] by using steric and electronic descriptors [58–60] in multiple linear regression models. In particular, the oxidative addition step was found to be mainly dominated by ligand electronics which agrees with the fact that better σ-donor ligands lead to lower oxidative addition barriers [61]. The computed energy barrier heights for the oxidative addition with the electron poorer $P(CF_3)_3$ was found to be higher than that for the electron-rich ligands $P(t\text{-Bu})_3$, PMe_3 and PPh_3.

The oxidative addition process commented so far are used to be described as a concerted process. Nevertheless, "nucleophilic attack" to the carbon center of the metal species [Pd(0)L_n] has been also proposed for the oxidative addition process (Fig. 3.5). Initial proposals for this process were done by Stille studying experimentally the oxidative addition of benzyl halides to Pd(0); the authors postulated a S_N2-type process with inversion of configuration at the benzylic center [62]. Such a substitution mechanism is commonly proposed in organic reactions mechanisms. The nucleophilic attack mechanism has been also postulated by means of theoretical studies on several oxidative addition processes [40, 41, 63, 64]. In the particular case of the oxidative addition of sp^3 carbons in α-sulfoxide systems the reaction was found to be fast and stereoselective, presenting an inversion of configuration [65]. The reaction mechanism for this process was investigated by DFT calculations for both the monophosphine and bisphosphine systems leading to qualitatively similar results. In all cases the nucleophilic substitution transition states showed lower barrier than their corresponding concerted pathways [66].

3.4 Phosphine Effects in Transmetalation

As we stated before, the mechanism for the transmetalation process is expected to show differences depending on the cross-coupling reaction since they differ in the nucleophile used. Thus, perhaps not surprisingly, the mechanism for this step has

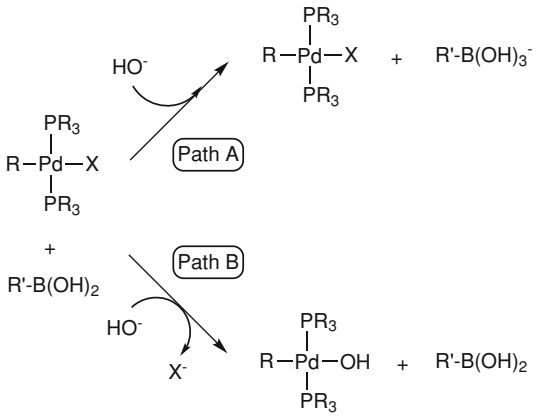

Fig. 3.6 Two main proposed reaction pathways for the role of the base in Suzuki–Miyaura reaction

been studied in less depth compared to the other ones, and the number of computational and experimental studies dealing with transmetalation is still lower. Among them, the Suzuki and Stille cross-coupling reactions are probably the most studied. Therefore, herein we present an overview of the reported studies on the transmetalation process within these two cross-coupling reactions, with special focus on the effects of phosphine ligands.

3.4.1 The Transmetalation Step in the Suzuki–Miyaura Reaction

Since the publication of the seminal paper of Miyaura et al. [31, 32] in 1979, some issues concerning the mechanistic details of the transmetalation step in the Suzuki–Miyaura reaction have appeared. For example, the role of the base was not clear and several proposals were made [67]. In order to cast light on this issue, many experimental studies were carried out [31, 32, 68, 69]. Particularly, two main pathways consisting on the base attacking first either the palladium complex or the organoboronic acid were proposed to account for the effect of the base in this step (Fig. 3.6).

The role of the base was unraveled through DFT-B3LYP studies by Maseras, Ujaque and co-workers [70] concluding that the role of the base was to react with the organoboronic acid to generate the anionic species $[RB(OH)_3]^-$; this is the reactive species taking part in the transmetalation process by substituting the halide and the subsequent transmetalation step.

With the role of the base established, another issue in the Suzuki–Miyaura reaction was to elucidate whether the mechanism for the transmetalation step involved either one or two phosphine ligands in the Pd catalytic species. On this issue, Maseras et al. reported a thorough computational study at DFT-B3LYP level of the full catalytic cycle for the coupling of vinyl bromide and vinylboronic acid $H_2C{=}CHB(OH)_2$ catalyzed by both $[Pd(PH_3)_2]$ and $[Pd(PH_3)]$ [71]. Moreover, alternative mechanisms for the transmetalation step depending on the *cis* or *trans*

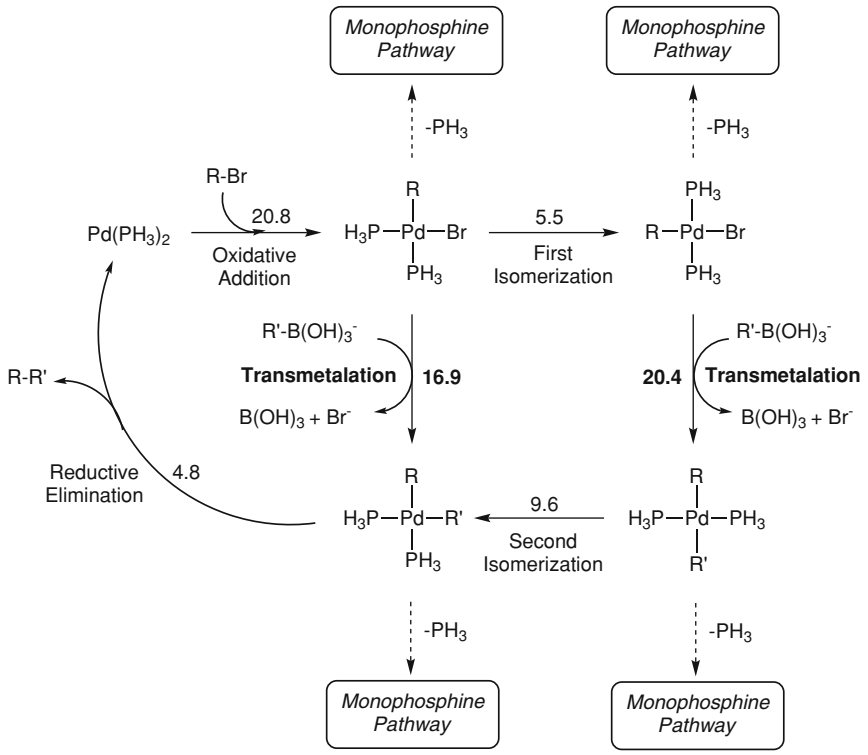

Fig. 3.7 Full reaction mechanism for the Suzuki reaction through bisphosphine Pd complexes theoretically analyzed by Maseras et al. [71] (Energies in kcal/mol)

isomery were also considered. According to their results, the transmetalation through both the bisphosphine pathways (Fig. 3.7) and the monophosphine pathways (Fig. 3.8) have reasonably low energy barriers, though lower energy barriers were found for the monophosphine reaction pathways.

However, special cautiousness should be taken when considering these mechanisms since it was generally assumed that the initial palladium complex (the one generated after the oxidative addition process) is a bisphosphine Pd complex when using regular phosphines. Thus, an additional energy for the dissociation of one of the phosphine ligands to generate the monophosphine species is required. A precise calculation of ligand dissociation processes in solution by means of static QM methods is not an obvious issue.

This study was later extended to aryls by the same authors obtaining qualitatively the same overall mechanism and suggesting that results of general validity can be obtained with the less computationally demanding vinyl systems [72]. Besides, this study also supported that the role of the base is to react with the boronate species regardless of which the electrophilic organic substrate is.

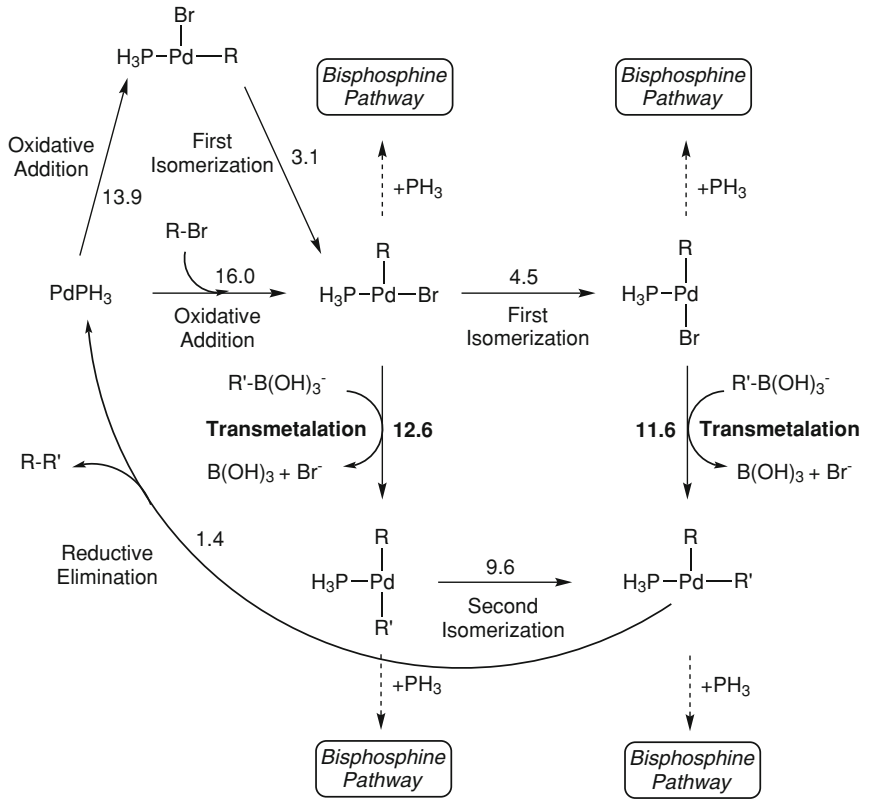

Fig. 3.8 Full reaction mechanism for the Suzuki reaction through monophosphine Pd complexes theoretically analyzed by Maseras et al. [71] (Energies in kcal/mol)

A related theoretical study on palladium-catalyzed borylation of iodobenzene with diboron was reported by Sakaki et al. [73]. Specifically, the mechanism for the transmetalation step between the Pd complexes $Pd(X)(Ph)(PH_3)_2$ (X = OH, F) and diboron $B_2(eg)_2$ (eg = $–OCH_2CH_2O–$) was investigated. Other theoretical studies, but now within the context of organic acids as electrophiles, were reported by Goo*ß*en et al. [74, 75]. The palladium catalyzed Suzuki reaction of carboxylic anhydrides with arylboronic acids was analyzed, showing that in those cases monophosphine complexes were also involved in the transmetalation process.

With the aim of designing new and more efficient catalysts for Suzuki reaction, the bulky and electron-rich dialkylbiaryl phosphine ligands (Fig. 3.9) were found to dramatically improve the efficiency and selectivity of this type of reactions [76]. In particular, Buchwald's group reported that the use of 2-(2′,6′-dimethoxybiphenyl)-dicyclohexylphosphine, SPhos (Fig. 3.9) in the palladium-catalyzed Suzuki reaction exhibited unprecedented scope, reaction rate, and stability [77]. More specifically, the use of this ligand conferred to the catalyst a unique activity allowing the coupling of boronic acids with aryl bromides and chlorides with low

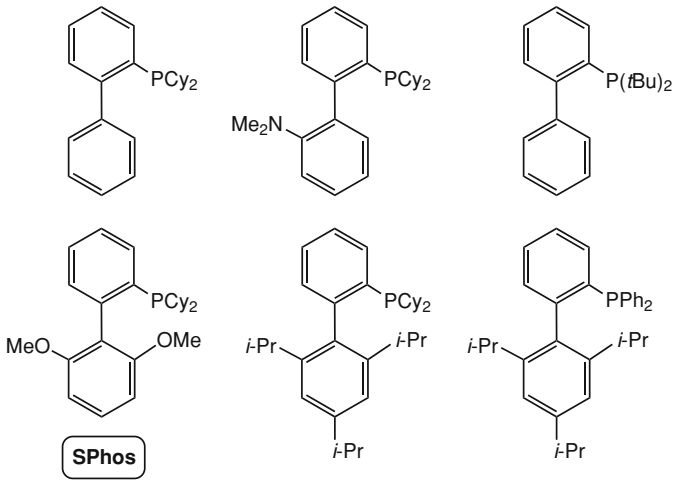

Fig. 3.9 Some examples of dialkylbiarylphosphines [76]

catalyst loadings. This enhanced reactivity was, in general, attributed by the authors to a combination of electronic and steric properties of this kind of ligands that favor the stabilization of the mono-ligated [PdL] intermediates, which are believed to be key species within the catalytic cycle [78]. So, this enhanced reactivity was not directly attributed to one step in particular, but to the full catalytic cycle in general.

The effect of different phosphine ligands over the Suzuki–Miyaura reaction was also experimentally and theoretically reported by Baillie et al. [79] and Hong et al. [80] respectively. In the first one, the effect of the size of phosphine ligands of type $P(biphenyl)_nPh_{3-n}$ in the palladium-catalyzed Suzuki reaction with aryl bromides and chlorides was investigated. Among the analyzed ligands, the highest conversions and turnovers were obtained using $P(biphenyl)Ph_2$, which the authors attributed to the contribution of both steric and electronic effects. On the other hand, in the study from Hong et al. [80], the effect of phosphorus and nitrogen chelating ligands (diphosphine, diimines, diamines) was computationally evaluated at DFT-B3LYP level for the palladium-catalyzed Suzuki reaction of phenyl chloride and phenylboronic acid. This type of ligands are particularly interesting within cross-coupling reactions because they provide kinetic and thermodynamic stability for the active species and further, forcing the entering ligands to be in a *cis* disposition with respect to each other; this allows to skip the *trans* to *cis* isomerization previous to the reductive elimination step. The results reported by Hong et al. with these chelating ligands revealed that the catalytic reaction employing diimine as the chelating ligand provide the most energetically feasible pathway. On the other hand, surprisingly high energies barriers in gas phase were found for the transmetalation processes with the different chelating ligands.

More recently, Hong et al. [81] reported a combined experimental and DFT-B3LYP computational study on bulky chelated ligands in which the application to

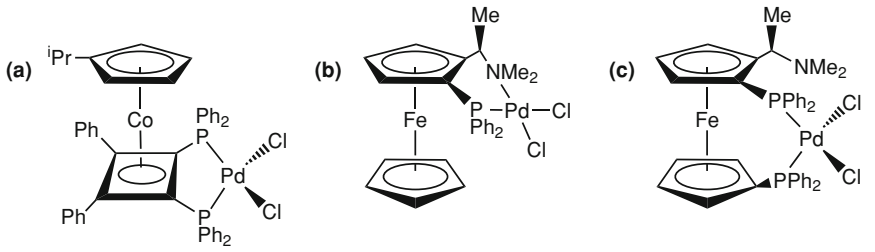

Fig. 3.10 Examples of Pd catalysts reported by Hong et al. [81]: **a** Pd complex synthesized by Hong et al. and applied to the Suzuki–Miyaura reaction. **b** and **c** Examples of other palladium complexes evaluated in their conformational study

the Suzuki reaction of a palladium-complex containing a cobalt sandwich diphosphine ligand [(η^5-$C_5H_4^i$Pr)Co(η^4-$C_4(PPh_2)_2Ph_2$)] was investigated (Fig. 3.10). The results reported therein showed that this ligand can be successfully applied in the synthesis of ferrocenylarenes. Furthermore, the computational analysis on various Pd complexes with different chelating ligands (Fig. 3.10) revealed that the most favorable conformation of these ligands in their corresponding Pd complexes is the one with a bite angle close to 90°.

Up until now, in most of the experimental and computational studies that were reviewed in this section, the effect of phosphine ligands such as electron-rich and bulky phosphine ligands in the Suzuki–Miyaura reaction has been analyzed as a global effect over the reaction rather than their isolated effect over the different steps within it. Harvey and co-workers very recently reported a DFT-B3LYP computational study on the effect of phosphine ligands over the different steps of the Suzuki–Miyaura reaction [57]. Therein, the effect of the phosphine ligands PMe_3, $P(CF_3)_3$, PPh_3 and P(*t*-Bu)$_3$ along the different steps in the full catalytic cycle was investigated by using steric and electronic descriptors in conjunction with DFT methods. Concerning the transmetalation step, the effects of those phosphine ligands were analyzed considering a mechanism in which the Pd complex had only one coordinated phosphine ligand. The transmetalation from a tetracoordinated square planar complex due to the chelating nature of boronate takes place through a four member ring transition state, resulting in a palladium complex with the two organic groups in a *cis* arrangement (Fig. 3.11). The results derived from this study revealed that both steric and electronic effects are important within this step. In particular, the computation of the steric descriptors showed that the bulkier ligands may produce higher energy barriers for this process probably due to the possible interactions with the rest of the substituents on the palladium complex in the rearrangement previous to the transition state. The conjuction of these steric and electronic effects resulted in the following order in the computed energy barriers with the different ligands: $P(CF_3)_3 < PPh_3 < PMe_3 <$ P(*t*-Bu)$_3$. Besides, the computation of the electronic descriptors pointed out that better π-acceptor phosphines may contribute to lowering the energy barrier for the transmetalation process. The authors rationalize this fact by the ability of these ligands to better stabilize the developing additional electron

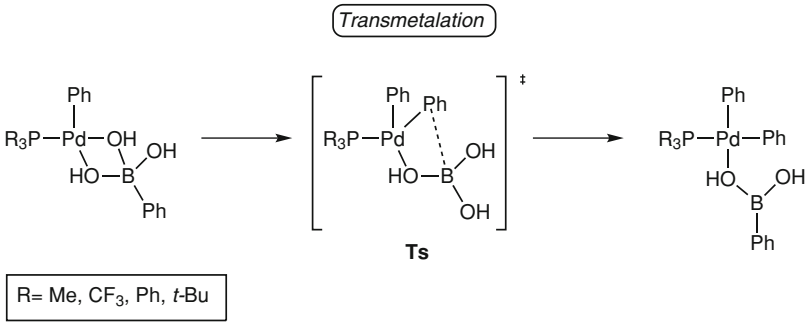

Fig. 3.11 Transmetalation process analyzed by Harvey et al. with different phosphine ligands

density on the metal as a result of the nucleophilic attack of the boronate phenyl group to the Pd atom.

3.4.2 The Transmetalation Step in the Stille Reaction

As stated in the beginning of the section, the Stille reaction along with the Suzuki–Miyaura reaction are the most broadly studied C–C cross-coupling reactions [82]. For the transmetalation process involved in the Stille reaction two main mechanisms dubbed as *cyclic mechanism* and *open mechanism* have been proposed in order to account for the reported experimental evidences (Fig. 3.12). In particular, the cyclic mechanism was proposed to account for the evidences of Stille processes in which the products exhibit retention of configuration at the transmetalated carbon [83], whereas the open mechanism was proposed for processes in which inversion of configuration was observed [84].

As far as concerns the cyclic mechanism (Fig. 3.12), it consists in a two step reaction process in which the first one corresponds to the substitution of a ligand L by the stannane. Afterwards, the transmetalation reaction between the stannane and palladium occurs via a cyclic four-coordinated transition state resulting in a square planar complex where the two organic groups are in a *cis* arrangement. Then, in order to afford the coupled product and regenerate the catalyst, the reductive elimination reaction is required.

In the cyclic mechanism the initial substitution of the ligand L by the stannane is, in general, believed to occur through a ligand exchange pathway [43, 85, 86] although other alternatives such as a dissociative mechanism [87] or a mechanism in which the catalytic species is the one generated after the substitution of a ligand L by a solvent molecule [88] have been also proposed. The latter, consisting in a solvent assisted process, was recently investigated through DFT-B3LYP calculations by Alvarez et al. [89] for the transmetalation reaction with vinylstannane. In particular, the results employing DMF as solvent showed lower energy barriers for the DMF-for-stannane substitution compared to the

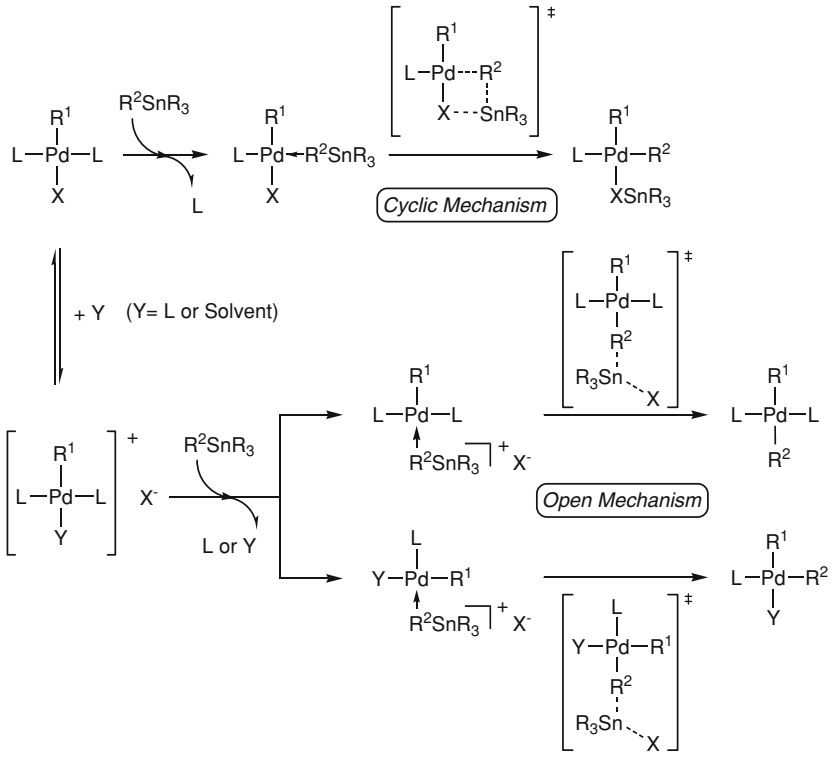

Fig. 3.12 The two mechanisms proposed for the transmetalation step in the Stille reaction

direct L-for-stannane substitution from the initial complex [PdR^1XL_2]. Similarly, the DFT-B3LYP results reported by Nova et al. [90] with THF as solvent showed lower energy barriers for the solvent assisted process. However, after considering the solvent-for-L exchange energy, the authors concluded that both processes may have competitive rates and one or the other might predominate depending on the solvent, the ligand L, and the concentration of this latter. The effect of model ligands (L = PH_3 and AsH_3) as well as the effect of the solvent (S = THF and PhCl) was computationally evaluated by the same authors [90]. According to their results, both the ligand-for-stannane substitution and the transmetalation process with L = PH_3 were found to be thermodynamically and kinetically less favored than those with L = AsH_3, which was consistent with the higher reaction rates experimentally observed for $AsPh_3$ as compared to PPh_3 [87, 88]. This enhanced reactivity is, in general, attributed to the easier dissociation of $AsPh_3$. On the other hand, the introduction of the solvent effects (THF and PhCl) in the transmetalation process with both ligands by means of a continuum model was found to increase the energies for both overall mechanisms, and thus, the authors suggested that the choice of solvents with small dielectric constants might favor this mechanism.

Lin and co-workers reported a DFT-B3LYP computational study on the effect of the leaving group X and the effect of the phosphine ligand for the transmetalation reaction of trimethyl vinyl tin with $L_nPd(Ar)(X)$ ($L = PH_3$, PMe_3; $X = Cl$, Br, I) [91]. Concerning the effect of the leaving group, their results revealed that the overall activation barrier for the transmetalation process (i.e. substitution of L by the stannane followed by the transmetalation reaction properly speaking) increases in the order: $Cl < Br < I$. However, although the transmetalation step with aryl chlorides was found to be faster than with the bromide and iodide analogues, the authors wisely emphasized that one should take into consideration that the oxidative addition step with aryl chlorides may be rate-determining, and therefore, the Stille reaction become more challenging. On the other hand, the evaluation of the effect of the ligands $L = PMe_3$ and $L = PH_3$ showed that the more electron-donating phosphine ligands increase the overall transmetalation barriers, which agreed with the Farina's et al. experimental observation that phosphine ligands of high donicity prevent transmetalation [87]. In particular, this enhancement of the reaction rates with less electron-donating phosphines was attributed by these authors to the less strong Pd–P bond, which facilitates the substitution of the phosphine by the stannane, and to the weaker *trans* influence on the Pd–vinyl bond, which stabilizes the transmetalation product.

As far as the open mechanism is concerned (Fig. 3.12), this mechanism consists of three steps. First, the substitution of the heteroatom X by a neutral ligand Y (Y = L or Solvent) occurs resulting in a cationic species $[PdYL_2R^1]^+$, which is supposed to be more reactive due to its higher electrophilic character. Afterwards, the coordination of the stannane to the palladium complex takes place via substitution of either the neutral ligand Y or a ligand L followed by the proper transmetalation step giving rise to the *trans* and *cis* transmetalated complexes, respectively.

The theoretical evaluation of this mechanism was also carried out by Nova et al. [90] revealing that this mechanism might be favored with catalysts containing good leaving groups (i.e. triflate) and with solvents with high dielectric constant because they facilitate and stabilize the formation of the cationic species. Conversely to the cyclic mechanism, the highest energy barrier within this mechanism was found to be the second step (i.e. the stannane-for-L substitution) and further, the energy barriers for phosphine resulted slightly lower than for the arsine ligand. On the other hand, the analysis of the *cis* and *trans* reaction pathways were found to be energetically comparable, thus confirming the experimental observations.

The Stille reaction mechanism was also evaluated by Alvarez et al. at DFT-B3LYP level obtaining similar conclusions: the open mechanism is favored when anionic ligands (i.e. triflate) are used, whereas the cyclic mechanism is favored for X = halides [92]. These authors also investigated the role of the additive LiCl in the Stille reactions of vinylbromide and vinyl triflate with trimethyl vinyl tin catalyzed by $Pd(PMe_3)_2$. According to their results, the added chloride anion drives the expected transmetalation step from the open one with triflates to the cyclic mechanism in the presence of the additive.

Table 3.1 Gibbs energy barriers calculated by Ariafard and Yates for the transmetalation reaction with different ligands L [54]

Ligand (L)	ΔG_{solv} (kcal/mol)
$P(t\text{-Bu})_3$	34.9
PPh_3	23.9
PPh_2Me	28.3
$PPhMe_2$	34.4
PMe_3	35.8

More recently, the reported accelerating effect of CsF [93] as well as the effect of different phosphine ligands on palladium(II) catalysts was analyzed at DFT-B3LYP level by Ariafard and Yates for the model Stille reaction of (vinyl)$SnMe_3$ with $L_nPd(Ph)(Cl)$ ($L = P(t\text{-Bu})_3$, PPh_3, PPh_2Me, $PPhMe_2$ and PMe_3) [54]. In particular, the effect of the additive CsF was analyzed for the transmetalation reaction with $L = P(t\text{-Bu})_3$ confirming that the addition of the anion F^- increases the reactivity of stannane reagents toward the transmetalation. Furthermore, to account for this enhanced reactivity with the additive, the transmetalation reaction with (vinyl)$SnMe_3$ was proposed to proceed with a lower energy barrier from the fluoro complex [$(P(t\text{-Bu})_3)Pd(F)(Ph)$] which is generated from the initial complex $(P(t\text{-Bu})_3)Pd(Cl)(Ph)$ by interaction of the F^- and following dissociation of the chloride. The evaluation of the effect of the different phosphine ligands for the same model reaction revealed that these ligands play a very important role in the transmetalation step (Table 3.1). For example, the use of very bulky ligands such as $P(t\text{-Bu})_3$ was shown to increase considerably the energy barrier for the transmetalation step because it makes the coordination of the stannane to the palladium complex more difficult.

In the case of the non bulky ligand PMe_3, it leads to a special case in which there is an over stabilization of the previously formed complex *trans*-$[Pd(L)_2(Cl)(Ph)]$ that increases the total energy barrier for the transmetalation process. This additional stabilization of the tetracoordinated complex was attributed by the authors to the less sterically demanding PMe_3 that binds stronger to Pd than the other L ligands. Furthermore, according to results from a previous study [94], the authors suggested that the strength of the Pd–L bond is positively correlated to the σ-donor ability of L; this is consistent with the conclusions previously reported by Lin et al. [91] that the stronger σ-donor ligand, the higher energy barrier for the transmetalation reaction. Alternatively, the moderate bulky ligand $L = PPh_3$ provided the lowest energy barrier for this process which can be rationalized to the right steric balance that this ligand confers. On the other hand the corresponding fine-tuned ligands $L = PPh_2Me$ and $L = PPhMe_2$ provided higher energy barriers for the transmetalation step than the ligand $L = PPh_3$, which is in agreement with the experimental findings of Farina et al. [87] concerning the higher reactivity of Pd(II)/PPh_3 compared to Pd(II)/PPh_2Me. On the basis of all the results, the authors concluded that in theoretical studies on the transmetalation step where the steric effects are very important, the use of PMe_3 to model PPh_3 is not good enough to provide accurate results.

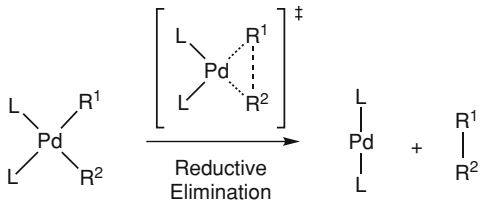

Fig. 3.13 Generally accepted mechanism for the reductive elimination step

3.5 Phosphine Effects in Reductive Elimination

To complete the full catalytic cycle a reductive elimination step is needed after the transmetalation process. This last step, in contrast with the other ones, which are frequently reversible [95], is irreversible. Thus, it is often taken for granted to be critical for the success of the whole reaction because it must pull the catalytic cycle forward. Even though the reductive elimination from a Pd(II) complex, in general, proceeds very readily and it is not rate-limiting, many efforts have been done to improve the efficiency of this step.

The generally accepted mechanism for this process is concerted, starting from the complex formed in the transmetalation step, having the two organic groups in *cis* position (Fig. 3.13). Otherwise, a *trans* to *cis* isomerization reaction previous to the reductive elimination is required. The transition state for this last step corresponds to a cyclic three-coordinated transition state which leads to the final C–C coupling and the regeneration of the catalytic species PdL_2.

Since the early theoretical works of Tatsumi, Hoffmann, Yamamoto and Stille [96] and Low and Goddard [97, 98], the reductive elimination step had received scant attention, but recently, extensive studies on the C–C reductive elimination have been carried out. In particular, in 2002 Ananikov, Musaev, and Morokuma reported a DFT-B3LYP study on the effects of different X ligands in the reductive elimination from bis-σ-vinyl complexes $[Pd(CH{=}CH_2)_2X_n]$ (X = Cl, Br, I, NH_3, PH_3). The results reported therein showed that activation barriers for the C–C bond formation reaction decreases in the following order: Cl > Br, NH_3 > I > PH_3 [99]. Lately, the same authors investigated theoretically most of the common types of coupling partners in the square-planar *cis*-$[PdRR'(PH_3)_2]$ complexes (R or R′ = Me, vinyl, Ph, ethynyl) [100]. The authors concluded that the energy barrier for the carbon–carbon coupling from the symmetrical complex $R_2Pd(PH_3)_2$ increases in the order: R = Vinyl < Ph < Ethynyl < Me. The activation free energies in gas phase for these reactions were found to range from 6.0 (R = vinyl) to 23.6 kcal/mol (R = Me), respectively. Besides, the energy barriers and the exothermicities for the asymmetrical coupling R–R′ from $RR'Pd(PH_3)_2$ resulted to be very close to the averages of the corresponding values with the symmetrical R–R and R′–R′ coupling reactions in $R_2Pd(PH_3)_2$ and $R'_2Pd(PH_3)_2$, respectively.

On the other hand, the nature of the ancillary L ligands is believed to have an important effect on the rate of the reductive elimination reaction. For example, the

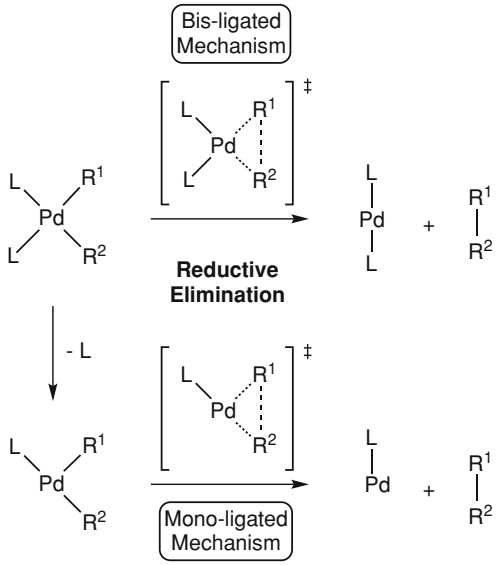

Fig. 3.14 Proposed mechanisms for the reductive elimination reaction from PdR_2L_2

steric effects provided by bulky phosphine ligands have been proposed to promote an accelerating effect on this reaction [101]. This effect can be rationalized as the repulsive interaction between the ancillary ligands and the two organic groups in the initial complex R_2PdL_2 that forces the two species to be very close from each other facilitating, thus, reductive elimination. Moreover, a reaction mechanism through the three-coordinated species formed by dissociation of one phosphine ligand from the initial complex has been also proposed to account for this enhanced reactivity, since the dissociation energy of bulky ligands is very low (Fig. 3.14) [102–105]. The use of phosphine ligands with low electron-donating character produces a clear enhancement in the rate of reductive elimination [106]. A possible explanation for this trend is that Pd(II) complexes which are more electrophilic than Pd(0) complexes, become more stable with phosphine ligands with high donicity [107]. Hence, these ligands stabilize the complex R_2PdL_2 compared to the corresponding transition state increasing the energy barrier for this process. In contrast, the influence of the bite angle in chelating diphosphine ligands showed that wide bite angle ligands destabilize the reactant and stabilize the transition state and therefore, accelerate the reaction [107].

In order to shed light on the influence of the steric and electronic properties of phosphine ligands in reductive elimination, several theoretical studies have been carried out very recently. Ananikov, Musaev and Morokuma reported a computational study by means of the ONIOM approach in which the Me–Me coupling from the complexes $[PdR_2L_n]$ ($L = PPh_3$, PCy_3, PMe_3, and PH_3; $n = 1, 2$) was investigated [108]. According to their results, the steric effects were found to mainly influence the energy of the initial complex, whereas the electronic effects have the largest impact on the energy of the transition state. Furthermore, the

Table 3.2 Relative energies (in kcal/mol) for the reductive elimination reaction from $PdMe_2L_n$ ($n = 1, 2$)

Ligand L	Bis ligated mechanism		Mono ligated mechanism	
	PdR_2L_2	Ts	$PdR_2L + L$	Ts
PMe_3	0.0	28.3	18.8 (0.0)	31.4 (12.6)
PH_3	0.0	23.3	14.2 (0.0)	26.1 (11.9)
PCl_3	0.0	13.2	10.3 (0.0)	20.7 (10.4)

Values in *parenthesis* are relative to $PdR_2L + L$

results revealed that different L ligands may involve different mechanisms of the reductive elimination (Fig. 3.14). In particular, the PCy_3 was proposed to facilitate the mono-ligated reaction pathway and to increase the reactivity, while the PMe_3 ligand stabilizes the four-coordinated complexes and decreases the reactivity toward reductive elimination. Alternatively, the PPh_3 ligand resulted to be a more universal choice, since it showed good reactivity for both mechanisms.

More recently, Ariafard and Yates investigated the steric and electronic effects of the model phosphine ligands L = PMe_3, PH_3, PCl_3 and the experimentally reported ligands L = PPh_3, PPh_2Me, $PPhMe_2$ on the Me–Me reductive elimination from the complexes [PdR_2L_2] and [PdR_2L] [109]. The computed energy barriers at DFT-B3LYP level with the model ligands from the four-coordinated and the three-coordinated complexes are listed in Table 3.2. These results are consistent with the experimental observations that reductive elimination is accelerated by the presence of ligands with low-electron donating properties. Interestingly, this feature has a significant effect on the energy of the transition state for the reductive elimination for the four-coordinated complex (bis-ligated mechanism), while its effect is much lower on the energy of the corresponding transition state for the three-coordinated species (mono-ligated mechanism). In the former case the greater the electron-donation of L, the higher the energy barrier for this process. In the latter case, it is the dissociation of the phosphine ligand that leads to the different overall energy barrier. This dissociation energy is also controlled by the basicity of L because the stronger electron donation leads to a stronger Pd–L bond, and thus a higher overall barrier.

According to the results shown in Table 3.2 the relative energy barriers for the mono-ligated pathways are higher than that through the bis-ligated ones. However, one should take into account that the introduction of the entropic effects may change these results, since a large positive entropy change is expected for the dissociation of one phosphine ligand from the initial Pd complex. The calculation of this process is not an easy task [71]. An estimation of the corresponding Gibbs free energies (which includes entropic contributions) can be roughly obtained by deducting 8–10 kcal/mol [110] from all the electronic energies in the mono-ligated pathway. With this correction, the mechanism via three-coordinated species is favored toward the bis-ligated mechanism, which is in agreement with the experimental observations.

On the other hand, the results obtained for the reductive elimination with the ligands L = PPh_3, PPh_2Me, $PPhMe_2$ (Table 3.3) showed an increase in the energy

Table 3.3 Relative energies (in kcal/mol) for the reductive elimination reaction from $PdMe_2L_n$ ($n = 1, 2$)

Ligand L	Bis ligated mechanism		Mono ligated mechanism	
	PdR_2L_2	Ts	$PdR_2L + L$	Ts
PPh_3	0.0	20.4	11.2 (0.0)	24.0 (12.8)
PPh_2Me	0.0	24.7	16.8 (0.0)	29.4 (12.6)
$PPhMe_2$	0.0	27.9	18.9 (0.0)	31.5 (12.6)

Values in *parenthesis* are relative to $PdR_2L + L$

barrier in the order $PPh_3 < PPh_2Me < PPhMe_2$. This trend was observed regardless of the mechanism, which agrees with the experimental observations [106]. Similarly to the reaction with the model ligands (Table 3.2), the energy barriers for the mono-ligated reaction pathways were found to be lower than those with the bis-ligated ones. Moreover, for all the L ligands the reductive elimination from PdR_2L was found to be almost independent of the bulk of the L ligand. This fact was supported by very small steric repulsions between the L and Me ligands calculated in the mono-phosphine species. Furthermore, the energy-decomposition analyses of the reaction barriers revealed that the electronic effects are very similar to each other and that the steric effects destabilize the initial complex PdR_2L_2 but not the transitions states; this involves a decrease in the barriers to reductive elimination compared to the smaller phosphine ligands.

The C–C coupling on the complex $[PdMe_2(PMe_3)_2]$ as well as on complexes $[PdMe_2(PMe_3)L]$ generated by the addition of coupling promoters (L = acetonitrile, ethylene, maleic anhydride (ma)), and on the tricoordinated intermediate $PdR_2(PMe_3)$ (represented as L = empty) was investigated by Alvarez, Maseras, Espinet and co-workers [111]. The computed activation energies at DFT-B3LYP level were found to increase in the order: ma < "empty" < ethylene < $PMe_3 \approx$ MeCN which confirmed that the energy barrier decreases with the π-acceptor ability of L. Consistently, ma produces a lower coupling barrier because it is a better π-acceptor than ethylene which in turn is better than PMe_3. Furthermore, the barrier with L = ma resulted to be lower to the point that the coupling is easier for the four-coordinated complex with ma than for the three-coordinated species ($\Delta G^{\ddagger}$ is 13.2 kcal/mol for L = empty and 8.6 kcal/mol for L = ma). Moreover, the effect of added olefins revealed that olefins with electron-withdrawing substituents facilitate the coupling through $[PdMe_2(PMe_3)(olefin)]$ intermediates with much lower activation energies than the starting complex or a three-coordinated intermediate.

3.6 Concluding Remarks

Cross-coupling reactions are one of the most common and useful organic tools in the laboratory. Several metal catalysts have been developed for this reaction but those based on Pd are the most developed ones. The stoichiometry of the Pd-based

catalyst uses to be PdL_2; as in many other transition metal catalysts phosphines are the most common ligands.

The reaction mechanism for the Pd-catalyzed cross-coupling reaction is commonly accepted that takes place in three main reaction steps: (1) oxidative addition, (2) transmetalation and (3) reductive elimination. The first and the third processes are common in many other catalytic reactions. The transmetalation, however, is quite particular of the cross-coupling reactions. The effect of the phosphine on each of these reaction steps studied by means of theoretical methods has been reviewed in this chapter.

As far as the oxidative addition is concerned, two different mechanisms are proposed for this step: a concerted mechanism and a nucleophilic attack mechanism. Calculations on the concerted mechanism show that the size of the phosphine does not significantly affect this process for monophosphine catalytic systems. In fact, it is experimentally shown that the rate constants for the oxidative addition depend more on the identity of the halide of the ArX electrophilic reactant than of the steric bulk of the phosphine ligands. The nature of the phosphine ligand may affect this process not because of the oxidative addition elementary step itself (where the effect is rather small), but due to its own intrinsic capability of generating mono- or bisphosphine catalysts. The oxidative addition process in monophosphine systems are more favorable than in their bisphosphine counterparts. In fact, the most active phosphine ligands known are the bulky and electron-rich dialkylbiaryl phosphines developed by Buchwald's group.

On the other hand, in the nucleophilic attack mechanism an inversion of configuration on the organic reaction was observed. For the particular case of sp^3 carbon atoms in α-sulfoxide systems the mechanism was proposed to be rather similar for both the mono- or bisphosphine catalysts.

The transmetalation process has been described for the Suzuki–Miyaura and the Stille cross-coupling reactions. For the first reaction, the computational analysis of the transmetalation process using a model PH_3 phosphine ligand showed that this step presents a relatively low energy barrier for both mono- and bisphosphine catalytic species, though mono-phosphine system was favored. Taking the monophosphine as the catalytic species the theoretical studies revealed that for this particular process the steric effects are more important than the electronic effects. Hence, the computation of steric descriptors showed that bulkier ligands may produce higher energy barriers whereas electronic descriptors revealed that better π-acceptor phosphines may contribute to lowering the energy barrier for this process.

In the case of the Stille reaction two different alternative mechanisms have been proposed: cyclic and open. The cyclic pathway is proposed for those cases where retention of configuration is observed, whereas the open pathway is proposed to take place when an inversion of configuration is obtained in the product. The cyclic pathway requires a ligand (phosphine) substitution process to coordinate the stannane species. Thus, the nature of the phosphine may significantly affect this process; phosphine ligands with high donor capacity should prevent transmetalation. As far as the open pathway is concerned, the theoretical study revealed that this pathway is favored for catalysts containing easily removal ligands (i.e. triflate) and

using solvents of high dielectric constants because they favor the formation of cationic intermediates. Regarding the phosphine effects, the theoretical evaluation points out that the use of bulky ligands increases considerably the energy barrier for the transmetalation step because prevents the coordination of the stannane to the metal center; good σ-donor phosphines also increases the barrier for the transmetalation due to the stabilization of the phosphine coordinated intermediates.

The reductive elimination can be considered the reverse pathway of the oxidative addition. Nevertheless, there is an important difference; the reductive elimination is an irreversible pathway within the catalytic cycle. The transition step for this process is calculated to be concerted leading to the final C–C coupling and regeneration of the Pd catalyst. Theoretical evaluation of the steric and electronic effects on this process showed that whereas the steric effects mainly influence the relative energy of the initial intermediate, electronic effects have the largest impact on the energy of the transition state. Thus, the use of low electron-donating phosphines diminishes the energy of the transition state therefore producing an enhancement of the reductive elimination rate. For chelating bisphosphine ligands theoretical studies showed that ligands with wide bite angle destabilize the initial intermediate and stabilize the transition state for the reductive elimination. The presence of coupling promoters acting as a second ligand along with the phosphine was also computationally evaluated. Theoretical analysis showed that the energy barrier for the coupling process decreases with the π-acceptor ability of the coupling promoter.

Overall a proper balance between steric and electronic effects is needed in the phosphine ligands in order to optimize the efficiency in cross-coupling reactions. Once again theoretical methods are shown as a valuable tool for analyzing reaction mechanisms, particularly the effect of the phosphine ligands in cross-coupling reactions. In spite of the great advances performed on the understanding of these processes, much work is still needed in order to have a more general picture of the cross-coupling reactions beside the Suzuki–Miyaura and Stille reactions.

Acknowledgments We thank the Ph.D. students and postdocs who have contributed to developing this research topic in our groups. Fruitful collaborations with experimental groups (Pablo Espinet, Gregorio Asensio, Rosana Alvarez and Angel Rodríguez de Lera) are also acknowledged. The Spanish MICINN is gratefully acknowledged for funding this research through projects CTQ2008-06866-C02-01, CTQ2008-06866-C02-02 and Consolider-Ingenio 2010 (CSD2007-00006 and CSD2006-0003).

References

1. Cornils B, Herrmann WA (2002) Applied homogeneous catalysis with organometallic compounds. Wiley-VCH, Weinheim
2. Hagen J (2006) Industrial catalysis: a practical approach, 2nd edn. Wiley-VCH, Weinheim
3. Miura M (2004) Rational ligand design in constructing efficient catalyst systems for Suzuki–Miyaura coupling. Angew Chem Int Ed 43:2201–2203
4. Chen W, Li R, Han B, Li B-J, Chen Y-C, Wu Y, Ding L-S, Yang D (2006) The design and synthesis of bis(thiourea) ligands and their application in Pd-catalyzed Heck and Suzuki reactions under aerobic conditions. Eur J Org Chem 1177–1184

5. Tolman CA (1977) Steric effects of phosphorus ligands in organometallic chemistry and homogeneous catalysis. Chem Rev 77:313–348
6. Brown TL, Lee KJ (1993) Ligand steric properties. Coord Chem Rev 128:89–116
7. Dias PB, de Piedade MEM, Martinho Simões JA (1994) Bonding and energetics of phosphorus (III) ligands in transition metal complexes. Coord Chem Rev 135(136):737–807
8. Bunten KA, Chen L, Fernandez AL, Poë AJ (2002) Cone angles: Tolman's and Plato's. Coord Chem Rev 233(234):41–51
9. Kühl O (2005) Predicting the net donating ability of phosphines- do we need sophisticated theoretical methods? Coord Chem Rev 249:693–704
10. Kamer PCJ, van Leeuwen PWNM, Reek JNH (2001) Wide bite angle diphosphines: Xantphos ligands in transition metal complexes and catalysis. Acc Chem Res 34:895–904
11. Wang Y, Wang J, Su J, Huang F, Jiao L, Liang Y, Yang D, Zhang S, Wender PA, Yu Z-X (2007) A computational designed Rh(I)-catalyzed two-component [5 + 2 + 1] cycloaddition of ene-vinylcyclopropanes and CO for the synthesis of cyclooctenones. J Am Chem Soc 129:10060–10061
12. Houk KN, Cheong PH-Y (2008) Computational prediction of small-molecule catalysts. Nature 455(7211):309–313
13. Ananikov VP, Orlov NV, Kabeshov MA, Beletskaya IP, Starikova ZA (2008) Stereodefined synthesis of a new type of 1,3-dienes by ligand-controlled carbon-carbon and carbon-heteroatom bond formation in nickel-catalyzed reaction of diaryldichalcogenides with alkynes. Organometallics 27:4056–4061
14. Abe Y, Kuramoto K, Ehara M, Nakatsuji H, Suginome M, Murakami M, Ito Y (2008) A mechanism for the palladium-catalyzed regioselective silaboration of allene: a theoretical study. Organometallics 27:1736–1742
15. Maseras F, Morokuma K (1995) IMOMM: A new integrated ab initio + molecular mechanics geometry optimization scheme of equilibrium structures and transition states. J Comput Chem 16:1055–1179
16. Ujaque G, Maseras F (2004) Applications of hybrid DFT/molecular mechanics to homogeneous catalysis. Struct Bond 112:117–149
17. Bo C, Maseras F (2008) QM/MM methods in inorganic chemistry. Dalton Trans 2911–2919
18. Carbo JJ, Maseras F, Bo C, van Leeuwen WNM (2001) Unraveling the origin of regioselectivity in rhodium diphosphine catalyze hydroformylation. A DFT QM/MM study. J Am Chem Soc 123:7630–7637
19. Garcia-Cuadrado D, de Mendoza P, Braga AAC, Maseras F, Echavarren AM (2007) Proton-abstraction mechanism in the palladium-catalyzed intramolecular arylation: substituents effects. J Am Chem Soc 129:6880–6886
20. Liu S, Saidi O, Berry N, Ruan J, Pettman A, Thomson N, Xiao J (2009) Electron-deficient phosphines accelerate the Heck reaction of electron-rich olefins in ionic liquids. Lett Org Chem 6:60–64
21. Moncho S, Ujaque G, Lledos A, Espinet P (2008) When are tricoordinated PdII species accessible? Stability trends and mechanistic consequences. Chem Eur J 14:8986–8994
22. de Meijere A, Diederich F (2004) Metal-catalyzed cross-coupling reactions. Wiley-VCH, Weinheim
23. Cross-Coupling reactions: A practical guide (2001) No 219. In: Miyaura N (ed) Topics in current chemistry. Springer, Berlin
24. Buchwald SL (ed) (2008) Cross-coupling. Acc Chem Res 41(special issue):1439–1564
25. Tamao K, Hiyama T, Negishi E (eds) (2002) 30 years of cross-coupling reaction. J Organomet Chem 653(special issue):1–303
26. Phapale VB, Cardenas DJ (2009) Nickel-catalyzed Negishi cross-coupling reactions: scope and mechanisms. Chem Soc Rev 38:1598–1607
27. Nicolaou KC, Bulger PG, Sarlah D (2005) Palladium-catalyzed cross-coupling reactions in total synthesis. Angew Chem Int Ed 44:4442–4489
28. Xue L, Lin Z (2010) Theoretical aspects of palladium-catalyzed carbon-carbon cross-coupling reactions. Chem Soc Rev 39:1692

29. Kosugi M, Sasazawa K, Shimizu Y, Migita T (1977) Reactions of allyltin compounds. 3. Allylation of aromatic halides with allyltributyltin in presence of tetrakis(triphenylphosphine) palladium(0). Chem Lett 3:301–302
30. Stille JK (1986) The palladium-catalyzed cross-coupling reactions of organotin reagents with organic electrophiles. Angew Chem Int Ed 25:508–524
31. Miyaura N, Yamada K, Suzuki A (1979) New stereospecific cross-coupling by the palladium-catalyzed reaction of 1-alkenylboranes with 1-alkenyl or 1-alkynyl halides. Tetrahedron Lett 36:3437–3440
32. Miyaura N, Suzuki A (1995) Palladium-catalyzed cross-coupling reactions of organoboron compounds. Chem Rev 95:2457–2483
33. Negishi E, King AO, Okukado N (1977) Selective carbon-carbon bond formation via transition-metal catalysis. 3. Highly selective synthesis of unsymmetrical biaryls and diarylmethanes by nickel-catalyzed or palladium-catalyzed reaction of aryl derivatives and benzylzinc derivatives with aryl halides. J Org Chem 42:1821–1823
34. Fuentes B, García-Melchor M, Lledos A, Maseras F, Casares JA, Ujaque G, Espinet P (2010) Palladium round trip in the Negishi coupling of trans-[PdMeCl($PMePh_2$)$_2$] with ZnMeCl: An experimental and DFT study of the transmetalation step. Chem Eur J 16:8596–8599
35. Braga AAC, Ujaque G, Maseras F (2008) Mechanism of palladium-catalyzed cross-coupling reactions. In: Morokuma K, Musaev DG (eds) Computational modeling for homogeneous and enzymatic catalysis. Wiley-VCH, Weinheim
36. Amatore C, Jutand A (2000) Anionic Pd(0) and Pd(II) intermediates in palladium-catalyzed Heck and cross-coupling reactions. Acc Chem Res 33:314–321
37. Galardon E, Ramdeehul S, Brown JM, Cowley A, Hii KK, Jutand A (2002) Profund steric control of reactivity in aryl halide addition to bisphosphane palladium(0) complexes. Angew Chem Int Ed 41:1760–1763
38. Hartwig JF (2007) Electronic effects on reductive elimination to form carbon-carbon and carbon-heteroatom bonds from palladium(II) complexes. Inorg Chem 46:1936–1947
39. Yandulov DV, Tran NT (2007) Aryl-Fluoride reductive elimination from Pd(II): Feasibility assessment from theory and experiment. J Am Chem Soc 129:1342–1358
40. Senn HM, Ziegler T (2004) Oxidative addition of aryl halides to palladium(0) complexes: A density-functional study including solvation. Organometallics 23:2980–2988
41. Gossen LJ, Koley D, Hermann HL, Thiel W (2005) Mechanistic pathways for oxidative addition of aryl halides to palladium(0) complexes: A DFT study. Organometallics 24: 2398–2410
42. Lam KC, Marder TB, Lin Z (2007) DFT studies on the effect of the nature of the aryl halide Y-C6H4-X on the mechanism of its oxidative addition to Pd0L versus Pd0L2. Organometallics 26:758–760
43. Casado AL, Espinet P (1998) Mechanism of the Stille reaction. 1. The transmetalation step. Coupling of R_1I and R_2SnBu_3 catalyzed by trans-[PdR_1IL_2] ($R_1 = C_6C_{l2}F_3$; R_2 = vinyl, 4-methoxyphenyl; L = $AsPh_3$). J Am Chem Soc 120:8978–8985
44. Sicre C, Braga AAC, Maseras F, Cid MM (2008) Mechanistic insights into the transmetalation step of a Suzuki-Miyaura reaction of 2(4)-bromopyridines: Characterization of an intermediate. Tetrahedron 64:7437–7443
45. Liu Q, Lan Y, Liu J, Li G, Wu Y-D, Lei A (2009) Revealing a second transmetalation step in the Negishi coupling and its competition with reductive elimination: Improvement in the interpretation of the mechanism of biaryl synthesis. J Am Chem Soc 131:10201–10210
46. Littke AF, Fu GC (2002) Palladium-catalyzed coupling reactions of aryl chlorides. Angew Chem Int Ed 41:4176–4211
47. Wolfe JP, Singer RA, Yang BH, Buchwald SL (1999) Highly active palladium catalysts for Suzuki coupling reactions. J Am Chem Soc 121:9550–9561
48. Zapf A, Ehrentraut A, Beller M (2000) A new highly efficient catalyst system for the coupling of nonactivated and deactivated aryl chlorides with arylboronic acids. Angew Chem Int Ed 39:4153–4155

49. Fleckenstein CA, Plenio H (2010) Sterically demanding trialkylphosphines for palladium-catalyzed cross-coupling reactions- alternatives to Pt-Bu_3. Chem Soc Rev 39:694–711
50. Kantchev EAB, O'Brien CJ, Organ MG (2007) Palladium complexes of N-Heterocyclic carbenes as catalysts for cross-coupling reactions. A synthetic chemist's perspective. Angew Chem Int Ed 46:2768–2813
51. Marion N, Nolan SP (2008) Well-defined *N*-Heterocyclic carbenes-palladium(II) precatalysts for cross-coupling reactions. Acc Chem Res 41:1440–1449
52. Ahlquist M, Fristrup P, Tanner D, Norrby P-O (2006) Theoretical evidence for low-ligated palladium(0): [Pd–L] as the active species in oxidative addition. Organometallics 25:2066–2073
53. Li Z, Fu Y, Guo Q-X, Liu L (2008) Theoretical study on monoligated Pd-catalyzed cross-coupling reactions of aryl chlorides and bromides. Organometallics 27:4043–4049
54. Ariafard A, Yates BF (2009) Subtle balance of ligand steric effects in Stille transmetalation. J Am Chem Soc 131:13981–13991
55. Barrios-Landeros F, Carrow BP, Hartwig JF (2009) Effect of ligand steric properties and halide identity on the mechanism for oxidative addition of haloarenes to trialkylphosphine Pd(0) complexes. J Am Chem Soc 131:8141–8154
56. Ahlquist M, Norrby P-O (2007) Oxidative addition of aryl chlorides to monoligated palladium(0): A DFT-SCRF study. Organometallics 26:550–553
57. Jover J, Fey N, Purdie M, Lloyd-Jones GC, Harvey JN (2010) A computational study of phosphine ligand effects in Suzuki-Miyaura coupling. J Mol Catal A 324:39–47
58. Fey N, Tsipis AC, Harris SE, Harvey JN, Orpen AG, Mansson RA (2006) Development of a ligand knowledge base, Part 1: Computational descriptors for phosphorus donor ligands. Chem Eur J 12:291–302
59. Fey N, Orpen GA, Harvey JN (2009) Building ligand knowledge bases for organometallic chemistry: Computational description of phosphorus(III)-donor ligands and the metal-phosphorus bond. Coord Chem Rev 253:704–722
60. Fey N (2010) The contribution of computational studies to organometallic catalysis: descriptors, mechanisms and models. Dalton Trans 39:296–310
61. Corbet J-P, Mignani G (2006) Selected patented cross-coupling reaction technologies. Chem Rev 106:2651–2710
62. Stille JK, Lau KS (1977) Mechanisms of oxidative addition of organic halides to group-8 transition metal complexes. Acc Chem Res 10:434–442
63. Feliz M, Freixa Z, van Leeuwen PWNM, Bo C (2005) Revisiting the methyl iodide oxidative addition to rhodium complexes: A DFT study of the activation parameters. Organometallics 24:5718–5723
64. Diefenbach A, de Jong GT, Bickelhaupt FM (2005) Activation of H–H, C–H, C–C and C–Cl bonds by Pd and PdCl. Understanding anion assistance in C–X bond activation. J Chem Theory Comput 1:286–298
65. Rodriguez N, Ramirez de Arellano C, Asensio G, Medio-Simon M (2007) Palladium-catalyzed Suzuki-Miyaura reaction involving a secondary sp3 carbon: Studies of stereochemistry and scope of the reaction. Chem Eur J 13:4223–4229
66. Gourlaouen C, Ujaque G, Lledos A, Medio-Simon M, Asensio G, Maseras F (2009) Why is the Suzuki–Miyaura cross-coupling of sp3 carbons in α-Bromo sulfoxide systems fast and stereoselective? A DFT study on the mechanism. J Org Chem 74:4049–4054
67. Miyaura N (2002) Cross-coupling reaction of organoboron compounds via base-assisted transmetalation to palladium(II) complexes. J Organomet Chem 653:54–57
68. Smith GB, Dezeny GC, Hughes DL, King AO, Verhoeven TR (1994) Mechanistic studies of the Suzuki cross-coupling reaction. J Org Chem 59:8151–8156
69. Matos K, Soderquist JA (1998) Alkylboranes in the Suzuki–Miyaura coupling: stereochemical and mechanistic studies. J Org Chem 63:461–470
70. Braga AAC, Morgon NH, Ujaque G, Maseras F (2005) Computational characterization of the role of the base in the Suzuki–Miyaura cross-coupling reaction. J Am Chem Soc 127:9298–9307

71. Braga AAC, Ujaque G, Maseras F (2006) A DFT study of the full catalytic cycle of the Suzuki-Miyaura cross-coupling on a model system. Organometallics 25:3647–3658
72. Braga AAC, Morgon NH, Ujaque G, Lledos A, Maseras F (2006) Computational study of the transmetalation process in the Suzuki-Miyaura cross-coupling of aryls. J Organomet Chem 691:4459–4466
73. Sumimoto M, Iwane N, Takahama T, Sakaki S (2004) Theoretical study of trans-metalation process in palladium-catalyzed borylation of iodobenzene with diboron. J Am Chem Soc 126:10457–10471
74. Gooβen LJ, Koley D, Hermann HL, Thiel W (2005) The palladium-catalyzed cross-coupling reaction of carboxylic anhydrides with arylboronic acids: a DFT study. J Am Chem Soc 127:11102–11114
75. Gooβen LJ, Koley D, Hermann HL, Thiel W (2006) Palladium monophosphine intermediates in catalytic cross-coupling reactions: a DFT study. Organometallics 25:54–67
76. Martin R, Buchwald SL (2008) Palladium-catalyzed Suzuki-Miyaura cross-coupling reactions employing dialkylbiaryl phosphine ligands. Acc Chem Res 41:1461–1473 (references therein)
77. Barder TE, Walker SD, Martinelli JR, Buchwald SL (2005) Catalysts for Suzuki-Miyaura coupling processes: scope and studies of the effect of the ligand structure. J Am Chem Soc 127:4685–4696
78. Christmann U, Vilar R (2005) Monoligated palladium species as catalyst in cross-coupling reactions. Angew Chem Int Ed 44:366–374
79. Joshaghani M, Faramarzi E, Rafiee E, Daryanavard M, Xiao J, Baillie C (2006) Efficient Suzuki cross-coupling reactions using bulky phosphines. J Mol Catal A 259:35–40
80. Huang Y-L, Weng C-M, Hong F-E (2008) Density functional studies on palladium-catalyzed Suzuki-Miyaura cross-coupling reactions assisted by N- or P-chelating ligands. Chem Eur J 14:4426–4434
81. Chang C-P, Weng C-M, Hong F-E (2010) Preparation of cobalt sandwich diphosphine ligand [(η^5–$C_5H_4{}^{i}Pr$)Co(η^4–$C_4(PPh_2)_2Ph_2$)] and its chelated palladium complex: application of diphosphine ligand in the preparation of mono-substituted ferrocenylarenes. Inorg Chim Acta 363:412–417
82. Espinet P, Echavarren AM (2004) The mechanisms of the Stille reaction. Angew Chem Int Ed 43:4704–4734
83. Ye J, Bhatt RK, Falck JR (1994) Stereospecific palladium/copper cocatalyzed cross-coupling of α-alkoxy- and α-aminostannanes with acyl chlorides. J Am Chem Soc 116:1–5
84. Labadie JW, Stille JK (1983) Mechanisms of the palladium-catalyzed couplings of acid chlorides with organotin reagents. J Am Chem Soc 105:6129–6137
85. Casares JA, Espinet P, Salas G (2002) 14-electron T-shape [PdRXL] complexes: evidence or illusion? Mechanistic consequences for the Stille reaction and related processes. Chem Eur J 8:4843–4853
86. Napolitano E, Farina V, Persico M (2003) The Stille reaction: a density functional analysis of the transmetalation and the importance of coordination expansion at Tin. Organometallics 22:4030–4037
87. Farina V, Krishnan B (1991) Large rate accelerations in the Stille reaction with tri-2-furylphosphine and triphenylarsine as palladium ligands: mechanistic and synthetic implications. J Am Chem Soc 113:9585–9595
88. Amatore C, Bahsoun AA, Jutand A, Meyer G, Ntepe AN, Ricard L (2003) Mechanism of the Stille reaction catalyzed by palladium ligated to arsine ligand: $PhPdI(AsPh_3)(DMF)$ is the species reacting with vinylstannane in DMF. J Am Chem Soc 125:4212–4222
89. Alvarez R, Faza ON, Lopez CS, de Lera AR (2006) Computational characterization of a complete palladium-catalyzed cross-coupling process: The associative transmetalation in the Stille reaction. Org Lett 8:35–38
90. Nova A, Ujaque G, Maseras F, Lledos A, Espinet P (2006) A critical analysis of the cyclic and open alternatives of the transmetalation step in the Stille cross-coupling reaction. J Am Chem Soc 128:14571–14578

91. Ariafard A, Lin Z, Fairlamb IJS (2006) Effect of the leaving ligand X on transmetalation of organostannanes (vinylSnR_3) with $L_nPd(Ar)(X)$ in Stille cross-coupling reactions. A density functional theory study. Organometallics 25:5788–5794
92. Alvarez R, Perez M, Faza ON, de Lera AR (2008) Associative transmetalation in the Stille cross-coupling reaction to form dienes: Theoretical insights into the open pathway. Organometallics 27:3378–3389
93. Littke AF, Schwarz L, Fu GC (2002) Pd/P(*t*-Bu)$_3$: a mild and general catalyst for Stille reactions of aryl chlorides and aryl bromides. J Am Chem Soc 124:6343–6348
94. Fazaeli R, Ariafard A, Jamshidi S, Tabatabaie ES, Pishro KA (2007) Theoretical studies of the oxidative addition of PhBr to $Pd(PX_3)_2$ and $Pd(X_2PCH_2CH_2PX_2)$ (X = Me, H, Cl). J Organomet Chem 692:3984–3993
95. Perez-Temprano MH, Nova A, Casares JA, Espinet P (2008) Observation of a hidden intermediate in the Stille reaction. Study of the reversal of the transmetalation step. J Am Chem Soc 130:10518–10520
96. Tatsumi K, Hoffmann R, Yamamoto A, Stille JK (1981) Reductive elimination of d^8-organotransition metal complexes. Bull Chem Soc Jpn 54:1857–1867
97. Low JJ, Goddard WA (1986) Theoretical studies of oxidative addition and reductive elimination. 2. Reductive coupling of H–H, H–C, and C–C bonds from palladium and platinum complexes. Organometallics 5:609–622
98. Low JJ, Goddard WA (1986) Theoretical studies of oxidative addition and reductive elimination. 3. C–H and C–C reductive coupling from palladium and platinum bis(phosphine) complexes. J Am Chem Soc 108:6115–6128
99. Ananikov VP, Musaev DG, Morokuma K (2002) Vinyl-vinyl coupling on late transition metals through C–C reductive elimination mechanism. A computational study. J Am Chem Soc 124:2839–2852
100. Ananikov VP, Musaev DG, Morokuma K (2005) Theoretical insight into the C–C coupling reactions of the vinyl, phenyl, ethynyl, and methyl complexes of palladium and platinum. Organometallics 24:715–723
101. Choueiry D, Negishi E-I (2002) Pd(0) and Pd(II) complexes containing phosphorus and other group 15 atom ligands. In: Negishi E (ed) Handbook of organopalladium chemistry for organic synthesis. Wiley, New York
102. Ozawa F, Ito T, Nakamura Y, Yamamoto A (1981) Mechanisms of thermal decomposition of trans- and cis-Dialkylbis(tertiary phosphine)palladium(II). Reductive elimination and trans to cis isomerization. Bull Chem Soc Jpn 54:1868–1880
103. Ozawa F, Kurihara K, Yamamoto T, Yamamoto A (1985) Alteration of reaction course in thermolysis of cis-diethylbis(tertiary phosphine)palladium(II) from reductive elimination to β-elimination process induced by addition of tertiary phosphine ligand. Bull Chem Soc Jpn 58:399–400
104. Brown JM, Cooley NA (1988) Carbon-carbon bond formation through organometallic elimination reactions. Chem Rev 88:1031–1046
105. Macgregor SA, Neave GW, Smith C (2003) Theoretical studies on C-heteroatom bond formation via reductive elimination from group 10 $M(PH_3)_2(CH_3)(X)$ species (X = CH_3, NH_2, OH, SH) and the determination of metal-X bond strengths using density functional theory. Faraday Discuss 124:111–127
106. Negishi E, Takahashi T, Akiyoshi K (1987) Palladium-catalyzed -or promoted reductive carbon–carbon coupling. Effects of phosphines and carbon ligands. J Organomet Chem 334: 181–194
107. Zuidema E, van Leeuwen PWNM, Bo C (2005) Reductive elimination of organic molecules from palladium-diphosphine complexes. Organometallics 24:3703–3710
108. Ananikov VP, Musaev DG, Morokuma K (2007) Critical effect of phosphane ligands on the mechanism of carbon-carbon bond formation involving palladium(II) complexes: a theoretical investigation of reductive elimination from square-planar and T-shape species. Eur J Inorg Chem 5390–5399

109. Ariafard A, Yates BF (2009) In-depth insight into the electronic and steric effects of phosphine ligands on the mechanism of the R–R reductive elimination from $(PR_3)_2PdR_2$. J Organomet Chem 694:2075–2084
110. Watson L, Eisenstein O (2002) Entropy explained: the origin of some simple trends. J Chem Educ 79:1269–1277
111. Perez-Rodriguez M, Braga AAC, Garcia-Melchor M, Perez-Temprano M, Casares JA, Ujaque G, de Lera AR, Alvarez R, Maseras F, Espinet P (2009) C–C reductive elimination in palladium complexes, and the role of coupling additives A DFT study supported by experiment. J Am Chem Soc 131(10):3650–3655